

UNIVERSITA' DEGLI STUDI DI NAPOLI FEDERICO II



SCUOLA POLITECNICA DELLE SCIENZE E DI BASE

Department of Chemical, Materials, and Industrial Production Engineering
(DICMAPI)

PhD in “Industrial Product and Process Engineering”

XXXV cycle

Development of an innovative and versatile nano-emulsion- based platform for the
active targeting

Supervisor:

Prof. Paolo Antonio Netti

Advisors:

Ing. Raffaele Vecchione

Coordinator:

Prof. Andrea D’anna

PhD candidate:

Elena Lagreca

Table of Contents

<i>Abstract.....</i>	<i>9</i>
<i>Chapter 1: Introduction.....</i>	<i>11</i>
1. Drug delivery system lipid base nano carriers	11
2. Nanotechnologies in medical field: from passive to active targeting	22
3. Biomimetic nanocarrier	27
Polymer and polysaccharides	28
Cell membrane coated materials.....	31
Bacteria coated nanocarrier	37
Exosome	39
Viral nanocarrier platforms.....	40
4. Application of nanotechnologies in nutraceutical and cosmetic field.....	41
5. Aim of the thesis.....	44
<i>Chapter 2: Tumour Cell membrane coated secondary Nanoemulsions.....</i>	<i>46</i>
Cell membrane-coated oil in water nano-emulsions as biomimetic nanocarriers for lipophilic compounds conveyance.....	46
<i>Abstract.....</i>	<i>46</i>
1. Introduction	47
2. Materials and Methods.....	49
Materials.....	49
Cell Culture	50
Cell Membrane Isolation and Characterization	50

Circular Dichroism (CD).....	51
Bicinchoninic Acid assay (BCA assay) membrane protein quantification.....	51
Ct-NEs preparation.....	51
CM-NEsoSome Preparation.....	52
Physio-chemical characterization and morphological characterization of the Ct-NE and CM-NEsoSome Particle Size and ζ -Potential Measurements.....	52
CM-NEsoSome Characterization by Confocal and STED Microscopy.....	53
Isolated cell membrane, Ct-NE and CM-NEsoSome Characterization by Cryo-TEM Microscopy	53
Cell Viability Assessment	54
Confocal Microscopy for NE uptake in HDF cells	54
3. Results and Discussion	54
Cell Membranes Extraction and Purification	54
CM-NEsoSome Preparation	56
CM-NEsoSome Characterization	56
CM-NEsoSome Biocompatibility Assessment	58
4. Conclusions.....	60
5. Supplementary Information	61
References.....	65
<i>Chapter 3: Macrophage biomimetic NEsoSome for inflamed tissue selective targeting.</i>	<i>69</i>
Abstract.....	69

1.	Introduction.....	69
2.	Material and methods.....	72
	Materials.....	72
	Cells Culture.....	72
	Membrane extraction and characterization.....	74
	Biomimetic NEsoSome development.....	76
	<i>In vitro</i> accumulation analysis in HUVECs.....	78
3.	Result and discussion.....	79
	THP-1 activation and cell membrane extraction.....	79
	Biomimetic NEsoSome development.....	82
	<i>In vitro</i> accumulation analysis in HUVECs.....	84
4.	Conclusion.....	88
	Supported information.....	89
	Biomimetic NEsoSome development.....	89
	<i>In vitro</i> accumulation analysis in HUVECs.....	90
	References.....	90
	<i>Chapter 4: Food grade secondary oil in water nanoemulsions with enhanced mucus-adhesion properties.....</i>	<i>94</i>
	Physicochemical and in vitro biological validation of food grade secondary oil in water nanoemulsions with enhanced mucus-adhesion properties.....	94
	<i>Abstract.....</i>	<i>94</i>

1. Introduction.....	96
2. Materials and Methods	97
Materials.....	97
Primary nano-emulsion preparation	98
Thermodynamic study of interaction between Ct and NEs	99
Ct-FITC Preparation.....	99
Ct salification with NAC	100
Materials characterization.....	100
Ellman’s test	100
¹ H-NMR.....	101
Secondary nano-emulsion preparation	101
Particle size and ζ-potential analysis.....	101
Morphological characterization: Cryo- Transmission electron microscopy (Cryo-TEM)	102
<i>In vitro</i> gastrointestinal digestion	102
CUR determination through UHPLC Q-Orbitrap HRMS	103
Ct and Ct-NAC NEs Treatment in InOA-chip.....	104
Microfluidic Device design and Fabrication	104
Caco-2 Cell culture in InOA-chip	104
On-line monitoring of Ct and Ct-NAC NEs treatment on Caco-2 monolayer seeded on InOA-chip	105

Fluorescence quantification analysis	105
3. Results and Discussion.....	107
DLS analysis of primary NEs	107
Isothermal titration calorimetry (ITC) on Ct-NEs	108
Ellman’s test	110
¹ H-NMR analyses of Ct.....	111
SNEs characterization by DLS and Cryo-TEM.....	114
<i>In vitro</i> bio-accessibility of free and encapsulated CUR.....	116
Ct and Ct-NAC NEs treatment of Caco-2 cells seeded on InOA-chip	118
4. Conclusions	121
Supporting Information.....	122
DLS analysis of FG primary NE 20 wt% in Oil	122
NMR characterization.....	124
Ellman’s test calibration curves and thiol groups determination in Ct-NAC .	124
DLS analysis of FG and PG Ct and Ct-NAC NEs	126
Mucoadhesive properties of CUR Ct-NAC NEs and Ct NEs in InOA-chip	133
References.....	134
<i>Chapter 5: Overall conclusion.....</i>	<i>138</i>
<i>Chapter 6: Side works.....</i>	<i>141</i>
<i>Tunable Release of Curcumin with an In Silico-Supported Approach from Mixtures of Highly Porous PLGA Microparticles.....</i>	<i>141</i>

Abstract.....	141
1. Introduction	142
2. Materials and Methods	144
Materials.....	144
Methods	144
3. Results and Discussion	147
CUR-MPs Production and Morphological Characterization	147
4. Conclusions.....	155
References.....	155
Engineered Bacterial Cellulose Nanostructured Matrix for Incubation and Release of Drug-Loaded Oil in Water Nanoemulsion	159
Abstract.....	159
1. Introduction.....	160
2. Material and methods	161
Materials.....	161
Methods	162
Infrared spectroscopy.....	164
Co-Q10-SNE production and characterization	164
3. Results and discussion.....	166
Cellulose production: morphological and chemical characterization	166
Ultrastructural characterization of BC	170

4. Conclusion.....	173
Supplementary Information	174
References.....	179
<i>List of publication.....</i>	<i>183</i>
<i>Acknowledgements.....</i>	<i>184</i>

Abstract

Nanoscale drug delivery systems represent a challenging area in pharmaceutical research, for the supply of therapeutics to the site of action, without affecting healthy tissues or organs. Herein, we report different strategies to engineer oil in water nano-emulsions (O/W NEs) to obtain a biomimetic nano-carrier employing both biological membrane and polymeric coating to increase the selective uptake into a selected compartment. Nowadays, a new bioengineered platform based on cell membrane cloaked nanoparticles has been developed to produce an innovative class of biomaterials able to combine the properties of cellular membranes with the engineering liveness of synthetic nanomaterials producing smart, biocompatible and biomimetic nanocarriers. This new class of cell membrane-camouflaged nanomaterials display numerous advantages such as high biocompatibility and prolonged blood circulation. Recently, we developed ultra-stable O/W NEs, able to carry both internal and external cargos (Somes) such as lipophilic compounds and hydrophilic coatings, respectively, that we call here NEsoSomes. O/W NEs are an excellent bioengineering tool for drug and molecules delivery due to their ability to dissolve a large number of hydrophobic compounds and protect them from hydrolysis and degradation under biological conditions. At present, no report is available on the combination of cell membrane coatings with such nanocarriers, probably due to their typical instability feature. Since that, we report for the first time a new cell membrane coated nanomaterial composed by membranes extracted from different cell lines including glioblastoma cancer cells (U87-MG) and THP-1 monocyte cell line deposited on NEsoSomes through a liquid–liquid interface method to produce highly controllable membrane coated nano-capsules. At first, we developed a biomimetic cancer cell based on secondary NEs (SNEs), named CM-NEsoSome, using as cell membrane source U87 glioblastoma cells as a suitable theranostic system to target cancer cells. CM-NEsoSomes were physicochemically characterized and *in vitro* validated. In detail, CM-NEsoSome biocompatibility was tested on a healthy model cell line, performing a cell cytotoxicity and uptake assay. The promising results of CM-NEsoSome led to the idea of building cell membrane coated nanoemulsions able to target inflamed tissue and more specifically atherosclerotic site. To target atherosclerotic lesions, we selected THP-1 as human monocyte cell line to obtain both human monocyte and macrophage membranes. THP-1 cells could be differentiated into macrophage-like phenotype cells (THP-1 macrophages, M0) by incubation with phorbol 12-myristate-13-acetate (PMA). Therefore, THP-1 were differentiated into macrophages to express cell membrane

markers and exploit macrophage active targeting into atherosclerotic lesions. We developed two cell membrane coated NEsoSomes using THP-1(M) and PMA-differentiated THP-1(M0) as membrane sources of monocyte and an unpolarized macrophage membranes, respectively. The two systems, indicated as Monocyte NEsoSome (M-NEsoSome) and Macrophage NEsoSome (M0-NEsoSome), joined together the biomimetic features coming from biological membrane with the physio-chemical and nano-sized characteristic of SNE. The uptake ability of two systems were evaluated both in a healthy endothelial cell (EC) layer (represent by Human Umbilical Vein Endothelial Cells, HUVECs) and in a model of inflamed ECs obtained by treating HUVEC cell layer with Tumour Necrosis Factor α (TNF α). Interestingly, M0-NEsoSome demonstrated a pronounced accumulation in the inflamed ECs model as compared to the healthy cell layer demonstrating the selective targeting of this innovative type of nano-vector. Finally, a food grade oral drug delivery system has been proposed to provide a formulation with enhanced mucus-adhesion to the intestinal barrier. In this case, the nanocarrier is based on a secondary O/W NE prepared by adding thiol groups to chitosan (Ct) via a simple non-covalent procedure based on N-acetylcysteine (NAC) salification, which is compliant with food supplement formulations. Pharma grade and food grade formulations, in different materials combinations, were prepared and physio-chemically characterized (DLS, ¹H-NMR, ITC, Cryo-TEM) showing similar behaviour. These systems were validated both in terms of bioaccessibility and mucus-adhesive properties employing respectively INFOGEST protocol and intestine on chip device (InOA-chip), which are able to mimic the complex intestinal functions. INFOGEST confirmed the improved bioaccessibility of encapsulated curcumin into our nano-system compared to the free molecule. Very interestingly, a significant enhancement in the mucus-adhesive properties of the proposed novel Ct-NAC NEs (due to the presence of thiol groups) was observed by comparing the two formulations behaviour through the InOA-chip.

In conclusion, O/W SNEs demonstrate to be a suitable starting building block for a different type of oil based nanocarrier with biomimetic properties and selective accumulation in a precise compartment depending on the most external layer characteristics.

Chapter 1: Introduction

1. Drug delivery system lipid base nano carriers

Nowadays the delivery and absorption of small molecules as well as of food supplements is a crucial aspect for the formulators. A plethora of drug delivery systems, from microparticles to nanoparticles (NPs), are widely used to protect the encapsulated sensitive molecules from being degraded in the physiological environments. Nanotechnology offers the opportunity to create nano-vehicles that can carry either single or multiple therapeutic cargos, as well as contrast agents, to tumours for improved treatment and imaging¹. Nanotechnology is defined by *European Medicines Agency (EMA)* as the production and application of structures, devices, and systems by controlling the shape and size of materials at nanometre scale (the nanometre scale ranges from the atomic level at around 0.2 nm (2 Å) up to around 100 nm) in agreement with the International Organization for Standardization (ISO)/Technical Committee (TC) 229 for nanotechnologies (ISO/TC 229)¹. Nanomedicines, resulting from the application of nanotechnology to medicine, are having an increasing impact on the treatment of several disease¹. Nanoscale drug delivery systems (NDDS) are well-known strategies used to improve the efficacy and safety of drug therapies and diagnostics^{2,3}. NDDS have numerous advantages such as cargo stability, specific delivery, high intracellular uptake, high surface-to-volume ratio, as well as the ability to enhance bioavailability^{1,2}.

For EMA, nanoparticles (NPs) are particles with a mean particles size between 1 and 1000 nm consisting in a pure active pharmaceutical ingredient (API), while British Standards Institution defined NPs as 3D nano-objects with 3 external dimensions with the nano range between 1 and 1000 nm¹.

Decades of research and development efforts produced a multitude of NDDS such as polymeric NPs, lipidic NPs [liposomes, micelles, solid lipid NPs (SLNs), nanostructured lipid carriers (NLCs), Nanoemulsions(NEs), Phytosomes], cyclodextrins, dendrimers, chitosan-based NPs, exosomes nanocomposites, and inorganic nanomaterials [i.e., graphene, iron oxides ($\text{Fe}_2\text{O}_3/\text{Fe}_3\text{O}_4$), gold (Au), silver (Ag), and mesoporous silica]⁴. Nevertheless, the majority of clinically approved NDDS involves polymeric or lipid based nanocarriers. The success of these particles in the clinic is linked to important parameters as robust and scalable fabrication strategies, physiochemical properties (a size range of 100 nm and a low surface charge), highly efficient encapsulation techniques, drug release potential, adequate product stability and, most importantly, minimum toxicity of the carrier itself⁴.

Different forms of lipid NPs (LNPs) have been proposed including liposomes, SLNPs, NLCs, microemulsions, NEs, phytosomes, lipid coated NPs (LCNs), and nano-assemblies with different advantages and limitations, which are reviewed in **Table 1**^{5,6}.

Table 1. Advantages and limitations of LPN.

Lipidic NPs	Advantages	Limitations
Liposomes	Biocompatible. Biodegradable. Non-immunogenic. Low toxicity.	High production cost. Drug leakage. Short half-life. Possible oxidation and hydrolysis of the used phospholipid.
Solid Lipid NPs (SLNs)	Biocompatible. Green synthesis. Reproducible and scalable manufacturing process. Release the drug in a modified released manner.	Low encapsulation efficiency due to perfect crystalline structure. High drug expulsion.
Nanostructured Lipid Carriers (NLCs)	Low drug expulsion. Improved physical stability. Prolonged release of the drug. Simple scaling up and preparation. High encapsulation efficiency. Increased aqueous medium dispersibility. Significant hydrophilic and lipophilic drug entrapment. Close contact with the stratum corneum, facilitating medication penetration into the skin or mucosa.	Possible cytotoxic effect depending on the matrix structure. Irritating action of some surfactants
Nanoemulsions (NEs)	Self-assembly. High penetration through the biological membranes. High absorption rate. Easily scale-up.	High concentrations of surfactants. Possible phase separation.
Phytosomes	Enhanced absorption. Low toxicity.	Phytochemical leaching. Low drug concentration.
Lipid Coated NPs (LCN)	Biocompatibility. Structural stability. Easily conjugation with targeting moieties.	Multi-step fabrication process Difficult scale-up
Nanoassemblies	Fast synthesis. Simple dispersibility. Low production cost.	Complicated particle size control Difficult scale-up. Low shelf-life stability.

Ethosomes	<p>Enhanced drug delivery from the vesicle into the deeper layers of the skin.</p> <p>Increased stability of the drug in the vesicle, thus allowing for a longer shelf-life.</p> <p>Improved safety profile due to the natural ingredients used in the formulation.</p> <p>Improved bioavailability due to the increased residence time of the drug in the vesicle.</p>	<p>Limited permeability of the vesicle.</p> <p>Sensitive to pH and temperature changes.</p> <p>Difficult to scale up in industrial production.</p> <p>The preparation and storage of the vesicles may require special equipment.</p>
-----------	---	--

LNPs have been used in a variety of biomedical applications, such as drug delivery, gene therapy, and imaging, such as fluorescence imaging and magnetic resonance imaging, to visualize and monitor the progress of a disease. LNPs possess enormous potential in treating diseases due to the ability to enhance the encapsulated drugs bioavailability and permeability, as well as improve the payload stability^{6,7}. LNPs improve the drug pharmacokinetics for insoluble API with low stability and low bioavailability as poorly water-soluble drugs which can be easily included in oil in water nanoemulsions and lipid solid NPs or liposomes⁵. LNPs have been used to improve the delivery and efficacy of various drugs, such as chemotherapeutic agents, anticancer drugs, and antiviral drugs. Furthermore, LNPs have been shown to be effective in delivering genetic materials, such as plasmids and short interfering RNA (siRNA), which can be used to modulate gene expression and treat genetic diseases^{4,8-10}. Nowadays, there are more than ten Food and Drug Administration (FDA) and EMA approved formulations based on employing LNPs to deliver drugs to disease sites. In **Table 2**, it is reported a list of marketed and FDA approved LNPs including liposome DOXIL®, the first FDA LNP approved in 1995 that is able to reduce the toxicity of doxorubicin. More recently, LNPs have come into the spotlight as an integral part of the development of mRNA vaccines and therapies against COVID-19^{11,12}.

Table 2. LPN approved and marketed formulations.

Name	Encapsulated drug	Indication	Company
-------------	--------------------------	-------------------	----------------

<i>AmBisome®</i>	Amphotericin B	Fungal infections Leishmaniasis	Gilead science
<i>Doxil®</i>	Doxorubicin	Kaposi's sarcoma Ovarian cancer Breast Cancer	Johnson & Johnson
<i>Caelyx®</i>	Doxorubicin	Kaposi's sarcoma Ovarian cancer Breast Cancer	Piscataway
<i>DaunoXome®</i>	Daunorubicin	Kaposi's sarcoma	Galen science
<i>Myocet®</i>	Doxorubicin	Breast cancer	Cephalon
<i>Abelcet®</i>	Amphotericin B	Aspergillosis	Enzon Pharmaceutical
<i>Amphotec®</i>	Amphotericin B	Invasive aspergillosis	Intermune
<i>Visudyne®</i>	Verteporfin	Wet macular degeneration	QLT
<i>Marqibo®</i>	Vincristine	Acute lymphoblastic leukemia	Spectrum Pharma
<i>Onyvide®</i>	Irinotecan	Metastatic pancreatic cancer	Ipsen Biopharma
<i>Vyxeos®</i>	Daunorubicin, Cytarabine	Acute lymphocytic leukemia	Jazz Pharma
<i>Onpattro®</i>	siRNA targeting transthyretin	Transthyretin induced amyloidosis (hATTR)	Anylam Pharmaceuticals
<i>L-Annamycin®</i>	Annamycin	Acute lymphocytic leukemia	Callisto Pharmaceuticals
<i>Mepact®</i>	Mifamurtide	Non-metastatic osteosarcoma	IDM Pharma
<i>DepoDur®</i>	Morphine sulphate	Analgesia (post- operative)	Pacira Pharmaceuticals
<i>DepoCyt®</i>	Cytarabine	Lymphomatous meningitis	Sigma-Tau

Comirnaty®	mRNA BNT162b2 vaccine	Active immunisation to prevent COVID-19 caused by SARS-CoV-2	BioNTech/Pfizer
Spikevax®	mRNA -1273 vaccine	Active immunisation to prevent COVID-19 caused by SARS-CoV-2	Moderna
Curosurf®/Poractant alpha®	Proteins SP-B and SP-C	Pulmonary surfactant for Respiratory Distress	Chiesei farmaceutici
Visudyne®	Verteporfin	Macular degeneration, wet age-related; myopia; ocular histoplasmosis	Bausch and Lomb
Estrasorb™	Micellar Estradiol	Menopausal therapy	Novavax

Some features of the most studied nanocarriers including NEs, SLNs, NLCs, phytosomes, liposomes are described below.

Liposomes. Liposomes are self-assembling colloidal vesicles obtained from cholesterol and natural or synthetic phospholipids^{6,13}. Liposomes are sphere-shaped particles with a size range of 10 nm to a few micrometres in which a lipid bilayer encapsulates a fraction of the surrounding aqueous medium while the fatty acid layer helps in the solubilization of hydrophobic agents. Liposomes can be prepared with several methods, such as thin film hydration, ethanol injection method¹⁴. Their properties are strictly related to their dimensions, composition (different phospholipids and cholesterol contents), charge (resulting from the charges of the composing phospholipids), and structure. According to the number of lipid bilayers contained, liposomes are classified into *unilamellar vesicles* (ULV), separated by aqueous compartments and consisting of only one phospholipid bilayer surrounding one aqueous compartment, *multilamellar vesicles* (MLV), consisting of several concentric bilayers, and *multivesicular vesicles* (MVV)^{15,16}. The liposome can be classified into anionic, cationic and neutral liposomes, based on the charge of the external phospholipids¹⁶. Usually, negatively charged liposomes have lower capacity to deliver gene drugs, while positively charged liposomes have less cytotoxicity. Doxil®, the first FDA-approved liposome-based formulation, was introduced in 1995 for the treatment of Kaposi's sarcoma, ovarian cancer, and breast cancer. Excitingly, liposomal formulations have been demonstrated to reduce cardiac risk factors associated with the administration of conventional chemotherapeutic doxorubicin in cancer patients⁴.

Solid Lipid Nanoparticles (SLNs). SLNs have been developed in the 1990s and they are the first generation of lipid colloidal systems in which the lipid phase is a solid matrix and surrounded and stabilized with a surfactant¹⁷⁻¹⁹. The API is dissolved or dispersed in the stable lipid matrix²⁰. SLNs can be obtained with different methods including high pressure homogenization (cold and hot homogenization), breaking of O/W microemulsion, solvent emulsification-evaporation or solvent emulsification–diffusion, solvent injection, preparation via water-in-oil-in-water double emulsion (W/O/W), high shear homogenization and/or ultrasound dispersion and preparation by using membrane contactor^{17,21}. They have strong *in vivo* tolerability and excellent biodegradability because they are mostly composed of physiologically acceptable and biodegradable components¹⁸. SLNs have been proposed as a means to improve the solubility and bioavailability of both hydrophilic and lipophilic drugs including small drug molecules, large biomacromolecules (polysaccharides, etc.), genetic material (DNA/RNA), vaccine antigens, antineoplastic, antimicrobial¹⁸. However, the crystalline structure of solid lipids at room temperature restricts their use as carriers. Their bulk structure is like a "*symmetric brick wall*", with only a few spaces for molecules, resulting in low drug loading efficacy. Moreover, the lipids rearrange the crystalline structure to become more stable and form gelation in the dispersed phase, causing drug leakage from the carriers and particles to aggregate over time²². Patents have been filed for different therapeutic applications of SNL, like oral, topical, parenteral, and cosmetic treatments. Additionally, the use of ligand-anchored surface-modified SLNs for the targeted delivery of anticancer drugs has also been patented²³.

Nanostructured Lipid Carriers (NLCs). NLCs are considered as a second generation SLNs since they were developed to overcome some of the drawbacks linked with SLNs such as drug expulsion over time by fabricating a less organized solid lipid phase^{19,22,24}. NLCs are a colloidal lipid particle stabilized by the adsorption of emulsifier molecules on the surface and dispersed in an aqueous phase. Compared to SLNs, NLCs have a less organized solid lipid phase. This phase is composed of a blend of solid lipids (fats) and liquid lipids (oils) in a weight ratio between 70:30 and 99.9:0.1, giving to the particles a more unstructured internal matrix. The presence of liquid lipids lowers the melting point of NLCs compared to SLNs, so the particles remain solid at body temperature. NLCs are stabilized with surfactants, usually in a 0.25-6% w/w concentration¹⁹. The benefits of SLNs, such as low toxicity, biodegradability, drug protection, gradual release, and avoidance of organic solvents in manufacturing, are also present in NLCs¹⁹. As a result, NLCs can be used to effectively deliver drugs to targeted areas, offering improved permeability, bioavailability, and fewer side effects than conventional drug carriers^{22,24}.

Phytosomes. Phytosomes are known to enhance absorption of active compounds across the intestinal wall. Phytosomes are designed to improve the bioavailability of phytochemicals, increasing their absorption and utilization in the body. They are a form of lipid NPs, which are very small particles made up of a lipid material and an active compound. Phytosomes are phyto-phospholipid complexes formed when a stoichiometric amount of phosphatidylcholine reacts with polyphenolic components or standardised extracts such as flavonoids, tannins, terpenoids, and xanthenes in a non-polar solvent. Common solvents used to create these complexes include aromatic hydrocarbons, methylene chloride, halogen derivatives, cyclic ethers, and ethyl acetate, but protic solvents like ethanol are often preferred due to their higher yield and lack of residues. Typically, phytosomes interact with solvents with a reduced dielectric constant. However, mixed solvent systems consisting of ethanol and dichloromethane, water and diethyl ether, and dichloromethane and methanol have also been used in some studies. There have been over 100 studies examining the various biological effects of phytosomes, which have been divided by body system (cardiovascular, central, and peripheral neurological, gastrointestinal, genitourinary, immunological, integumentary, musculoskeletal, and respiratory).

Ethosomes. Ethosomes are phospholipid nanovesicles utilised to transfer chemicals to the skin and through the skin²⁵. Ethosomes are lipid NPs that are composed of a mixture of phospholipids, such as phosphatidylcholine, and surfactants. These particles are characterized by their ability to penetrate the skin and enhance the delivery of active ingredients. An example of such technology is the incorporation of ethosomes into a topical cream, which can be used to deliver an active ingredient deep into the skin²⁶. Ethanol, a powerful permeation enhancer, is believed to act by disrupting the intercellular spaces of the stratum corneum. These soft, flexible vesicles range in size from tens of nanometres to microns, allowing for the alteration and optimization of skin absorption^{25,27}.

Nanoemulsions (NEs). NEs are an emulsion system with droplet size in the nanometre scale, wherein oil or water droplets are finely dispersed in the opposite phase with the help of a suitable surfactant for stabilization. These droplets usually range from 0.1 to 500 nm in size, and may vary depending on the drug particles, mechanical energy, composition, and relative amount of the surfactants. NEs are also known as miniemulsions, fine-dispersed emulsions, or submicron emulsions, which may either be O/W (oil in water) or W/O (water in oil) emulsions. O/W NEs usually contain 5-20% w/w of oil, and sometimes a mixture of oils may be used to improve drug solubilization in the oil phase. Co-surfactants and co-solvents may also be used to facilitate the stabilization process. NEs differ from other emulsion systems in that they show different physical and rheological properties as droplet size decreases. The main advantages of NEs are their stability and ability to penetrate biological barriers, due to their very fine particle size and low surface tension between the oil and water molecules. This makes NEs much more stable than other emulsion systems, and thus more translucent. Furthermore, NEs can be used to facilitate the absorption of drug molecules from the gastrointestinal tract (GIT) or to cross the skin barrier. NEs can also be used as a precise drug carrier to deliver drugs to targeted areas. NEs for oral administration have been proposed as an excellent option for improving the solubility of lipophilic medicaments and increasing their bioavailability. This approach is particularly favoured for *Class 2 & 4* (Biopharmaceutics Classification System, BCS) drugs which are characterized by high permeability and low solubility (*Class 2*) and low permeability, low solubility (*Class 4*). The NEs used in this route are made up of food grade oils and generally recognized as safe (GRAS) excipients, making them safe and edible for oral drug delivery. However, NEs although more stable than emulsions due to their small droplet size they still are typically thermodynamically unstable, but the deposition of a polymeric layer can be used to improve their stability. Recently, a successful strategy to improve the stability of completely nature-based O/W NEs was implemented by optimizing process and composition. This enabled the successful encapsulation of lipophilic substances, such as Curcumin²⁸ (CUR), Co-Enzyme-Q10^{29,30} (Co-Q10) and Lycopene³¹. Furthermore, their stability allowed for the implementation of different functionalization strategies, such as layering, to improve their stability in the biological environment and modify/add new properties to the formulations. These include active targeting, cell membrane bilayer penetration and antifouling through biomimetic coatings of polyethylene glycol (PEG)³² or cell membrane (CM) coating³³. Layer-by-layer (LbL) approaches can be used to create a stable coating on the surface of the nanoemulsion droplets. This method involves the

sequential deposition of polymeric layers of opposite charge, which interact electrostatically and create a stable coating on the nanoemulsion droplets. This coating can help to protect the droplets from destabilizing factors and increase the overall stability of the nanoemulsion. Additionally, the layers form a stable structure that can encapsulate active ingredients and protect them from external influences. By controlling the size and number of layers, the properties of the nanoemulsion can be tailored to fit a specific application, making them an attractive option for use in drug delivery, cosmetics, and food formulations.

Lipid coated NPs (LCNs). LCNs are tiny particles composed of a core material including metal, silica, polymeric or a combination of both, that is surrounded by a lipid bilayer³⁴. These NPs have attracted a lot of attention due to their potential applications in drug delivery, diagnosis and imaging³⁵. They have an advantage over other drug delivery systems because thanks to the bilayer nature of the lipid coating, they are able to fuse with the lipid bilayer of the cell membrane and allow cell membrane crossing. Additionally, this lipid bilayer confers a biomimetic nature to the helping them to stay in the body for a longer period of time, thus, allowing for the controlled release of drug³⁵. Previous techniques for the synthesis of LCNPs involved a two-step process which necessitated the formation of a lipid shell and a polymeric core, followed by the fusion of the two layers. However, the more preferred approach in recent times is the single-step approach, which offers enhanced convenience and simplicity during the preparation of LCNPs³⁴.

2. Nanotechnologies in medical field: from passive to active targeting

NPs can be “*smart designed*” with enhanced drug delivery, phototherapy, vaccination, immunotherapy, and imaging. In particular, NDDS take benefits from enhanced permeability and retention (EPR) effect, typical of many solid tumours, which show a leaky vasculature and absent or lessened lymphatic drainage⁸. EPR effect allows the accumulation of high molecular weight molecules as well as small particles of diameter ~20–500 nm within the tumour tissue through passive targeting mechanism^{36,37}. However, the new findings raise questions about the real efficacy of EPR due to complicated tumour microenvironment (TME), the EPR effect with many well-designed nanocarriers failed in clinical application^{36,38}. Far from the initial prospects, only 50 nanoformulations have been approved for marketing and the translational rate from preclinical study to clinical use is no more than the 6%³⁹. These statistic data have re-examined the role in

tumour-targeting of the EPR effect. In detail the EPR effect has some limitations as a targeting strategy, including:

- Not all tumors have the same level of EPR, so the effectiveness of the targeting may vary.
- The EPR effect also occurs in other diseased tissues, such as inflammation, which can lead to non-specific delivery of the NPs^{40,41}.
- EPR-dependent drug delivery is obstacle by high tumor interstitial fluid pressure (IFP), irregular vascular distribution, and poor blood flow inside tumors^{40,42,43}.
- The NPs may be cleared from the body quickly by the reticuloendothelial system (RES) which limits the residence time of the particles in the targeted site^{36,44}.

The size value of the NPs also plays an important role in the EPR effect. NPs which are too small may not be able to extravasate while NPs that are too large may not be able to enter the tumour vasculature⁴⁰. The EPR effect is also limited by the fact that it only works in the tumour vasculature and not in the tumour interstitial space⁴⁴. Most of the researchers are currently focused on improving and overcoming the clinical limitations of EPR effects by TME^{43,45}, as well as developing alternative tumour targeting mechanisms as active mechanisms. To enhance EPR effects, both physical stimuli, such as radiation or heat, and pharmacological approaches have been proposed³⁷. Pharmacological approach may involve the management of a drug to modify the TME or nanocarrier physiochemical characteristics to improve permeability in tumour tissues⁴². Since all anticancer nanocarriers take advantage from EPR effects, it is recommended to combine both passive and active targeting strategies in the design and development of nanomedicines to facilitate EPR-based tumour accumulation for better therapeutic efficacy and reduced adverse effects. Active targeting is a well-established strategy for the direct transport of drug in the selected action site. This strategy is a complex mechanism which involves the molecular recognition between the ligand which decors the nanocarrier surface and an overexpressed receptor on the selected tissue allowing the receptor mediated endocytosis and higher drug uptake. This mechanism exploits the altered gene and protein expression profile of malignant cells by targeting the specific molecular components overexpressed in tumours. This includes targeting G-protein-coupled receptors, growth factor receptors, interleukins, transferrin, and polysaccharide moieties. By doing so, it is possible to develop treatments that specifically target and inhibit tumour growth and metastasis. This mechanism is due to higher understating of disease progression and molecular targets^{5,45}.

An active targeting could be obtained by surface functionalization of NDDS with antibodies, proteins, small molecules, aptamers and ligand-mimicking peptides that allows the penetration of a specific biological compartment⁴⁵⁻⁵⁰. This approach enhances the drug delivery and minimizes side effects by increasing the drug localization in the desired compartment, potentially improving treatment efficacy. A plain nanoparticle, when reaching the bloodstream, is destined for Kupffer cells in the liver, leading to unintended uptake by these cells⁴⁶. By decorating the same nanoparticle with specific ligands, it can be directed to the intended cells, minimizing involuntary uptake by normal cells. Additionally, active targeting can bypass the P-glycoprotein (P-GP) drug efflux mechanism⁴⁶. Different strategies have been proposed for target tumour tissue the most successful included:

- *angiogenesis-associated targeting*: vascular endothelial growth factor receptor, $\alpha_v\beta_3$ integrin, vascular cell adhesion molecule, matrix metalloproteinases⁵¹
- *uncontrolled cell proliferation targeting*: folate receptors, transferrin receptors, human epidermal receptor⁵¹
- *specific tumor cell targeting*: breast cancer HER-2 receptor, luteinizing hormone releasing hormone (LHRH) , prostate specific membrane antigen (PSMA)⁵¹.

As well as, active targeting can be used to improve the delivery of chemotherapy drugs and the effectiveness of gene therapies for other diseases such as heart disease, diabetes, inflammation, and neurological disorders. However, one of its most impressive uses is for neurological disease, as nanocarriers are modified with ligands that interact with the blood brain barrier (BBB) to be taken up and transported across the brain endothelium. This is achieved through receptor-mediated transcytosis, transporter-mediated transcytosis, and other physiological mechanisms.

However, the presence of targeting moieties can make NPs vulnerable to the cleaning action of the RES due to their hydrophobicity and immunogenicity, they can also accidentally trigger a local immune response when they reach the blood vessels and organs⁵². For example, positively charged peptide targeting ligands often induce nonspecific adsorption with negatively charged endogenous proteins, leading to a universal recognition of negative cell membranes and impairing the targeting ability and circulation stability of the NPs. Additionally, some receptors can be expressed on the normal cell surface, resulting in non-specific binding during the circulation

process. This may lead to unfavourable side effects, making it important to achieve controlled shielding of targeted ligands in the blood circulation⁵²⁻⁵⁴.

The next frontiers of active targeting strategy are represented by cell membrane derived nanocarriers, which not only are biomimetic presenting a very high antifouling behaviour, but they can also claim, thanks to the presence of cell membrane protein, a so-called “**homing effect**”. Cell homing is the process by which specific cell types, including stem cells, progenitors, and mature, specialized T cells, move towards a point of destination, such as a tissue in distress or a niche environment that can promote their self-renewal. The cell homing effect occurs when certain cell types are injected into the bloodstream of a mouse, they are drawn to certain organs and tissues. This phenomenon, known as **homing**, became the basis for further studies in cell migration. Cell homing effect has been increasingly studied in the context of stem cell transplantation, with the goal of achieving remission of neurodegenerative diseases.

By learning the lesson from nature, the cell homing effect was studied and for the development of active targeted nanocarrier. Following this discovery, cell-homing peptides have been used to direct the delivery of nanocarriers to specific types of cells with enhanced efficiency⁴⁹. The cell-homing effect of nanocarriers has been used for various applications, such as targeted drug delivery and gene therapy. NPs can be coated or prepared with native extract and components of cell membranes to achieve homotypic targeting, which is beneficial in terms of self-recognition with cancer cells. Additionally, this approach increases the immune tolerance and nanomaterial stability in biological fluids, such as the blood, making it an effective tool for both targeting and delivery purposes. These nanocarriers are specifically designed to interact with specific cell surface receptors, allowing them to be actively guided to their target cells. This strategy offers a more precise delivery of drugs, thereby improving the efficacy and reducing the toxicity of therapeutic agents. These nanocarriers are typically composed of a lipid bilayer, which can contain lipids, proteins, peptides, and other molecules, allowing them to interact with various cell surface receptors⁵⁵. These receptors may be specific to certain types of cells, allowing the nanocarriers to be actively guided to specific types of cell. Specifically, the homotypic aggregation is basically due to self-adherence of cancer cells thanks to the presence of the adhesion molecules such as Thomsen–Friedenreich antigens and E-cadherin⁵⁶. Therefore, the adherence between cancer cells provides a new opportunity for cancer cell membrane-derived NPs to actively target tumours and track and capture cancer cells in the blood. NPs coated with the

membrane of 4T1 breast cancer cells have been found to retain some adhesion molecules such as Thomsen–Friedenreich antigen, E-cadherin, Cluster of differentiation 44 (CD44), and Epithelial cell adhesion molecule expression (CD326) and facilitate the delivery of paclitaxel to primary as well as metastatic tumours. However, it is important to take into account the diversity of cancer cells for achieving desired homotypic targeting⁵⁶.

Platelet membrane derived NPs can target and accumulate in tumour tissue due to the presence of P-selectin which can bind to CD44 molecules expressed on the surface of tumour cells⁵⁵⁻⁵⁷. The ability to target relies on a specific molecule called lymphocyte function-associated antigen 1 (LFA-1), this molecule is found on lymphocytes and can bind to a molecule called intercellular adhesion molecule 1 (ICAM-1) on inflamed cells. Additionally, macrophages and monocytes have a specific protein on their surface that can be recruited to the tumour site by C-C Motif Chemokine Ligand 2 (CCL2). Neutrophils use a combination of binding interactions, including CD44 with L-selectin, LFA-1 with ICAM-1, and β 1 integrin with vascular cellular adhesion molecule 1 (VCAM-1), to target circulating tumour cells. The ability to target relies on a specific molecule called LFA-1, which is found on lymphocytes and can bind to a molecule called ICAM-1 on inflamed cells. Additionally, macrophages and monocytes have a specific protein on their surface that can be recruited to the tumour site by CCL2. Neutrophils use a combination of binding interactions, including CD44 with L-selectin, LFA-1 with ICAM-1, and β 1 integrin with VCAM-1, to target circulating tumour cells⁵⁶.

Cell membrane coated nanomaterials can also be employed to target inflamed tissue or bacteria to treat other diseases. In detail, platelets and lymphocytes have been investigated to target inflamed tissues and bacteria. Platelets and leukocytes play a crucial role in the healing process by traveling to areas of injury and inflammation to stop bleeding and aid in the formation of extracellular matrices. As a result, these cells are commonly used as a natural coating for NPs. Leukocyte-coated NPs have been found to be able to cross the endothelium, and porous silica NPs have been shown to have this ability as well due to the retention of specific proteins such as cluster of differentiation 45 (CD45), T-cell receptor T3 zeta chain (CD3z) and LFA-1. This opens the potential for trans-endothelium drug delivery. Platelets, on the other hand, have been found to bind to collagen in the sub-endothelium which is exposed when the upper endothelium layer is damaged. This property has been used in the treatment of coronary restenosis, which is a condition where the intima overgrows in response to injury, narrowing the artery and restricting

blood flow. The retention of glycoprotein IV allows platelet-coated NPs (PNPs) to also bind to exposed collagen such as that found in a damaged artery which is susceptible to coronary restenosis. When loaded with the drug docetaxel, PNPs have been shown to bind to exposed collagen in denuded rat arteries and almost completely prevent the overgrowth of the intima⁵⁶.

PNPs have been developed to target opportunistic antibiotic-resistant bacteria methicillin-resistant *Staphylococcus aureus* (MRSA), as they exploit platelets to shield themselves from the immune system and localize to certain vulnerable tissues^{57,58}. Binding between platelets and bacteria is varied and complex, occurring through either direct adhesion via bacterial surface proteins or involving plasma bridging molecules. *Hu et al.* fabricated PNPs capable of multiple biological interactions, and they have demonstrated that coating vancomycin-loaded PNPs can improve binding to MRSA 12-fold compared to bare NPs. This efficient binding greatly improves bacteria killing efficacy, decreasing overall bacterial load in the organs of mice better than free vancomycin at just one-sixth the clinical dose in a systemic MRSA challenge mouse model^{56,58}.

In conclusion, the use of cell membrane coating as active targeting strategy has the potential to revolutionize the delivery of therapeutic agents, allowing for more precise, efficient, and safer treatments.

3. Biomimetic nanocarrier

In the last decade, researchers have been focusing on improving tissue specificity by proposing increasingly complex formulations based on mechanics dependent on pH, temperature, redox reactions, or enzyme-responsive materials. Moreover, to reduce non-self recognition by the immune system, new synthetic and natural biomimetic materials have been introduced as surface components. In detail, NCs may be rapidly adsorbed by biological molecules such as plasma proteins, antibodies, and complement components, which leads to opsonization and rapid removal by the Mononuclear Phagocyte System (MPS). Composed of dendritic cells, monocytes, and macrophages, the MPS is part of the innate immune system that phagocytoses foreign substances, particles, or pathogens, including NPs. This process is especially important in fenestrated vessels of the liver via Kupffer cells and in the spleen by splenic macrophages, limiting the circulation time of conventional NCs. To solve this issue, various strategies have been implemented to cover the surfaces of NCs with different molecules to obtain

biomimetic NCs. Biomimetic nanocarriers are nanomaterials that mimic the natural structures and functions of biological molecules and systems. They are designed to interact with biological systems in a way that mimics natural processes, such as the uptake of drugs by cells. These nanocarriers can be used to deliver drugs, genes, and other therapeutic agents to specific cells or tissues in the body. They can also be used to target and deliver drugs to specific sites in the body, such as tumours. These efforts have led to the development of the current generation of nanocarriers, which range from polymer-coated materials to biohybrid systems. Coated NCs with polymers, particularly PEG, has become the most popular approach since the early 1990s. Indeed, PEGylated NCs have shown to significantly extend the circulation time, resulting in increased tumour accumulation. Despite the promising results to date, there are important issues related to the use of PEG that are increasingly relevant. Common biomimetic strategies to improve the effectiveness of nanocarriers include camouflaging them with cell membranes, viruses, and vegetation, or delivering them with immune cells or extracellular vesicles. Among these, cell membrane coated materials are being more and more used as valid substitute to PEGylation for the development of delivery systems.

Polymer and polysaccharides

Polymeric/ polysaccharides coated nanocarriers represent the first type of stealth. It is well established that stealth systems can be obtained by surface coating with hydrophilic polymers that prevent/reduce the opsonization process⁵⁹. Moreover, stealth nanocarriers have been found to display long circulation profiles even after extensive opsonization⁵⁹. The main features of polymers used to confer stealth properties to NPs and nanovesicles are high flexibility and hydrophilicity. Both natural and semisynthetic polysaccharides and polymers have been employed for these purposes. The most employed natural polysaccharides are dextran (Dex), polysialic acid (PSA), hyaluronic acid (HA), chitosan (Ct), and heparin. Synthetic polymers include polyvinyl pyrrolidone (PVP), polyvinyl alcohol (PVA), polyacrylamide (Pam), PEG, and PEG-based copolymers such as poloxamers, poloxamines, and polysorbates⁵⁹. One of the first biomimetic nanomaterials employed for the development of nanocarriers was the PEG.

PEG is a FDA-approved biocompatible hydrophilic polymer and PEGylation is a process in which PEG is attached to the surface of NPs⁶⁰. This process confers stealth properties to the NPs, as the PEG forms a hydrophilic steric wall that prevents opsonization and recognition by the RES. As a result, PEGylated NPs have a longer circulation time in the bloodstream. PEGylation

is an FDA-approved biocompatible process, making it a safe and effective method for improving the pharmacokinetics of NPs^{60,61}. Additionally, the distal end of surface projected PEG chains of PEGylated NPs can be modified to promote active targeting on intravenous injection. This can be done by attaching targeting molecules such as antibodies, peptides, or small molecules to the distal end of the PEG chains⁶². These targeting molecules can bind to specific receptors on the surface of cells, allowing the PEG chains to be actively targeted to the desired cells. Additionally, the distal end of the PEG chains can be modified with polymers or other molecules to increase the hydrophilicity of the PEG chains, which can help them to be more easily taken up by cells^{52,62}. The functionalized PEG layers were used for instance to modify the surface of metal and semiconductor NPs, allowing them to be used in a variety of biological assays. These functionalized NPs can be used to detect and quantify various biological molecules, such as proteins, DNA, and enzymes. They can also be used to detect and quantify small molecules, such as hormones and drugs. Furthermore, these functionalized NPs can be used to image and monitor biological processes, such as cell signalling pathways and gene expression⁶⁰.

A typical example of FDA regulatory-approved and marketed PEGylated formulation is the doxorubicin loaded liposome Doxil®, known as Caelyx® in Europe, which is now used in treatment/management of different tumours⁶⁰. Doxil® success story is due to several characteristics^{52,59-61}:

- Doxil® utilizes PEGylated nano-liposomes which have a prolonged circulation time and avoid the RES, allowing for a larger dose of drug to reach its target.
- Doxil® transmembrane ammonium sulphate gradient allows for high and stable remote loading of doxorubicin as well as its release at the tumor.
- Doxil® liposome lipid bilayer is in a “liquid ordered” phase composed of high melting Temperature (T_m) (53 °C) phosphatidylcholine and cholesterol, which allows for its passive targeting to tumours.

The EPR effect allows for doxorubicin to be released from the liposome and available to the tumour cells. On the other hand, the success of PEGylation also addressed the "PEG safety dilemma". It is proved that the immune system can produce antibodies that recognize PEG chains⁶³: animal studies have revealed that anti-PEG immunity is mainly an Immunoglobulin M (IgM) response mediated by a type-2 T-cell independent pathway⁶³. This response is mediated

by B-cells and typically results in the production of antibodies that target the PEG molecules specifically. The antibodies produced in this immune response can have a range of effects, including inhibition of the therapeutic effects of the PEG-based drug⁶³. The risk of anti-PEG immunity should be considered before using PEG-based drugs in clinical settings.

To assess the effect of accelerated blood clearance (ABC) phenomenon, a study was conducted to compare the performance of NPs carrying a cleavable methoxy-PEG-lipid conjugate with a carbonate linkage and a non-cleavable methoxy-PEG-lipid with a carbamate linkage, in which the PEG molecular weights were varied between 350 Da and 5000 Da. The results of the experiment revealed that raising the molecular weight of cleavable PEG linkages only provided limited mitigation of the anti-PEG IgM production and ABC phenomenon⁶⁴. However, a higher molecular weight of non-cleavable PEG derivatives could reduce the production of anti-PEG IgM while still preserving the long circulation time. This suggests that increasing the molecular weight of PEG is a viable option to reduce the ABC phenomenon while sustaining long-term circulation⁶⁴. Another important factor influencing the protection of NPs against macrophage ingestion and complement activation is the surface heterogeneity of the PEGylated layer. Variations in surface properties can lead to differences in particle uptake and complement activation, thus providing a protective effect. These findings could account for why a small percentage of intravenously injected long-circulating NPs (such as Doxil®) are quickly sequestered by Kupffer cells⁶². Finally, an overlooked area is the actual fate of intracellular PEG molecules. Indeed, PEG accumulation in lysosomes might alter lysosome density and eventually modify or modulate the activity of lysosomal enzymes and membrane glycoproteins, thereby affecting efflux of metabolic products from the lysosomes as well as lysosome fusion with recycling vesicles.

Due to limitations of PEG, researchers have investigated a variety of alternative materials for disguising nanoparticle surfaces, as zwitterionic polybetaines, polyglycerols, glycopolymers, copolymers, polyoxazolines, polysaccharides. Additionally, it has been found that there is a difference in macrophage recognition of stealth NPs between species. For example, polyoxazoline-coated NPs are long-circulating in mice, and *in vitro*, these NPs do not activate the murine complement system or fix C3b and iC3b⁶⁵. However, these NPs are potent activators of the C1q-dependent classical pathway of the human complement system and the recognition of polyoxazoline-coated NPs by human macrophages is strictly complement-dependent^{52,65}. These observations underscore the importance of testing the supposed "*stealth*" properties of NPs with

human materials instead of solely relying on animal sources, as immune responses could be different⁵². As above mentioned, another example of stealth coating can be achieved with polysaccharides. Stealth coated NPs can be prepared using derivatives of chitosan, dextran, hyaluronic acid, and heparin, which provide hydrophilic shells on the surface of the NPs²⁴. These polysaccharides have several advantages, such as being biodegradable, non-immunogenic, and non-toxic, and having functional groups that can be used for conjugation of drugs or cell-interactive ligands. These polysaccharides coated NCs are able to extend the circulation time and enhance their accumulation in tumours. Chitosan, in particular, has a positive charge and can improve cellular interactions of NPs at weakly acidic pH, which can be utilized to achieve specific drug delivery to acidifying tumors⁶⁶. However, the use of these polymers is correlated to their physio-chemical characteristics. Chitosan often finds little application due to its poor hydrophobicity. Researchers resolved this issue through chemical modification of the selected polymer⁶⁷. Furthermore, the polymeric coating is often not very efficient to prevent the protein corona effect⁶⁸. Overall, these data show that the stealth behaviour of long circulating nanocarriers is a very complex mechanism and it cannot be reduced to the simple opsonin repulsion underlining some additional and relevant effects operated by the steric coating on the nanocarrier surface.

Cell membrane coated materials

Cell membrane coated NPs have become increasingly popular in the medical field for drug delivery applications. The use of cellular membrane materials for nanoparticle preparation is a top-down bioinspired strategy that has the benefit of faithfully replicating the antigenic diversity of source cells. This approach of creating NPs directly from cellular membranes eliminates the need for proteomics and the engineering hurdles associated with multivalent nanoparticle functionalization. As a result, researchers have been able to create NPs with many desirable features. The idea of isolating the red blood cell (RBC) vesicles was reported in 1994 and gained significant research interest in utilizing cell membrane vesicles for coating onto a template to design cell membrane nanocarriers in 2011²⁰⁻²³. The cell membrane is the outermost defensive layer of a cell with a thickness of around 5–10 nm, generally made of lipids, proteins, and carbohydrates, and it interacts and performs complex biological functions with the surrounding environment for survival and proliferation²⁴. The first and mandatory step to obtain cell membrane vesicles from source cells is cell lysis followed by membrane purification/collection and vesicle

production⁶⁹. There are both chemical and physical method for cell rupture as high-speed centrifugation, sonication, extrusion, using of dounce homogenizers, pipetting by a fine pipette, repetitive freeze-thaw, and hypotonic lysis which can be used alone or in combination⁶⁹. The selection of the method for breaking the cell membrane depends on the source of the cells, the size of the preparation, and the purpose of the cell membrane. However, the method is mostly selected considering the capability to better preserve the structure and integrity of the membrane proteins expressed by the selected cellular source. The selection of the method for breaking the cell membrane depends on the source of the cells, the size of the preparation, and the purpose of the cell membrane. If done correctly, the cell membrane will maintain its functionality after isolation and its coating will enhance its biointerfacing capabilities. The gentlest method for membrane extraction is hypotonic lysis, which involves treating the expanded cell line with a lysis buffer made with a hypotonic solution. This method is widely used as it helps to prevent denaturing of proteins on the surface of the cell⁶⁹. For nucleated cells, the lysis must be followed by a purification step which can be done through differential centrifugation or sucrose gradient with very little contamination from those intracellular contents. A sucrose gradient is a solution of increasing concentrations of sucrose, from low to high. The cell membrane will float to the top of the gradient, while the other components will remain at the bottom. The cell membrane can then be collected from the top of the gradient. Alternatively, the cell membrane can be purified using a differential centrifugation. This involves spinning the sample at high speeds in a centrifuge. The cell membrane will form a pellet at the bottom of the tube, while the other components will remain in the supernatant. The pellet can then be washed with a buffer to remove any remaining contaminants. Major methods to fuse/ coat core-NPs with cell membranes comprise membrane extrusion³⁴, sonication method³⁵, microfluidic electroporation or by cell-membrane-templated gelation technique³⁶, microfluidic system³⁷, *in situ* packaging of nanomaterials using live cells³⁸, which offer fully coating of the particles and retaining cell surface proteins in a right-side-out manner³⁵.

The most used method is membrane extrusion. This method involves applying mechanical pressure to the cell membrane to allow the NPs to penetrate the phospholipid bilayer. It is a convenient and effective way to prepare cell membrane-coated NPs with homogeneous particle sizes, but it is not suitable for large-scale production^{69,70}. Sonication is a convenient and effective way to produce NPs without the need for extrusion. Ultrasonic waves create cavitation bubbles that break down the membrane structure, allowing the reassembly of the membranes around the

NPs through simple co-incubation. This one-step fabrication process is quick and easy, but the power, frequency, and duration of the sonication must be modified to maximize fusion efficiency and minimize protein denaturation^{69,70}. Cell membrane coated nanocarriers (CM-NCs) possess unique characteristics, such as superior biocompatibility, decreased uptake by macrophage cells, prolonged circulation lifetimes, evasion of the immune system, simplified imaging *in vivo*, improved therapeutic efficacy, and increased drug accumulation into specific targeted sites. This is due to the fact that CM-NCs inherently mimic the surface properties of the source cells, allowing them to take advantage of the nature of the shell-membrane^{25,26}.

As a result, many types of CM-NC have been proposed employing different cell sources for the external shell of membranes, including red blood cells²⁷, white blood cells²⁸, leukocyte⁶⁰, cancer cells^{29,55,69}, platelets⁵⁷, bacteria³⁶, stem cells⁷¹, macrophages³⁰, β -cells⁷², neutrophils³⁵, T-cells⁷³, hybrid membrane cells³⁶, epithelial cells⁷⁴, natural killer cells⁷³, leukemic cells⁷⁵, fibroblasts, patient-derived tumour cells^{55,69,76}, dendritic cells⁷¹ and, more recently, the outer intracellular membrane from the mitochondria⁴⁴ with a synthetic core of different kind of materials such as polymers³¹, gold³², and silica³³ are reported. The selection of the appropriate cell type or cell membrane is crucial for ensuring site-specific distribution and targeting as well as for minimizing adverse interactions with complementing systems *in vivo*⁷⁷. Cell membrane layer should not be considered an unmodifiable structure but a very versatile biological material that can be modified to support the aim of the final nanocarrier. For instance, the cell membrane layer can be labelled using multiple methods (fluorescence, radiolabelling, and genetic engineering) for tracking and diagnostic purposes^{39,40}. To introduce additional functionalities (i.e. active targeting for RBC membrane) researchers have developed conjugation methods like lipid insertion, membrane hybridization, metabolic engineering, and genetic modification^{41–43} which can be classified in pre-modification carried out before breaking the source cells and post-modification obtained by introducing exogenous components into cell membranes after separation and purification. Pre-modification strategies include genetic modification and metabolic engineering, while cell membrane post-modification includes lipid insertion and membrane hybridization.

These approaches contribute diverse functions in a non-disruptive fashion while preserving the natural function of the cell membranes. They also improve on the multifunctional and multitasking ability of cell membrane coated NPs, making them more adaptive to the complexity of biological systems. The validity of a drug delivery system is essentially given by the

ability to evade the immune system, cross the biological barriers of the body and localize at target tissues. Here, we report and describe the principal source of cell membrane used in last years, which are also summarized in **Table 3**.

Circulating blood cells. Circulating blood cells in the body possess innate properties that make them suitable for drug delivery purposes. As previously reported RBC coated nanoparticle have been the first type of CM-NCs in early 1970. RBCs have a long circulation time in the body, with a lifetime of 100–120 days before immune clearance. This long circulation time is due to physicochemical properties (e.g., membrane composition, shape, surface charge, and the ability to deform) and the interaction between CD47, the “*marker-of-self*” protein found on the RBC surface, and signal-regulatory protein α (SIRP α) expressed by phagocytic cells. Moreover, the absence of a nucleus makes erythrocytes highly deformable, and this deformability is highly critical for their longer life span. RBC-coated NCs preserve the stealth properties of the source cells; however, the targeting ability of this nanocarrier is not extremely specific. To enhance the targeting capability of RBCs, ligands that specifically bind to inflammation tissue or tumour cells can be added to the RBC membrane to improve targeting and cellular uptake. Common targeting ligands include peptides and small molecules such as angiopep-2, folate, triphenyl phosphonium, small heterodimer partner (SHp), and arginylglycylaspartic acid (RGD). The incorporation of these properties will expand the native function of RBCs and may have a significant impact on the biological outcome. However, this modification process can be complex, especially for mass production. Moreover, another solution is represented by hybrid nanovesicle which can be easily obtained thanks to the unique ability of RBC membrane to fuse with other cell.

The use of other cell types as coating materials for cell membrane coating to evade the immune system has been expanded as circulating cells. Among circulating cells, white blood cells (WBC) or leukocytes, including macrophages, neutrophils, T-cells, and natural killer cells (NK cells) bring a great attention for the development of drug delivery systems to treat inflammatory disorder, cancer as well as bacterial infection⁷⁸. WBC works as guardians to protect our bodies from infections and injuries. Furthermore, leukocytes are able to penetrate the injured BBB, in addition to inflamed vessels, via membrane proteins which interact with the vascular endothelial cells^{57,79}. As for RBC-NCs, WBC-NCs are uniquely able to target disease sites due to their natural cellular surface ligands, improving drug transport by traversing the endothelial layer, and reducing phagocytic uptake through self-recognition⁷³. In recent years, different types

of WBC-NC have been proposed. *Parodi and colleagues* created nano porous silicon synthetic NPs that were coated with plasma membranes collected from leukocytes, called leuko-like vectors (LLVs). The leukocyte membrane coating was achieved through chemical conjugation and electrostatic interactions between the negatively charged membranes and positively charged synthetic NPs. These LLVs were found to exhibit similar functions as leukocytes and were able to pass through the inflamed endothelial cell layer both *in vitro* and *in vivo*. It is suggested that the coating of LLVs with membrane proteins allows for the activation of signalling pathways in endothelial cells, which subsequently increases vascular permeability. This enables the NPs to penetrate inflamed vessels like leukocytes. T-cell membranes have been coated onto paclitaxel-loaded PLGA NPs (TNPs) which leads to a reduction in phagocytosis by macrophages and allows for targeted cancer therapy through interactions with surface adhesion molecules such as LFA-1 and ICAM-1 on vascular endothelium. More recently, WBC-NPs have been developed to inherit important surface receptors from their parent cells, allowing them to bind and block viruses from interacting with their intended host targets. For example, T-cell membrane coated PLGA NPs (TNPs) have been used in the neutralization of HIV. It is also worth noting that platelet membrane-coating has been studied for the treatment of various diseases. Platelets have a long circulation lifespan in the bloodstream (half-life of 30 h) and play a role in thrombus formation by being recruited to sites of injured vessel walls and becoming a main component of thrombi. Given the unique properties of platelets, NPs coated with platelet membranes have been investigated for their use in cancer and inflammatory disease treatment, such as infections and atherosclerosis⁵⁷. As RBC membrane, platelet cell membrane express CD47 receptors which act as a “*don't eat me*” indicator by selectively binding to SIRP α expressed by macrophages⁸⁰. The presence of CD47 inhibits the immune cell-mediated clearance of NPs and allows passive drug targeting of NPs through the extension of their circulation in the blood. However, platelet membrane coated NPs have a targeting ability that allows them to adhere to tumours and damaged blood vessels unlike RBC-NC. As previously described, platelet cells are able to interact with cancer cells through highly expressing ligands on the tumour cell surface⁸¹. *Chi et al.* developed a platelet membrane-coated docetaxel-loaded PLGA NPs (PM/PLGA/DTX) for lung cancer therapy⁸². These PM/PLGA/DTX were found to decrease the toxicity of antitumor chemotherapy drugs and inhibit the growth of lung tumours. Platelet membranes are also involved in coagulant activity and are recruited by vascular damaged components of the subendothelial matrix, including collagen, fibronectin and von Willebrand factor. This role led to platelet NCs as a targeting strategy to treat

vascular diseases as atherosclerosis and ischemic injury. *Xu et al.* designed a nanoparticle system that is coated with platelet membranes and responds to thrombin, allowing for the sequential, specific delivery of tissue plasminogen activator (t-PA) and the neuroprotectant ZL006 to the thrombus region and ischemic brain tissue⁸³. These nanocarriers proved to release t-PA in a thrombin-triggered manner via degradation of the thrombin cleavable linker. As well as, platelet coated NCs have been proved to target atherosclerotic plaque, rheumatoid arthritis synovial tissue. In detail compared to bare NC, the planted NC showed a 4.98-fold higher targeting efficiency towards atherosclerotic arterial⁸⁴. Additionally, the evolution of atherosclerosis was significantly reduced and atherosclerotic plaques were stable in ApoE^{-/-} mice⁵⁷.

Cancer cell. Cancer cell coated nanocarriers are considered a promising solution to escape immune surveillance and homing tumour targeting^{75,85}. The stealth properties are basically due to the attitude of cancer cells to neutralize and/or evade immune surveillance using sophisticated tools. The homing or homologous targeting is reached through numerous functional proteins, including membrane proteins mediating homologous binding (selectins, integrins, etc.), biomarkers of self-recognition and immune escape (CD47, etc.), and immune activation-related tumour antigens (tumour-associated Thomsen-Friedenreich, glycoantigen, etc.)⁸⁶. The first study in this subfield revealed that cancer cell membrane coated PLGA NPs showed 40- and 20-fold increases of uptake by homologous cancer cells compared with RBC coated and bare NPs, respectively. Another advantages of cancer cell is an indefinite proliferation and fast *in vitro* expansion which make the possibility of isolating cell membranes in a large number⁸⁷. *Wu et al.* developed a nanocarrier coated with cell membranes from the lung cancer cell line H975 and loaded with doxorubicin and icotinib⁸⁸. This nanocarrier was found to be successful in treating chemotherapeutic drug-resistant non-small cell lung cancer (NSCLC), showing advantages such as high stability and efficient tumour inhibition (killing 87.56% of tumour cells)⁸⁸. Additionally, the use of NPs coated with 4T-1 cell membranes was found to significantly enhance the distribution of NPs in lung tumours and suppress lung metastasis in breast cancer⁸⁹. However, the use of cancer cell-derived membranes raises safety concerns and potential risks of inducing tumorigenesis, which limits its clinical applications⁸⁰.

Stem cell membrane. Stem cells have the ability to migrate towards tumors⁹⁰, a property known as tumour tropism, which is mediated by the binding of lymphocyte LFA-1 to ICAM-1 making them suitable for use in cell-based drug delivery. In detail, mesenchymal stem cells (MSC)

express homing receptors, such as CXC motif chemokine receptor 4 (CXCR4), CXCR2, and cluster of differentiation 74 (CD74), in response to the corresponding cytokines expressed in tumour sites or injured tissues, such as stromal cell-derived factor. Among these, the CXCR4 receptor constitutes one of the surface receptors expressed on the stem cell membrane that is crucial for nano system recognition⁷¹. Overall, mesenchymal stem cells (MSCs) tumour tropism involves three different stages:

- access to the circulatory system through direct administration or enrolment from bone marrow.
- rolling, capture, adhesion and extravasation over the epithelial cells into injury surrounding area driven by chemokine gradients;
- migration towards the tumour sites.

Thanks to tumour tropism, MSCs-NC have been developed and analysed. In detail, PLGA-PTX or PLGA-DOX loaded MSCs showed to be concentrated in the tumour tissues as prostate cancer tissue, lung, and glioma tissue⁹¹. *Yang et al.* demonstrated the efficacy in targeted lung tumour treatment of PLGA NPs coated with MSCs membranes. In detail, they employed MSC membrane from Human umbilical cord-derived mesenchymal which managed to considerable tumour growth inhibition and induced clear apoptosis within tumour lesions⁹². However, there is a risk that stem cells may differentiate into tumour cells, activating the complement system and reducing their effectiveness in treating disease.

Bacteria coated nanocarrier

Bacteria membranes caught the attention as vaccination materials since they have a huge number of immunogenic antigens with intrinsic adjuvant properties and express several pathogen associated-molecular patterns that stimulate innate immunity and promote adaptive immune responses⁷⁶. *Gao et al.* proposed a bacterial membrane-coated nanoparticle system as antibacterial vaccine. In detail, they employed, as model, pathogen *Escherichia coli* to coat small gold NPs (AuNPs). The resulting bacterial membrane-coated AuNPs (BM-AuNPs) showed significant stability in biological buffer solutions. When tested on mice, the BM-AuNPs induced rapid activation and maturity of dendritic cells in the lymph nodes, generated a strong antibody response and induced elevated production of interferon gamma (INF γ) and interleukin-17 (IL-17) but not interleukin-4 (IL-4). This suggests that the BM-AuNPs can generate strong T helper cell

type 1 (Th1) and T helper cell type 17 (Th17) based cell responses against the source bacteria. These results indicate that using natural bacterial membranes to coat synthetic NPs has great potential for designing effective antibacterial vaccines⁹³. Studies have also shown that using the outer membrane of *Helicobacter pylori* as a coating for NPs can effectively prevent bacteria from binding to gastric epithelial cells and stomach tissue⁹⁴.

Table 3. Biomarkers, advantages, and limitations of biological membrane source.

Sources	Biomarkers	Advantages	Limitations
RBCs	CD47	Long circulation time, simple techniques for membrane surface decoration	Lack targeting, low drug-loading capacity
Platelets	P-selectin, CD47	Inflammation targeting, immune escape	Limited assessment of immunogenic potential,
Cancer cells	T antigen-galectin-3	Homologous targeting	Potential concerns regarding safety
MSCs	CXCR4 and other chemokine receptors	Inherent tumour-tropic and inflammatory migratory	High preparation cost
Immune cells	α 4 integrins, CD45, CD47	Immune evasion, metastatic tumour targeting	Complex workflow to extract and purify membrane, immunogenicity
Bacteria	Virulence actors	Immune activation	Potential concerns regarding safety

Exosome

Exosomes are small extracellular vesicles with high compatibility and low risk of an immune response, making them an attractive option for drug delivery. They are released by various cells and can retain the targeting properties of the cells that produced them. However, as autologous biologics, exosomes have been subject to clinical investigation. Limitations in production yield, functionalization, and purification have hindered their biomedical applications. Cell-derived exosome-mimetic nanovesicles, which coat intact cell-derived membranes on their surface, have recently been proposed as an alternative. They have higher production yields and can preserve the biological functions of cell membranes while allowing for tuneable physicochemical properties. The main clinical application of exosomes is their use as biomarkers, therapeutic agents, drug delivery carriers and cancer vaccines. They are derived from human or plant sources and are utilized in various clinical trials. Exosomes from the circulatory system are most used for biomarker experiments. MSCs and dendritic cells (DCs) are two widely used cell sources for exosome production. MSC-derived exosomes are utilized for inflammation treatment

and drug delivery, while DC-exosomes are employed to induce inflammation response in cancer patients. Despite their potential, the clinical application of exosomes faces various questions and challenges, and translation of exosome-based clinical trials is required to meet good manufacturing practices (GMP)⁹⁵.

Viral nanocarrier platforms

Viruses, due to their small size, stability in various conditions, and ability to be produced in large quantities, play a crucial role in nanoscale engineering. One aspect of this is the use of viral-like particles (VLPs) and Viral NPs (VNPs) as nanoscale scaffolds to encapsulate a variety of materials, such as nucleic acids, proteins, peptides, and drugs. VNPs and virus-like particles VLPs are like viruses in their structure and properties. VNPs are actual viral particles that contain viral genetic material, while VLPs are NPs that mimic the structure of viruses but do not contain any viral genetic material^{96,97}. The exterior of VLPs can be modified through genetic or chemical means and can also be targeted to specific cells using ligands or peptides⁹⁷. These characteristics make VLPs useful in a variety of applications, such as drug delivery, bioimaging, tissue engineering, vaccine production, and disease detection⁹⁶⁻⁹⁸. Several plants based VNP and VLP are being developed for various nanomedical applications. These include *Tobacco mosaic virus* (TMV), *Cowpea mosaic virus* (CPMV), *Cowpea chlorotic mottle virus* (CCMV), *Physalis mottle virus* (PhMV), and *Potato virus X* (PVX). Additionally, bacteriophages such as MS2, P22, Q β and M13 are also being explored as VNP and VLP platforms⁹⁹. Currently, the most advanced method for delivering genes to human patients is using mammalian virus vectors, several of which are being tested in clinical trials. However, newer VNP/VLP platforms using bacteriophages and plant viruses are being developed as these are considered safer for human use. Studies have evaluated the distribution, pharmacokinetics, and potential side effects of certain NPs, such as CPMV, CCMV, Q β , and M13 in mice and found that they have a wide distribution in the body⁹⁹ with no observed toxicity⁹⁶. As well as plant virus NPs (PVNPs) have achieved considerable success in preclinical studies in cancer immunotherapies¹⁰⁰.

4. Application of nanotechnologies in nutraceutical and cosmetic field

From the drug delivery vehiculation, nano scale materials have gained the attention of both cosmetic and food industry. This interest is basically due to the unique characteristics related to nanometre size, such excellent physicochemical properties in terms of diffusivity, solubility, bioavailability, low toxicity, optics, thermodynamics, high encapsulation efficacy and payload stability. For example CUR loaded nano-formulations are able to enhance CUR physicochemical stability and to overcome the natural barriers and improve its bioavailability¹⁰¹. LPN are among the most promising nano-encapsulation technologies available in food industry.

Lipid formulations can be easily produced using technologies already widely used by the food industry such as high-pressure homogenization and micro-fluidization. These systems, to be usable and marketable, must be safe for food use, economically advantageous, and must not negatively affect the sensory properties of the product. Several types of LPN are cited in the literature. NEs, NLCs, nano-suspensions, SLNs, liposomes and nanoliposomes are among the most developed and studied food grade delivery systems as food grade nanocarriers.

NEs have significant importance in the food industry for food protection and supplementation of foods with useful components¹⁰². Due attention is given to encapsulated vitamins, antioxidants, omega-3 fatty acids, phytochemicals, and other nutraceuticals/dietary supplements or ingredients used to fortify food and meet the standard of foods for special medical purposes. The nutraceutical market has grown significantly in recent years due to increasing consumer demand for products that promote health and wellness, as well as, an aging population that is more concerned about maintaining health as they age. The market is highly competitive, with many companies competing for a share of the market through product innovation, marketing, and distribution. Some of the key players in the nutraceuticals market include Nestlè®, GSK®, Pfizer®, and Herbalife®. As result, there is a great interest to improve nutraceuticals bioavailability. The amount of nutraceutical that reaches the bloodstream in an active form after oral sub-ministration is known as its oral bioavailability. Additionally, the use of edible coatings and smart packaging materials to increase shelf life and enhance food quality is also addressed. There are several examples of nano-formulated nutraceutical. Recent studies have shown that the stability of resveratrol when exposed to UV rays can be improved by encapsulating it in NEs¹⁰³.

Another example is Co-Q10, that due to its high hydrophobicity and high molecular weight (MW 863.34 g/mol), has poor pharmacokinetic properties and low bioavailability^{72,104}. Various strategies have been reported in literature to improve Co-Q10 bioavailability such as oil solutions¹⁰⁵, liposomes¹⁰⁶, polymeric or lipid NPs^{107,108}, nano-crystals, and NEs^{30,109}. In particular, a significant increase in Co-Q10 bioavailability has been demonstrated when encapsulated in lipid formulations such as NEs and conventional emulsions⁷². To effectively deliver a drug or nutraceutical to the body, it is necessary to know its bioavailability. In the pharmaceutical field, a classification system known as the Biopharmaceutical Classification System (BCS) is used to divide drugs into four categories based on their permeability and solubility. Given the extreme usefulness of the BCS for the development of pharmaceutical forms, an analogous system for nutraceuticals has been developed, known as the Nutraceutical Bioavailability Classification Scheme (NuBACS). This method is based on the limiting factors of the bioavailability of nutraceuticals, which are classified into three classes based on bioaccessibility, absorption, and transformation in the gastrointestinal tract (GIT). More in detail, O/W NEs of food grade type are among the most used delivery systems for lipophilic substances since they are able to incorporate/solubilize large amount of compound. The interest in NEs compared to conventional emulsions and other types of nano-vectors is essentially due to the numerous advantages offered^{110,111}. They can be prepared from generally recognized as safe (GRAS) raw materials and using simple processes compared to multiple emulsions and SLN:

- They are of particular interest to the food industry as food grade oils and emulsifiers are available.
- The presence of numerous lipases allows for rapid digestion of the NEs, digestion of these systems can also be controlled by varying the dimensional distribution, the type of emulsifier and the composition of the lipophilic phase.
- They can increase the bioavailability of lipophilic bioactive compounds due to the solubilization capacity of the molecules and the small size of the nanocarrier.
- They are able to protect the encapsulated compounds within the oily phase during preparation procedures preserving the physio-chemical stability of the product and the organoleptic properties (colour, taste, appearance).
- They are relatively stable to separation and aggregation (compared to emulsions).
- They can be used for different routes of administration (oral, cutaneous, parenteral, nasal).

- They can be used in place of liposomes and micelles.

Despite all these properties, for certain applications it is necessary to use more sophisticated systems such as multilayer NEs: the interfacial deposition of polymeric layers can be considered a valid strategy to increase the stability of the emulsion and protect the encapsulated bioactive compounds^{112,113}. In addition, the chitosan coating prevents phase separation in the NEs and inhibits degradation of the compound when exposed to UV radiation and thermal treatments¹¹⁴. In addition to systems based on chitosan alone, nano-carriers have been developed in which the polymer is appropriately functionalized. *Vecchione et al.* have verified the importance of the different degree of chitosan functionalization with 2-iminothiolane, the size of the NEs comparing systems with sizes between 110 and 230 nm, and the effects of co-administration with piperine which, as known, increases the bioavailability of CUR. From these studies it emerged that NEs of smaller size coated with chitosan with a higher degree of functionalization and containing CUR and piperine presented a better bioavailability and in addition the therapeutic activity of CUR conveyed by such systems is preserved²⁸. From the same group, multilayer NEs based on chitosan were developed using CUR as a drug model, in particular a multilayer coating based on polysaccharides (chitosan glycolate and heparin) covalently bound through a cross-linked bond was developed¹¹⁵. This system was obtained by alternating layers of chitosan glycolate and heparin, respectively modified with a thiolic residue and an allyl residue, UV irradiation allows to obtain the formation of a covalent bond between the two residues without the use of photoinitiators or metal catalysts. This is therefore a *click reaction* that allows to obtain as a result a completely biocompatible and biodegradable nano-carrier much more stable than systems based on electrostatic interactions alone¹¹⁵. It has also been shown that the interaction of NEs with a coating consisting of chitosan glycolate functionalized with N-acetylcysteine and containing CUR with *in vitro* models of the intestinal barrier preserves their structural integrity, and the anti-inflammatory activity of CUR is preserved, showing that this system is able to protect it from degradation¹¹⁶. More recently, it has been shown that O/W NEs can be formed using different types of oils (extra virgin olive oil and olive pomace oil) and non-ionic emulsifiers to effectively incorporate Co-Q10¹¹⁷. These systems have shown good chemical-physical stability over time when stored at 4°C and 25°C, in particular, all formulations remained in the nanometric size range for 3 months⁷⁴. In conclusion, all these results show a promising application of such delivery systems for the oral administration of lipophilic and sensitive drugs and nutraceuticals, such as CUR and Co-Q10.

5. Aim of the thesis

NDDS are well-known strategies used to overcome the problems associated with the direct administration of naked drug and to obtain a controlled release of drug content into a selective target site. The principal purpose of this thesis is the development of O/W layered NEs as versatile targeting NDDS for different applications including tumour cells or atherosclerotic lesions targeting and intestine barrier. Among NDDS, the bioinspired nanocarriers, based on biomimetic coating of cell membrane shows interesting features, particularly the ability to avoid the immune response and to improve drug bioavailability.

Here, we present a new study focused on the design of a novel biomimetic nano-carrier based on O/W NEs. The O/W NEs are a unique system due to their excellent properties such as high encapsulation efficiency for lipophilic molecules to make them highly bioavailable^{44,45}. NEs are a biphasic system in which one phase is dispersed in the other in the form of minute droplets, which generally have an average diameter between 50 and 500 nm⁴⁶. The kinetic stability of O/W NEs is usually increased with layer-by-layer strategies; moreover, its surfaces can be modified with specific ligand, such as peptide, to reach an active targeting^{16,47}. We propose an oil liquid core with a cell membrane shell, which represents an innovative biomimetic system able to combine the biomimetic nature of cell membrane, and the excellent properties of the ultrastable secondary O/W NEs developed in our group, previously mentioned^{48,49}.

However, cell membrane coating has never been applied on liquid nanocarriers such as O/W NEs, most probably due to the delicacy of such a system. In our group, we have experience with O/W NEs coated with a polymer layer which are highly stable and can easily undergo further coatings. In this context, the aim was to design a new biomimetic nanocarrier, which is based on cell membrane - O/W NEs able to carry several internal and external cargos (Some) CM-NEs. Together with the biomimetic feature, one objective coming from cell membrane coating is to promote an active targeting by exploiting the homotypic adhesion properties towards cancer cells by cell membranes. Additionally, the proposed chitosan-based secondary NEs proved to be able to firmly encapsulate hydrophobic compounds such as therapeutic nutraceuticals including CUR⁴⁵, lycopene⁵⁰ and Co-Q10⁵¹ and safely reach the intestine barrier, due to the high gastro resistance provided by the chitosan coating and accumulate on such barrier

thanks to the high mucus-adhesion property of the physically thiol functionalized chitosan coated on the nanoemulsion.

The **chapter 2** was mainly dedicated to the assembly of this innovative biomimetic nanocarrier. For that purpose U87-MG, a human primary glioblastoma cell line, was selected¹. U87-MG was elected as model tumour cell line to develop an easy and scalable protocol for the assembly of CM-NEsoSome. As reported in the previous paragraph, nanomedicine-based treatment strategies have been extensively used in antitumor therapy.

The **chapter 3** was focused on targeting atherosclerotic lesions with different strategies exploiting the homing effect of macrophages membrane layer. In detail, in **chapter 3** we proposed a macrophages membrane coated NEsoSome. To target atherosclerotic lesions, we selected THP-1 as human monocyte cell line to obtain human monocyte (M) and macrophage (M0) membranes. THP-1 were activated at macrophages to express cell membrane markers and exploit macrophage “**homing**” and an active targeting into atherosclerotic lesions. At first, selective accumulation of both monocyte NEsoSome (M-NEsoSome) and macrophage NEsoSome (M0-NEsoSome) were compared and evaluated by *in vitro* uptake in a tumour Necrosis Factor α (TNF α) treated HUVEC cell layer, elected as a model to inflamed endothelial cells, with confocal microscopy. As well as, the *in vitro* internalization was performed in healthy HUVEC cell layer to prove the effective selectivity for the inflamed endothelial cells.

O/W NEs is well established formulation for lipophilic compounds such as Co-Q10, lycopene and CUR. In **chapter 4** it is reported a food grade secondary CUR loaded O/W NEs with enhanced mucus-adhesion properties thanks to the presence of N-acetylcysteine salified chitosan. In detail, the developed NEs were completely physiochemical characterized, and its mucus adhesive properties are validated in an intestine on chip device (InOA-chip). Additionally, we evaluated *in vitro* through the INFOGEST® protocol the bioavailability of loaded CUR.

In summary, during this PhD project, we focused on the active targeting promoted with a nanocarrier based on an O/W nanoemulsion, which, thanks to its high stability, could be properly coated for that purpose and keeping its stability in *in vivo* like conditions such as blood in the case of cell membrane coated NEs and GIT in the case of high adhesive chitosan coated NEs.

Chapter 2: Tumour Cell membrane coated secondary Nanoemulsions

Cell membrane-coated oil in water nano-emulsions as biomimetic nanocarriers for lipophilic compounds conveyance

Martina Profeta^{1§}, Concetta Di Natale^{1,2§}, Elena Lagreca¹, Valentina Mollo¹, Paolo Antonio Netti^{1,2,3} and Raffaele Vecchione^{1*}

¹Center for Advanced Biomaterials for Health Care (CABHC), Istituto Italiano di Tecnologia, Largo Barsanti e Matteucci 53, Napoli, Italy

²Interdisciplinary Research Centre on Biomaterials (CRIB), University of Naples Federico II, P.le Tecchio 80, Naples, 80125, Italy

³Department of Chemical Materials and Industrial Production (DICMAPI), University of Naples Federico II, P.le Tecchio 80, Naples, 80125, Italy

[§]These authors equally contributed to the work

*Correspondence: Raffaele.vecchione@iit.it

Published article: *Pharmaceutics* 2021, 13(7), 1069; <https://doi.org/10.3390/pharmaceutics13071069>

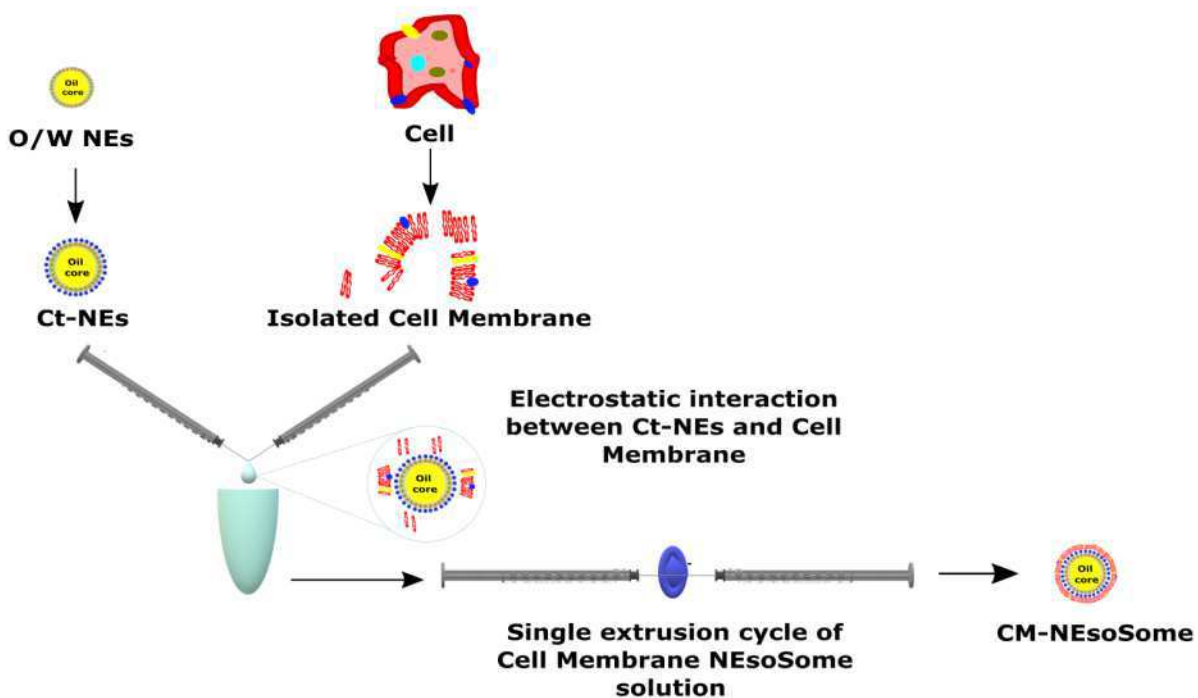
Received: 8 June 2021 / Revised: 4 July 2021 / Accepted: 8 July 2021 / Published: 12 July 2021 (This article belongs to the Special Issue [Complementary and Alternative Medicine \(CAM\) and Nanomedicine: Advances in Cancer and Cardiovascular Diseases](#))

Abstract

Nowadays, a new bioengineered platform based on cell membrane cloaked nanoparticles has been developed to produce a cutting-edge class of biomaterials able to combine the properties of cellular membranes with the engineering liveness of synthetic nanomaterials producing smart, biocompatible, and biomimetic nanocarriers. This new class of cell membrane-camouflaged nanomaterials displays numerous advantages such as high biocompatibility and prolonged blood circulation. Recently, we developed ultra-stable oil in water nano-emulsions (O/W NEs), able to carry both internal and external cargos (Somes) such as lipophilic compounds and hydrophilic coatings, respectively, that we call here NEsoSomes. O/W NEs are an excellent

bioengineering tool for drug and molecules delivery due to their ability to dissolve a large number of hydrophobic compounds and protect them from hydrolysis and degradation under biological conditions. At present, no report is available on the combination of cell membrane coatings with such nanocarriers, probably due to their typical instability feature. Since that, we report for the first time a new cell membrane (CM) coated nanomaterial composed by membranes extracted from glioblastoma cancer cells (U87-MG) deposited on NEsoSomes through a liquid–liquid interface method to produce highly controllable membrane caked nano-capsules, namely CM-NEsoSomes. Moreover, CM-NEsoSomes biocompatibility was tested on healthy model cell line, performing cell cytotoxicity and uptake assay.

Keywords: Nano-emulsions, cell membrane, biomimetic approach.



1. Introduction

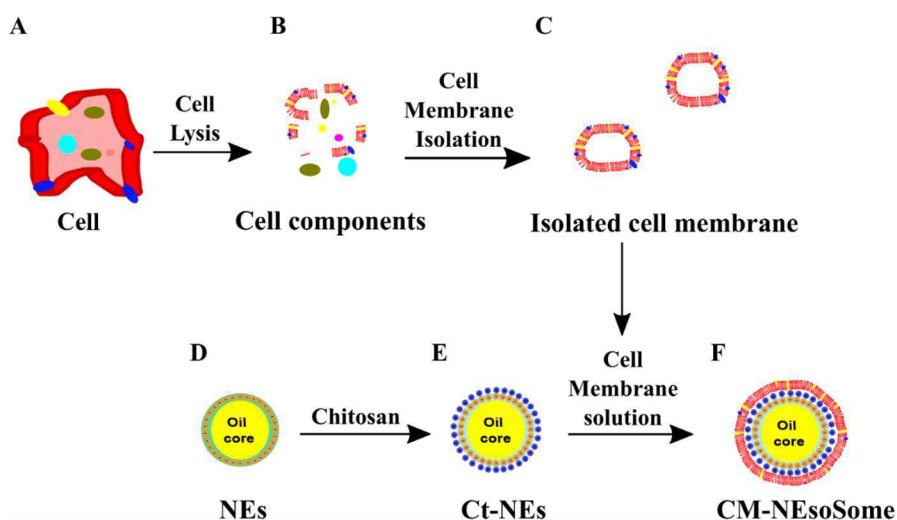
Nanoscale drug delivery systems (NDDS) are widely investigated to improve the efficacy and safety of drug therapy and diagnostic. Among these, oil in water nano-emulsions (O/W NEs)

are an ideal system for the encapsulation of lipophilic molecules^{1,2}. The kinetic stability of O/W NEs is usually increased *via* layer-by-layer strategies and their surfaces can be decorated with specific ligands such as proteins, polymers, and cell-penetrating peptides (CPP) able to target cells or tissues^{1,3-6}. However, they have some limitations including short circulation time, immune recognition, poor tumour accumulation and penetration^{3,7,8}. Recently, improving nano-carrier circulation times has gained considerable attention and, among all current proposed strategies, the most innovative is based on biomimetic systems deriving by extracted cell-membranes⁹. Cell membrane-coated nano-carriers consist in a core formed by different materials and in a shell of cell derived membranes; this coating strategy is known to elude the immune system, simplify *in vivo* imaging, improve therapeutic efficacy and increase the drug accumulation into specific targeted sites depending on the nature of the coated-membrane^{10,11}. Many types of cell membrane-coated nano-carriers based on external shell of membranes from red blood cells^{9,12,13}, white blood cells¹⁴, cancer cells^{11,15} and bacteria¹⁶ with a synthetic core of different kind of materials such as polymers¹⁷, gold¹², and silica¹⁸ are reported in literature. The current cell membrane-coated nano-carriers are obtained by electrostatic attraction¹⁵, sonication method¹⁹ and by cell-membrane-templated gelation technique²⁰, microfluidic system²¹, *in situ* packaging of nanomaterials using live cells²², which offer a full coating of the particles and retaining cell surface proteins in a right-side-out manner¹⁹. Up to now the only example of cell membrane coated nano-emulsion is based on a recent red blood membrane coated perfluorocarbons (PFC)-nano-formulation, which has been reported as an oxygen delivery vehicle²³. Despite the excellent obtained results, it is well-known that perfluorinated compounds are not biodegradable and most of them show a poor solubility in ethanol or acetone that are the most common solvents used to solubilize/disperse several compounds for therapeutic or diagnostic purposes. By contrast, vegetable oil involved in our O/W NEs, is biocompatible, biodegradable and highly miscible with ethanol and acetone and so able to encapsulate lipophilic substances such as curcumin²⁴, Co-enzyme Q10⁶ and lycopene²⁵. Moreover, our O/W NEs coated by a layer of chitosan (Ct), namely secondary nano-emulsions (SNE), was optimized in terms of formulation and process, in order to provide a shelf life over 1 year²⁶ and a consequent exceptional ability to be stably coated with several materials, such as polymers as well as inorganic materials²⁷⁻²⁹.

In the light of these considerations, here we present for the first time a biocompatible and nature-based O/W NE –membrane system (CM-NEsoSomes) as potential biomimetic nanocarrier of lipophilic compounds. Cell membranes were extracted from U87-MG cells and, after membrane

purification, the layer was obtained through a liquid–liquid interface by an electrostatic interaction between negative charged cell membrane and positive charged Ct-NE (**Scheme 1**). Furthermore, CM-NEsoSomes were characterized, and their biocompatibility was tested on HDF, by means of cell cytotoxicity and uptake assay.

In this scenario, thanks to the Ct-NE versatility and the biomimetic feature provided by the cell membrane coating, one can envision innovative and highly performing delivery systems with increased bioavailability and metabolic stability of the carried drugs.



Scheme 1. Schematic representation of CM-NEsoSome preparation: **A**) Cell, **B**) Cell components, **C**) Isolated Cell Membrane, **D**) O/W NEs, **E**) Chitosan deposition and **F**) final CM-NEsoSome.

2. Materials and Methods

Materials

Surfactant Lipoid E80 (egg lecithin powder 80%–85% enriched with phosphatidyl choline (PC) and 7%–9.5% content in phosphatidyl ethanolamine (PE)) were purchased from Lipoid GmbH. Millipore Milli-Q water was used for the preparation of all nano-emulsions and solutions. Soybean oil (density at 20 °C of 0.922 g mL⁻¹), Fluorescein-isothiocyanate (FITC) and chitosan (Ct, LMW 90–150 kDa, DDA 84% determined via ¹H-NMR) were purchased from Sigma Aldrich (Milan, Italy). Hoechst 33342, Trihydrochloride, Trihydrate (Hoechst), CellMask™ Orange plasma membrane stain (CellMask™-543) and Wheat Germ Agglutinin, Alexa Fluor™ 488 Conjugate (WGA-488) were purchased from Thermo Fisher Scientific.

Cell Culture

Human glioma cell line (U87-MG) was purchased from ATCC® and used as cancer cells model for membrane extraction. Primary human dermal fibroblasts (HDF) were purchased from ATCC® and used as healthy tissue model, to test the biological effect of the final system.

U87-MG cells were cultured with EMEM supplemented with 10% FBS, 1% of glutamine and antibiotics. Cells were sub-cultured in T150 cell culture flask for membrane extraction, in a humidified controlled atmosphere with 5% of CO₂, at 37 °C. The medium was changed every 2-3 days.

HDF cells were cultured in Eagle's minimal essential medium (EMEM) supplemented with 20% Fetal Bovine Serum (FBS, Gibco), 1% of glutamine, 100 U/mL penicillin, 100 mg mL⁻¹ streptomycin and 2X nonessential aminoacids. Cells were maintained in cell culture plates of 100 mm diameter in a humidified controlled atmosphere with 5% of CO₂, at 37 °C. The medium was changed every 2–3 days.

Cell Membrane Isolation and Characterization

Cells membranes were isolated from the cancer cells U87-MG, according to the procedure reported by *Balasubramanian et al.*³⁰ with modifications.

Prior to cell detachment, cell culture medium was removed and 3 mL of a PBS solution containing 0.01% of Hoechst, 0.1% of WGA-488 and 0.1% of CellMask™ -543 was added to each flask. In this way, cell nuclei, cell membrane glycoproteins and plasma cell membranes were stained, respectively. After 10 min of incubation in a humidified controlled atmosphere with 5% of CO₂, at 37 °C, 10⁹ U87-MG cells were detached from the T150 cell culture flasks by trypsinization, and centrifuged at 500g for 5 min. The resulting cell suspension was washed three times with PBS buffer by centrifuging at 500g for 4 min, and then suspended in hypotonic lysing buffer at a 1:10 ratio pellet/lysing buffer. The lysis buffer was composed as follows: 20 mM Tris-HCl pH 7.5; 10 mM KCl; 2 mM MgCl₂. The cells were disrupted by pipetting them thoroughly and spinning the solution at 3.200×g for 5 min. The resulting pellet was dissolved again in the hypotonic lysing buffer solution, pipetted and spun down by centrifugation at 3.200 ×g for 6 min. After that, the supernatants were collected, mixed and centrifuged at 18.000 ×g for 20 min at 4°C. The pellet

was collected, characterized, and used as purified cancer cell membrane for the subsequent experiments.

The membrane extraction protocol was performed in triplicate to validate its reproducibility and the purity of the final sample. The pellets or the supernatants of each step of the purification process were observed by confocal microscope (Leica Microsystems TCS SP5 II, Germany) with a 25X water immersion objective. Images were acquired with a resolution of 1024x1024 pixels (**Figure S1**). For cell membrane deposition on nanoemulsion (see following paragraphs), WGA staining was avoided.

Circular Dichroism (CD)

CD spectroscopy is a well-established technique for studying the secondary structures of soluble proteins and it has a special relevance in the study of membrane proteins embedded in different environments such as lipid vesicles, detergent micelles, oriented bilayers or nanoparticles^{31,32}. CD spectra of membrane solutions before (371.1 µg) and after deposition (150 µg) were recorded using a Jasco J-1500 spectro-polarimeter (J-1500-150, Japan) in a 1.0 cm path-length quartz cell. CD spectra were registered at 25 °C in the far UV region from 260 to 190 nm^{33,34}. The spectra were obtained with an average of 3 scans by subtracting them from blank samples (**Figure S2**)³⁵⁻⁴¹.

Bicinchoninic Acid assay (BCA assay) membrane protein quantification

Protein quantification of cell membranes was evaluated using the Bicinchoninic Acid assay (BCA assay) (Bicinchoninic Acid Kit, Merk). The assay was carried out according to the manufacturer's instructions^{42,43}. The absorbance at 562 nm was measured using an EnSpire® Multimode Plate Reader and the relative titration curve was reported in **Figure S3**.

Ct-NEs preparation

The substrate for cell membrane deposition was a secondary nano-emulsion (SNE) which consists of an O/W NE, called "primary nano-emulsion", coated with a layer of an opposite charge polyelectrolyte (chitosan, Ct). Briefly, the oil phase was prepared by dissolving 5.8 g of Lipoid E 80 in 24 mL of soybean oil at 60 °C using an immersion sonicator (Ultrasonic Processor VCX500 Sonic and Materials); after, 5 mL of an ethanol solution of fluorescein-5-isothiocyanate (FITC) (0.6

w/v %) was added to the oil phase and the evaporation of the alcoholic solvent was carried out at 60 °C for 30 min. Then, the prepared oil phase was added dropwise to the water phase (Milli-Q water) and mixed again using an immersion sonicator to obtain a pre-emulsion. A low temperature was maintained throughout this process by using an ice-bath. Finally, this pre-emulsion was passed at 2000 bar through the high-pressure valve homogenizer (Microfluidics, M110PS) to greatly reduce the initial size²³. In the end, to achieve the Ct-NE, a first layer of Ct was deposited above the O/W NEs by following a previously developed procedure⁴. Concisely, a 0.1 M acetic acid solution of Ct pH 4 (0.2 w/v%) was prepared, to that solution was quickly added, under vigorous stirring, the O/W NEs 20 wt % oil and kept under stirring for 15 min to allow uniform chitosan deposition. The secondary NEs were re-dispersed through a high-pressure valve homogenizer at 700 bar for around 100 continuous steps, and finally re-processed after one week under the same conditions and stored at room temperature. The final concentrations of oil and Ct were 10 and 0.1 w/v %, respectively, while the pH of the final secondary NEs was 4.24.

CM-NEsoSome Preparation

Starting from the positive Ct-NE, the second layer of cells membranes was deposited using two syringe pumps (HARVARD APPARATUS 11 PLUS) by adapting a procedure developed for multilayer system preparation²⁷. Particularly, a cell membrane solution of c.a.0.3 µg was mixed 1:1 (v:v) with the Ct-NE (10 wt% oil - 0.1 w/v % Ct) suspension at flow rate of 0.4 mL/min through two micrometric capillaries interfaced at their extremities in order to form a single drop because of the high surface tension. Each drop was then collected inside a glass tube and stored at 4 °C for further analysis.

Physio-chemical characterization and morphological characterization of the Ct-NE and CM-NEsoSome Particle Size and ζ-Potential Measurements

Ct-NE and CM-NEsoSome were characterized by measuring size, polydispersity index (PDI) and ζ-potential values through dynamic light scattering (DLS) instrument (Zetasizer ZS, Nanoseries ZEN 3600, Malvern Instruments Ltd., Malvern, UK, λ = 632.8 nm) (**Table S1**). All the samples were diluted up to a droplet concentration of approximately 0.025 wt% by using Milli-Q water. A detecting angle of 173° was used. A default refractive index ratio (1.5900) and three runs for each measurement (1 run lasting 100 s) were used in the calculations of the particle size

distribution. ζ -potential analysis was carried out by setting 30 runs for each measurement. Stability assay was performed with the same parameters up 30 days (**Table S2**).

CM-NEsoSome Characterization by Confocal and STED Microscopy

For STED analysis of fluorescent Ct-NEs, the samples are pre-pared by following a developed procedure²⁷. Each sample was diluted (a 1:10 dilution) with a 20 mM acetic acid buffer solution at pH 4 and was put in a FD3510 dish for 30 min to allow it to adhere to the surface of the dish. Then, three washes with a 5 wt% DABCO antifade solution were made and the sample observation was done by leaving the central part of the dish full of DABCO. DABCO antifade was needed to reduce the bleaching effects on the dyes. Samples were imaged using a Leica TCS SP5 STED-CW gated microscope (Leica-Microsystems, Mannheim, Germany). The resolution of the microscope was estimated to be <70 nm. The STED-CW beam power was 150 mW, measured at objective back focal plane and the time gate was 1.2 ns. For each different sample, 10 images were acquired and analysed by ImageJ[®] software (**Figure S4 A-D**). A number of nanoparticles >100 for both Ct-NEs and CM-NEsoSome were analysed by fitting their extracted profile by Gaussian. This approximation was performed to obtain the size value from the full width at half maximum (FWHM)⁴⁴. The same was performed for CM-NEsoSome, also adding a laser source of 543 nm to excite the Cell Mask[™] -543 used to monitor cell membrane shell.

Isolated cell membrane, Ct-NE and CM-NEsoSome Characterization by Cryo-TEM Microscopy

Cryo-TEM samples of isolated membranes obtained from glioblastoma multiform U87-MG cell line, Ct-NEs and CM-NEsoSomes 0.25 wt% oil were prepared by Plunge freezing technique by using the Vitrobot Mark IV (Fei Company). 3 μ L of each specimen were applied on 200 mesh quantifoil copper grid in Vitrobot chamber and subsequently reduced in volume by blotting for 1 s with filter paper to yield a final thin film about 100-200 nm in thickness. To prevent sample evaporation, the Vitrobot was settled to 95% humidity and 4°C with a waiting time of 60 s before plunging in liquid propane. After grid transfer in liquid nitrogen, each sample was mounted on Gatan Cryo holder, then observed by transmission electron microscope TECNAI G2-20 (Fei Company) equipped by Gatan CCD camera 2HS, in Cryo mode. The imaging was performed in low dose mode, at 200 KV in a range of magnification from 20000 to 50000.

Cell Viability Assessment

To evaluate CM-NEsoSome cytotoxic effects, cell survival was quantified by Alamar Blue Assay. 5×10^4 HDF cells per well were seeded in a 96-well plate. 24 h after seeding, cells were treated with cell culture medium alone, secondary NEs, cell membranes and CM-NEsoSome at three different time points and two concentrations. The tested times were 12, 24 and 48 h, while the chosen concentrations were 4% and 10% of nano-carrier.

Cell viability was evaluated by Alamar Blue assay. Briefly, after 12, 24 or 48 of incubation, samples were washed twice with PBS to remove the non-internalized compounds and then incubated for 3 h with a solution containing 10% of Alamar Blue cell viability reagent (Invitrogen) in cell culture medium. After incubation, supernatants were collected, and their fluorescence was measured at $\lambda_{\text{ex}} = 570 \text{ nm}$ and $\lambda_{\text{em}} = 610 \text{ nm}$ (Wallac Victor 1420, Perkinelmer), according to the manufacturer's procedure. Data were reported as the percentage of viable cells normalized to non-treated cells. All experiments were performed in triplicate.

Confocal Microscopy for NE uptake in HDF cells

5×10^4 HDF cells were seed on a 24 well plate. Cells were incubated with Ct-NE, CM *as is*, CM-NEsoSome and cell medium alone as positive control, at a final concentration of 10% of nanoemulsion for 12, 24 and 48 hours at 37 °C in 5% CO₂. Then, samples were washed two times with PBS to remove the non-internalized compounds and fixed with paraformaldehyde 4% for 20 min. Finally, cells were incubated with DRAQ5 (Abcam) diluted 1:1000 in PBS for 10 min at room temperature for cell nuclei staining. Samples were observed by confocal multiphoton microscope (Leica TCS SP5 MP, Solms, Germany) with a 25X water immersion objective. Images were acquired with a resolution of 1024 X 1024 pixels. All experiments were performed in triplicate.

3. Results and Discussion

Cell Membranes Extraction and Purification

Cell membranes were isolated from U87-MG according to the procedure reported by *Balasubramanian et al.*³⁰ with some modifications (**Scheme 1A-C**). The procedure consists in a gentle rupture of hypotonically swollen cells, evacuation of most of the cell contents by repeated washing, and isolation of cell membrane “ghosts” by a bunch of centrifugations at different

speeds, avoiding the final extrusion steps. The membrane extraction protocol was performed in triplicate to validate its reproducibility and the purity of the final sample. The pellet or the supernatants of each step of the purification process were observed by confocal microscopy. Indeed, prior to membrane extraction, cell nuclei (blue) (**Figure S1**), cell membrane glycoproteins (green) and plasma cell membranes (red) were stained. **Figure 1A** show that cell membranes integrity was preserved (red signal) as long as the presence of the glycoproteins (green signal). Moreover, images qualitatively show a good degree of purity of the final sample. For cell membrane deposition on nano-emulsion only the plasma cell membrane was stained (**Figure 1B and C**).

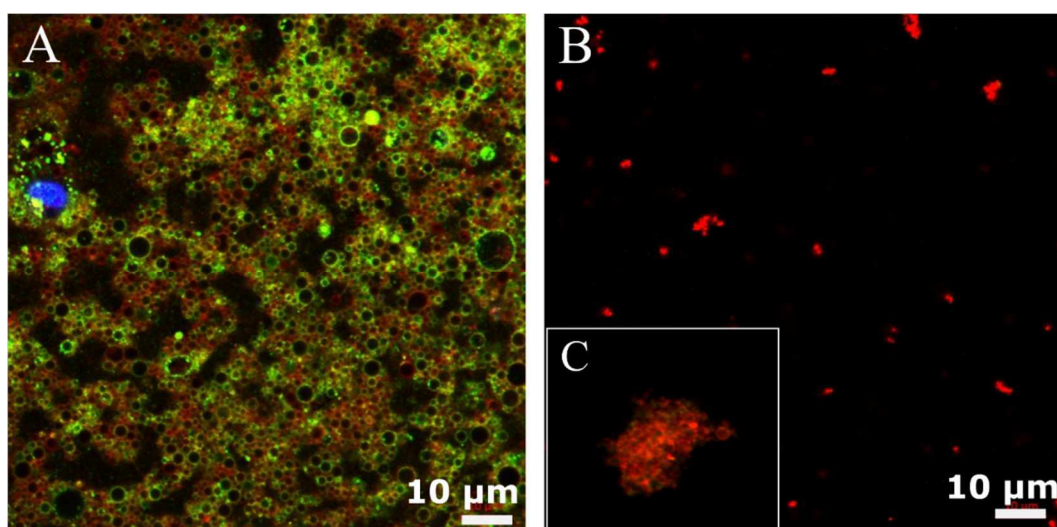


Figure 1. Confocal images of purified cell membrane; **(A)** cell membrane glycoproteins stained in **green** and plasma cell membranes stained in red, **(B)** isolated plasma cell membranes stained in red. **Inset C)** shows a zoom-in of a single extracted membrane in **Figure B**.

Moreover, in order to study the efficiency of the cell membrane extraction and purification process, together with the analysis of the correct secondary structure preserved by membrane proteins, a circular dichroism analysis was performed³¹.

Results, shown in **Figure S2**, underline two important aspects: i) the extraction and purification processes were performed in a correct way, indeed no DNA bands, usually found at 260 nm^{45,46}, were exposed and ii) ⁴⁷displaying a typical α -helix conformation with two shoulders, one negative at 205 nm and one positive at 190 nm which are typical feature of ellipticity. Same good results were obtained after the deposition process, as reported in Figure S2-blu spectrum,

membrane proteins retained their ellipticity showing the two principal α -helix related bands at 205 nm (negative peak) and 190 nm (positive peak).

CM-NEsoSome Preparation

As previously reported, O/W-NEs were employed as starting building blocks of CM-NEsoSome (**Scheme 1**). Our group has already demonstrated the ability of NEs to improve the bioavailability of lipophilic substances^{6,48}, making this system suitable as potential drug delivery system^{26,27} as well as diagnostic^{28,49,50}. In the present work we confer a new aptitude to our NE, making it a biomimetic system thanks to the addition of a cell membrane shell able to avoid the protein corona effects and obtain a specific delivery system for targeting tumour cells⁵¹. Secondary NEs (Ct-NEs) were obtained from primary emulsions coated with a layer of Ct, a positive biocompatible polyelectrolyte (**Scheme 1D-E**). Ct deposition is fundamental for the electrostatic deposition of cell membranes, it provides a positive charged surface able to establish an attractive interaction between positive Ct-NEs droplets and negative charged cell membranes (**Scheme 1F**). The cell membrane shell ($371.1 \pm 18.71 \mu\text{g}$ of membrane determined by Bicinchoninic Acid (BCA) assay as reported in **SI Figure S3**) was obtained by adapting a previous procedure^{24,25,27-29,49-52}. In particular, to obtain a system with the highest degree of monodispersion (**Figure 2**), a single extrusion cycle was added after the liquid – liquid interface technique, in contrast with the current methodologies⁵³.

CM-NEsoSome Characterization

Size, PDI and ζ -potential of Ct-NEs and CM-NEsoSomes were evaluated by DLS analysis, and the obtained results were reported in **Table S1**. A slight increase in terms of size and PDI was observed from Ct-NEs ($96.0 \pm 0.1 \text{ nm}$, 0.119 ± 0.02) to the final system ($105.9 \pm 0.66 \text{ nm}$, 0.088 ± 0.013) due to cell membrane shell around Ct-NEs confirming the correct deposition. Furthermore, the ζ -potential decreased in absolute value, from $+38.0 \pm 1.2 \text{ mV}$ for Ct-NEs to $+31.8 \pm 0.88 \text{ mV}$ for CM-NEsoSomes, stating even more the formation of the membrane shell on Ct-NEs (**Table S1**). CM-NEsoSomes dimensional stability over time was also evaluated by DLS analysis for 30 days (**Figure 2**). As reported in **Table S2** and **Figure S3-D**, the CM-NEsoSome stability was confirmed by a constant size; moreover, PDI values remained below the conventional stability rank of 0.1. A deepest morphological analysis of our systems was performed by STED and Confocal microscopy. Nanocarrier sizes were calculated as full width at half maximum

(FWHM) as detailed in SI. STED results revealed, in agreement with the DLS measurements, a size value of 120 nm for the Ct-NEs and 150 nm for the final system (**Figure S4A-D** and **Figure 2B-C**) underlying as our novel deposition approach is able to maintain the correct Ct-NE and membrane protein structure (**Figure S2**-pink spectrum). The efficacy of our system was also confirmed by confocal microscopy in which, as shown in **Figure 2F**, a perfect match between the green colour (related to FITC inside Ct-NEs) (**Figure 2D**) and red one (Cell Mask™-543 coloured cell membrane, **Figure 2E**) was revealed. In addition, a TEM analysis was performed. Samples were imaged by using Cryo-TEM technique in order to preserve their structure and integrity. **Figure 3A and B** show the isolated membranes and the Ct-NE morphology, respectively and were used as positive control. **Figure 3C** shows CM-NEsoSome which appears shape-rounded and homogenously dispersed, in agreement with the DLS data. Moreover, the inset in **Figure 3C** clearly show the presence of a layer on the nanoemulsion structure, further proving cell membrane deposition on the nanocarrier template, in accordance with the data reported in the confocal analyses.

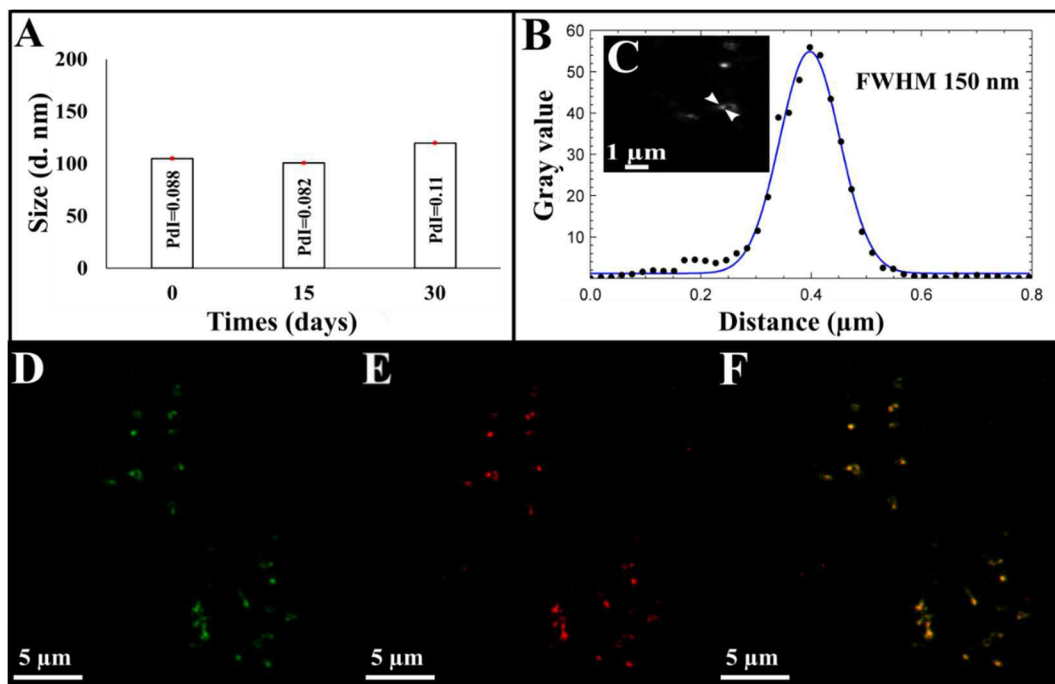


Figure 2. **A)** Stability of CM-NEsoSomes over the time by DLS analysis, **B)** corresponding line profile of CM-NEsoSome intensities by STED analysis: the black dots depicted in the panel show the intensities of the corresponding pixel values in the image, blue line is the Gaussian fit of the values. Nanocarrier size was extracted from image C, **C)** STED image of CM-NEsoSome (Scale bar 1 μm). Confocal images of CM-NEsoSomes **D)** green channel related to FITC signal of Ct-NEs, **E)** red channel signal of cell membrane,

F) overlay (Scale bar 5 μm).

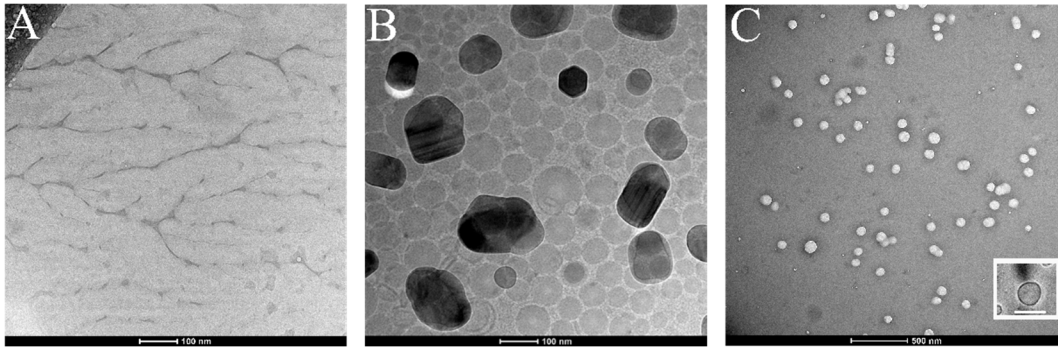


Figure 3. Cryo-TEM images of **A)** purified cell membrane, **B)** Ct-NE and **C)** CM-NEsoSome. Inset in panel C shows a single CM-NEsoSome at higher magnification; scale bar 100 nm.

CM-NEsoSome Biocompatibility Assessment

To verify nanocarrier biocompatibility, HDF (Human Dermal Fibroblast) were chosen as model line of healthy cells. HDF were incubated with the CM-NEsoSomes at a final nanoemulsion concentration of 4 and 10% for 12, 24 and 48 h. Moreover, the CM as is and the Ct-NE biocompatibility were also tested, at the same nanocarrier concentrations and incubation times, to further verify the biosafety of the nanocarrier components. Finally, cells were treated with cell medium alone as positive control. After incubation, a quantitative evaluation of cell viability (normalized to positive control, which is set to 100%) was obtained by Alamar Blue Assay (**Figure 4**). Data show that all the tested compounds do not affect cell viability considerably. The latter outcomes were obtained for all contact times and all concentrations.

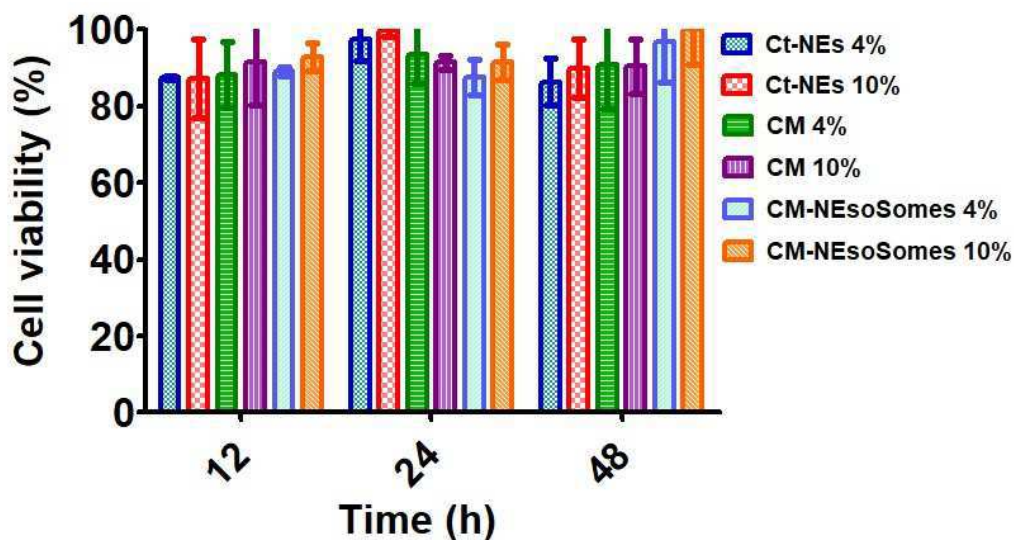


Figure 4. Cell Viability Assessment obtained by Alamar Blue Assay.

In addition, the nanocarrier uptake by HDF cells was confirmed by confocal microscopy. Cells were treated with cell culture medium alone (**Figure 5A-E-I**), Ct-NE (**Figure 5B-F-L**), CM as is (**Figure 5C-G-M**), and CM-NEsoSomes (**Figure 5D-H-N**) for 12, 24 and 48h at a final NE concentration of 10% wt. The FITC-loaded Ct-NE core is represented with a green signal, the CellMask™-543-tagged membrane is visualized using a red colour, while yellow hotspots show the merge of the two fluorophores in the same pixel. From a qualitative evaluation of the images, Ct-NE treated cells (**Figure 5B-F-L**) exhibit a spotted green signal emerging from the FITC-loaded NE that increases increasing the incubation time. A very low signal comes from the CM-as is treated cells, showing a very low uptake by cells which is probably due to the negative ζ -potential of the CM as-is (-18.5 ± 4.50 mV; data not shown). The latter findings are in agreement with the literature, indeed it is well known that the presence of positively charged groups on nanoparticles surface can enhance the *in vitro* cellular uptake, compared to negatively charged nanoparticles⁵⁴. Finally, the yellow spotted signal in **Figure 5D-H-N** originates from the colocalization of the red and green channels, suggesting that the CM-NEsoSome integrity is preserved in the extracellular environment until the internalization. These observations are consistent with those of the stability tests reported in **Table S2**. Moreover, even in this case, the fluorescence signal increases, increasing the incubation time suggesting a time-dependent uptake mechanism.

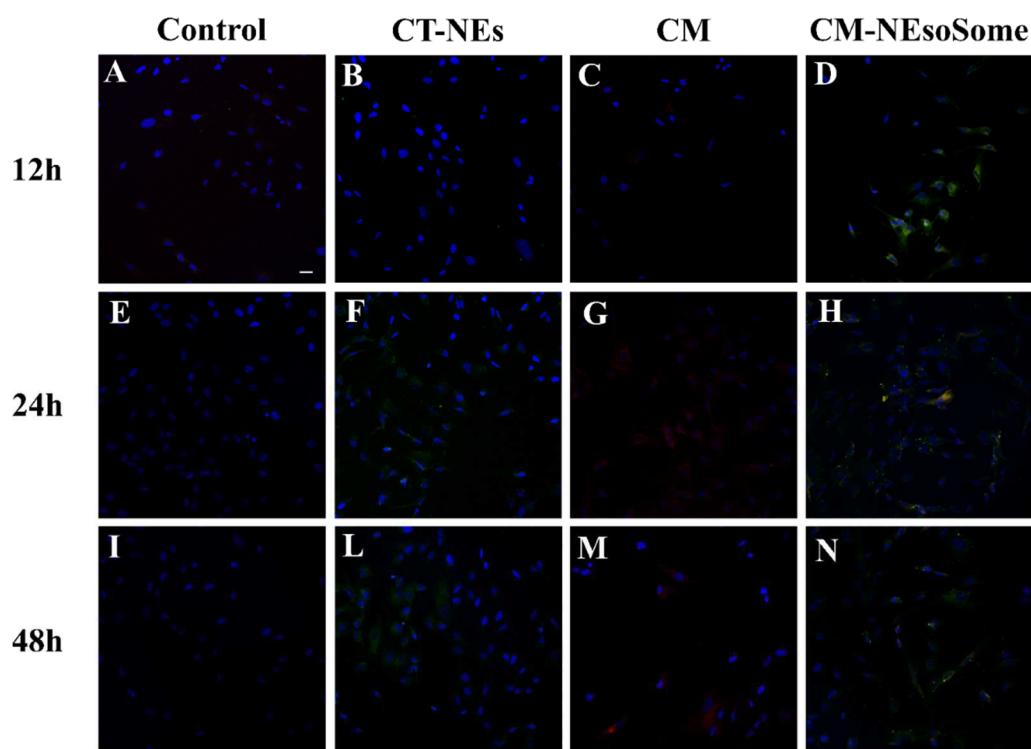


Figure 5. Confocal images of HDF uptake of cell medium alone (**A, E, I**), **CT-NEs (B, F L)**, **CM (C, G, M)** and **CM-NEsoSomes (D, H, N)** after 12, 24 and 48 h of incubation. Scale bar 30 μm .

Taken all together, these results show that the empty nanocarrier can be up taken by healthy cells without inducing cytotoxicity. This is a fundamental nanocarrier requirement to be assessed before moving to the applications, which in this case can range from the delivery of lipophilic drugs and biomolecules to the conveyance of lipophilic contrast agent compounds.

4. Conclusions

The developed nanocarrier is an innovative cell-derived biocompatible system able to combine the biological nature of cell membranes with the excellent synthetic properties of Ct-NEs in terms of stability and high drug encapsulation efficacy. These data highlight as the proposed purification and deposition process combined to the mechanical stability of the oil core template herein used could be a powerful tool in the field of biomimetic cell-membrane camouflaged nanocarriers. Indeed, the adopted purification and deposition strategy is quite gentle going beyond the limits of current processes that usually lead to protein degradation and instability⁵⁵ and it allows the use of oil core based nanocarriers, which opens to the conveyance of several

lipophilic compounds ranging from drugs and biomolecules to contrast agents compounds. Therefore, these results, even if preliminary, pave the way for the possible use of this biocompatible system for the treatment and diagnosis of several human diseases, including cancer as long as for vaccination¹⁶ and prevention from viral infection⁵⁶.

5. Supplementary Information

The following are available online at www.mdpi.com/xxx/s1, **Figure S1**: Cell nuclei (**blue**) contained in the first pellet of the purification process., **Figure S2**: Overlay of CD spectra of: **pink**) bare membrane after extraction and purification processes (371.1 μ g) and **blue**) cell membrane proteins deposited on Ct-NE (150 μ g). **Figure S3**: Cell membrane quantification by BCA assay. Titration curve. **Table S1**: Size, PDI and ζ -potential data of Ct-NEs and CM-NEsoSome. **Table S2**: Size and PDI of CM-NEsoSome over time obtained by DLS analysis. Data are expressed as mean \pm SD (n=3). **Figure S4**: STED analysis of Ct-NE (**A-B**) and CM-NEsoSome (**C-D**). **A-C**) STED images, **B-D**) Deconvolution spectra analysis by ImageJ® software extracted respectively from images **A-C**. For the confocal analysis, the images were acquired with a confocal microscope (Leica Microsystems TCS SP5 II, Germany). Laser source of 488 nm was used to excite the FITC in oil core.

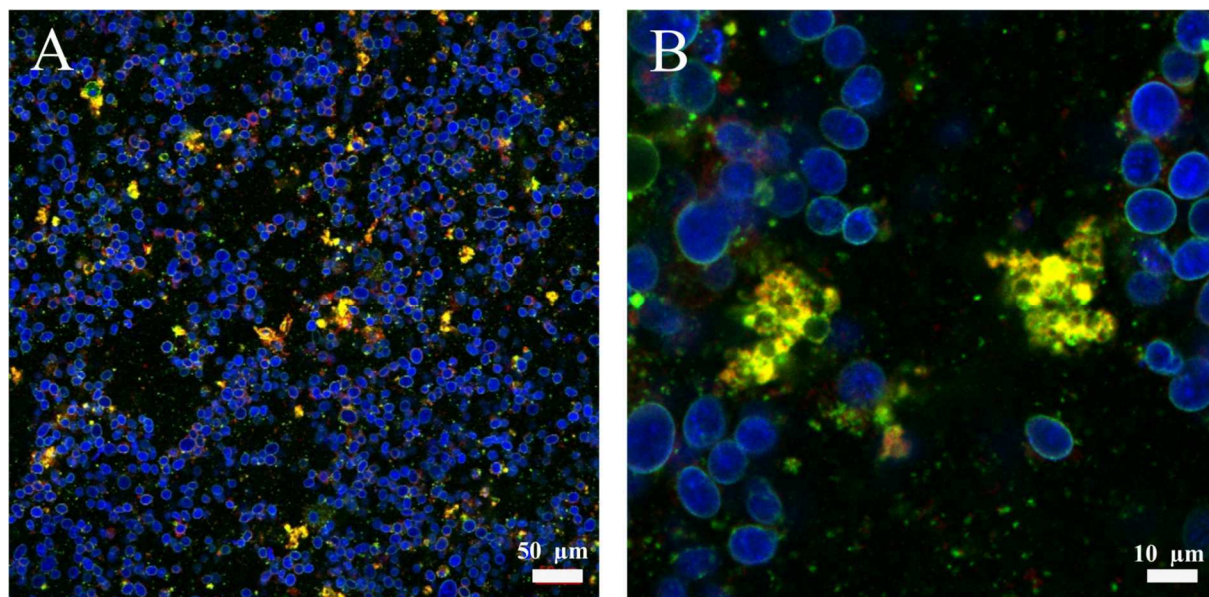


Figure S1. Cell nuclei (blue) contained in the first pellet of the purification process.

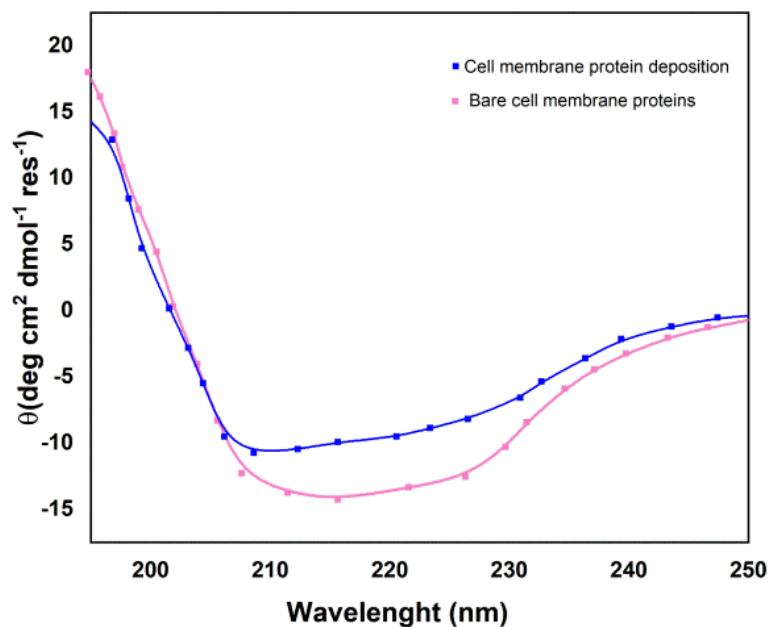


Figure S2. Overlay of CD spectra of **pink**) bare membrane after extraction and purification processes (371.1 μ g) and **blue**) cell membrane proteins deposited on Ct-NE (150 μ g).

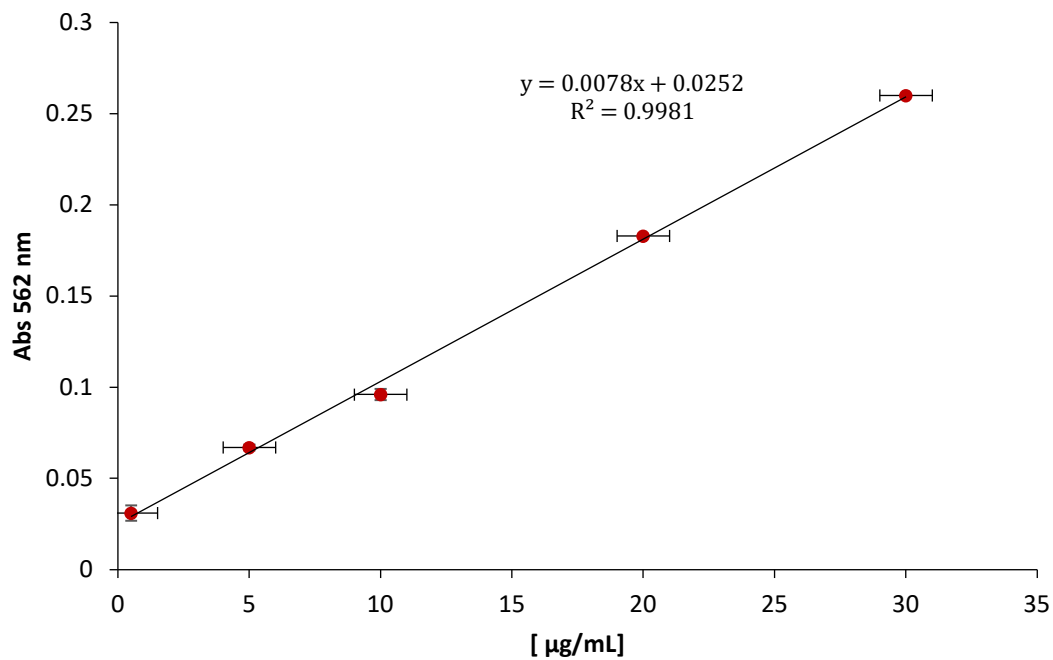


Figure S3. Cell membrane quantification by BCA assay. Titration curve.

Table S1. Size, PDI and ζ -potential data of Ct-NEs and CM-NEsoSome

Samples	Size /d. nm	PDI	ζ-potential / mV
Ct-NEs	96.0 \pm 0.1	0.119 \pm 0.02	+38.0 \pm 1.2
CM-NEsoSome	105.9 \pm 0.66	0.088 \pm 0.013	+31.8 \pm 0.88

Table S2. Size and PDI of CM-NEsoSome over time obtained by DLS analysis. Data are expressed as mean \pm SD (n=3).

Time / days	Size /d. nm	Pdl
0	105.9 \pm 0.66	0.088 \pm 0.013
1	108.0 \pm 4.71	0.086 \pm 0.02
7	105.5 \pm 0.089	0.089 \pm 0.010
15	100.8 \pm 0.55	0.082 \pm 0.09
30	119.8 \pm 1.02	0.118 \pm 0.017

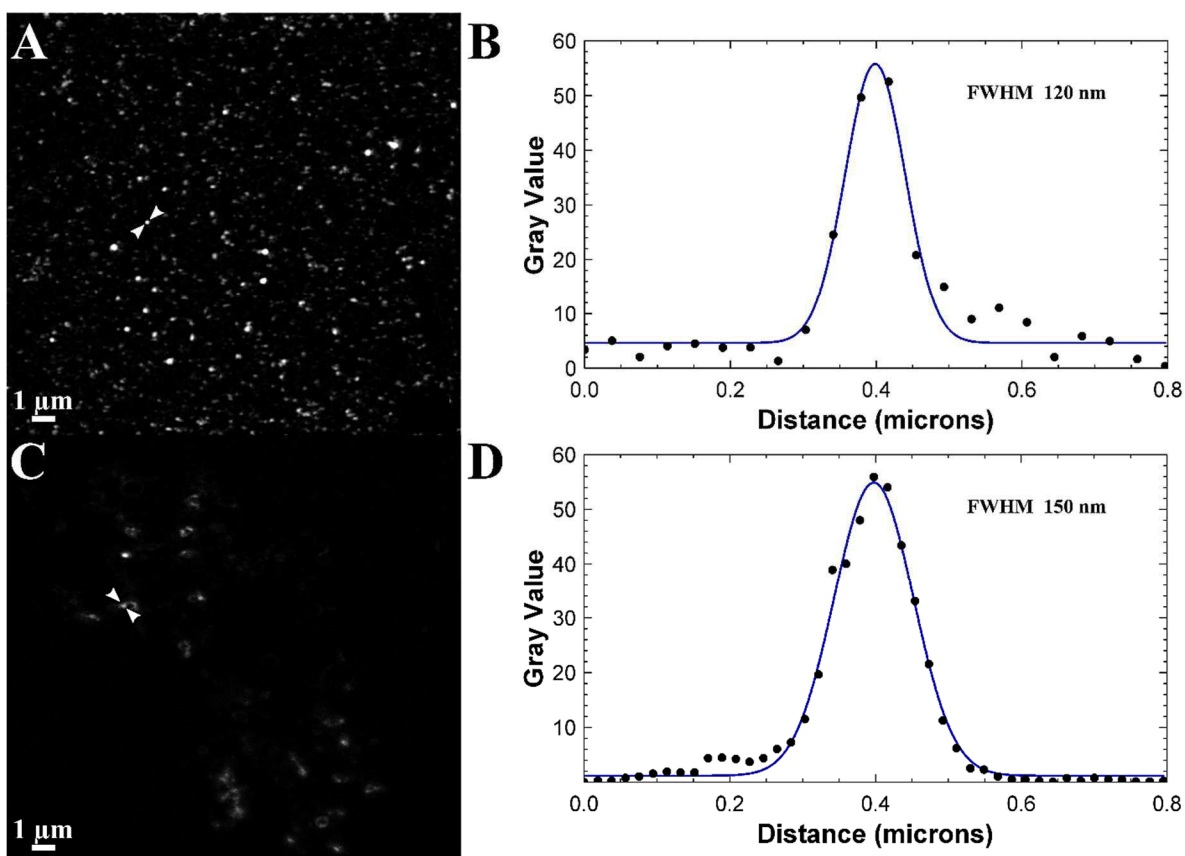


Figure S4. STED analysis of Ct-NE (A-B) and CM-NEsoSome (C-D). A-C) STED images, B-D) Deconvolution spectra analysis by ImageJ® software extracted respectively from images A-C.

For the confocal analysis, the images were acquired with a confocal microscope (Leica Microsystems TCS SP5 II, Germany). Laser source of 488 nm was used to excite the FITC in oil core.

Author Contributions: “Conceptualization, R.V.; methodology, R.V., C.D.N., M.P., E.L., V.M; investigation, M.P., C.D.N, E.L., V.M; data curation, C.D.N, M.P., E.L., V.M.; writing—original draft preparation M.P.,C.D.N, E.L; writing—review and editing, R.V. C.D.N, M.P., E.L., V.M.; visualization, C.D.N, M.P., E.L.; supervision, R.V., P.A.N. All authors have read and agreed to the published version of the manuscript.”

Acknowledgments: The authors want to thank Dr. Fabio Formiggini for his support in confocal imaging.

References

- 1 McClements, D. J. Nanoemulsion-based oral delivery systems for lipophilic bioactive components: nutraceuticals and pharmaceuticals. *Therapeutic delivery* **4**, 841-857 (2013).
- 2 Iaccarino, G., Profeta, M., Vecchione, R. & Netti, P. A. Matrix Metalloproteinase-Cleavable Nanocapsules for Tumor-Activated Drug Release. *Acta biomaterialia* (2019).
- 3 Blanco, E., Shen, H. & Ferrari, M. Principles of nanoparticle design for overcoming biological barriers to drug delivery. *Nature biotechnology* **33**, 941 (2015).
- 4 Fotticchia, T. *et al.* Enhanced drug delivery into cell cytosol via glycoprotein H-derived peptide conjugated nanoemulsions. *ACS nano* **11**, 9802-9813 (2017).
- 5 Iaccarino, G., Profeta, M., Vecchione, R. & Netti, P. A. Matrix metalloproteinase-cleavable nanocapsules for tumor-activated drug release. *Acta Biomaterialia* **89**, 265-278 (2019).
- 6 Vecchione, R. *et al.* Curcumin bioavailability from oil in water nano-emulsions: In vitro and in vivo study on the dimensional, compositional and interactional dependence. *Journal of Controlled Release* **233**, 88-100 (2016).
- 7 Ganta, S., Talekar, M., Singh, A., Coleman, T. P. & Amiji, M. M. Nanoemulsions in translational research—opportunities and challenges in targeted cancer therapy. *Aaps Pharmscitech* **15**, 694-708 (2014).
- 8 Di Natale, C., De Benedictis, I., De Benedictis, A. & Marasco, D. Metal–Peptide Complexes as Promising Antibiotics to Fight Emerging Drug Resistance: New Perspectives in Tuberculosis. *Antibiotics* **9**, 337 (2020).
- 9 Rao, L. *et al.* Erythrocyte membrane-coated upconversion nanoparticles with minimal protein adsorption for enhanced tumor imaging. *ACS applied materials & interfaces* **9**, 2159-2168 (2017).
- 10 Kroll, A. V., Fang, R. H. & Zhang, L. Biointerfacing and applications of cell membrane-coated nanoparticles. *Bioconjugate chemistry* **28**, 23-32 (2017).
- 11 Chen, Z. *et al.* Cancer cell membrane–biomimetic nanoparticles for homologous-targeting dual-modal imaging and photothermal therapy. *ACS nano* **10**, 10049-10057 (2016).

- 12 Gao, W. *et al.* Surface functionalization of gold nanoparticles with red blood cell membranes. *Advanced Materials* **25**, 3549-3553 (2013).
- 13 Chai, Z. *et al.* A facile approach to functionalizing cell membrane-coated nanoparticles with neurotoxin-derived peptide for brain-targeted drug delivery. *Journal of Controlled Release* **264**, 102-111 (2017).
- 14 Fang, R. H., Jiang, Y., Fang, J. C. & Zhang, L. Cell membrane-derived nanomaterials for biomedical applications. *Biomaterials* **128**, 69-83 (2017).
- 15 Bose, R. J., Paulmurugan, R., Moon, J., Lee, S.-H. & Park, H. Cell membrane-coated nanocarriers: the emerging targeted delivery system for cancer theranostics. *Drug Discovery Today* **23**, 891-899 (2018).
- 16 Gao, W. *et al.* Modulating antibacterial immunity via bacterial membrane-coated nanoparticles. *Nano letters* **15**, 1403-1409 (2015).
- 17 Hu, C.-M. J. *et al.* Erythrocyte membrane-camouflaged polymeric nanoparticles as a biomimetic delivery platform. *Proceedings of the National Academy of Sciences* **108**, 10980-10985 (2011).
- 18 Jakobsson, U. *et al.* Preparation and in vivo evaluation of red blood cell membrane coated porous silicon nanoparticles implanted with ¹⁵⁵Tb. *Nuclear Medicine and Biology* (2020).
- 19 Pang, Z. *et al.* Detoxification of organophosphate poisoning using nanoparticle bioscavengers. *ACS nano* **9**, 6450-6458 (2015).
- 20 Zhang, J., Gao, W., Fang, R. H., Dong, A. & Zhang, L. Synthesis of Nanogels via Cell Membrane-Templated Polymerization. *Small* **11**, 4309-4313 (2015).
- 21 Rao, L. *et al.* Microfluidic electroporation-facilitated synthesis of erythrocyte membrane-coated magnetic nanoparticles for enhanced imaging-guided cancer therapy. *ACS Nano* **11**, 3496-3505 (2017).
- 22 Silva, A. K. A. *et al.* Cell-derived vesicles as a bioplatfrom for the encapsulation of theranostic nanomaterials. *Nanoscale* **5**, 11374-11384 (2013).
- 23 Kaneda, M. M., Sasaki, Y., Lanza, G. M., Milbrandt, J. & Wickline, S. A. Mechanisms of nucleotide trafficking during siRNA delivery to endothelial cells using perfluorocarbon nanoemulsions. *Biomaterials* **31**, 3079-3086 (2010).
- 24 Quagliariello, V. *et al.* Cardioprotective effects of nanoemulsions loaded with anti-inflammatory nutraceuticals against doxorubicin-induced cardiotoxicity. *Nutrients* **10**, 1304 (2018).
- 25 Quagliariello, V. *et al.* Nano-encapsulation of coenzyme Q10 in secondary and tertiary nano-emulsions for enhanced cardioprotection and hepatoprotection in human cardiomyocytes and hepatocytes during exposure to anthracyclines and trastuzumab. *International Journal of Nanomedicine* **15**, 4859 (2020).
- 26 Vecchione, R. *et al.* Tunable stability of monodisperse secondary O/W nano-emulsions. *Nanoscale* **6**, 9300-9307 (2014).
- 27 Vecchione, R. *et al.* Ultrastable liquid-liquid interface as viable route for controlled deposition of biodegradable polymer nanocapsules. *Small* **12**, 3005-3013 (2016).

- 28 Jakhmola, A. *et al.* Bioinspired oil core/silica shell nanocarriers with tunable and multimodal functionalities. *Advanced healthcare materials* **4**, 2688-2698 (2015).
- 29 Vecchione, R. *et al.* Multilayered silica-biopolymer nanocapsules with a hydrophobic core and a hydrophilic tunable shell thickness. *Nanoscale* **8**, 8798-8809 (2016).
- 30 Balasubramanian, V. *et al.* Biomimetic engineering using cancer cell membranes for designing compartmentalized nanoreactors with organelle-like functions. *Advanced Materials* **29**, 1605375 (2017).
- 31 Miles, A. J. & Wallace, B. A. Circular dichroism spectroscopy of membrane proteins. *Chemical society reviews* **45**, 4859-4872 (2016).
- 32 Di Natale, C. *et al.* Design of biodegradable bi-compartmental microneedles for the stabilization and the controlled release of the labile molecule collagenase for skin healthcare. *Journal of Materials Chemistry B*, doi:10.1039/D0TB02279A (2020).
- 33 Di Natale, C. *et al.* Engineered β -hairpin scaffolds from human prion protein regions: Structural and functional investigations of aggregates. *Bioorganic Chemistry* **96**, 103594 (2020).
- 34 Di Natale, C. *et al.* Effects of surface nanopatterning on internalization and amyloid aggregation of the fragment 264-277 of Nucleophosmin 1. *Colloids and Surfaces B: Biointerfaces* **197**, 111439 (2020).
- 35 Di Natale, C. *et al.* Molecularly endowed hydrogel with an in silico-assisted screened peptide for highly sensitive small molecule harvesting. *Chemical Communications* **54**, 10088-10091 (2018).
- 36 Di Natale, C. *et al.* Proteostasis unbalance of nucleophosmin 1 in Acute Myeloid Leukemia: An aggregomic perspective. *International Journal of Biological Macromolecules* (2020).
- 37 Di Natale, C. *et al.* Engineered β -hairpin scaffolds from human prion protein regions: structural and functional investigations of aggregates. *Bioorganic Chemistry*, 103594 (2020).
- 38 Di Natale, C. *et al.* Structural insights into amyloid structures of the C-terminal region of nucleophosmin 1 in type A mutation of acute myeloid leukemia. *Biochimica et Biophysica Acta (BBA)-Proteins and Proteomics* **1867**, 637-644 (2019).
- 39 Di Natale, C. *et al.* Nucleophosmin contains amyloidogenic regions that are able to form toxic aggregates under physiological conditions. *The FASEB Journal* **29**, 3689-3701 (2015).
- 40 Celetti, G., Di Natale, C., Causa, F., Battista, E. & Netti, P. A. Functionalized poly (ethylene glycol) diacrylate microgels by microfluidics: In situ peptide encapsulation for in serum selective protein detection. *Colloids and Surfaces B: Biointerfaces* **145**, 21-29 (2016).
- 41 Jamaledin, R. *et al.* Recombinant Filamentous Bacteriophages Encapsulated in Biodegradable Polymeric Microparticles for Stimulation of Innate and Adaptive Immune Responses. *Microorganisms* **8**, 650 (2020).
- 42 Bainor, A., Chang, L., McQuade, T. J., Webb, B. & Gestwicki, J. E. Bicinchoninic acid (BCA) assay in low volume. *Analytical Biochemistry* **410**, 310-312, doi:<https://doi.org/10.1016/j.ab.2010.11.015> (2011).

- 43 Walker, J. M. in *Basic Protein and Peptide Protocols* (ed John M. Walker) 5-8 (Humana Press, 1994).
- 44 Šileikaitė, A., Puišo, J., Prosyčevas, I. & Tamulevičius, S. Investigation of silver nanoparticles formation kinetics during reduction of silver nitrate with sodium citrate. *Materials Science (Medžiagotyra)* **15**, 21-27 (2009).
- 45 Musumeci, D. *et al.* DNA-based strategies for blocking HMGB1 cytokine activity: design, synthesis and preliminary in vitro/in vivo assays of DNA and DNA-like duplexes. *Molecular bioSystems* **7**, 1742-1752 (2011).
- 46 Roviello, G. N. & Musumeci, D. Correction: Synthetic approaches to nucleopeptides containing all four nucleobases, and nucleic acid-binding studies on a mixed-sequence nucleo-oligolysine. *RSC advances* **6**, 78486-78486 (2016).
- 47 Keles, H., Naylor, A., Clegg, F. & Sammon, C. Studying the release of hGH from gamma-irradiated PLGA microparticles using ATR-FTIR imaging. *Vibrational Spectroscopy* **71**, 76-84, doi:<https://doi.org/10.1016/j.vibspec.2014.01.012> (2014).
- 48 Langella, A. *et al.* In vitro study of intestinal epithelial interaction with engineered oil in water nanoemulsions conveying curcumin. *Colloids and Surfaces B: Biointerfaces* **164**, 232-239 (2018).
- 49 Calcagno, V. *et al.* Oil core–PEG shell nanocarriers for in vivo MRI imaging. *Advanced healthcare materials* **8**, 1801313 (2019).
- 50 Vecchione, R. *et al.* Oil/water nano-emulsion loaded with cobalt ferrite oxide nanocubes for photo-acoustic and magnetic resonance dual imaging in cancer: In vitro and preclinical studies. *Nanomedicine: Nanotechnology, Biology and Medicine* **13**, 275-286 (2017).
- 51 Zhai, Y. *et al.* Preparation and Application of Cell Membrane-Camouflaged Nanoparticles for Cancer Therapy. *Theranostics* **7**, 2575-2592, doi:10.7150/thno.20118 (2017).
- 52 Ban, C. *et al.* Enhancing the oral bioavailability of curcumin using solid lipid nanoparticles. *Food chemistry* **302**, 125328, doi:10.1016/j.foodchem.2019.125328 (2020).
- 53 Frisken, B., Asman, C. & Patty, P. Studies of vesicle extrusion. *Langmuir* **16**, 928-933 (2000).
- 54 Guarnieri, D., Malvindi, M. A., Belli, V., Pompa, P. P. & Netti, P. Effect of silica nanoparticles with variable size and surface functionalization on human endothelial cell viability and angiogenic activity. *Journal of nanoparticle research* **16**, 2229 (2014).
- 55 Drachuk, I., Gupta, M. & Tsukruk, V. Biomimetic Coatings to Control Cellular Function through Cell Surface Engineering. *Advanced Functional Materials* **23**, 4437-4453, doi:10.1002/adfm.201300038 (2013).
- 56 Rao, L. *et al.* A biomimetic nanodecoy traps zika virus to prevent viral infection and fetal microcephaly development. *Nano letters* **19**, 2215-2222 (2018).

© 2020 by the authors. Licensee MDPI, Basel, Switzerland. This article is an open access article distributed under the terms and conditions of the Creative Commons Attribution (CC BY) license (<http://creativecommons.org/licenses/by/4.0/>).

Chapter 3: Macrophage biomimetic NEsoSome for inflamed tissue selective targeting.

This project was carried out in collaboration with Prof. Pasquale Maffia, Prof. Armando Ialenti and Dr. Elisabetta Caiazzo from the Department of Pharmacy, University Federico II of Naples and School of Infection & Immunity, University of Glasgow (UK).

Abstract

By taking inspiration from nature, the biomimetic approach has been involved into drug nanocarriers (NCs) development for the active targeting of various diseases thus ranging from cancer therapy to neuronal disease and inflammation disease. This success is related to the capability to endow the inner nanomaterials with the biological identity and some of the functions of the cells from whom they are derived. Recently, macrophage membrane coated nanomaterials emerged as an ideal delivery system to target the inflamed vascular tissue as the atherosclerotic plaques. Herein, we developed two biomimetic NCs using THP-1 and Phorbol 12-myristate 13-acetate (PMA) differentiated THP-1 (M0) as membrane sources to obtain respectively monocyte and macrophage ones. We used as inner core a secondary oil in water nanoemulsion (SNE) which already reported to retain good plasma circulating stability and the capability of increasing the payload of lipophilic compounds. Two different biomimetic systems were produced, joining the biomimetic features coming from biological membrane with the physio-chemical and nano sized characteristic of SNEs. These systems were named: Monocyte NEsoSome (M-NEsoSome) and Macrophage NEsoSome (M0-NEsoSome). Their uptake ability was evaluated in a tumour Necrosis Factor α (TNF α) treated HUVEC cell layer, elected as a model to inflamed endothelial cells. In agreement with the expectations, M0 membrane coating provides a faster internalization compared to the monocyte one and the bare NCs. In conclusion, M0-NEsoSome NCs could be a potential therapeutic system for the targeted delivery of anti-inflammatory drug in the atherosclerotic site.

1. Introduction

Atherosclerosis (AS) is the main pathological cause of coronary heart disease (CHD). Traditional oral treatments (as statins, antiplatelet, and vasodilators) demonstrated some

limitations for a AS therapy due to their non-specific distribution, poor water solubility and poor bioavailability. Additionally, long-term therapy may produce significant side effects, as liver damage, muscle pain, and diabetes mellitus. The spread of nanotechnologies in drug delivery development has put nano-carriers (NCs) as promising approach for AS therapy¹. The reasons behind the great success of NCs can be related to the many advantages of the improvement of drug bioavailability and long-term stability. In detail, NCs showed a passive targeting attitude for dysfunctional endothelial cells, since they are able to specifically distribute in plaques through permeable endothelial cells (ECs) or dysfunctional neovascularization, defeating the limitations of traditional oral drugs². Nevertheless, the passive targeted effect of NCs may still be not sufficient for effective and safe therapeutic standards of heterogeneous AS therapy. Recently, formulators proposed several types of NCs able to target the lesion sites by binding with different receptors including intercellular cell adhesion molecule 1 (ICAM-1), vascular cell adhesion protein 1 (VCAM-1), integrin $\alpha_v\beta_3$, and P-selectin¹. However, considerable challenges remain in targeting efficiency and controllable drug release at the lesion sites^{3,4}. It should be considered that a valid drug delivery system should be able to evade the immune system, have an extended blood circulation and accumulation in the targeted selected tissues⁵. A biomimetic delivery technology utilizes immune evasion and intracellular uptake strategies of pathogens such as viruses^{6,7} and bacteria⁸. This technology seeks to overcome the limitations of drug delivery systems by learning the lesson from biological elements. In detail, circulating cells of the immune system (leukocytes, macrophages) have all these properties since they are involved in the immune response mechanisms⁹.

Thanks to these innate properties, the researchers proposed the assembly of leukocyte membrane derived NC which proved to be able to evade the immune system, cross the biological barriers of the body and localize the target tissues¹⁰. Among immune system cells, macrophage have a crucial role in several diseases, including cancer, atherosclerosis, rheumatoid arthritis, infection, and inflammation, due to the recognition and engulfment function of removing substances and pathogens^{11,12}. In detail, macrophages play a significant role in the pathogenesis of AS by promoting plaque formation¹³. The “*homing*” into AS lesions is due to the expression of integrin $\alpha_4\beta_1$ which can actively bind to VCAM-1 highly expressed in the inflamed endothelium¹⁴. As consequence, the macrophage membrane could be employed to target inflamed tissue or tumour sites exploiting the recognition of antigens. In literature, there are reported several types of macrophage derived NCs which demonstrate to protect synthetic nanoparticles from

phagocytosis by macrophages and targeted activated ECs *in vitro*¹⁴. Moreover, macrophage coated nanoparticles demonstrated to efficiently target and accumulate in lesions *in vivo*. At the present, macrophage membrane-camouflaged nanoparticles are in the embryonic phase of development, there is huge potential and challenge to explore the conversion mode in the clinic¹⁵. The aim of this work has been the development of oil in water secondary nanoemulsions (O/W SNEs) with a macrophage membrane layer able to retain the properties of cell source and target the inflamed atherosclerotic plaque. The O/W SNEs are a well-established nano-delivery system for the delivery of lipophilic substances¹⁶⁻²¹. SNEs represent a raw material that could be easily modified for different applications. SNEs could be the starting building block for multilayer nanoemulsions^{22,23} and its properties are related to the selected coating strategies (i.e. stimuli responsive system^{24,25}, active targeting²⁶, blood brain barrier (BBB) overcoming²⁷). We referred to this type of NC with term NEsoSome to highlight this nanosized features joined with is lipophilic soul with the ability to carry both internal and external cargos. In 2021, we proposed a CM-NEsoSome as biomimetic NC provided of a cancer cell membrane layer, which showed a good stability and with the potential to be a suitable NC for tumour targeting²⁸. In this context, we focused the attention on the development of biomimetic nanoemulsions to reach AS plaques and to selectively be internalized by the inflamed endothelin cells. With this aim, we decided to assemble two biomimetic NCs employing monocyte and macrophage membranes as external layers. We selected THP-1 as human monocyte cell line to obtain human macrophages membranes. THP-1 cells could be differentiated into macrophage-like cells (THP-1 macrophages) by incubation with phorbol 12-myristate-13-acetate (PMA), which leads to a macrophage-like phenotype. Therefore, THP-1 cells were activated at macrophages to express cell membrane markers and exploit macrophage “*homing*” and an active targeting toward AS lesions. The two systems were assembled employing THP-1 and PMA differentiated THP-1 as membrane sources, respectively for monocyte (M) and an unpolarized macrophage (M0) NEsoSome, indicted as M-NEsoSome and M0-NEsoSome. The systems were morphologically analysed by dynamic light scattering (DLS), ζ -potential and cryo electron transmission microscopy (Cryo-TEM). The uptake ability of the systems was evaluated in a Tumour Necrosis Factor α (TNF α) treated HUVEC cell layer, elected as a model of inflamed ECs by confocal microscopy.

2. Material and methods

Materials

Surfactant Lipoid E80 (egg lecithin powder 80%–85% enriched with phosphatidyl choline (PC) and 7%–9.5% content in phosphatidyl ethanolamine (PE)) were purchased from Lipoid GmbH. Millipore Milli-Q water was used for the preparation of all nano-emulsions and solutions. Soybean oil (density at 20 °C of 0.922 g mL⁻¹) and Fluorescein-isothiocyanate (FITC) and chitosan (Ct, LMW 90–150 kDa, DDA 84% determined via ¹H-NMR) were purchased from Sigma Aldrich (Milan, Italy). Hoechst 33342, Trihydrochloride, Trihydrate (Hoechst), CellMask™ Orange plasma membrane stain (CellMask™-543) were purchased from Thermo Fisher Scientific. Phosphate-buffered saline (PBS), Glutaraldehyde, sodium cacodylate, osmium tetroxide, potassium ferrocyanide, Spuur's resin, uranyl acetate, copper grids were purchased from electron microscopy sciences. Ethanol and tannic acid were purchased from Merck.

RPMI-1640 (Gibco), Fetal Bovine Serum (FBS, Gibco), antibiotics (glutamine, 100 U/mL penicillin, 100 mg mL⁻¹ streptomycin, Gibco), Phorbol 12-myristate 13-acetate (PMA) were purchased Thermo Scientific Chemicals. Vasculife® VEGF Endothelial Medium Complete Kit were purchased from Lifeline cell Technologies. Sodium pyruvate, 2-Mercaptoethanol and Gelatin were purchased from Merck.

Cells Culture

THP1 Culture and Activation to Unpolarized macrophages

THP-1 cells, passage 3, were seeded at a density of 5x10⁵ cells/mL with RPMI-1640 supplemented with 10% inactivated Fetal Bovine Serum (FBS), 1% of antibiotics (glutamine, 100 U/mL penicillin, 100 mg mL⁻¹ streptomycin), 1 mM sodium pyruvate and 0.05 mM 2-mercaptoethanol. Cells were sub-cultured in T75 cell culture flask for membrane extraction, in a humidified controlled atmosphere with 5% of CO₂, at 37 °C. The medium was changed every 2-3 days. For differentiation in unpolarized macrophages, namely M0, and membrane extraction, cells were seeded in a 6-well plate and treated with 50 ng phorbol 12-myristate 13-acetate (PMA) for 16 h followed by 48 h resting to obtain M0²⁹ (**Figure 1**).

Cell differentiation after PMA treatment was verified by evaluating cell adhesion and spreading under an optical microscope. More in detail, cell differentiations were estimated by Invitrogen™ EVOS™ Digital Color Fluorescence Microscope and Transmission Electron Microscope (TEM) analysis for both suspension cells (PMA free THP-1, M) and adherent cells (PMA differentiated THP-1, M0). Prior to plasma membrane extraction, both PMA differentiated and undifferentiated cells from THP-1 were treated with phosphate-buffered saline (PBS) solution containing 0.01% of Hoechst, and 0.1% of CellMask™ -543 was added to each flask / plate for 10 min to stain nuclei and plasma membrane and washed with PBS.

Transmission electron microscopy (TEM analysis)

Monocytes (PMA-free THP-1, M) were centrifuged at 1200 rpm for 5 min in each washing/changing media step. Macrophages (differentiated THP-1, M0) sample preparation was conducted in Petri dish for all steps, then scraped and centrifuged at 1200 rpm for 5 min before dehydration step.

Samples were fixed in 2.5% glutaraldehyde in 0.1M sodium cacodylate buffer at 4°C overnight, then washed in the same buffer three times (5 min each step) and post fixed in a solution of 1% osmium tetroxide/1% potassium ferrocyanide in sodium cacodylate for 1 h at 4°C. After 3 washing in sodium cacodylate, specimens were stained with 1% uranyl acetate aqueous solution (electron microscopy sciences) overnight at 4°C, in the dark. The next day after washing in chilled water, specimens were incubated with 0.15% tannic acid aqueous solution for 3 min then rinsed again in chilled distilled water before dehydration. The dehydration was carried out by using ascending series of ethanol (30°, 50°, 70°, 95° (two times) 100° (three times)) for 10 min for each step on ice. The last step in ethanol was performed at room temperature before overnight infiltration in 1:1 Spurr's resin/ethanol mixing. Samples were embedded in fresh Spurr's resin for 2 days before polymerization at 70°C. Each sample was cut with a diamond knife (diatome) at an ultramicrotome FC7-UC5 Leica (thickness 80 nm) and collected on 200 mesh thin bar copper grids. The imaging was performed by using TEM Tecnai G2, 20_Thermofisher Company equipped by Veleta side-view camera, at 120 KV in a range of magnification between 5KX and 50 KX.

HUVECs Culture

HUVEC cells, passage 4, were grown with VascuLife® VEGF Endothelial Medium Complete Kit in T-75 cell culture flask treated for 30 min with 1% (w/v) gelatine, in a humidified controlled atmosphere with 5% of CO₂, at 37 °C. The medium was changed every 2-3 days. To obtain inflamed cell layer, HUVECs were cultured in 8-well and treated with TNF α (Sigma-Aldrich) for 24h. The 8-wells were pre-treated with 1% (w/v) gelatine (Sigma-Aldrich) for 30 min.

Membrane extraction and characterization

Plasma membranes were isolated from the PMA differentiated THP-1 cells or M0 and as control from PMA free THP-1 cells or M, according to the procedure reported by *Profeta et al.* with some modifications³⁰ after cell staining. Briefly, monocyte cells (M) were washed with PBS collect by centrifuge at 1200 rpm for 5 min, then suspended in hypotonic lysing buffer at a 1:10 ratio pellet/lysis buffer. Macrophage adherent cells were detached with a cell scraper, washed with PBS and collect by centrifuge at 1200 rpm for 5 min, then suspended in hypotonic lysing buffer at a 1:10 ratio pellet/lysis buffer. The lysis buffer was composed as follows: 20 mM Tris-HCl pH 7.5; 10 mM KCl, 2 mM MgCl₂ and 20 mM sucrose. Both cell types were disrupted by pipetting them thoroughly and spinning the solution at 3.200 $\times g$ for 5 min. The resulting pellets was dissolved again in the hypotonic lysing buffer solution, pipetted, and spun down by centrifugation at 3.200 $\times g$ for 6 min. After that, the supernatants were collected, mixed, and centrifuged at 20.000 $\times g$ for 20 min at 4 °C. M and M0 membrane pellets were obtained by a final 100.000 $\times g$

at 4 °C for 15 min. The pellet redispersed in 1 mL of PBS 1x, characterized, and used as purified M and M0 membrane for the subsequent experiments.

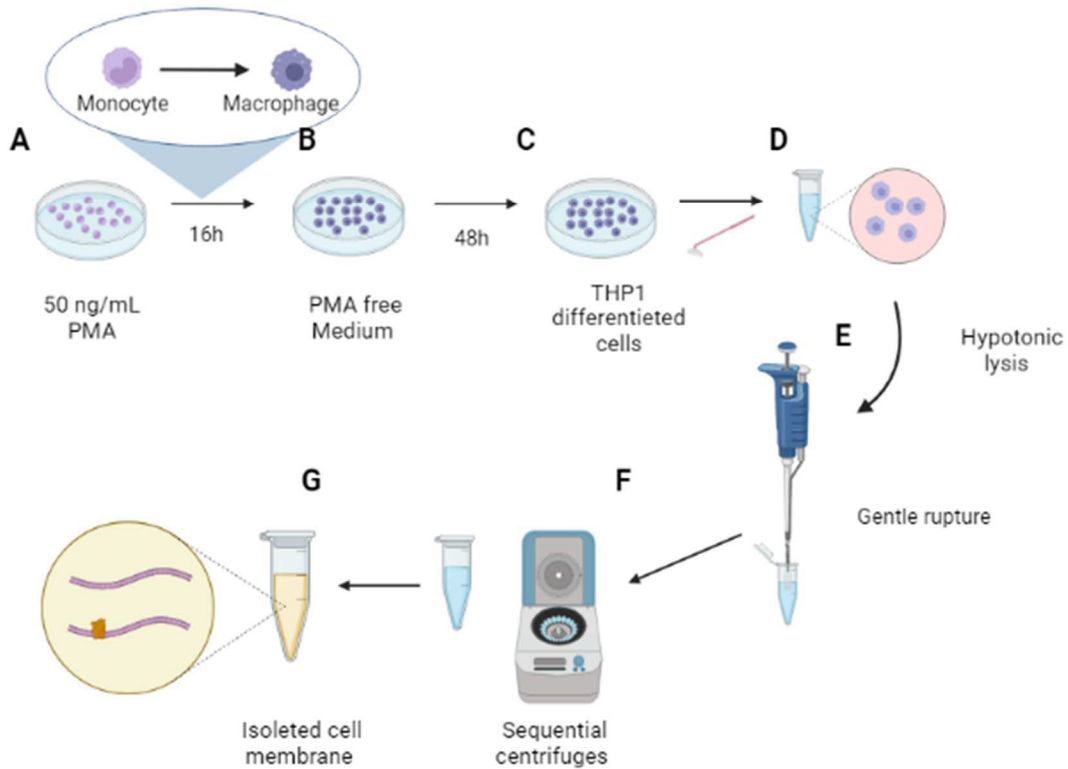


Figure 1. Schematic representation of THP1 activation with PMA (A-C) and plasma membrane extraction procedure (E-F). Created with BioRender.

The membrane extraction protocol was performed in triplicate to validate its reproducibility and the purity of the final sample. The pellets or the supernatants of each step of the purification process were observed by confocal microscope (Leica Microsystems TCS SP5 II, Wetzlar, Germany) with a 25X water immersion objective. Images were acquired with a resolution of 1024 × 1024 pixels. Protein quantification of cell membranes was assessed by the Bicinchoninic Acid assay (BCA assay) (Bicinchoninic Acid Kit, Merck). The test was carried out according to the manufacturer's instructions^{31,32}. The absorbance at 562 nm was measured using an EnSpire® Multimode Plate Reader and the relative titration curve was reported in **Figure 2**.

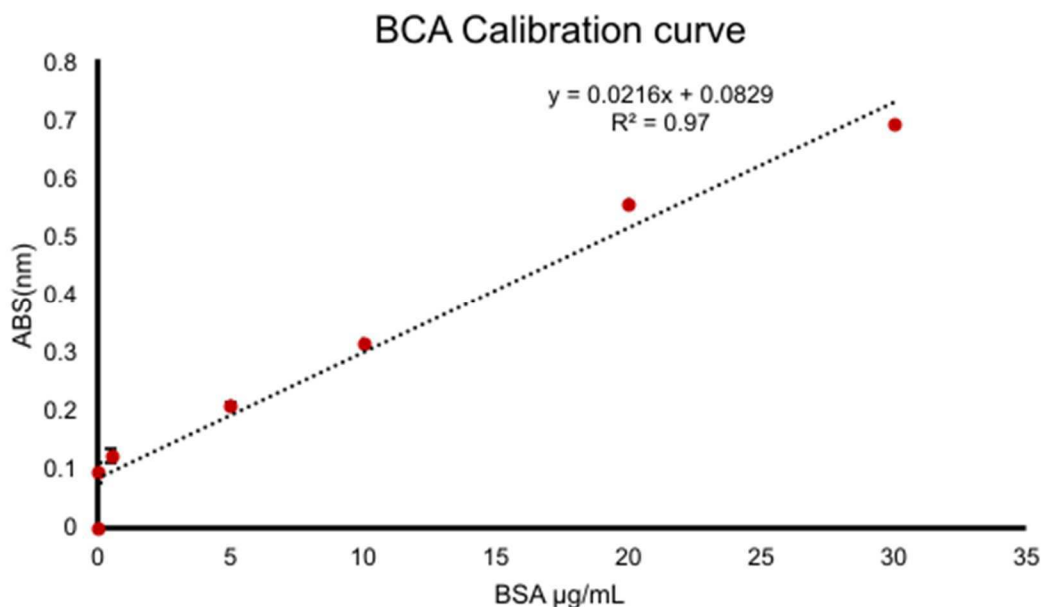


Figure 2. BCA calibration curve.

As reported in *Profeta et al.* The membrane protein integrity was evaluated by circular dichroism. Briefly, CD spectra of membrane solutions (3 µg/mL s.d. 0.05 and 2.4 µg/mL s.d. 0.06 for monocytes and macrophages, respectively) were recorded using a Jasco J-1500 spectropolarimeter (J-1500-150, Tokyo, Japan) in a 1.0 cm path-length quartz cell. CD spectra were registered at 25 °C in the far UV region from 260 to 200 nm. The spectra were obtained with an average of three scans by subtracting them from blank samples.

Biomimetic NEsoSome development

SNEs preparation: Chitosan layered NEs (Ct-NEs)

The inner core was a SNEs which involves an O/W NE, called “primary nano-emulsion”, layered with a sheet of an opposite charge polyelectrolyte (chitosan, Ct), this NC is indicated as Ct-NEs. Briefly, the oil phase was prepared by dissolving 5.8 g of Lipoid E 80 in 24 mL of soybean oil at 60°C using an immersion sonicator (Ultrasonic Processor VCX500 Sonic and Materials); after, oil phase was added dropwise to the water phase (Milli-Q water) and mixed again using an immersion sonicator to obtain a pre-emulsion. A low temperature was maintained throughout this process by using an ice-bath. Finally, this pre-emulsion was passed at 2000 bar through the high-

pressure valve homogenizer (Microfluidics, M110PS) to greatly reduce the initial size³³. The polyelectrolyte coating was achieved by deposition of fluorescent Ct prepared above the O/W NEs by following a previously developed procedure²⁷. More in detail, Ct was chemically labelled with Fluorescein 5(6)-isothiocyanate (FITC) as described in a previous work¹⁶. 100 mg of Ct (0.50 mmol) was dispersed in 10 mL of 0.1 M of acetic acid solution. Once complete the dissolution, a FITC (5.0 mg in 500 μ L of Dimethyl sulfoxide, DMSO) solution was added dropwise. The reaction was kept overnight at room temperature, then precipitated by correcting the pH to 10 with NaOH and washed with water by means of several centrifugations (Thermo-Scientific SL16R 9000 rpm, 15 min). Finally, the purified product was freeze-dried (Freeze Dryer CHRIST Alpha 1–4 LSC) for 48 h. The obtained Ct FITC was employed for the assembly of SNEs. In detail, a 0.1 M acetic acid solution of Ct FITC pH 4 (0.2 w/v%) was prepared, to that solution was quickly added, under vigorous stirring, the O/W NEs 20 wt% oil and kept under stirring for 15 min to allow uniform chitosan deposition. Ct-NEs were re-dispersed through a high-pressure valve homogenizer at 700 bar for around 100 continuous steps, and finally re-processed after one week under the same conditions and stored at room temperature. The final concentrations of oil and Ct were 1 and 0.01 w/v%, respectively, while the pH of the final Ct-NEs was 4.24.

Biomimetic NEsoSome assembly and characterization

The isolated Macrophage (M0) and Monocyte (M) membrane was deposited on Ct-NEs surface exploiting the electrostatic interaction between positive charged of Ct-NEs and negative charge membrane. At first cell membrane was redispersed by 21 passes of extrusion with Avanti Polar Lipids extruder using 0.1 μ m membrane (PC Membranes 0.1 μ m Avanti Polar Lipids). The extruded membrane was deposited on Ct-NEs surface by adapting the CM-NEsoSome procedure²⁸. Briefly, Ct-NEs was quickly added, under vigorous stirring, to the extruded cell membrane solution and kept under stirring for 15 min to allow uniform cell membrane deposition and then co-extruded for 21 passes with Avanti Polar Lipids Extruder using 0.1 μ m membrane (PC Membranes 0.1 μ m Avanti Polar Lipids). Biomimetic NEsoSome with monocyte and macrophage membrane were both characterized by DLS and Cryo-TEM according to the procedure reported in a previous work³⁴.

Ct-NEs, M-NEsoSome and M0-NEsoSome were typified by measuring size, polydispersity index (Pdl) and ζ -potential values through DLS instrument (Zetasizer ZS, Nanoseries ZEN 3600,

Malvern Instruments Ltd., Malvern, UK, $\lambda = 632.8$ nm). All the samples were diluted up to a droplet concentration of approximately 0.01 wt% by using Milli-Q water. A detecting angle of 173° was used, a default refractive index ratio (1.5900) and three runs for each measurement (1 run lasting 100 s) were used in the calculations of the particle size distribution. ζ -potential analysis was carried out by setting 30 runs for each measurement.

Cryo-TEM samples of M-NEsoSome and M0-NEsoSome were prepared by Plunge freezing technique by the Vitrobot Mark IV (Fei Company). 3 μ L of each sample were put in on 200 mesh quantifoil copper grid in Vitrobot chamber and then decreased in volume by blotting for 1 s with filter paper to yield a final thin film about 100-200 nm in thickness. To avoid sample evaporation, the Vitrobot was settled to 95% humidity and 4 $^\circ$ C with a waiting time of 60 s before plunging in liquid propane. After grid transfer in liquid nitrogen, each sample was mounted on Gatan Cryo holder, then observed by transmission electron microscope TECNAI G2-20 (Fei Company) equipped by Gatan CCD camera 2HS, in Cryo mode. The imaging was performed in low dose mode, at 200 KV in a range of magnification from 20000 to 50000.

***In vitro* accumulation analysis in HUVECs**

The targeting ability of the prepared NCs to the activated ECs of AS site was evaluated by mimicking the activated ECs on the plaque with HUVECs stimulated with TNF- α ^{10,35}. In detail, 5×10^4 HUVEC cells were seeded on an 8-well plate and inflamed with 10 ng/mL TNF- α for 24h. Cells were incubated with M0-NEsoSomes, M-NEsoSomes, Ct-NEs and cell medium alone as positive control (**Figure S1 in SI**), at a final concentration of 0.2 wt% of oil in water concentration for 30 min, 24 and 48 h at 37 $^\circ$ C in 5% CO₂. As well as to prove the selectivity for inflamed tissue, the up-take experiments were also made in not inflamed HUVECs in the same way. Then, samples were washed three times with PBS to remove the non-internalized compounds and fixed with paraformaldehyde 4% for 10 min, glycine 100 mM for 5 min and bovine serum albumin (BSA) 1% for 30 min. Finally, cells were incubated with Hoechst diluted 1:10.000 in PBS for 10 min room temperature for cell nuclei staining. Samples were observed by Confocal Zeiss Axio Observer.Z1 using a 20X objective. All experiments were performed in triplicate.

3. Result and discussion

THP-1 activation and cell membrane extraction

The macrophage membranes were selected as an ideal biomimetic shell candidate thanks to the presence in their surface, of functional proteins that regulate the inflammatory responses and cell recruitment during the pathogenesis of AS¹⁴. THP-1 cells line was chosen as membrane source for both monocyte and, once activated, macrophage membranes. The THP-1 cells were differentiated by 16h of PMA treatment in order to induce the first step of macrophage maturation/differentiation, i.e., unpolarized macrophages (M0), scheme in **Figure 1A-C**.

The differentiation was evaluated through cell morphological changes by microscope evaluation and TEM analysis. After 16h of PMA treatment, as expected THP-1 cells showed the typical hallmarks of macrophages, characterized by cell adhesion, spread morphology, increased granularity, and irregular nucleus shape, as detected by optical and TEM images (**Figure 2 B and D**). More in detail, macrophagic cells (**B and D**) can be typified by a wide cytoplasm abundant in lysosomes and mitochondria. Frequently, macrophage nucleus presents an increasing size and polymorphic and multilobate aspects (**Figure 2 D**)^{36,37}.

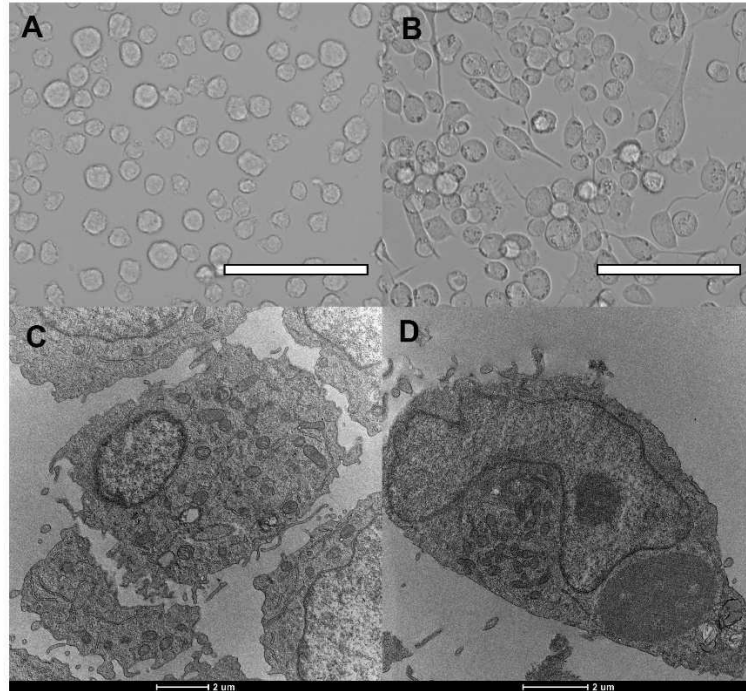


Figure 3. Morphological analysis of control and PMA treated THP-1: Top optical microscopy images of **A)** THP-1 monocyte cells, **B)** THP-1 PMA activated macrophages for 16h, scale bar 100 μm ; Below TEM images of **C)** THP-1 monocyte and **D)** THP-1 PMA activated macrophage for 16h.

Cell membranes were isolated from both differentiated THP-1 (Macrophage, M0) and THP-1 (Monocyte, M) according to the procedure reported by *Profeta et al.* with some modifications (**Figure 1 A-C**). The technique involves a gentle rupture of hypotonic treated cells. Cell contents removal and cell membrane “ghosts” isolation were obtained through repetitive and sequential washing and centrifugation at different speeds. The pellet and the supernatants of each step of the purification process were collected and examined by confocal microscopy. Indeed, preceding the membrane extraction, cell nuclei (blue) (**Figure 3 A**), and plasma cell membranes (red) were marked. **Figure 3A** and **B** showed the first surnatant containing isolated cell nuclei for both cell sources (**Figure 3 A M** and **Figure 3 C M0**). **Figure 3 B** and **D** shows the final pellet of the monocyte and macrophage membrane extractions, from the images the blue signal of the nuclei is not observed in both samples. Therefore, a good degree of purification can be deduced for both cell lines.

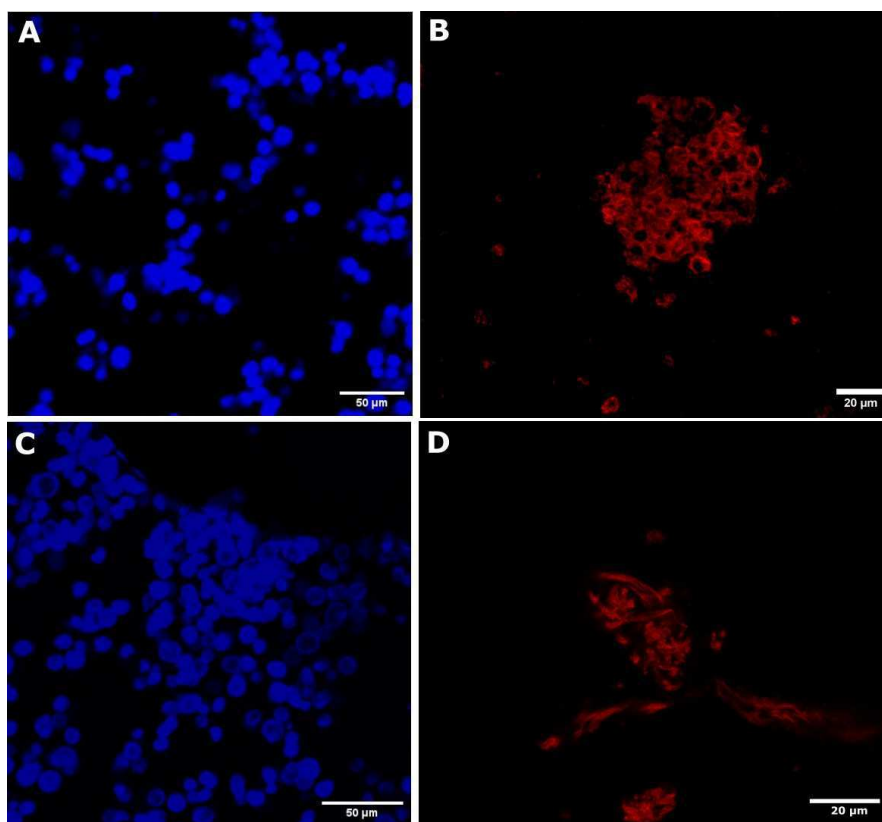


Figure 4. Confocal images of initial pellet with nuclei of **A)** monocyte (M) and **C)** macrophage (M0) scale bar 50 μ m, and final membrane pellet of **B)** monocyte(M) and **D)** macrophage (M0) scale bar 20 μ m.

After the last purification step, the protein membrane content, for both cell sources, was evaluated through the BCA test and a concentration of 3 μ g/mL and 3.4 μ g/mL was calculated for monocytes and macrophages, respectively. Moreover, to corroborate BCA and confocal analysis and evaluate if the correct secondary structure was preserved by membrane proteins, CD analysis was performed³⁸. The results of recorded CD spectra, as showed in **Figure 4**, confirm that the extraction and purification processes were performed in a correct way for both cell membrane sources, as no DNA bands, usually found at 260 nm, were revealed. Moreover, the membrane proteins retained their secondary structure displaying a typical mixed α -helix and β -sheet conformations with the presence of the minimum at 222 and 205 nm and a maximum a 195 nm.

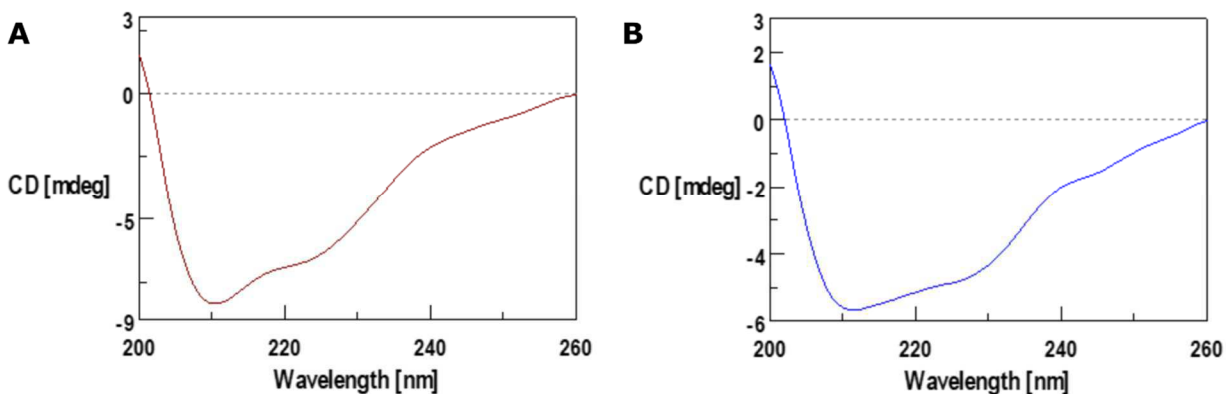


Figure 5. CD spectra for isolated plasma membrane of **A)** monocyte and **B)** macrophage.

Biomimetic NEsoSome development

Once obtained cell membranes, the step forward was to use them as a coating around Ct-NEs to provide highly biomimetic NCs with active targeting functionality. Ct-NEs (or NEsoSomes), representing the inner core of the final NCs, were obtained through a well-established procedure. The dimension of Ct-NEs was 102.5 nm s.d. 0.96 with a poly dispersion index (Pdl) of 0.09 s.d.0.01 (**Figure 3** green line) and a ζ -potential value of +30 mV. The obtained extruded membrane was added quickly to the Ct-NEs solution under vigorous stirring and kept under stirring for 15 min followed by one extrusion cycle of 21 passages through a 100 nm polycarbonate to allow uniform membrane coating. Biological membrane coating on Ct-NEs was driven by electrostatic and hydrophobic interactions between the negatively membrane layered and the positively charged Ct-NEs, as observed for other kinds of cell membrane layered materials^{10,28}. The fate and behaviour of NCs is strictly related to the particle size and ζ -potential values that were therefore monitored. All formulations showed a distribution in size less than 140 nm. In particular, DLS analysis revealed an increase in terms of size for both kinds of cell source of ~ 20 nm (M0-NEsoSome 121.2 nm s.d. 1.2 , Pdl 0.14 s.d. 0.02, **Figure 3** red line; M-NEsoSome Size 122 nm s.d.1.23, Pdl 0.15 s.d. 0.04 **Figure 3** blue line) as compared to Ct-NEs (Size 102.5 nm s.d. 0.96 , Pdl 0.09 s.d. 0.01) which is in agreement with the thickness of the coated macrophage bilayer membrane³⁵. As compared to Ct-NEs, it was observed a decrease of ζ -potential value of ~10 mV due to the typical negative charge of phospholipid membrane of cell sources (Ct NEs +25 mV, M0-NEsoSome +11 mV and M-NEsoSome +12 mV, in **SI**). The overall positive charge is

helpful for cellular uptake considering that cell membranes are negatively charged³⁴. To corroborate and prove the membrane coating also a Cryo-TEM analysis was performed (**Figure 6**). Both biomimetic NCs showed a nanometric size and the presence of external layer given by cell membrane coating.

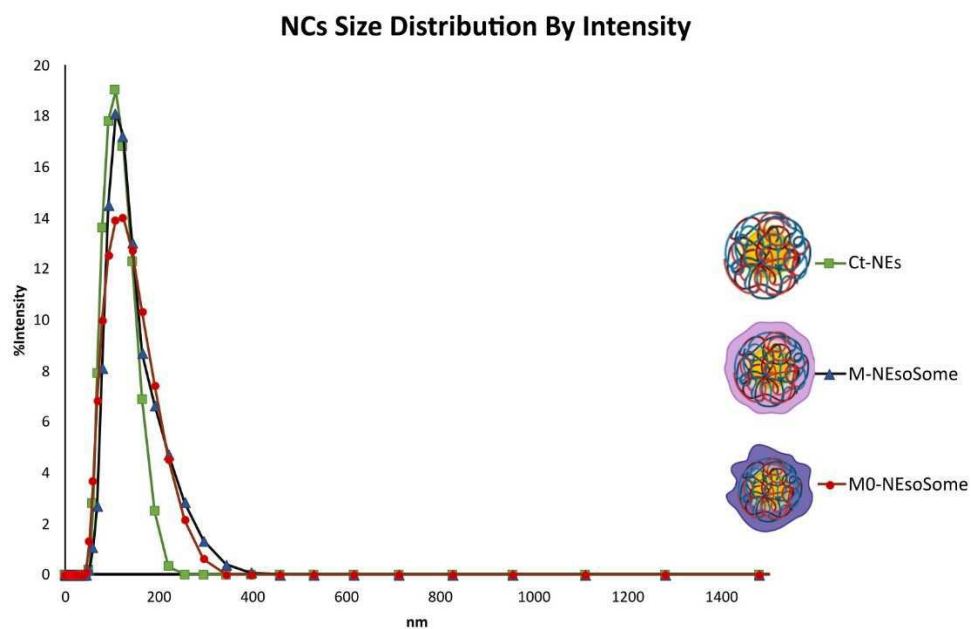


Figure 6. NCs size distribution by intensity of Ct NEs (green line and box), M-NEsoSome (blue line and triangle) and M0-NEsoSome (red line and circle).

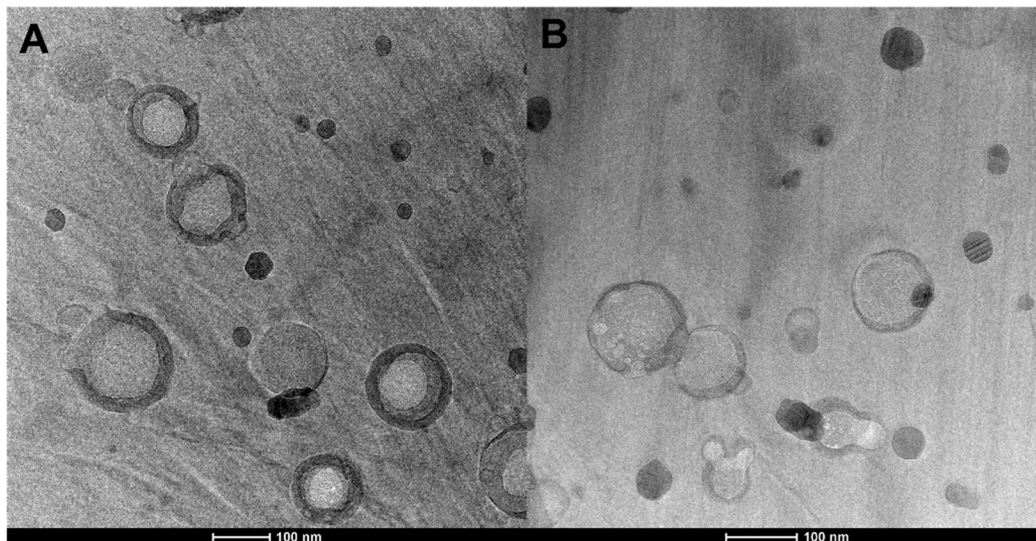


Figure 7. Cryo-TEM images of **A)** M0-NEsoSome and **B)** M-NEsoSome, Scale bar 100 nm.

***In vitro* accumulation analysis in HUVECs**

The ability to target the inflamed site was evaluated by comparing the uptake of M0-NEsoSome, M-NEsoSome and uncoated NEsoSome, namely Ct-NEs, at 0.2 wt% of final oil in water concentration and cell medium alone as positive control (**Figure S1 in SI**) in TNF α treated HUVECs and control HUVECs at different time points (30min, 24h and 48h) by confocal analysis. HUVECs activated with TNF- α could overexpress VCAM-1, ensuring the interaction specificity with integrin $\alpha 4\beta 1$ on the macrophages³⁹. As reported in **Materials and Methods**, the extracted cell membrane and Ct polymer were stained with CellMask™-543 (red) and FITC (green), respectively, to follow its signal during the internalization analysis with confocal microscopy. Therefore, Ct-NE correspond to the green signal, whereas M and M0-NEsoSome correspond to yellow hotspots given by the merge of the two fluorophores in the same pixel. In **Figure 8** it is reported the NCs *in vitro* accumulation in TNF α treated HUVECs at different time points. As we can see from the **Figure 8C**, for M0-NEsoSomes the accumulation process started already at 30 min (yellow spots, red box inset) and increased overtime **Figure 8 F**.

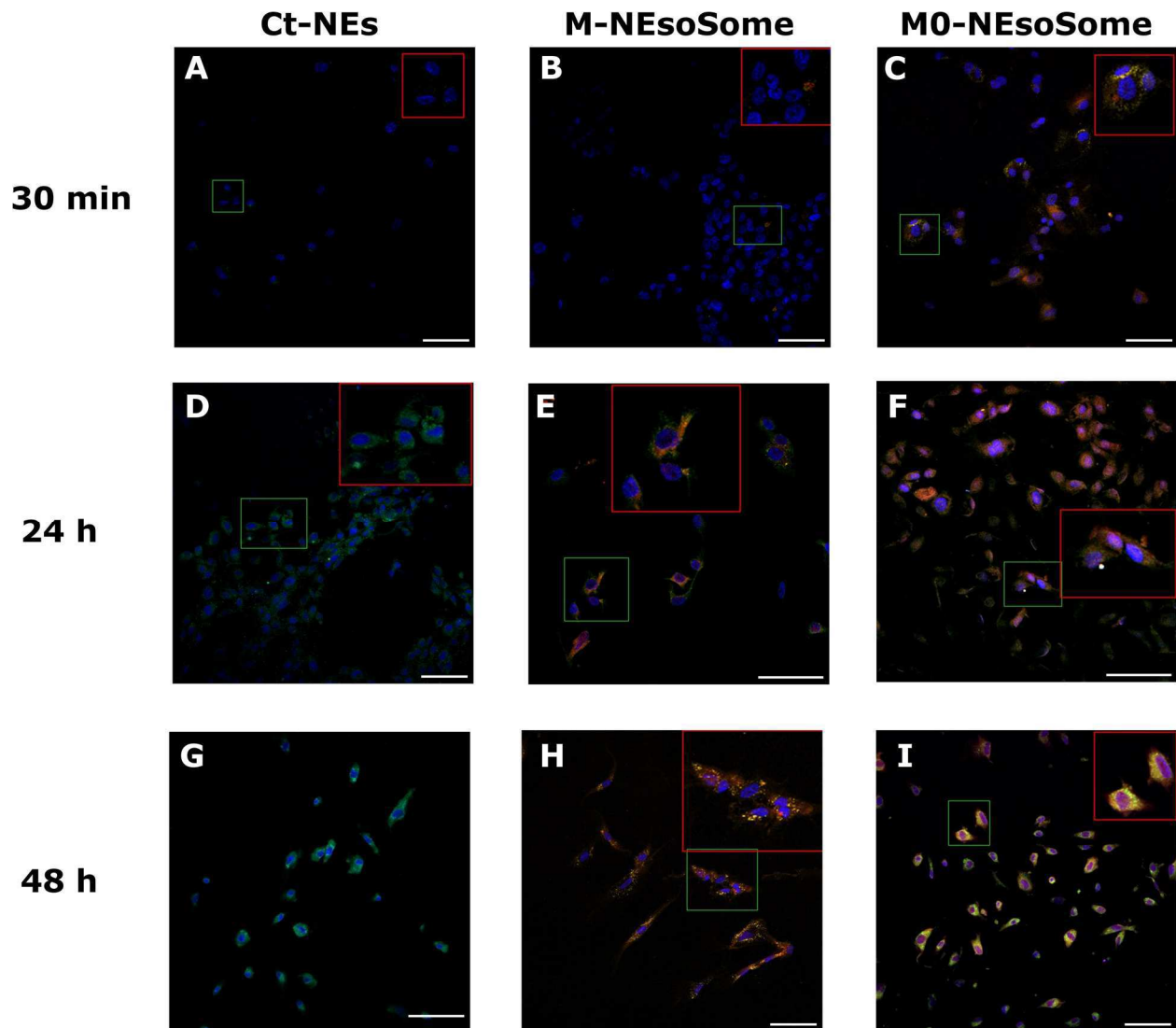


Figure 8. *In vitro* uptake of Ct-NEs (A, D, G), M-NEsoSome (B, E, H), M0-NEsoSome (C, F, I) in TNF α treated HUVECs.

In detail, the images after 30 min of treatment highlighted a better interaction and therefore accumulation and uptake of M0-NEsoSome (Figure 8 C, red box inset) with inflamed HUVEC as compared to M-NEsoSomes (Figure 8 B, red box inset) and even more to uncoated NEsoSome (Figure 8 A, red box inset) which showed no accumulation and therefore internalization at this time. However, M-NEsoSomes yellow signal was more evident after 24h and 48h as highlighted in the two red box insets present in each figure (Figure 8 E and H) suggesting a slower accumulation compared to M0-NEsoSomes, (Figure 8 F and I). More in

depth, we can suggest that the M-NEsoSome accumulation in stimulated HUVECs is located on the half between M0-NEsoSomes and Ct-NEs (**Figure 8 A, D, G**). These results can be explained by the blood-circulating monocytes behaviour during inflammatory responses as they are driven to the sites of inflammation where they differentiate into tissue macrophages. At 24h and 48h of treatment we can see that also the uncoated Ct-NEs (green spots, **Figure 8 D and G**) was able to internalize. This results could be justified by positive ζ -potential value of Ct-NEs due to the presence of high charge density areas at the cell surface is able to mediate endocytosis of positively charged particles⁴⁰. After 24h and 48h, both M0 (**Figure 8 F and I**) and M-NEsoSome (**Figure 8 E, H**) showed an intense signal (yellow spots) suggesting a time dependent internalization, although still stronger in the M0-NEsoSome. Of course, in dynamic *in vivo* conditions the time is crucial since a delay in the NC internalization may result in a wash out of the NC itself nullifying its effect.

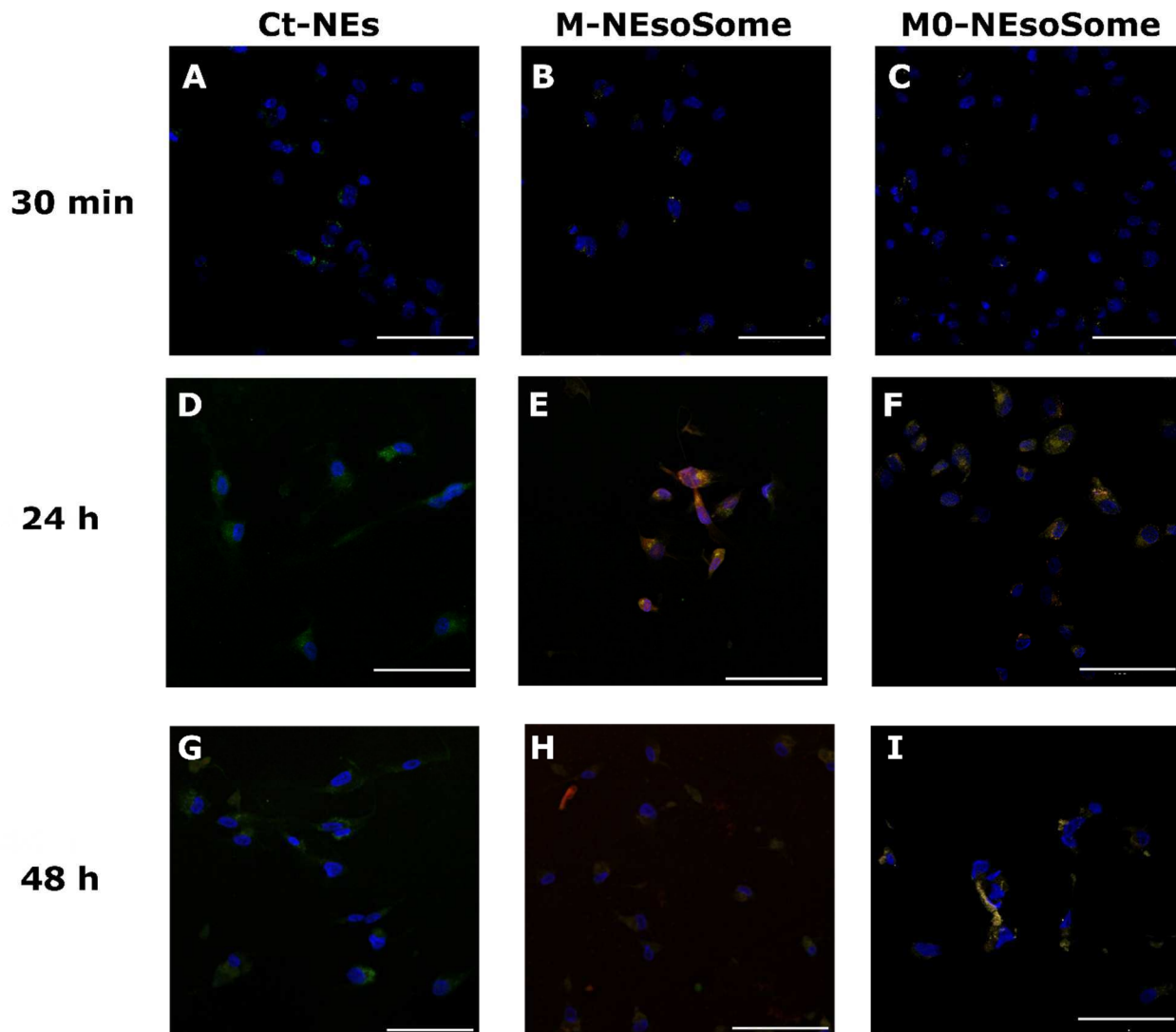


Figure 9. *In vitro* uptake of Ct-NEs (A, D, G), M-NEsoSome (B, E, H), M0-NEsoSome (C, F, I) in HUVECs.

In control HUVECs, we can observe M0-NEsoSome slowly accumulated in the cells (**Figure 9 C**) in respect to TNF α treated HUVECs (**Figure 8 C**). In control HUVECs, the three kinds of NCs behave in a similar way, the internalization process appears to be almost zero in the first 30 min of treatment and tends to intensify in the following 24h (**Figure 9 F**). Nonetheless, after 24h and 48h all the formulations have been internalized in control HUVECs (**Figure 9 G, H, I**). This result demonstrates a greater selectivity of the macrophages towards the inflamed

endothelium compared to the healthy one. In this case also the uncoated nanocarrier has an uptake capacity comparable to that of the membrane-coated analogues.

This different behavior can be explained by the expression of fewer adhesion molecules in normal endothelial cells than in infected ones. Therefore, monocytes and macrophage coated NEsome adhere poorly to them, and their accumulation and uptake result slower compared to the inflamed ECs model. These results highlighted the selectivity to the inflamed ECs for M0 and M membrane coated NCs compared to uncoated Ct-NEs.

4. Conclusion

At present the existing therapies for treating AS, based on free drugs, are not always completely efficient due to side effects associated with treatments which limit their systemic administration. Thanks to the recent advances in the nanomedicine systems, researchers are working on the development of nanosized formulations specifically designed for either drug delivery, visualization of atherosclerotic plaques, or possibly the combination of both these and other functionalities. Among the proposed NCs, cell membrane camouflaged NCs have become the new trend in the nano drug delivery system technologies thanks to their numerous advantages inherited from the cell membrane source. To target AS plaque, lymphocyte and macrophage coated NCs have been proposed. Here, we proposed two different cell membrane coated O/W secondary nanoemulsions employing monocyte and macrophage as cell membrane source. We assessed the two systems in term of physical characteristics (i.e., DLS and Cryo-TEM) and *in vitro* behaviour in both in an inflamed (TNF α treated HUVEs) and in a healthy ECs layer (HUVECs). Morphological analysis proved the nanosized dimensions and the presence of cell membrane layer. The results showed that the presence of macrophage membrane allowed higher and faster internalization in TNF α HUVECs compared to M-NEsome and uncoated Ct-NEs. Moreover, it could be highlighted a selective internalization in TNF α HUVEC cell layer of the cell membrane coated materials in respect of not TNF α treated HUVEC cell layer. These results agree with the natural behaviour of macrophage and monocyte, which are able to reach the typically activated ECs due to the presence of cell adhesion molecules. Our findings open a route for both therapeutic and potentially diagnostic management of AS disease. Specifically, our system could be a suitable drug delivery system for lipophilic molecules thanks to huge payload

capability^{16,22,23,41-43}. Nevertheless, these findings need to be corroborated by an *in vivo* analysis and immune evasion test.

Supported information

Biomimetic NEsoSome development

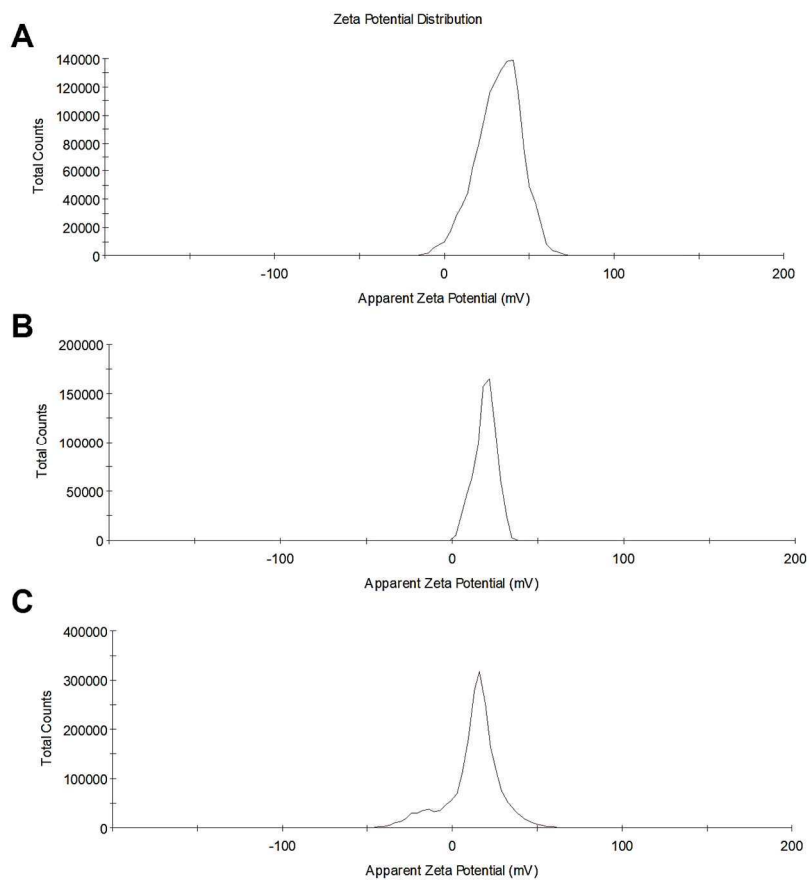


Figure S1. ζ -potential distributions of **A)** Ct NEs, **B)** M-NEsoSome and **C)** M0-NEsoSome.

In vitro accumulation analysis in HUVECs

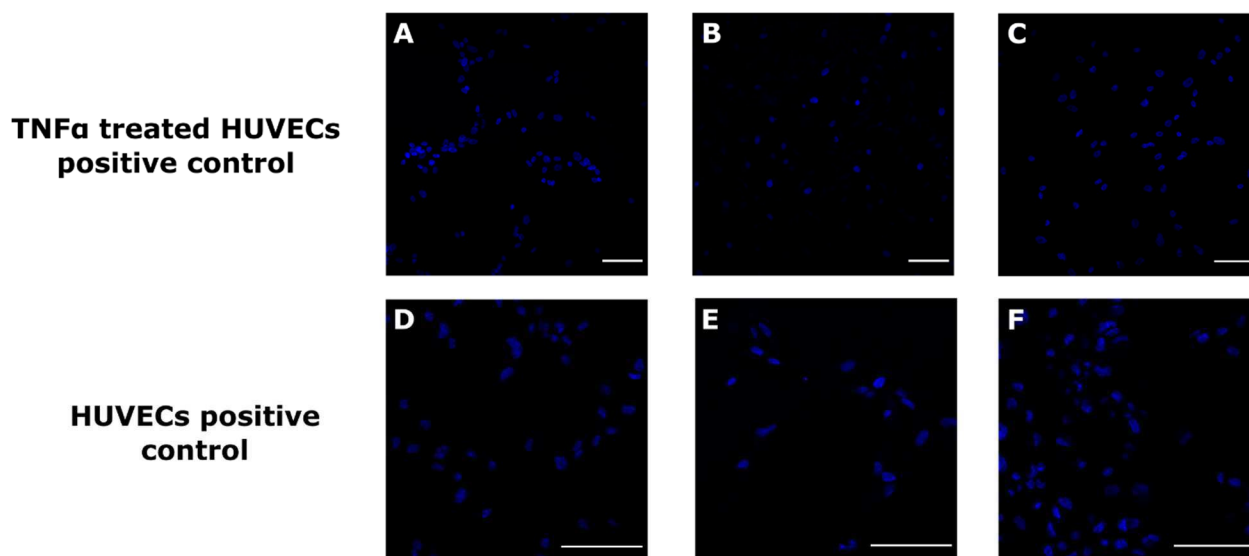


Figure S2. Positive control (treatment with cell medium) at different time point of TNF α treated HUVECs (A, B, C) and healthy HUVECs (D, E, F).

Acknowledgments

The authors would like to thank Dr. Valentina Mollo for her great support in TEM and Cryo-TEM imaging and Dr. Fabio Formigini for his support in confocal imaging.

References

- 1 Chen, J. *et al.* Recent advances in nanomaterials for therapy and diagnosis for atherosclerosis. *Advanced Drug Delivery Reviews* **170**, 142-199, doi:<https://doi.org/10.1016/j.addr.2021.01.005> (2021).
- 2 Lobatto, M. E., Fuster, V., Fayad, Z. A. & Mulder, W. J. Perspectives and opportunities for nanomedicine in the management of atherosclerosis. *Nature Reviews Drug Discovery* **10**, 835-852 (2011).
- 3 Feng, S. *et al.* Nanoparticles responsive to the inflammatory microenvironment for targeted treatment of arterial restenosis. *Biomaterials* **105**, 167-184 (2016).
- 4 Fang, F. *et al.* Inflammatory endothelium-targeted and cathepsin responsive nanoparticles are effective against atherosclerosis. *Theranostics* **12**, 4200-4220, doi:10.7150/thno.70896 (2022).
- 5 Salmaso, S. & Caliceti, P. Stealth Properties to Improve Therapeutic Efficacy of Drug Nanocarriers. *Journal of Drug Delivery* **2013**, 374252, doi:10.1155/2013/374252 (2013).

- 6 Alvandi, N., Rajabnejad, M., Taghvaei, Z. & Esfandiari, N. New generation of viral nanoparticles for targeted drug delivery in cancer therapy. *Journal of Drug Targeting* **30**, 151-165, doi:10.1080/1061186X.2021.1949600 (2022).
- 7 Rao, L. *et al.* A Biomimetic Nanodecoy Traps Zika Virus to Prevent Viral Infection and Fetal Microcephaly Development. *Nano Letters* **19**, 2215-2222, doi:10.1021/acs.nanolett.8b03913 (2019).
- 8 Almeida, I. *et al.* Bacterial cellulose membranes as drug delivery systems: An in vivo skin compatibility study. *European Journal of Pharmaceutics and Biopharmaceutics* **86**, 332-336 (2014).
- 9 Wang, D. *et al.* White Blood Cell Membrane-Coated Nanoparticles: Recent Development and Medical Applications. *Advanced Healthcare Materials* **11**, 2101349, doi:<https://doi.org/10.1002/adhm.202101349> (2022).
- 10 Parodi, A. *et al.* Synthetic nanoparticles functionalized with biomimetic leukocyte membranes possess cell-like functions. *Nature Nanotechnology* **8**, 61-68, doi:10.1038/nnano.2012.212 (2013).
- 11 Ulbrich, W. & Lamprecht, A. Targeted drug-delivery approaches by nanoparticulate carriers in the therapy of inflammatory diseases. *Journal of The Royal Society Interface* **7**, S55-S66, doi:doi:10.1098/rsif.2009.0285.focus (2010).
- 12 Zhang, Y. *et al.* Macrophage Membrane Biomimetic Drug Delivery System: for Inflammation Targeted Therapy. *Journal of Drug Targeting*, 1-47, doi:10.1080/1061186X.2022.2071426 (2022).
- 13 Bobryshev, Y. V., Nikiforov, N. G., Elizova, N. V. & Orekhov, A. N. in *Macrophages: Origin, Functions and Biointervention* (ed Malgorzata Kloc) 273-298 (Springer International Publishing, 2017).
- 14 Wang, Y. *et al.* Macrophage membrane functionalized biomimetic nanoparticles for targeted anti-atherosclerosis applications. *Theranostics* **11**, 164-180, doi:10.7150/thno.47841 (2021).
- 15 Dash, P., Piras, A. M. & Dash, M. Cell membrane coated nanocarriers - an efficient biomimetic platform for targeted therapy. *Journal of Controlled Release* **327**, 546-570, doi:<https://doi.org/10.1016/j.jconrel.2020.09.012> (2020).
- 16 Vecchione, R. *et al.* Curcumin bioavailability from oil in water nano-emulsions: In vitro and in vivo study on the dimensional, compositional and interactional dependence. *Journal of Controlled Release* **233**, 88-100, doi:10.1016/j.jconrel.2016.05.004 (2016).
- 17 Lagreca, E. *et al.* Physicochemical and in vitro biological validation of food grade secondary oil in water nanoemulsions with enhanced mucus-adhesion properties. *Colloids and Surfaces A: Physicochemical and Engineering Aspects* **654**, 129998 (2022).
- 18 Langella, A. *et al.* In vitro study of intestinal epithelial interaction with engineered oil in water nanoemulsions conveying curcumin. *Colloids and Surfaces B: Biointerfaces* **164**, 232-239 (2018).
- 19 Natale, C. D., Onesto, V., Lagreca, E., Vecchione, R. & Netti, P. A. Tunable release of Curcumin with an in Silico-supported approach from mixtures of highly porous PLGA microparticles. *Materials* **13**, doi:10.3390/MA13081807 (2020).

- 20 Quagliariello, V. *et al.* Cardioprotective effects of nanoemulsions loaded with anti-inflammatory nutraceuticals against doxorubicin-induced cardiotoxicity. *Nutrients* **10**, 1304 (2018).
- 21 Quagliariello, V. *et al.* Nano-encapsulation of coenzyme Q10 in secondary and tertiary nano-emulsions for enhanced cardioprotection and hepatoprotection in human cardiomyocytes and hepatocytes during exposure to anthracyclines and trastuzumab. *International Journal of Nanomedicine* **15**, 4859 (2020).
- 22 Vecchione, R. *et al.* Multilayered silica-biopolymer nanocapsules with a hydrophobic core and a hydrophilic tunable shell thickness. *Nanoscale* **8**, 8798-8809, doi:10.1039/c6nr01192f (2016).
- 23 Vecchione, R. *et al.* Ultrastable liquid-liquid interface as viable route for controlled deposition of biodegradable polymer nanocapsules. *Small* **12**, 3005-3013 (2016).
- 24 Di Cicco, C. *et al.* Biocompatible, photo-responsive layer-by-layer polymer nanocapsules with an oil core: in vitro and in vivo study. *Journal, of the Royal Society Interface* **19**, 20210800 (2022).
- 25 Iaccarino, G., Profeta, M., Vecchione, R. & Netti, P. A. Matrix metalloproteinase-cleavable nanocapsules for tumor-activated drug release. *Acta Biomaterialia* **89**, 265-278 (2019).
- 26 De Capua, A. *et al.* Active targeting of cancer cells by CD44 binding peptide-functionalized oil core-based nanocapsules. *RSC Advances* **11**, 24487-24499 (2021).
- 27 Fotticchia, T. *et al.* Enhanced drug delivery into cell cytosol via glycoprotein H-derived peptide conjugated nanoemulsions. *ACS nano* **11**, 9802-9813 (2017).
- 28 Profeta, M. *et al.* Cell Membrane-Coated Oil in Water Nano-Emulsions as Biomimetic Nanocarriers for Lipophilic Compounds Conveyance. *Pharmaceutics* **13**, 1069 (2021).
- 29 Pinto, S. M. *et al.* Comparative proteomic analysis reveals varying impact on immune responses in phorbol 12-myristate-13-acetate-mediated THP-1 monocyte-to-macrophage differentiation. *Frontiers in Immunology*, 2241 (2021).
- 30 Profeta, M. *et al.* Cell membrane-coated oil in water nano-emulsions as biomimetic nanocarriers for lipophilic compounds conveyance. *Pharmaceutics* **13**, doi:10.3390/pharmaceutics13071069 (2021).
- 31 Bainor, A., Chang, L., McQuade, T. J., Webb, B. & Gestwicki, J. E. Bicinchoninic acid (BCA) assay in low volume. *Analytical Biochemistry* **410**, 310-312, doi:<https://doi.org/10.1016/j.ab.2010.11.015> (2011).
- 32 Walker, J. M. in *Basic Protein and Peptide Protocols* (ed John M. Walker) 5-8 (Humana Press, 1994).
- 33 Kaneda, M. M., Sasaki, Y., Lanza, G. M., Milbrandt, J. & Wickline, S. A. Mechanisms of nucleotide trafficking during siRNA delivery to endothelial cells using perfluorocarbon nanoemulsions. *Biomaterials* **31**, 3079-3086 (2010).
- 34 Han, Y. *et al.* Macrophage membrane-coated nanocarriers Co-Modified by RVG29 and TPP improve brain neuronal mitochondria-targeting and therapeutic efficacy in Alzheimer's disease mice. *Bioactive Materials* **6**, 529-542, doi:<https://doi.org/10.1016/j.bioactmat.2020.08.017> (2021).

- 35 Li, Y. *et al.* CD47- and Integrin $\alpha 4/\beta 1$ -Comodified-Macrophage-Membrane-Coated Nanoparticles Enable Delivery of Colchicine to Atherosclerotic Plaque. *Advanced Healthcare Materials* **11**, 2101788, doi:<https://doi.org/10.1002/adhm.202101788> (2022).
- 36 Spano, A., Monaco, G., Barni, S. & Sciola, L. Expression of cell kinetics and death during monocyte–macrophage differentiation: effects of Actinomycin D and Vinblastine treatments. *Histochemistry and Cell Biology* **127**, 79-94, doi:10.1007/s00418-006-0227-9 (2007).
- 37 Gatto, F. *et al.* PMA-Induced THP-1 Macrophage Differentiation is Not Impaired by Citrate-Coated Platinum Nanoparticles. *Nanomaterials* **7**, 332 (2017).
- 38 Miles, A. J. & Wallace, B. A. Circular dichroism spectroscopy of membrane proteins. *Chemical society reviews* **45**, 4859-4872 (2016).
- 39 Wei, X. *et al.* Nanoparticle functionalization with platelet membrane enables multifaceted biological targeting and detection of atherosclerosis. *ACS nano* **12**, 109-116 (2018).
- 40 Hillaireau, H. & Couvreur, P. Nanocarriers' entry into the cell: relevance to drug delivery. *Cellular and Molecular Life Sciences* **66**, 2873-2896, doi:10.1007/s00018-009-0053-z (2009).
- 41 Vecchione, R. *et al.* Tunable stability of monodisperse secondary O/W nano-emulsions. *Nanoscale* **6**, 9300-9307 (2014).
- 42 Vecchione, R. *et al.* Nanocapsules: Ultrastable Liquid–Liquid Interface as Viable Route for Controlled Deposition of Biodegradable Polymer Nanocapsules (Small 22/2016). *Small* **12**, 2935-2935 (2016).
- 43 Vecchione, R. *et al.* Oil/water nano-emulsion loaded with cobalt ferrite oxide nanocubes for photo-acoustic and magnetic resonance dual imaging in cancer: In vitro and preclinical studies. *Nanomedicine: Nanotechnology, Biology and Medicine* **13**, 275-286 (2017).

Chapter 4: Food grade secondary oil in water nanoemulsions with enhanced mucus-adhesion properties.

Physicochemical and in vitro biological validation of food grade secondary oil in water nanoemulsions with enhanced mucus-adhesion properties.

Elena Lagreca^{1,2}, Raffaele Vecchione^{1*}, Chiara Di Cicco^{1,2}, Federica D'Aria³, Alessia La Rocca^{1,2,4}, Vincenza De Gregorio⁶, Luana Izzo³, Raffaele Crispino^{1,2,4}, Valentina Mollo¹, Emiliano Bedini⁵, Giorgia Imparato^{1,2,4}, Alberto Ritieni³, Concetta Giancola³ and Paolo Antonio Netti^{1,2,4}

¹Center for Advanced Biomaterials for Health Care (CABHC), Istituto Italiano di Tecnologia, Largo Barsanti e Matteucci 53, Napoli, Italy.

²Department of Chemical Materials and Industrial Production (DICMaPI), University of Naples Federico II, P.le Tecchio 80, Naples, 80125, Italy.

³Department of Pharmacy, University of Naples Federico II, Via Domenico Montesano 49, Naples, 80131, Italy.

⁴ Interdisciplinary Research Centre on Biomaterials (CRIB), University of Naples Federico II, P.le Tecchio 80, Naples, 80125, Italy

⁵Department of Chemical Sciences, University of Naples Federico II, Complesso Universitario Monte S. Angelo, via Cintia 4, I-80126 Napoli, Italy

⁶Department of Biology, University of Naples Federico II, Complesso Universitario Monte S. Angelo, via Cintia 4, I-80126 Napoli, Italy.

* Corresponding Author: E-mail address: raffaele.vecchione@iit.it

Published article: *Colloids and Surfaces A: Physicochemical and Engineering Aspects*, 654 (5), December 2022, 129998, <https://doi.org/10.1016/j.colsurfa.2022.129998>

Received 31 May 2022, Revised 14 August 2022, Accepted 16 August 2022, Available online 18 August 2022, Version of Record 12 September 2022.

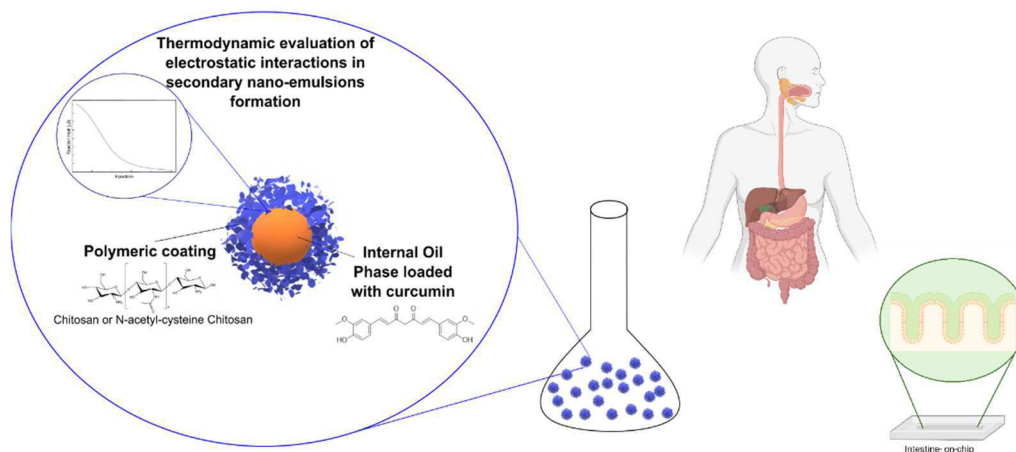
Abstract

Among oral delivery systems, oil in water nano-emulsions (O/W NEs) are of particular interest to improve pharmacokinetics of lipophilic compounds. Recently, we have implemented a successful strategy to improve O/W NEs stability, based on a polymeric coating on an oil core, using pharma grade formulations. However, in the field of food supplements, food grade materials are the top choice since they combine safety and cost effectiveness. Here, we have replaced

pharma grade (PG) with food grade (FG) materials in the preparation of the polymer coated O/W NEs, namely secondary O/W NEs, and performed a comparative study between the two formulations to assess the FG one. Additionally, to provide formulations with enhanced mucus-adhesion to the intestinal barrier, secondary O/W NEs were prepared by adding thiol groups to chitosan (Ct) via a simple non-covalent procedure based on N-acetylcysteine (NAC) salification, which is compliant with food supplement formulations. PG and FG formulations, in different materials combinations, were prepared and physico-chemically characterized (DLS, ¹H-NMR, ITC, CRYO-TEM) showing similar behaviour. In this work we validated this system both in terms of bioaccessibility and of physiological behaviour by employing some of the most recent and innovative techniques. FG formulations (NEs, Ct-NEs and Ct-NAC-NEs) loaded with curcumin were prepared and compared with the free drug in terms of drug bioaccessibility through the INFOGEST protocol confirming improved bioaccessibility. Very interestingly, by comparing mucus-adhesion properties of the two polymeric coatings (Ct and Ct-NAC) within an intestine on chip device able to mimic the complex intestinal functions, a significant enhancement in the mucus-adhesive properties of Ct-NAC was observed with respect to Ct due to the presence of thiol groups. Nonetheless, *in-vivo* assays are required as a final assessment of the proposed system.

Keywords: Food supplements, Isothermal Titration Calorimetry, Food-grade nano-emulsions, Oral Delivery, Intestine on chip, Curcumin, INFOGEST

FOOD GRADE NANO-EMULSIONS



1. Introduction

Food grade nano-formulations are becoming a promising option for the encapsulation of many bio-active molecules (dietary supplements, nutrients, vitamins, mineral and nutraceuticals) with limited oral bioavailability due to physicochemical and physiological events within the gastrointestinal tract (GIT) after their ingestion¹⁻³. For that reason, there is an increasing interest towards efficient nano-encapsulation strategies not only for pharmaceutical industry but also for food and beverage companies. Oil in water nano-emulsions (O/W NEs) are an ideal oral delivery system, thanks to their interesting physicochemical and functional properties, such as high encapsulation efficiency for lipophilic molecules, high bioavailability^{4,5} and time stability. Recently, we have implemented a successful strategy to improve the stability of completely nature-based O/W NEs by optimizing process and composition⁶. Since then, many lipophilic substances have been encapsulated into these O/W NEs such as Curcumin^{5,7}, Co-Enzyme-Q10^{8,9}, Lycopene¹⁰. Additionally, thanks to their stability, it has been possible to easily handle such O/W NEs and implement different functionalization strategies including layering with the aim to improve their stability in the biological environment¹¹ and modify/add new properties to the formulations including active targeting, cell membrane bilayer penetration¹², stimuli-responsive reactivity¹³⁻¹⁵, active targeting¹⁶, antifouling through biomimetic coatings by polyethylene glycol (PEG)¹⁷ or more recently by cell membrane coating¹⁸. In this work, we suggest the assembly and an in-depth characterization of a completely food grade (FG) secondary O/W NE for oral delivery of lipophilic substances, which was compared to the pharmagrade (PG) counterpart. Then, an *in vitro* simulated digestion evaluation of FG-formulations as well as an *in vitro* test within a gut on chip device to assess mucus-adhesion properties were performed. For the comparison with the PG formulation, each single PG component of the nano-carrier was replaced step by step and compared with the FG analogous in terms of size distribution by DLS and in terms of materials interaction, which is connected to the final stability of the formulation by isothermal titration calorimetry (ITC). ITC, well-known as an universal detection and quantification technique for studying macromolecular interactions¹⁹, has been, indeed, recently extended¹⁹⁻²² to the study of layer-by-layer interactions in nano-systems¹⁹⁻²². Furthermore, with the aim to enhance Ct-NEs mucus-adhesion properties, we developed a Ct salification reaction with a food grade N-acetyl-cysteine (NAC)²³. These not covalent thiolated chitosan represent a good solution for simplify the production procedure since salification is not a covalent reaction and does not need activator agents, thus there is no need to remove secondary reaction products, with an advantage in terms

of regulatory affairs of the final products. Firstly, this derivative was employed for building SNEs with an improved mucus adhesive property in substitution of covalent derivatives. The Ct salification was evaluated by Ellman's test ²⁴ and ¹H-NMR²¹. Then, we analyzed the role of Ct layer and the influence of thiolated group on CUR-NEs digestion. Here, a modified INFOGEST method was adopted to evaluate the impact of drug encapsulation into food grade primary and secondary nanoemulsions (NEs, Ct-NEs and Ct-NAC-NEs). Finally, to further characterize the proposed FG nano-formulation in terms of mucus-adhesion we exploited an organ on chip, which is a microfluidic cell culture system, with controlled dynamic conditions able to replicate the assembly, function and physiology of a human organs *in vitro* ²⁵. We designed an Intestine-on-a-chip (InOA-chip) platform composed of a single PDMS microfluidic channel on which human intestinal epithelial cells were seeded and cultivated in a controlled and human similar environment ^{26,27}. InOA-chip platform was produced by culturing human colorectal adenocarcinoma (Caco-2) cell line under dynamic fluid flow on PDMS. In these conditions Caco-2 cells form a polarized epithelial monolayer that is able to mimic adsorptive enterocytes. In this case the aim was to evaluate and compare mucus-adhesion properties of polymeric coating (Ct and Ct-NAC) by InOA-chip. More in detail, confocal imaging was used to qualitatively estimate the transport and localization of Ct and Ct-NAC NEs. The analysis of the mucus adhesive properties is crucial for oral delivery formulations as the materials' properties appreciably affects the release of the encapsulated active molecule.

2. Materials and Methods

Materials

Surfactant Lipoid E80 (egg lecithin powder 80%–85% enriched with phosphatidyl choline (PC) and 7%–9.5% content in phosphatidyl ethanolamine (PE)) is a PG product used in parenteral nutrition because of their well-known biodegradability and they were purchased from Lipoid GmbH (Ludwigshafen, Germany), used without further purification. FG egg lecithin was purchased from Hunan Insen Biotech Co., Ltd (Shanghai, China). Millipore Milli-Q water was used for the preparation of all nano-emulsions and solutions. Soybean oil (density at 20 °C of 0.922 g mL⁻¹), deuterium oxide (D₂O), deuterated trifluoroacetic acid (CD₂COOF₃, TFA) and 5, 5'-dithiobis (2-nitrobenzoic acid) (DTNB, also known as Ellman's reagent), NaOH, Dimethylsulfoxide (DMSO), Fluorescein-5-isothiocyanate (FITC), Chitosan Low Molecular Weight (PG Ct, 90–150 kDa) (Ct)

were purchased from Sigma Aldrich (Milan, Italy). Food grade turmeric 99% curcuminoids, food grade chitosan HD 80 Mesch (FG Ct) and N-acetyl-L-cysteine (FG NAC) were kindly provided by Labomar (Istrana, Italy) and were from Zhejiang Aoxing Biotechnology Co., Ltd (Yuhuan Zhejiang, China) and Giusto Faravelli spa (Milan, Italy), respectively. Polydimethylsiloxane (PDMS) and Poly(methyl methacrylate) (PMMA) were purchased from Sylgard 184 Mascherpa and Goodfellow, respectively. For cellular studies, human colon adenocarcinoma epithelial cell line, Caco-2 cells, were obtained from American Type Cell Culture (ATCC, Manassas, VA) and grown in Dulbecco Modified Eagle Medium (DMEM, Microtech) with 10% of fetal bovine serum (FBS, Microtech), 100 $\mu\text{g mL}^{-1}$ L-glutamine (Himedia), 100U mL^{-1} penicillin/streptomycin (Himedia). Phosphate-buffered saline (PBS 1X) and fibronectin human plasma solution were purchased from Sigma-Aldrich.

For digestion INFOGEST protocols: methanol (MeOH), ethanol (EtOH), acetic acid (AcOH), formic acid (FA), and acetonitrile (AcN), water UHPLC grade, were purchased from Merck (Darmstadt, Germany). Potassium chloride (KCl), potassium thiocyanate (KSCN), monosodium phosphate (NaH_2PO_4), sodium sulfate (Na_2SO_4), potassium persulphate ($\text{K}_2\text{S}_2\text{O}_8$), sodium chloride (NaCl), sodium bicarbonate, (NaHCO_3), sodium carbonate (Na_2CO_3), hydrochloric acid (HCl), calcium chloride dihydrate ($\text{CaCl}_2 \cdot 2\text{H}_2\text{O}$), sodium hydroxide (NaOH), α -amylase enzyme from human saliva, pepsin (250 U/mg solid) from porcine gastric mucosa, pancreatin (4 USP) from porcine pancreas, protease from *Streptomyces griseus*, also named Pronase E (3.5 U/mg solid) and Viscozyme L were purchased from Sigma Aldrich (Milan, Italy).

Primary nano-emulsion preparation

Both FG and PG lecithin based primary nano-emulsions were prepared as reported in a previous work ⁶. Briefly, for a 20 wt% oil in water pre-emulsion preparation, 5.8 g of lecithin was dissolved in 24 mL of soy-bean oil at 60 °C and then added to the aqueous phase (Milli-Q water) by an immersion sonicator (Ultrasonic Processor VCX500 Sonic and Materials). Then, the pre-emulsion was homogenized for 200 steps at 2000 bar by a high-pressure homogenizer (Microfluidics M110PS) to obtain the final nano-emulsion. The same protocol was performed both with PG and FG lecithin. For bio-accessibility evaluations, FG NEs were loaded with 100 mg curcumin (CUR) in 24 mL of oil phase as reported in a previous work ^{7,12,28,29}.

Thermodynamic study of interaction between Ct and NEs

The electrostatic interaction between Ct and lecithin stabilized nano-emulsions were thermodynamically characterized by ITC¹⁹. ITC experiments were performed using a Nano ITC Low Volume from TA Instruments (Lindon, UT, USA) with a cell volume of 170 μL . Stepwise titrations were performed at 25 °C with 50 μL syringe at a stirring rate of 250 rpm. The sample cell was always filled with 1.1 wt% O/W NE (size = 97.15 nm; PDI = 0.082; ζ = -21.5 mV) and the reference cell with Milli-Q water. 0.7 w/v % Ct (2 μL , 25 injections, 200 s interval) was titrated into the cell filled with the 1.1 wt% O/W NE, meanwhile the reference cell was filled with Milli-Q water. The pH of each solution was evaluated and adjusted when required before each experiment to reduce dilution heat and to ensure the same values in the cell and in the syringe. The relative amount of polymer and NE was expressed as ratio (R) between the concentration of Ct and the concentration of NE, both expressed as a weight percentage. Ct solution, both FG and PG, was prepared dissolving 10 mg of polymer in 1 mL (1 w/v %) of acetic acid solution 0.1 M (pH = 4) by vigorous stirring overnight. Ct solutions at different concentrations were obtained diluting the bulk solution with acetic acid solution 0.1 M pH =4. Dilution heat was subtracted from each measurement by titrating each polymer into the buffer alone as a control experiment. The interaction heat for each injection was calculated after the correction of the heat coming from polymer dilution. The resulting corrected injection heats were plotted as a function of the weight ratio between polymer and O/W NE concentrations, fitted with a model for one set of binding sites and analyzed with a nonlinear least-squares minimization algorithm, using the program NanoAnalyze Software v2.4.1 (TA instruments). $\Delta_b H$ (binding enthalpy change in kJ mol^{-1}), K_b (binding constant in M^{-1}), and stoichiometry (N= binding sites, calculated as the ratio between polymer and O/W NE concentrations) were the fitting parameters. The Gibbs energy and the entropy change contributions were calculated using the following relationships:

$$\text{Eq. 1 } \Delta_b G^\circ = -RT \ln K_b, (R = 8.314 \text{ J mol}^{-1}\text{K}^{-1}, T = 298 \text{ K})$$

$$\text{Eq. 2 } T\Delta_b S = \Delta_b H^\circ - \Delta_b G^\circ.$$

Ct-FITC Preparation

For the in fluorescence analysis *in vitro* digestion with InOA-chip, Ct was chemically labelled with Fluorescein 5(6)-isothiocyanate (FITC) as reported in a previous work⁷. Briefly, 100 mg of Ct (0.50 mmol) was dissolved in 10 ml of 0.1 M of acetic acid solution. After complete

dissolution, a solution of FITC (5.0 mg in 500 μ L of DMSO) was added dropwise. The reaction proceeded overnight at room temperature. Sample was then precipitated adjusting the pH to 10 with NaOH and the precipitate was collected by centrifuge (Thermo-Scientific SL16R 9000 rpm, 15 min). Sample was washed with water by means of several centrifugations. Finally, the purified product was freeze-dried (Freeze Dryer CHRIST Alpha 1–4 LSC) for 48 h.

Ct salification with NAC

100 mg of Ct (0.6 mmol) was uniformly dispersed in MilliQ water (5 mL). Then, a NAC solution was prepared solubilizing NAC (1.2 mmol) in MilliQ water (3 mL) and added dropwise to the Ct solution. The resulted mixture (pH 2) was under stirring overnight. The final modified polymer was purified by dialysis with 12-14 KDa MWCO membrane (Spectrum Laboratories Inc.) and freeze dried (Freeze Dryer CHRIST Alpha 1–4 LSC) for 48 h. The same protocol was performed both with PG and FG materials with different combinations of Ct and NAC. The final polymers were compared by proton nuclear magnetic resonance (^1H NMR) and Ellman's test. Also, a Ct-FITC was salified with NAC for the evaluation of mucus-adhesion properties for InOA-chip experiments through fluorescence analysis.

Materials characterization

Ellman's test

Ellman's test, a colorimetric assay, was used to determine the amount of thiol groups on the polymers^{24,30,31}. The calibration curve for Ellman's test was obtained using NAC as standard. NAC at different concentrations was dissolved by using 0.1 M acetic acid. Then, 0.5 mL of each standard were added to 3.5 mL of a solution of 0.2 mg/mL 5, 5'-dithiobis (2-nitrobenzoic acid) (DTNB, Ellman's reagent) in 0.5 M buffer phosphate at pH 8.03. The final pH resulted 7-8, a value necessary for the essay. At $t = 0$ the baseline was registered in order to subtract the absorbance due to DTNB at 410 nm (Varian Cary Scan 100 Spectrophotometer). Then, standards were stored in the dark at 25 $^{\circ}\text{C}$ for 2 h. Finally, absorbance was measured for each sample and the value at 410 nm was used to obtain a calibration curve. Same protocol was followed for each Ct-NAC sample. In particular, 0.15 mg of polymer was dissolved in 0.1 M acetic acid and each solution reacted with 3.5 mL of a solution of 0.2 mg/mL DTNB in 0.5 M buffer phosphate at pH 8.03 to reach as said a final pH between 7 and 8. At $t=0$ the baseline was registered in order to subtract the absorbance due to DTNB at 410 nm. Then, samples were stored in the dark at 25 $^{\circ}\text{C}$ for 2 h.

Finally, absorbance was measured for each sample and the value at 410 nm was used to obtain a calibration curve.

¹H-NMR

¹H-NMR analysis was performed to characterize both FG and PG Ct and NAC and Ct salified with NAC in each food and pharma grade combinations and NMR spectra were recorded using an Agilent 600 MHz (14 T) spectrometer equipped with a DD2 console and a One NMR HX probe. Ct samples, eventually salified, were prepared at 10 mg/mL, in deuterium oxide, containing 1 % (v/v) TFA, and N-acetylcysteine (NAC) samples at 30 mg/mL in deuterium oxide. NMR spectra were recorded with a total of 64 transients. To saturate the HDO residual peak for spectra measured in D₂O-based solvents, PRESAT sequence was used. Spectra analysis was performed using VNMRJ 4.0 software.

Secondary nano-emulsion preparation

Secondary nano-emulsions (SNEs), obtained by depositing chitosan on the NEs oil core, (Ct-NEs) were prepared both with PG and FG components, in terms of lecithin, Ct and NAC. Secondary nano-emulsion preparation was performed in accordance with a previous work ⁶. Briefly, a 20 wt% O/W nano-emulsion was added to a 0.02 M HAc solution of chitosan-based polymer (0.2 w/v %) under vigorous stirring for 15 min. The volume ratio between the solutions was respectively 1:1. In the final formulations, oil and chitosan concentrations were respectively, 10 wt% and 0.1 w/v %. For bio-accessibility assay with modified INFOGEST method, SNEs were loaded with curcumin, while for mucus-adhesion evaluation we prepared fluorescent formulations employing Ct-FITC and Ct-NAC-FITC polymer.

Particle size and ζ-potential analysis

Primary and secondary nano-emulsions were characterized and monitored over time by a laser dynamic light scattering (DLS, Malvern Instruments Ltd., Malvern, U.K) instrument ($\lambda = 632.8$ nm), detecting angle of 173°. All samples were diluted to an oil concentration of 0.025 wt% by using Milli-Q water for primary nano-emulsion and 20 mM HAc for secondary nano-emulsion. Furthermore, to evaluate the formulation stability in physiological conditions, the size particle distribution of all sample was analyzed at 37°C in Caco-2 cell medium using poor DMEM (w/o Phenol red) at different time points (0, 3h, 24h and 48h). To mimic the dilution level undergoing

oral ingestion, each sample was diluted 1:8 with cell medium. Particle size distribution calculations and polydispersity index (PDI) were performed using a default refractive index ratio (1.59) and 5 runs for each measurement (1 run lasting 100 s). For ζ -potential determinations, a particle electrophoresis instrument (Zetasizer zs nano series ZEN 3600, Malvern Instruments Ltd., Malvern, U.K.) was used, setting 50 runs for each analysis. Samples were diluted as in particle size analysis.

Morphological characterization: Cryo- Transmission electron microscopy (Cryo-TEM)

Cryo-TEM samples of Ct and Ct-NAC NEs were prepared by Plunge freezing technique by using the Vitrobot Mark IV (Fei Company). Overall, 3 μ L of each specimen were applied on 200 mesh quantifoil copper grid in Vitrobot chamber and subsequently reduced in volume by blotting for 1 s with filter paper to yield a final thin film about 100–200 nm in thickness. To prevent sample evaporation, the Vitrobot was settled to 95% humidity and 4 °C with a waiting time of 60 s before plunging in liquid nitrogen. After grid transfer in liquid nitrogen, each sample was mounted on Gatan Cryo holder, then observed by transmission electron microscope TECNAI G2-20 (Fei Company, Hillsboro, OR, USA) equipped by Gatan CCD camera 2HS, in Cryo mode. The imaging was performed in low dose mode, at 200 KV in a range of magnification from 20,000 to 50,000.

***In vitro* gastrointestinal digestion**

The *in vitro* GIT digestion was performed in accordance with the digestion model proposed by INFOGEST network and includes oral, gastric, and intestinal stages³². To simulate the oral stage, 3 mL of samples were mixed with 3.5 mL of simulated salivary fluid (SSF) together with 500 μ L of α -amylase enzyme from human saliva (1500 U/mL), 25 μ L of 0.3M calcium chloride dihydrate, 0.975 mL of water and then manually mixed. The pH value was adjusted to 7 by using HCl 1 M and the mixture incubated for 2 min in an orbital shaker at 150 rpm (KS130 Basic IKA, Argo Lab, Milan, Italy). To simulate the gastric stage, 7.5 mL of simulated gastric fluid (SGF), 1.6 mL porcine pepsin enzyme (25000 U/mL), 5 μ L of 0.3 M calcium chloride dihydrate and 0.675 mL of water were added to the oral bolus. The pH value was adjusted to 3 by using HCl 6 M and the mixture incubated for 2 h in an orbital shaker at 150 rpm (KS130 Basic IKA, Argo Lab, Milan, Italy). To simulate the intestinal stage, 11 mL of simulated intestinal fluid (SIF), 5 mL of pancreatin from porcine pancreas (800 U/mL), 2.5 mL of fresh bile (160 mM), 40 μ L of 0.3 M calcium chloride

dihydrate and 1.3 mL of water were added to the gastric chyme. The pH value was adjusted to 7 by using NaOH 6 M and the mixture incubated for 2 h in an orbital shaker at 150 rpm (KS130 Basic IKA, Argo Lab, Milan, Italy). At the end of each step, the tube was centrifuged for 5 min at 5000 rpm, the supernatant was collected and lyophilized. Afterward, the residue was solubilized in methanol, diluted and analysed through UHPLC Q-Orbitrap HRMS.

CUR determination through UHPLC Q-Orbitrap HRMS

The qualitative and quantitative analyses of loaded and free CUR were conducted through UHPLC (Dionex UltiMate 3000, Thermo Fisher Scientific) equipped with a degassing system, a quaternary UHPLC pump working at 125 MPa and a refrigerated auto-sampler device. Chromatographic separation was carried out with a thermostated ($T = 25^{\circ}\text{C}$) Kinetex Biphenyl 1.7 μm column ($50 \times 1 \text{ mm}$, 100 \AA Phenomenex) coupled to a guard column and an inline filter. The mobile phase consisted of water (A) and methanol (B) both containing 0.1% formic acid. The injection volume was 5 μL , and the flow rate was 0.150 mL/min. Separation was achieved in a total run-time of 5 min under the following gradient started with 5% B, increased to 30% B in 0.4 min and again to 100% B in 1.1 min, kept for 1.5 min at 100% B and then the column was re-equilibrated at 5% B for 1.5 min before the next injection. The Q-Orbitrap HRMS system was operated in negative ionization mode. Full scan and data-independent all-ion fragmentation spectra were collected.

The following scan parameters were used in full MS mode: mass resolution power of 70,000 full width at half maximum, scan range 120 to 400 m/z , automatic gain control target 5×10^6 , maximum inject time set to 50 ms, and scan rate 3 scan/s. The ion source parameters were as follows: sheath gas ($\text{N}_2 > 95\%$) 11, auxiliary gas ($\text{N}_2 > 95\%$) 2, spray voltage 3.3 kV; capillary temperature 320°C ; S-lens RF level 50; and auxiliary gas heater temperature 320°C . The following scan parameters were used in all-ion fragmentation mode: mass resolution power of 70,000 full width at half maximum, scan range 120 to 400 m/z , automatic gain control target 5×10^6 , maximum inject time set to 50 ms, and scan rate 3 scan/s; scan time = 0.10 s; isolation window 5.0 m/z ; and retention time 30 s. The collision energy was set to 15 eV to obtain representative product ion spectra. A mass tolerance below 5 ppm was set for the identification of the molecular ion and fragments. Data processing was performed by using Xcalibur software, version 3.1.66.10 (Thermo Fisher Scientific).

Ct and Ct-NAC NEs Treatment in InOA-chip

Microfluidic Device design and Fabrication

InOA-chip devices were fabricated by means of rapid prototyping techniques, which used polydimethylsiloxane (PDMS) (Sylgard 184, Mascherpa) to build the biochip through the replica molding from a Polymethyl methacrylate (PMMA, Goodfellow) slab. The PMMA master was designed in AutoCAD and carved with a micromilling machine (Minithech CNC Mini-Mill)²⁶. Pre-polymerized PDMS was worked with a curing agent at the ratio 10:3 (w/w) and the mixture was, then, degassed under vacuum for 10 min, poured on PMMA master, evened out by means of a bubble level, and then degassed once again for an additional time (10 min), in order to remove air bubbles. Subsequently, the entire set-up was incubated at 80°C for 60 min to achieve the complete polymerization of the devices, which were then peeled off from the master molds. In order to obtain an ultra-thin device, the device was sealed with PDMS. Briefly, a PDMS mixture was uniformly distributed in a Petri dish (11 cm diameter, Corning), pre-incubated at 90°C for about 8 min and used as a bonding layer for the complete closure of the PDMS slide. The entire set-up was incubated at 80°C overnight to achieve irreversible bonding. Inlet and outlet holes were punched with 1.5 mm biopsy punch (DifaCooper). Then plastic feeding tubes, 22ga x 25mm (Instech Laboratories, Inc), attached under sterile conditions to barbed male luer lock connectors (Harvard Apparatus) were inserted into the inlet and outlet. Tygon tubes (CM Scientific, UK, ID 1/16") were inserted into the inlets and outlets and barbed female luer lock connectors (Harvard Apparatus) were added to the end of tubes to obtain the single layer InOA-chip device channel with dimensions of 2 cm long channel with 2 x 1-mm rectangular cross-section and channel branches of 0.5 cm length and 2 x 0.6-mm rectangular cross-section (**Figure 1-A and 1-B**). The different height chosen for the branches allowed a wider layer of PDMS in these regions, ensuring overall better stability for the punching and the insertion of the connectors. Furthermore, the devices, tubes, and connectors were sterilized before cell seeding, by filling with ethanol 70% (v/v) for 15 min. Then, the sterilization procedure was continued washing the devices twice with a Penicillin-Streptomycin solution 2% (v/v) and to complete under UV overnight. Following, the microfluidic platforms were ready to host the cell culture.

Caco-2 Cell culture in InOA-chip

Before the cell seeding, a coating of human fibronectin for 45 min at RT was carried out

into the microchannel to allow cell adhesion. Then, Caco-2 cells were directly seeded on chip at a seeding density of 5×10^5 cells/cm², to produce an intestinal monolayer. After Caco-2 cells adhesion, cell medium was fluxed to eliminate not adhered residual cells. Then, InOA-chip platforms were incubated at 37°C and 5% CO₂ in dynamic conditions by using a syringe pump (Harvard Apparatus) with a flow rate of 2 μL/min, to allow the intestine cells to grow, proliferate and polarize.

Cell growth was monitored daily by using brightfield microscopy (Olympus CKX41) and high-quality monolayers were consistently obtained. After five days, Caco-2 cells monolayer were ready for the treatment.

On-line monitoring of Ct and Ct-NAC NEs treatment on Caco-2 monolayer seeded on InOA-chip

To mimic the dilution level undergoing oral ingestion, each sample (Ct-FITC NEs and Ct-NAC-FITC NEs) was diluted 1:8 with cell medium using poor DMEM (w/o Phenol red) and was added on the single-channel of the InOA-Chip platforms using a syringe pump (Harvard Apparatus) with a flow rate of 2 μL/min. For the treatment, the devices were mounted on the stage of an inverted epifluorescence microscope (Carl Zeiss Axio Observer z1), equipped with Hamamatsu Orca Flash 4 camera and chamber incubator XL (Pecon, Germany) for CO₂, temperature and humidity control and controlled by Zen 3.3 software (**Figure 1-C**). Time lapse and tile scan were carried out with a 20x objective, focusing cells monolayer and acquiring 4 regions along the channel each 15 min for 2 h of the dynamic treatment. After 2 h, samples were washed with PBS (to remove excess of nano-emulsions) and fixed with Paraformaldehyde (4%) to observe the Ct-FITC NEs and Ct-NAC-FITC NEs adhesion on the monolayer of Caco-2 cells. The confocal images were acquired using 20x objective by using confocal microscopy (TCS SP5 II Leica, Milan, Italy).

Fluorescence quantification analysis

From the time lapse and tile scan acquisitions, 9 complete reconstructions of the 4 regions were obtained for Ct-FITC NEs and Ct-NAC-FITC NEs treatments. The fluorescence quantification was performed by the selection of 4 Regions of Interest (ROIs) around the object of each reconstruction by using Fiji software. After threshold evaluation, the ratio between Intensity and Areas obtained for each ROI were calculated. The mean ratio of the 9

reconstructions were obtained and the fluorescence intensity was measured in arbitrary units. The same analysis was performed using the confocal images obtained after fixing the systems. Statistical analyses were performed with Student's t-test and ANOVA test followed by the Tukey HSD test. P-values of <0.05 denote statistically significant differences. For all data sets, experiments were repeated in independent studies.

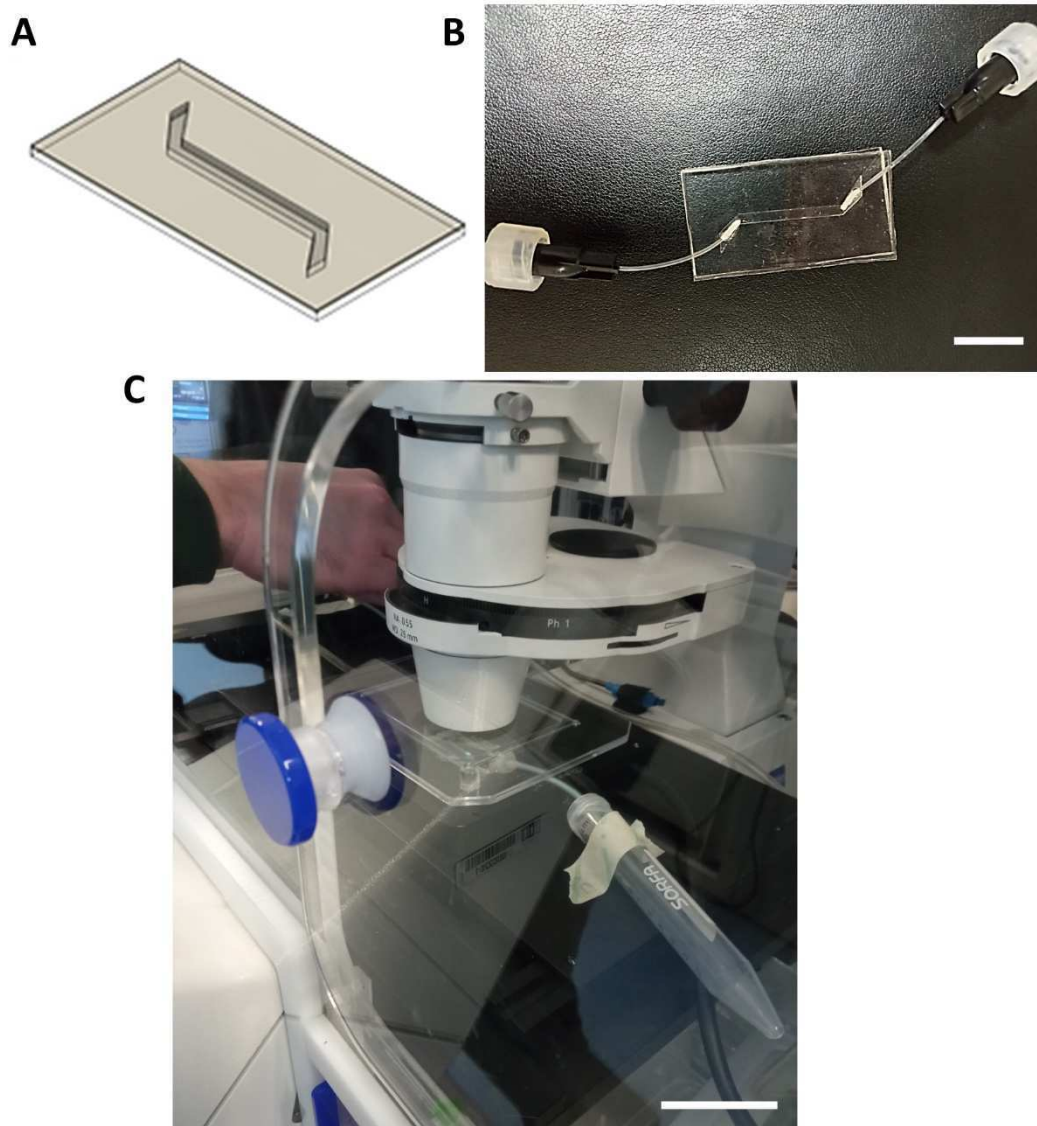


Figure 1. InOA-chip device. **A)** AutoCAD design of the single-layer device. **B)** Top view of the ultra-thin, single-layer InOA-chip device; scale bar 200µm; **C)** Experimental set up; scale bar 40cm.

3. Results and Discussion

DLS analysis of primary NEs

To the aim of replacing PG with FG materials in the preparation of O/W NEs, a first assessment has been a comparison in terms of morphology. DLS analyses show that particle size distribution, more in detail the polydispersity index value (PDI) was ≤ 0.1 for both PG (size = 100.3 ± 1.7 nm, PDI = 0.09 ± 0.07 , ζ -Pot. -35.5 ± 0.4 mV) and FG (size = 88.4 ± 0.5 nm, PDI = 0.08 ± 0.04 , ζ -Pot. -45.5 ± 0.6 mV) primary O/W NEs (see Supplementary Information (SI) **Table 1**). In particular, the more negative ζ -potential value of the FG formulation may justify the stabilization of a slightly smaller hydrodynamic diameter during the process, considering the stabilizing effect of the absolute ζ -potential value⁶.

As explained in **Materials and Methods**, the protocol to prepare PG based O/W⁶ was adopted also for FG one. Results of long-time monitoring of the FG NEs stability (**Figure 2-A**, see SI **Table 2**) confirmed that such protocol was well adapted to the new formulation, providing a size distribution under 100 nm (PDI ≤ 0.1). In the same way CUR-FG-NEs were also characterized in terms of size distribution through DLS analysis showing a particle size distribution of 90.58 ± 1.31 nm with a PDI value of 0.06 ± 0.04 and ζ -potential value of -24.50 ± 1.72 mV (see SI, **Table 1**); moreover, the dimensional stability was evaluated over the time **Figure 2-B**.

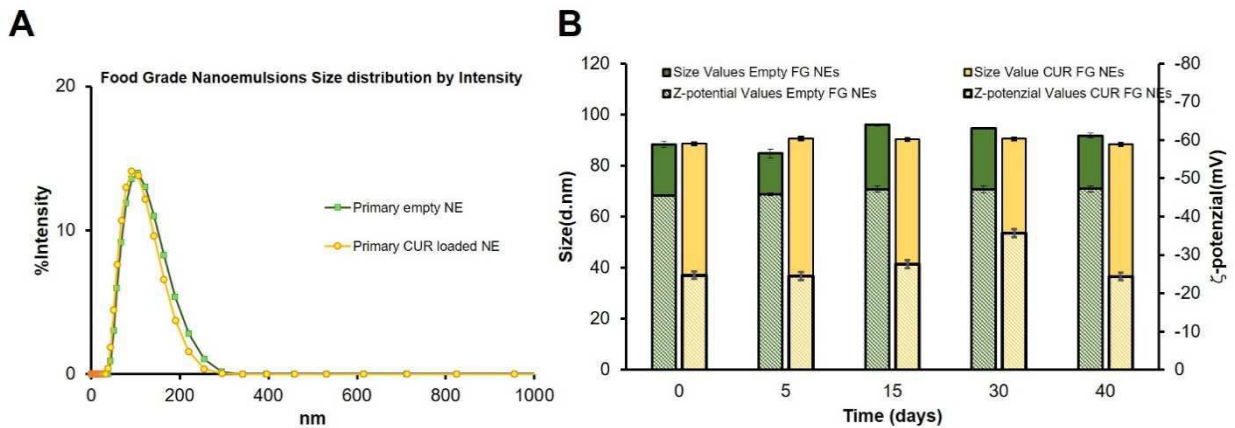


Figure 2. A) Primary FG NE size distribution by Intensity: empty NE (green) and CUR loaded NE (yellow). B) Stability over time in terms of dimensional stability of empty FG NE (green) and CUR FG NE (yellow) and corresponding ζ -potential value (line green for FG NE) and (line yellow for CUR FG NE). Data

are reported as mean (n=3).

Isothermal titration calorimetry (ITC) on Ct-NEs

Once dealing with secondary NEs, namely NEs coated with a polymer layer, such as chitosan, the stability of the final product as well as the optimal concentration of the polymer coating can be thermodynamically predicted by carrying out a calorimetric analysis¹⁹. ITC experiments allowed to identify an exothermic binding event followed by an aggregation for both PG Ct and FG Ct due to electrostatic interaction between the negative O/W NEs and the positive charged Ct. **Figure 3-A** and **B** show thermograms for the binding of FG Ct or PG Ct to the O/W NE at 25 °C along with the integrated heats and the corresponding best fit binding models for each system. The thermodynamic data are collected in **Table 1**. The binding was characterized by unfavorable enthalpic contribution, but favorable entropic contribution to Gibbs energy change, as already found in a previous work¹⁹, where the O/W NE was titrated with PG Ct in similar solution conditions. The ITC proved that the interaction between polymer and NE is not influenced by the degree (FG or PG) of Ct and the thermodynamic parameters determined for the two types of Ct are comparable (**Figure 3-C**), confirming that the typologies of chitosan did not affect the electrostatic interaction between polymer and NE.

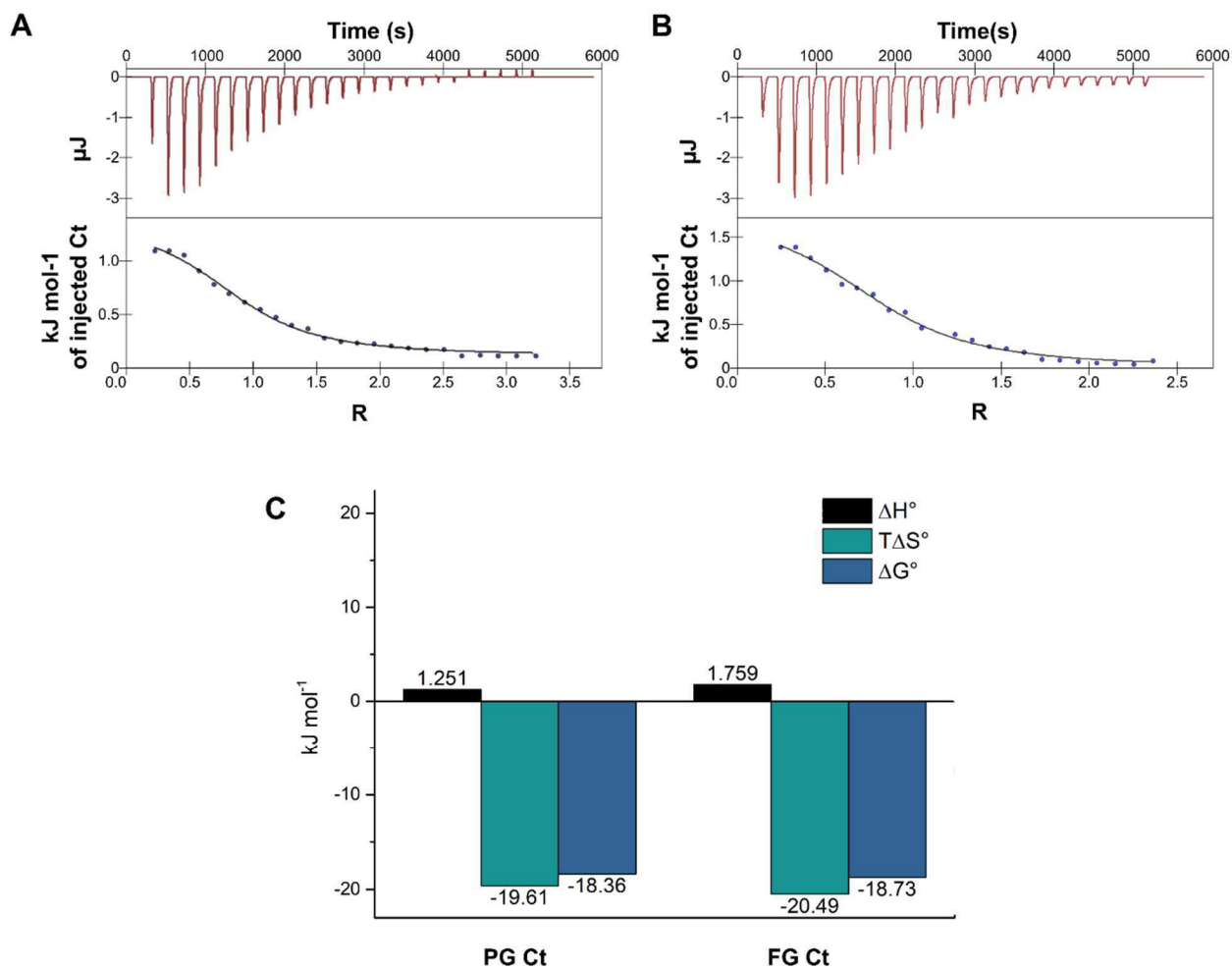


Figure 3. Titration by 25 injection of 0.7 w/v % PG Ct (**A**) and FG Ct (**B**) into O/W NE 1.1wt% oil at 25 °C and relative fitting obtained by independent model site. The heat flow (red) and the respective integrated binding heat, corrected for dilution heat, are plotted as a function of R. The solid line is the binding curve, according to the independent-site model. Diagram of the thermodynamic parameters (**C**).

Table 1. Thermodynamic parameters of the interaction between 0.7 w/v % FG Ct and PG Ct and O/W nano-emulsion at 1.1wt% oil with PG lecithin.

	ΔH° (kJ mol ⁻¹)	$-T\Delta S^\circ$ (kJ mol ⁻¹)	ΔG° (kJ mol ⁻¹)	K_d (M)	K_b (M ⁻¹)	N
PG Ct NEs with PG Lecithin	1.25±0.21	-19.6±1.1	-18.4±0.9	6.08 x10 ⁻⁴	1.64 x10 ³	0.9±0.6
FG Ct NEs with PG Lecithin	1.76±0.30	-20.5±1.0	-18.7±1.0	5.22 x10 ⁻⁴	1.91x10 ³	0.8±0.8

Ellman's test

As said in the introduction, final aim of the proposed NEs is the nano-encapsulation and oral delivery of lipophilic compounds such as curcumin. To this aim it is paramount to provide a strong mucus-adhesion to enhance the absorption of the molecule in the intestine. It has been previously demonstrated the enhanced absorption promoted by surface exposure of thiol groups. Here, we have proposed a non-covalent functionalization of chitosan with NAC based thiol groups to the aim of avoiding activator agents, thus any removal of secondary reaction products, with an advantage in terms of regulatory affairs of the final products. As reported in **Materials and Methods**, for each Ct-NAC, %NAC was calculated determining thiol groups' concentration by Ellman's test as colorimetric assay to quantify free thiol groups. Molar extinction coefficient (ϵ_{410}) was calculated by Ellman's test using NAC as standard (**Figure S2**). The values of ϵ_{410} calculated for NAC was 13199 M⁻¹cm⁻¹. Ellman's test results, evaluated by applying **Eq S1**, show very similar %NAC (average value $\approx 15.8 \pm 1.1$ %) independently from the kind of Ct (**Figure 4**) showing similar chemical reactivity regardless of FG or PG materials.

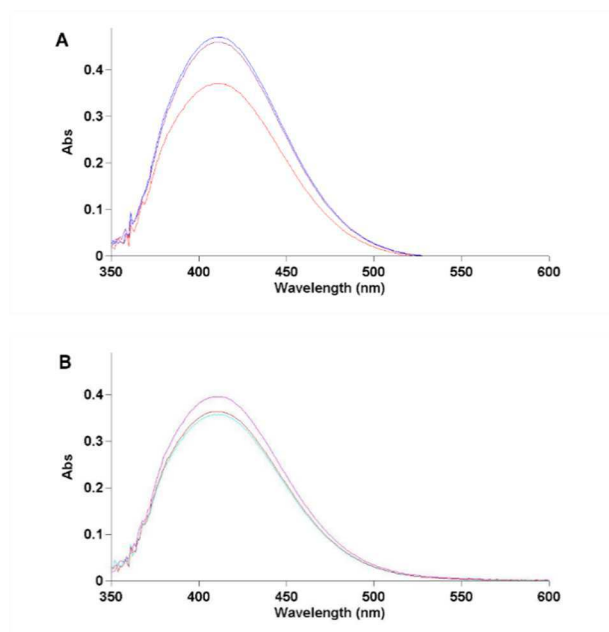


Figure 4. The absorbance spectra of the two typologies of Ct-NAC in triplicate: PG Ct-NAC (A), FG Ct-NAC (B).

¹H-NMR analyses of Ct

To corroborate Ellman's test results, both FG and PG chitosan have been chemically characterized by ¹H-NMR before and after characterization with NAC. To evaluate possible differences in the chemical structure of FG and PG Ct, ¹H-NMR spectra of these samples was acquired (**Figure 5-A**) and N-acetylation degree, %DA, was calculated using the following equation (**Eq. 3**)³³:

$$\text{Eq. 3 } \%DA = \frac{I_{H_{AC}}/3}{(I_{H_{AC}}/3) + I_{H-2(D)}} \times 100$$

Experimental %DA calculated for PG and FG Ct were 34% and 13%, respectively. ¹H-NMR spectrum of NAC was also acquired (**Figure 5-B**).

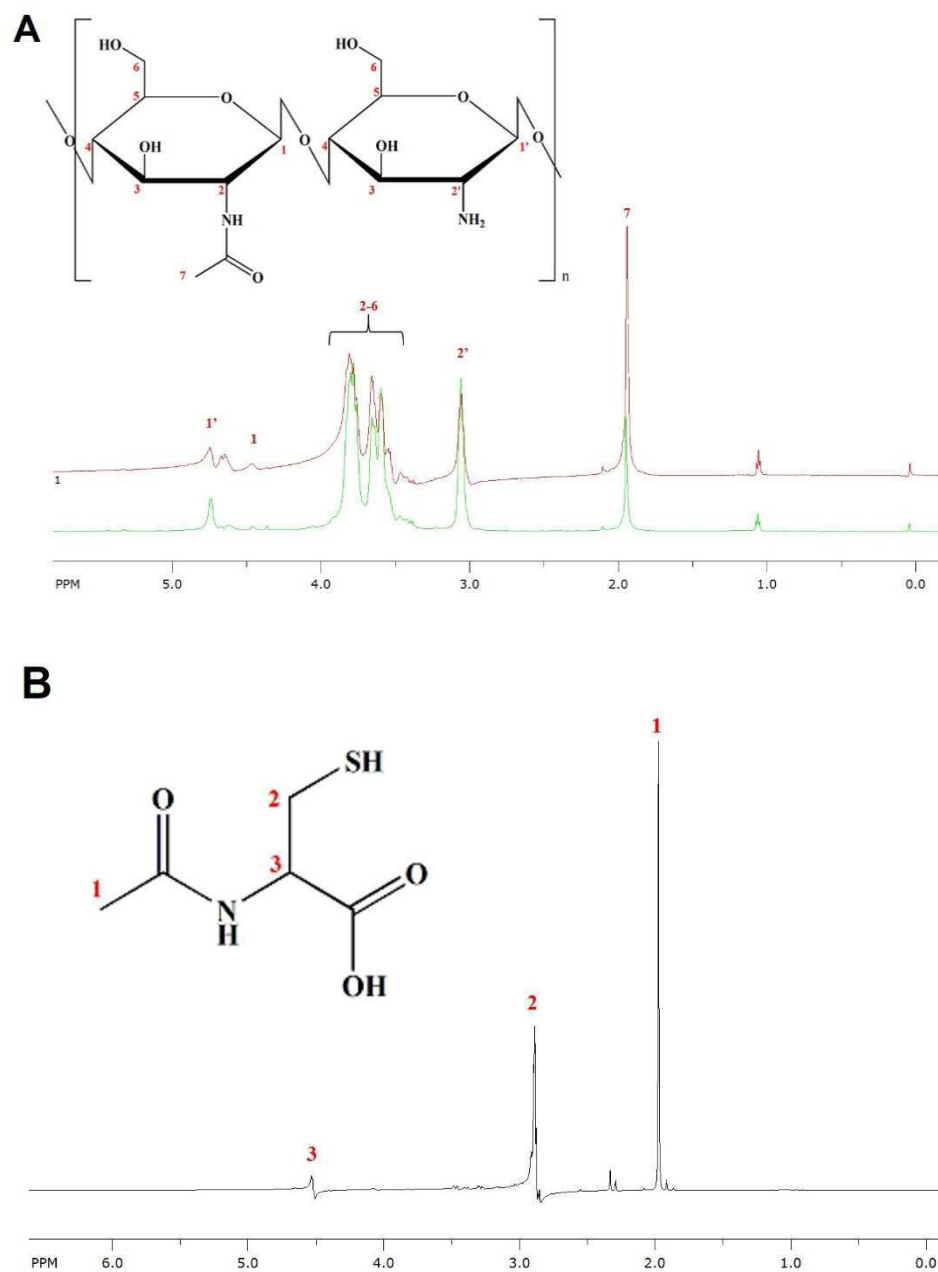


Figure 5. $^1\text{H-NMR}$ spectra of Ct and NAC: **A**) $^1\text{H-NMR}$ spectra of PG (red) and FG (green) Ct and relative assignments to the monomeric unit of chitosan, **B**) $^1\text{H-NMR}$ spectra of NAC chemical structure and assignments.

Ct-NEs functionalized with NAC is of particular interest to obtain nano-carriers with enhanced mucus-adhesion properties^{34,35}. As described in **Materials and Methods**, Ct-NAC was prepared with a salification step between FG and PG Ct and N-acetylcysteine (FG Ct-NAC, PG

Ct- NAC). $^1\text{H-NMR}$ spectra were acquired for the two products (**Figure 6**). Each spectrum shows a triplet signal at 3 ppm (H-2-2'), indicative of the absence of covalent bonds between Ct and NAC, which acts like Ct counter-ion by salification. The Ct-NAC % DA was calculated by **Eq. 3**. The % DA results from two N-acetyl contributions due to Ct and NAC simultaneously. Subtracting chitosan % DA previously calculated, it was possible to extrapolate the % DA just due to N-acetyl-cysteine contribution, which represents % NAC salified Ct (average value $\approx 50\%$). The uniform value of % DA (**Table 2**) for each Ct-NAC, regardless of FG or PG of the components, is an indication that the salification protocol gives uniform and reproducible results and it is independent on the kind of Ct.

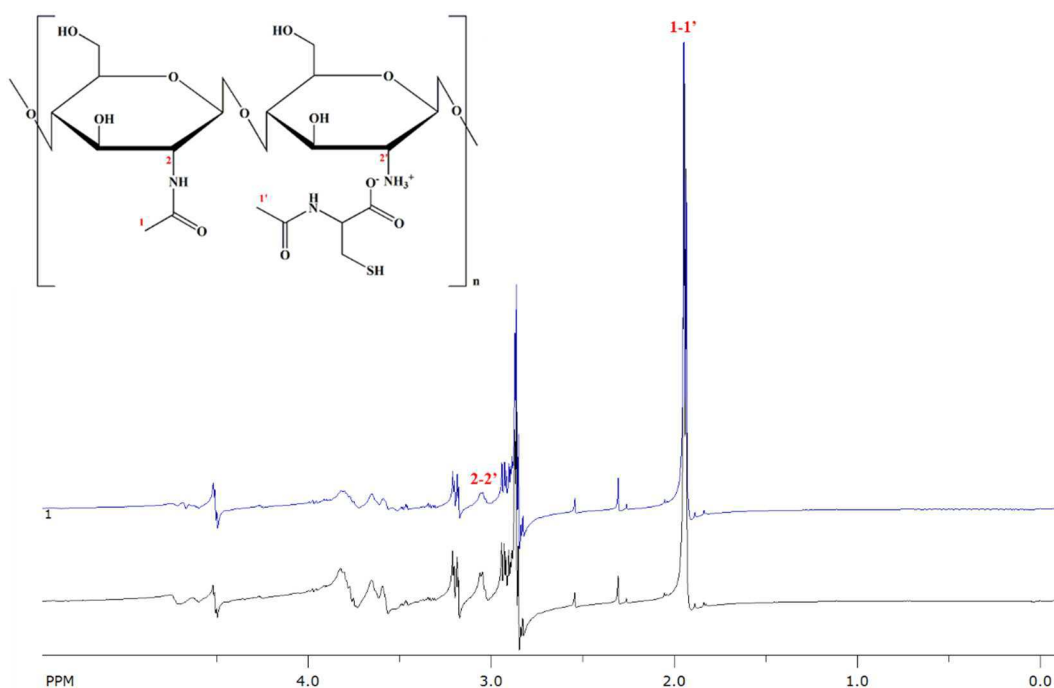


Figure 6. $^1\text{H-NMR}$ spectra of different combination of salified Ct: PG Ct- NAC (blue), FG Ct- NAC (black).

Table 2. Deacetylation degree (%DD) and Acetylation degree (%DA) in PG and FG Ct NAC calculated by ¹H-NMR analysis.

Polymer	%DD	%DA
PG Ct-NAC	81%	47%
FG Ct-NAC	68%	55%

SNEs characterization by DLS and Cryo-TEM

Once chemically characterized all Ct polymer configurations, primary NEs were coated with each of them by following the procedure previously described in **Materials and Methods** section. The coating of primary NE produces a charge switching from a negative to a positive ζ -potential value. For all the formulations, the coating produced a little increase of hydrodynamic diameter of NE droplets, although remaining monomodal, in agreement with the introduction of a nanometer shell around the oil core. Additionally, PDI values ($\ll 0.2$) demonstrated that all final formulations were still narrowly distributed, therefore not affected by FG or PG components. PDI is a very important parameter because a narrow distribution corresponds to less tendency to Ostwald ripening³⁶. Ct NEs and Ct-NAC NEs were monitored by DLS analysis for several months. The samples were stored at room temperature and periodically characterized. As reported in SI **Figure 1**, a constant size for both systems were observed. Their stability was also confirmed by unchanged value of PDI, which remains below the conventional stability rank of 0.1. ζ -potential values showed a little increase over time which is connected to an increase of stability due to the electrostatic repulsion between secondary nano-emulsion droplets with same charge (detailed DLS data are reported in **Table 4** and **5** in SI)^{37,38}. No significant differences in terms of stability over time were observed between FG and PG formulations enabling the exploitation of entirely FG based O/W Ct NEs of interest for the food supplement field.

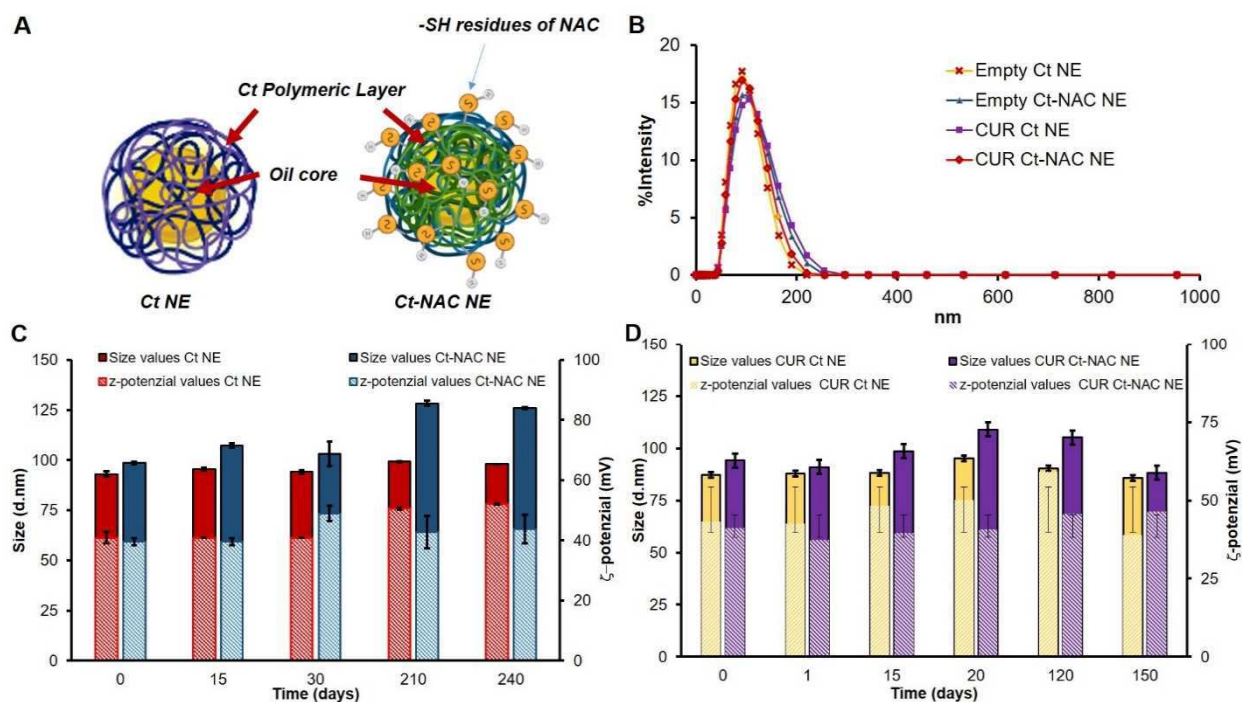


Figure 7. Top: **A)** Schematic representation of Ct NE (right) and Ct-NAC (left) **B)** Size value distributions of SNEs 10 wt% oil - 0.1 w/v % polymer: empty Ct NE. Down: stability over time of SNEs 10 wt% oil - 0.1 w/v % polymer in term of size and ζ -potential values: **C)** FG Ct (red) and Ct-NAC (blue), **D)** CUR FG Ct (yellow) and CUR FG Ct-NAC (violet). Data are reported as mean (n=3) (s.d.).

As described in **Materials and Methods**, for an applicative perspective, 10 times more concentrated secondary Ct and Ct-NAC NEs (10 wt % oil and 0.1 w/v % polymer) were also prepared. Also in this case, stability over time was assessed by DLS monitoring (**Figure 6-C**, detailed data are reported in SI **Table 6, 7, 8 and 9**). Furthermore, food grade Ct and Ct-NAC NEs (10 wt % oil and 0.1 w/v % polymer) loaded with curcumin (CUR) were also prepared and checked by DLS showing again maintenance in values (**Figure 7-D**) (Particle size distribution of 94.17 ± 0.30 nm; PDI value of 0.01 ± 0.02 ; ζ -potential value of 43.3 ± 0.6 mV for curcumin loaded Ct-NAC NEs; Particle size distribution of 87.16 ± 0.62 nm; PDI value of 0.07 ± 0.02 ; ζ -potential value of 43.3 ± 0.6 mV for curcumin loaded Ct NEs) with results which are comparable to FG empty formulations (**Figure 7-C**) (Particle size distribution of 98.58 ± 0.70 nm; PDI value of 0.099 ± 0.004 ; ζ -potential value of 39.5 ± 2.0 mV for empty Ct-NAC NEs; Particle size distribution of 93.03 ± 0.9 nm; PDI value of 0.088 ± 0.001 ; ζ -potential value of 35.0 ± 0.9 mV for empty Ct NEs). As reported in **Materials and Methods**, the stability of empty and loaded Ct and Ct-NAC NEs in

physiological conditions (1:8 dilution in cell medium at 37°C) at different time points (0, 3h, 24h, 48h) was evaluated. This study confirmed the stability of these formulations (data reported in **SI Figure S4, Table S10-S11**). However, a little increase in size distribution value was observed after 24h. Nevertheless, up to 48h all formulations were stable, as demonstrated by their PDI (<0.3). The Cryo-TEM analysis performed on Ct and Ct-NAC NEs are shown in **Figure 8**. It is evident from the morphological analysis the presence of the polymeric layer for both Ct and Ct-NAC (as control, in SI are reported the Cryo-TEM characterization also for primary NEs **Figure S1**.), as well as the level of mono-dispersion of the basic carrier, and the size distributions are corroborated by DLS analysis.

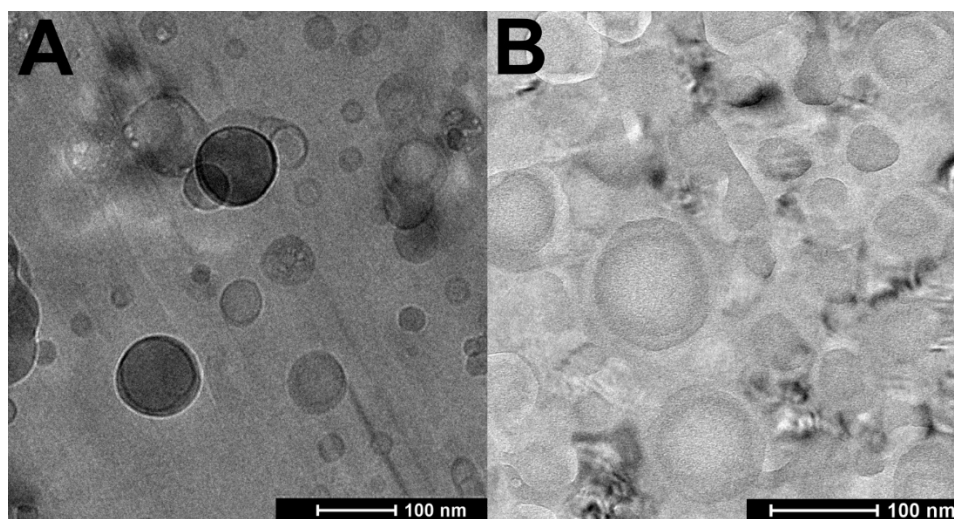


Figure 8. Cryo-TEM characterization of Ct NEs (A) and Ct-NAC NEs (B).

***In vitro* bio-accessibility of free and encapsulated CUR**

Although CUR is responsible for several biological activities e.g., antioxidant, anti-inflammatory, anti-tumor, and anti-microbial properties, its application as a functional ingredient is currently limited caused by its low bio-accessibility and poor water solubility^{39,40}. Bio-accessibility is defined as the portion of active compounds released from the matrix in the gastrointestinal tract and available for absorption. As a lipophilic ingredient, bio-accessibility of CUR was calculated taking into account the theoretical loading of the formulations and the encapsulation efficiency^{41,42}. In this context, focused on the FG formulations, the bio-accessibility

of three different nano-formulations: (1) Ct NEs, (2) Ct-NAC NEs and (3) NEs loaded with CUR as reported in **Material and Method** was evaluated during an *in vitro* GIT digestion and compared with the digestion of unformulated CUR (**Table 3 and 4**). Results showed that the bio-accessibility of unformulated CUR was very low, as expected. Conversely, all the formulated CUR systems showed enhanced CUR bio-accessibility with a slight higher bio-accessibility of Ct-NAC NEs in the gastric and intestinal stages. In literature ⁴¹, it was used an *in vitro* digestion model to examine some of the major factors that impact the bio-accessibility of CUR encapsulated within emulsion-based delivery systems including size and charge ⁴³. Several nano-carriers were proposed for curcumin nanoparticle formulation including CUR nanocrystals ⁴⁴, nanoparticles ⁴⁵, micelles ⁴⁶, nano-emulsions ⁴⁷, and nanogel ⁴⁸. Nanotechnology has proved to be a very effective strategy for enhancing the therapeutic potential of CUR ⁴⁹. We also confirmed that nano-formulations of CUR within the proposed structures significantly increased the bio-accessibility of CUR compared to the free CUR digestion and could successfully stabilize it against CUR degradation, as shown in **Table 3 and 4**.

Table 3. *In vitro* GIT distributions of CUR release from nano-formulations. Results are expressed as mg of CUR and standard deviation of three independent replication.

Stage	CUR Ct NEs		CUR Ct-NAC NEs		CUR NEs	
	CUR (mg)	%	CUR (mg)	%	CUR (mg)	%
Oral	0.288±0.00 1	24.0	0.135±0.01 5	11.3	0.182±0.009	15.1
Gastric	0.591±0.02 9	49.2	0.673±0.01 4	56.1	0.643±0.039	53.6
Intestinal	0.026±0.00 1	2.2	0.071±0.00 2	5.9	0.048±0.002	4.4
Total	0.905	75.4	0.879	73.3	0.873	73.1

Table 4. *In vitro* GIT digestion of free CUR (1.2 mg) and their bio-accessibility through oral, gastric, and intestinal stages. Results are expressed as mg of CUR and standard deviation of three independent replication.

CUR standard digestion		
Stage	CUR (mg)± s.d.	% Recovery
Oral stage	0.001±0.000	0.05
Gastric stage	0.027±0.007	0.32
Intestinal stage	0.003±0.000	0.24
Total	0.032	2.6

Ct and Ct-NAC NEs treatment of Caco-2 cells seeded on InOA-chip

Stated the ability to reach the intestine another fundamental aspect to analyze is the mucus adhesive properties of the nanocarrier. Therefore, as reported in **Materials and Methods**, the mucus adhesive properties of Ct and Ct-NAC NEs have been assessed through an InOA-chip device in which a monolayer of Caco-2 cells was cultured. A plethora of possible *in vitro* approaches to quantify mucus permeation are reported in literature ⁵⁰, including microfluidic systems that reproduce the formation of an intestinal dynamic mucus architecture ⁵¹. However, the recent 3D Intestine *in vitro* models, used to investigate absorption process, were more complex systems and formed by biopsies of human intestinal tissues that are difficult to obtain them ⁵². Here instead, we propose a more simplified, available, and innovative InOA-chip platform able to induce a spontaneous differentiation and proliferation of Caco-2 cells monolayer and to recapitulate many features of the small intestinal epithelium, including mucus production, throughout the continuous perfusion. We used this functional microfluidic platform for the first time to monitor *in situ* real-time the intestinal microenvironment formation and to simulate the Ct and Ct-NAC NEs interaction with the intestine. For this purpose, we investigated the formulations' behavior with confocal analysis following the fluorescence signal of FITC labelled polymer coating of the NEs, as a positive control to monitor the cellular uptake and retention of nanoemulsions on

the mucus layer⁵³. In addition, we also monitored the interaction of curcumin-loaded Ct and Ct-NAC NE with the mucus layer detecting the fluorescence signal of curcumin. The confocal images showed that both formulations had the same behavior as Ct and Ct-NAC NEs labelled with FITC, as shown in the SI Figures S5. The Caco-2 monolayers treated with FITC-Ct NEs and Ct-NAC NEs showed a tight junction-modulation, due to chitosan ability to open the intercellular tight junctions to enhance paracellular permeability⁵⁴ (**Figure 9-A and B** high magnification views), differently from the not treated Caco-2 monolayer (**Figure 9-C**). In addition, we observed a spread signal of FITC in Caco-2 monolayers treated with Ct NEs (**Figure 9-D**) compared with Ct-NAC NEs in which a strong FITC signal was revealed together with aggregates of monolayer in some areas (**Figure 9 -E**). To monitor FITC signal of Ct NEs and Ct-NAC NEs, we performed the analysis of time-dependent fluorescence intensity over 140 min (**Figure 9-F**). Both formulations reached the same plateau after 1 h of treatment, probably due to the spread signal of FITC that did not allow to detect the differences of fluorescence intensity during dynamic treatment. For this reason, we washed the channel to remove the excess of the two systems and analyzed and better discriminated the fluorescence intensity of FITC in Ct NEs and Ct-NAC NEs. The images show a very low FITC signal of Ct NEs linked to mucus membrane of Caco-2 cells (**Figure 9-G**), compared with Ct-NAC NEs (**Figure 9-I**), shown also in the high magnification insets (**Figure 9-H and J** respectively), indicating much higher adhesion in respect to Ct- NEs. As we can see in the graph (**Figure 9-K**) after washing, the intensity of Ct-NEs signal decreased whereas Ct-NAC showed a greater intensity due to a steady adhesion to the mucus layer.

As reported in literature, for the covalent bounded Ct-NAC nanocarriers^{31,54}, also in the case of the proposed salified Ct-NAC NE, we expect that the enhanced mucus-adhesions properties of Ct-NAC NEs are due to the formation of covalent S–S bonds by free thiol groups of Ct-NAC and mucus cysteine domains plus the electrostatic interactions between the positively charged Ct and the negatively charged mucosa layer^{23,55}.

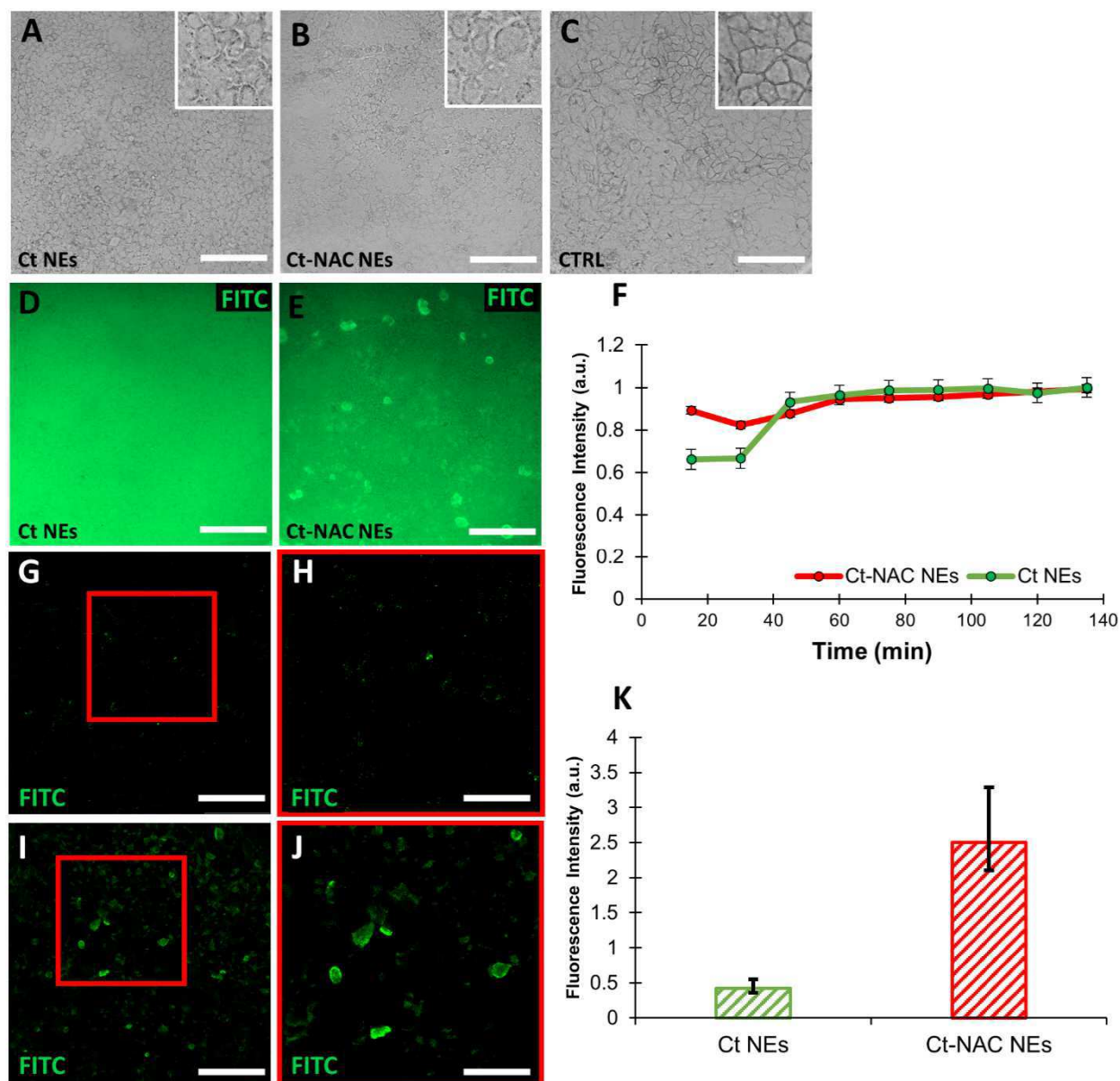


Figure 9. Analyses of mucus adhesions properties of Ct-FITC NEs and Ct-NAC-FITC NEs. Bright-field images of **A)** Ct NEs, **B)** Ct-NAC NEs and **C)** CTRL with high magnification views of Caco-2 monolayers; FITC images of Caco-2 monolayer treated with **D)** Ct NEs and **E)** Ct-NAC NEs; scale bar 100 μm . **F)** Graph of fluorescence intensity of Ct-FITC NEs and Ct-NAC-FITC NEs time-dependent. FITC images of **G)** Ct NEs and **I)** Ct-NAC NEs after washing and fixing and high magnification views shown in red squares (**H,** **J**); scale bar 100 μm and 70 μm . **K)** Graph of fluorescence intensity of Ct-FITC NEs and Ct-NAC-FITC NEs after washing and fixing.

4. Conclusions

In the last year, FG delivery systems have reached a key role in the food industry^{1,2} and have been proposed to improve bio-availability and stability⁵⁶ of different biomolecules such as vitamin D⁵⁷, curcumin⁵⁸, quercetin⁵⁹, β -carotene⁶⁰ or omega-3 oils⁶¹. Herein, we present for the first time, a totally FG delivery system based on a secondary O/W NE coated with a non-covalent thiol modified Ct with enhanced mucus-adhesion properties. We proposed a novel coating for NEs, which involved a not covalent thioled Ct derivative, with a good storage stability and a proved mucus adhesive property. FG and PG formulations have been morphologically, thermodynamically, and chemically compared. We found that the size of PG formulations is comparable to the FG one as well as the stability over time. By ITC it was shown that lecithin/Ct interaction is entropically driven for both FG Ct and PG Ct. Then, by ¹H-NMR and Ellman's test it was characterized the degree of Ct %N-acetylation functionalization showing similar results for both Ct configurations. Cryo-TEM characterizations confirmed the presence of polymer coating around the NEs for both Ct and Ct-NAC polymers and corroborated the DLS results. Afterwards, an *in vitro* bioavailability assay was performed using the INFOGEST protocol where both Ct NE and Ct-NAC NE demonstrated to improve CUR bio-accessibility properties thanks to the protective action of Ct against lipid digestion. Finally, the Ct and Ct-NAC mucus adhesive properties were compared for the first time within an innovative and accessible intestine-on-chip platform, InOA-chip, and we proved that thiolated Ct NE possesses a much higher mucus adhesion as expected because of the formation of S-S bonds with the mucin produced by the Caco-2 monolayers. The proposed totally FG system open a route in nutraceutical field, with a novel emulsion-based formulation possessing enhanced mucus-adhesive property thanks to the Ct functionalization with NAC together with the improved lipophilic substance bio-accessibility as compared to the free molecule. Nonetheless, the chosen not-covalent thiol functionalization of chitosan opens the door to an immediate use of such formulation with no need for safety clinical tests.

Contributions

E.L., C.D.C. and E.B performed modification and characterization of polysaccharides; E.L., C.D.C and R.C. carried out experiments on nano-emulsions and related characterizations; E.L. and F.D.A performed isothermal titration calorimetric experiments, E.L. and C.D.C. performed NMR experiments; V.M. performed Cryo-TEM characterization, L.I. carried out experiments and analyses on formulations and curcumin bioaccessibility assay by INFOGEST; A.L.R. carried out experiments and analyses on formulations treatments with InOA-chip; R.V., C.G., A.R., E.D.G. G.I. and P.A.N. supervised and provided theoretical support; R.V., and P.A.N. conceived the work; E.L. and R.V. contributed to develop the manuscript. All authors contributed to write-review and edit the manuscript giving approval to the final version of the manuscript.

Supporting Information

DLS analysis of FG primary NE 20 wt% in Oil

Table S1. PG and FG O/W primary nano-emulsions DLS analysis. Data are reported as mean (n=3).

Sample	Size (nm)	ζ-Pot. (mV)
PG O/W NE	100.3 ±1.7	-35.5 ±0.4
FG O/W NE	88.4 ±0.5	-45.5 ±0.6
CUR FG O/W	90.58±1.31	-24.50±1.72

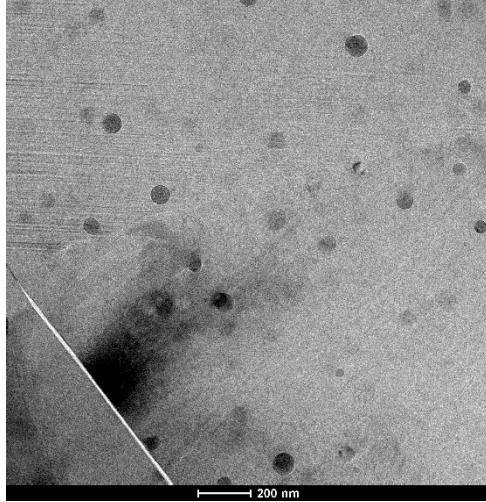


Figure S1. Cryo-TEM characterization of primary NEs.

Table S2. Size (PDI \leq 0.1) and ζ -Potential data of FG primary NE 20wt% in oil. Data are reported as mean (n=3).

Time (days)	Size (nm)	ζ -Pot. (mV)
0	88.36 \pm 1.20	-45.5 \pm 0.1
7	84.75 \pm 1.80	-45.8 \pm 0.4
15	95.98 \pm 0.53	-47.2 \pm 0.8
30	94.57 \pm 0.11	-47.2 \pm 0.9

NMR characterization

Table S3. Deacetylation degree (%DD) and Acetylation degree (%DA) in PG and FG Ct-NAC calculated by $^1\text{H-NMR}$ analysis.

Polymer	%DD	%DA
PG Ct-NAC	81%	47%
FG Ct-NAC	68%	55%

Ellman's test calibration curves and thiol groups determination in Ct-NAC

As described in **Result and Discussion**, we measured the absorbance and the TNB^{2-} values at 410 nm for NAC. Then, these values were fitted to obtain the calibration curves (each measurement was in triplicate, **Figure S1**). The value of NAC ϵ was $13199 \text{ M}^{-1} \text{ cm}^{-1}$, respectively. Starting from this value of ϵ , Ellman's test was performed for Ct-NAC and the degree of thiol groups (% NAC, $\sim 15.8 \pm 1.1 \%$) was calculated as explained in **Results and Discussion** (data reported in **Table S4**) by applying the equation **Eq S1**.

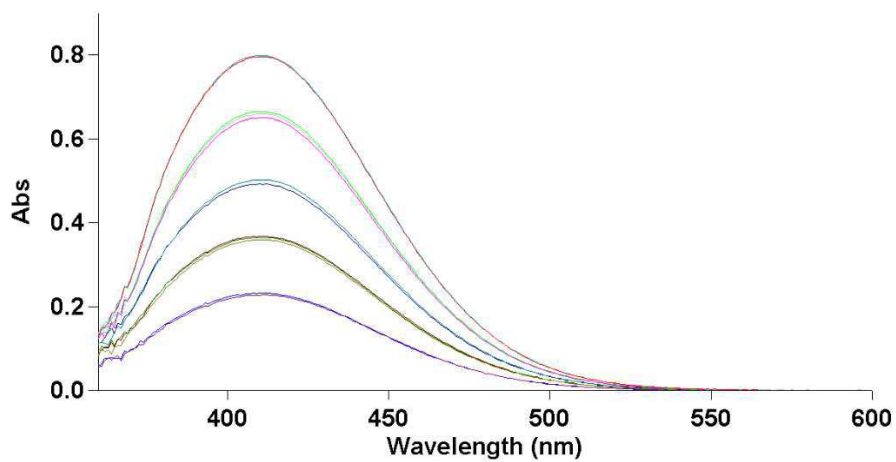
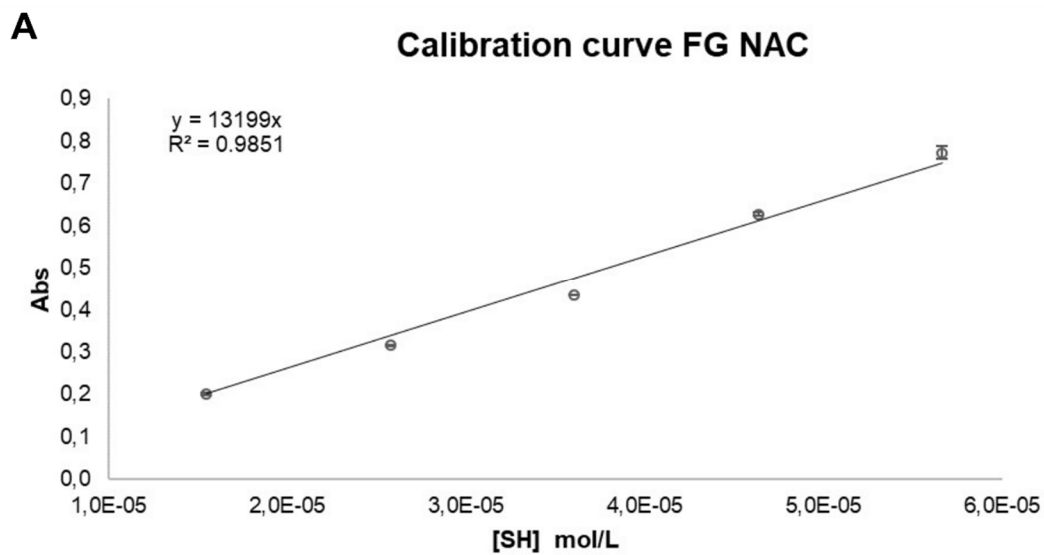


Figure S3. A) Ellman's test calibration curve of NAC. Each measure was done in triplicate. **B)** The absorbance spectra of NAC at different concentration for the calibration curve, each measure was performed in triplicate.

$$\text{Eq. S1} \quad \%SH = \frac{\text{mol/g SH}}{\text{mol tot./g}} \times 100$$

DLS analysis of FG and PG Ct and Ct-NAC NEs

Table S4. Size (PDI \leq 0.1) and ζ -potential data of PG and FG secondary NE 1 wt% in oil and 0.01 w/v% Ct. Data are reported as mean (s.d.) in triplicate.

Time (d)	Pharma Grade		Food Grade	
	Size (nm)	ζ -Pot. (mV)	Size (nm)	ζ -Pot. (mV)
0	101.4 \pm 0.8	+ 22.1 \pm 3.8	100.3 \pm 2.2	+ 25.5 \pm 1.9
4	104.5 \pm 3.3	+ 35.7 \pm 1.5	104.1 \pm 0.3	+ 31.5 \pm 6.3
7	104.2 \pm 1.4	+ 39.0 \pm 0.9	102.0 \pm 0.9	+ 36.6 \pm 3.7
14	110.3 \pm 0.1	+ 40.2 \pm 0.6	107.9 \pm 4.3	+ 37.9 \pm 3.3

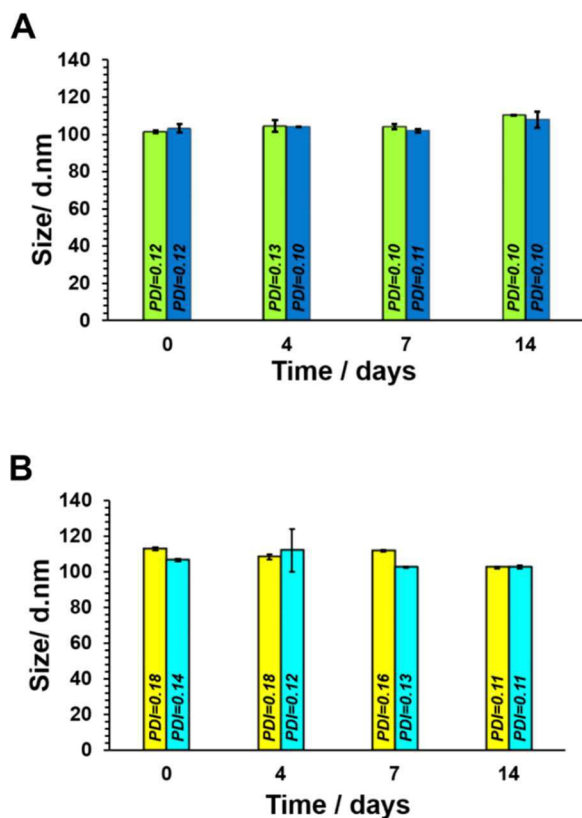


Figure S3. Stability over time of secondary NEs 1 wt% oil - 0.01 w/v % polymer: **A**) FG Ct (green) and PG Ct (blue), **B**) FG Ct-NAC (yellow) and PG Ct-NAC (light blue). Data are reported as mean (n=3).

Table S5. Size (PDI ≤ 0.1) and ζ-potential data of secondary NE 1 wt % in oil and 0.01 w/v % Ct-NAC in each PG and FG combinations. Data are reported as mean (s.d.) in triplicate.

Time (d)	PG Ct-NAC		FG Ct-NAC	
	Size (nm)	ζ-Pot. (mV)	Size (nm)	ζ-Pot. (mV)
0	112.7 ±0.9	+29.5 ±5.0	106.4 ±0.7	+25.5 ±1.8
4	108.1 ±1.4	+29.2 ±1.8	111.9 ±1.2	+28.7 ±2.3
7	111.6 ±0.7	+29.2 ±5.0	102.2 ±0.4	+30.4 ±4.0
14	102.2 ±0.4	+34.1 ±4.4	102.5 ±0.8	+36.3 ±2.8

Table S6. Size (PDI \leq 0.1) and ζ -potential data of FG secondary NE 10 wt% in oil and 0.1 w/v % Ct. Data are reported as mean (s.d.) in triplicate.

Time (d)	Size (nm)	ζ-Pot. (mV)
0	93.03 \pm 0.9	+ 35.0 \pm 0.9
15	95.41 \pm 0.8	+ 41.9 \pm 2.4
60	94.1 \pm 0.7	+ 52.7 \pm 1.4
210	99.2 \pm 0.1	+47.2 \pm 1.6
240	97.91 \pm 0.3	+52.4 \pm 0.9

Table S7. Size (PDI \leq 0.1) and ζ -potential data of FG secondary NE 10 wt% in oil and 0.1 w/v % Ct-NAC. Data are reported as mean in triplicate.

Time (d)	Size (nm)	ζ-Pot. (mV)
0	98.58 \pm 0.70	39.53 \pm 2.0
15	107.3 \pm 1.06	39.40 \pm 1.20
60	102.9 \pm 6.2	48.9 \pm 2.5
210	128.3 \pm 1.3	42.7 \pm 2.2
240	125.9 \pm 0.5	43.70 \pm 2.8

Table S8. Size (PDI \leq 0.1) and ζ -potential data of FG secondary CUR NE 10 wt% in oil and 0.1 w/v % Ct. Data are reported as mean in triplicate.

Time (d)	Size (nm)	ζ-Pot. (mV)
0	87.16 \pm 0.62	+ 43.3 \pm 0.6
15	87.72 \pm 0.48	+ 42.6 \pm 0.6
30	88.22 \pm 1.06	+ 48.2 \pm 0.79
60	95.26 \pm 0.1	+50.1 \pm 0.93
180	90.21 \pm 0.64	+59.1 \pm 2.02

Table S9. Size (PDI \leq 0.1) and ζ -potential data of FG secondary CUR NE 10 wt% in oil and 0.1 w/v % Ct-NAC. Data are reported as mean in triplicate.

Time (d)	Size (nm)	ζ-Pot. (mV)
0	94.17 \pm 0.30	41.1 \pm 1.85
15	90.96 \pm 0.60	37.2 \pm 2.27
30	98.58 \pm 0.70	39.5 \pm 1.20
60	108.95 \pm 0.62	40.7 \pm 1.90
180	105.1 \pm 2.24	45.7 \pm 0.98

Table S10. Size (PDI \leq 0.1) FG secondary NE 10 wt% in oil and 0.1 w/v % Ct FITC and Ct-NAC FITC. Data are reported as mean in triplicate.

Time (h)	Size value Ct-FITC NEs	Size value Ct-NAC FITC NEs
0	98.74 \pm 3.26	116.0 \pm 4.05
3	99.5 \pm 4.6	119.4 \pm 7.4
24	135.4 \pm 3.7	137.8 \pm 3.1
48	147.5 \pm 4.5	144.8 \pm 4.6

Table S11. Size (PDI \leq 0.2) FG secondary NE 10 wt% in oil and 0.1 w/v % Ct-NAC loaded with curcumin. Data are reported as mean in triplicate.

Time (h)	Size value Ct-NEs CUR	Size value Ct-NAC NEs CUR
0	115.6 \pm 2.4	138.1 \pm 2.9
3	123.5 \pm 1.0	151.1 \pm 0.9
24	130.9 \pm 2.5	59.6 \pm 3.4
48	131.1 \pm 2.2	154.7 \pm 4.1

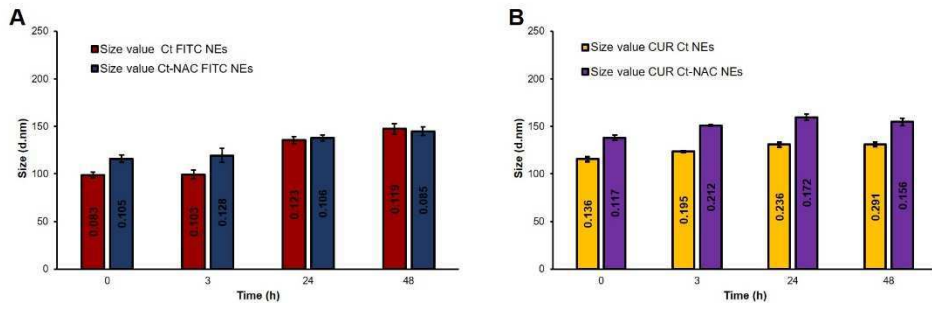


Figure S4. Stability at 37° in Caco-2 cell Medium at different time point (0,3h, 24h, 48h) of unloaded and loaded NEs 10 wt% oil - 0.1 w/v % polymer: **A)** Ct FITC NEs (red) Ct-NAC FITC NEs (blue), **B)** Ct NEs (yellow) and Ct-NAC NEs (violet) loaded with curcumin. Data are reported as mean (n=3).

Mucoadhesive properties of CUR Ct-NAC NEs and Ct NEs in InOA-chip

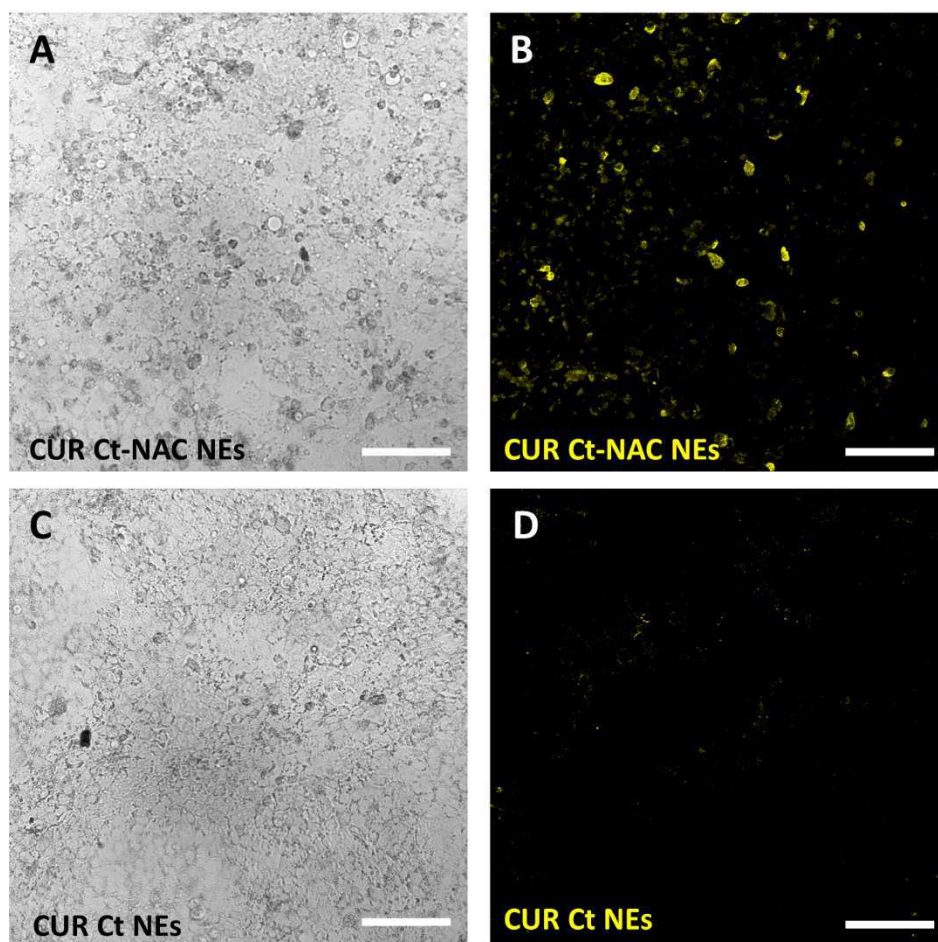


Figure S5. Mucoadhesive properties of Ct-NAC NEs and Ct NEs loaded with curcumin (CUR Ct-NAC NEs and CUR Ct NEs) in InOA-chip platform. Brightfield images of Ct-NAC NEs (**A**) and Ct NEs (**C**); scale bar 150 μm . Fluorescent signal of curcumin in CUR Ct-NAC NEs (**B**) and Ct NEs (**D**); scale bar 150 μm .

References

- 1 Dasgupta, N. & Ranjan, S. *An introduction to food grade nanoemulsions*. Vol. 13 (Springer, 2018).
- 2 McClements, D. J. & Rao, J. Food-grade nanoemulsions: formulation, fabrication, properties, performance, biological fate, and potential toxicity. *Critical reviews in food science and nutrition* **51**, 285-330 (2011).
- 3 Tripathi, A. D., Sharma, R., Agarwal, A. & Haleem, D. R. Nanoemulsions based edible coatings with potential food applications. *International Journal of Biobased Plastics* **3**, 112-125 (2021).
- 4 Marhamati, M., Ranjbar, G. & Rezaie, M. Effects of emulsifiers on the physicochemical stability of Oil-in-water Nanoemulsions: A critical review. *Journal of Molecular Liquids* **340**, 117218 (2021).
- 5 Li, J., Hwang, I.-C., Chen, X. & Park, H. J. Effects of chitosan coating on curcumin loaded nano-emulsion: Study on stability and in vitro digestibility. *Food Hydrocolloids* **60**, 138-147 (2016).
- 6 Vecchione, R. *et al.* Tunable stability of monodisperse secondary O/W nano-emulsions. *Nanoscale* **6**, 9300-9307 (2014).
- 7 Vecchione, R. *et al.* Curcumin bioavailability from oil in water nano-emulsions: In vitro and in vivo study on the dimensional, compositional and interactional dependence. *Journal of Controlled Release* **233**, 88-100 (2016).
- 8 Quagliariello, V. *et al.* Nano-encapsulation of coenzyme Q10 in secondary and tertiary nano-emulsions for enhanced cardioprotection and hepatoprotection in human cardiomyocytes and hepatocytes during exposure to anthracyclines and trastuzumab. *International Journal of Nanomedicine* **15**, 4859 (2020).
- 9 Di Natale, C. *et al.* Engineered Bacterial Cellulose Nanostructured Matrix for Incubation and Release of Drug-Loaded Oil in Water Nanoemulsion. *Frontiers in Bioengineering and Biotechnology* **10**, doi:10.3389/fbioe.2022.851893 (2022).
- 10 Quagliariello, V. *et al.* Cardioprotective effects of nanoemulsions loaded with anti-inflammatory nutraceuticals against doxorubicin-induced cardiotoxicity. *Nutrients* **10**, 1304 (2018).
- 11 Vecchione, R. *et al.* Ultrastable liquid–liquid interface as viable route for controlled deposition of biodegradable polymer nanocapsules. *Small* **12**, 3005-3013 (2016).
- 12 Fotticchia, T. *et al.* Enhanced drug delivery into cell cytosol via glycoprotein H-derived peptide conjugated nanoemulsions. *ACS nano* **11**, 9802-9813 (2017).
- 13 Di Cicco, C. *et al.* Biocompatible, photo-responsive layer-by-layer polymer nanocapsules with an oil core: in vitro and in vivo study. *Journal, of the Royal Society Interface* **19**, 20210800 (2022).
- 14 Calcagno, V. *et al.* Biostability enhancement of oil core—polysaccharide multilayer shell via photoinitiator free thiol-ene ‘click’ reaction. *Colloids and Surfaces B: Biointerfaces* **142**, 281-289 (2016).

- 15 Iaccarino, G., Profeta, M., Vecchione, R. & Netti, P. A. Matrix metalloproteinase-cleavable nanocapsules for tumor-activated drug release. *Acta Biomaterialia* **89**, 265-278 (2019).
- 16 De Capua, A. *et al.* Active targeting of cancer cells by CD44 binding peptide-functionalized oil core-based nanocapsules. *RSC Advances* **11**, 24487-24499 (2021).
- 17 Calcagno, V. *et al.* Oil core–PEG shell nanocarriers for in vivo MRI imaging. *Advanced healthcare materials* **8**, 1801313 (2019).
- 18 Profeta, M. *et al.* Cell Membrane-Coated Oil in Water Nano-Emulsions as Biomimetic Nanocarriers for Lipophilic Compounds Conveyance. *Pharmaceutics* **13**, 1069 (2021).
- 19 Fotticchia, I. *et al.* Thermodynamic signature of secondary nano-emulsion formation by isothermal titration calorimetry. *Langmuir* **30**, 14427-14433 (2014).
- 20 Fotticchia, I., Fotticchia, T., Mattia, C. A. & Giancola, C. Chitosan-based nanoparticles studied by isothermal titration calorimetry. *Journal of Thermal Analysis and Calorimetry* **125**, 585-593 (2016).
- 21 Boonsongrit, Y., Mueller, B. W. & Mitrevej, A. Characterization of drug–chitosan interaction by ¹H NMR, FTIR and isothermal titration calorimetry. *European Journal of Pharmaceutics and Biopharmaceutics* **69**, 388-395 (2008).
- 22 Thongngam, M. & McClements, D. J. Characterization of interactions between chitosan and an anionic surfactant. *Journal of Agricultural and Food Chemistry* **52**, 987-991 (2004).
- 23 Bravo-Osuna, I., Vauthier, C., Farabollini, A., Palmieri, G. F. & Ponchel, G. Mucoadhesion mechanism of chitosan and thiolated chitosan-poly (isobutyl cyanoacrylate) core-shell nanoparticles. *Biomaterials* **28**, 2233-2243 (2007).
- 24 Ellman, G. L. Tissue sulfhydryl groups. *Archives of biochemistry and biophysics* **82**, 70-77 (1959).
- 25 Xiang, Y. *et al.* Gut-on-chip: Recreating human intestine in vitro. *Journal of Tissue Engineering* **11**, 2041731420965318 (2020).
- 26 De Gregorio, V. *et al.* Intestine-on-chip device increases ECM remodeling inducing faster epithelial cell differentiation. *Biotechnology and Bioengineering* **117**, 556-566 (2020).
- 27 De Gregorio, V. *et al.* Intestine-liver axis on-chip reveals the intestinal protective role on hepatic damage by emulating ethanol first-pass metabolism. *Frontiers in bioengineering and biotechnology* **8**, 163 (2020).
- 28 Di Natale, C., Onesto, V., Lagreca, E., Vecchione, R. & Netti, P. A. Tunable release of curcumin with an in silico-supported approach from mixtures of highly porous PLGA microparticles. *Materials* **13**, 1807 (2020).
- 29 Langella, A. *et al.* In vitro study of intestinal epithelial interaction with engineered oil in water nanoemulsions conveying curcumin. *Colloids and Surfaces B: Biointerfaces* **164**, 232-239 (2018).
- 30 Riddles, P. W., Blakeley, R. L. & Zerner, B. Ellman's reagent: 5, 5'-dithiobis (2-nitrobenzoic acid)—a reexamination. *Analytical biochemistry* **94**, 75-81 (1979).
- 31 Kast, C. E. & Bernkop-Schnürch, A. Thiolated polymers—thiomers: development and in vitro evaluation of chitosan–thioglycolic acid conjugates. *Biomaterials* **22**, 2345-2352 (2001).

- 32 Minekus, M. *et al.* A standardised static in vitro digestion method suitable for food—an international consensus. *Food & function* **5**, 1113-1124 (2014).
- 33 Hirai, A., Odani, H. & Nakajima, A. Determination of degree of deacetylation of chitosan by ¹H NMR spectroscopy. *Polymer Bulletin* **26**, 87-94 (1991).
- 34 Gajdziok, J. & Vetchý, D. Mucoadhesive polymers in medical forms. *Chemicke Listy* **106** (2012).
- 35 Schuerer, N. *et al.* Effects of chitosan and chitosan N-acetylcysteine solutions on conjunctival epithelial cells. *Journal of EuCornea* **1**, 12-18 (2018).
- 36 Prakash, A. & Vadivel, V. Citral and linalool nanoemulsions: impact of synergism and ripening inhibitors on the stability and antibacterial activity against *Listeria monocytogenes*. *Journal of Food Science and Technology* **57**, 1495-1504 (2020).
- 37 Ogawa, S., Decker, E. A. & McClements, D. J. Production and characterization of O/W emulsions containing cationic droplets stabilized by lecithin– chitosan membranes. *Journal of agricultural and food chemistry* **51**, 2806-2812 (2003).
- 38 Ogawa, S., Decker, E. A. & McClements, D. J. Influence of environmental conditions on the stability of oil in water emulsions containing droplets stabilized by lecithin– chitosan membranes. *Journal of Agricultural and Food Chemistry* **51**, 5522-5527 (2003).
- 39 Rauf, A., Imran, M., Orhan, I. E. & Bawazeer, S. Health perspectives of a bioactive compound curcumin: A review. *Trends in food science technology* **74**, 33-45 (2018).
- 40 Ullah, F. *et al.* High bioavailability curcumin: an anti-inflammatory and neurosupportive bioactive nutrient for neurodegenerative diseases characterized by chronic neuroinflammation. *Archives of Toxicology* **91**, 1623-1634 (2017).
- 41 Ahmed, K., Li, Y., McClements, D. J. & Xiao, H. Nanoemulsion-and emulsion-based delivery systems for curcumin: Encapsulation and release properties. *Food chemistry* **132**, 799-807 (2012).
- 42 Fricker, G. *et al.* Phospholipids and lipid-based formulations in oral drug delivery. *Pharmaceutical research* **27**, 1469-1486 (2010).
- 43 Pinheiro, A. C. *et al.* Unravelling the behaviour of curcumin nanoemulsions during in vitro digestion: effect of the surface charge. *Soft Matter* **9**, 3147-3154 (2013).
- 44 Onoue, S. *et al.* Formulation design and photochemical studies on nanocrystal solid dispersion of curcumin with improved oral bioavailability. *Journal of pharmaceutical sciences* **99**, 1871-1881 (2010).
- 45 Sun, M. *et al.* Enhancement of transport of curcumin to brain in mice by poly (n-butylcyanoacrylate) nanoparticle. *Journal of Nanoparticle Research* **12**, 3111-3122 (2010).
- 46 Gou, M. *et al.* Curcumin-loaded biodegradable polymeric micelles for colon cancer therapy in vitro and in vivo. *Nanoscale* **3**, 1558-1567 (2011).
- 47 Ganta, S. & Amiji, M. Coadministration of paclitaxel and curcumin in nanoemulsion formulations to overcome multidrug resistance in tumor cells. *Molecular pharmaceuticals* **6**, 928-939 (2009).

- 48 Mangalathillam, S. *et al.* Curcumin loaded chitin nanogels for skin cancer treatment via the transdermal route. *Nanoscale* **4**, 239-250 (2012).
- 49 Gera, M. *et al.* Nanoformulations of curcumin: An emerging paradigm for improved remedial application. *Oncotarget* **8**, 66680 (2017).
- 50 Wright, L., Joyce, P., Barnes, T. J. & Prestidge, C. A. Mimicking the Gastrointestinal Mucus Barrier: Laboratory-Based Approaches to Facilitate an Enhanced Understanding of Mucus Permeation. *ACS Biomaterials Science & Engineering* (2021).
- 51 Lindner, M., Laporte, A., Block, S., Elomaa, L. & Weinhart, M. Physiological Shear Stress Enhances Differentiation, Mucus-Formation and Structural 3D Organization of Intestinal Epithelial Cells In Vitro. *Cells* **10**, 2062 (2021).
- 52 Shi, M. *et al.* Phytochemicals, Nutrition, Metabolism, Bioavailability, and Health Benefits in Lettuce—A Comprehensive Review. *Antioxidants* **11**, 1158 (2022).
- 53 TM, M. W., Lau, W. M. & Khutoryanskiy, V. V. Chitosan and Its Derivatives for Application in Mucoadhesive Drug Delivery Systems. *Polymers (Basel)* **10**, doi:10.3390/polym10030267 (2018).
- 54 Vllasaliu, D. *et al.* Tight junction modulation by chitosan nanoparticles: comparison with chitosan solution. *International journal of pharmaceutics* **400**, 183-193 (2010).
- 55 Noi, I., Schlachet, I., Kumarasamy, M. & Sosnik, A. Permeability of novel chitosan-g-poly (methyl methacrylate) amphiphilic nanoparticles in a model of small intestine in vitro. *Polymers* **10**, 478 (2018).
- 56 Bhushani, A. & Anandharamakrishnan, C. in *Nanoscience in Food and Agriculture 4* 99-139 (Springer, 2017).
- 57 Mehmood, T. & Ahmed, A. Tween 80 and soya-lecithin-based food-grade nanoemulsions for the effective delivery of vitamin D. *Langmuir* **36**, 2886-2892 (2020).
- 58 Jung, H. J. *et al.* Development of food-grade curcumin nanoemulsion and its potential application to food beverage system: antioxidant property and in vitro digestion. *Journal of food science* **81**, N745-N753 (2016).
- 59 Iqbal, R., Mehmood, Z., Baig, A. & Khalid, N. Formulation and characterization of food grade O/W nanoemulsions encapsulating quercetin and curcumin: Insights on enhancing solubility characteristics. *Food and Bioproducts Processing* **123**, 304-311 (2020).
- 60 Yuan, Y., Gao, Y., Zhao, J. & Mao, L. Characterization and stability evaluation of β -carotene nanoemulsions prepared by high pressure homogenization under various emulsifying conditions. *Food Research International* **41**, 61-68 (2008).
- 61 Walker, R., Decker, E. A. & McClements, D. J. Development of food-grade nanoemulsions and emulsions for delivery of omega-3 fatty acids: Opportunities and obstacles in the food industry. *Food & function* **6**, 41-54 (2015).

Chapter 5: Overall conclusion

The new era of NDDS is focused on the development of biomimetic NCs able to reach a specific compartment employing both passive and active targeting strategies. With this aim several approaches, using both synthetic and natural materials, have been proposed and developed. The NC physio-chemical properties are crucial for an effective specific targeting.

The attention of this thesis is focused on the construction of three SNEs based biomimetic nanocarriers able to reach a chosen site based on the characteristics of the most external layer, which was opportunely selected and modified for each application (cancer cell targeting, AS plaques accumulation and improved mucus adhesion for food applications).

Firstly, taking inspiration from the natural behaviour of cancer cells and immune circulating cells (i.e., monocytes and macrophages), biomimetic NCs with active targeting features were assembled, characterized and *in vitro* validated. This new generation of NCs demonstrated to retain the natural features of the biological sources. These results can be achieved by preserving the protein membrane integrity during all membrane extraction steps. The protein preservation of each membrane extraction was proved by CD analysis, which demonstrates the retention of membrane proteins with their secondary structure and the purity of membrane solutions, i.e. no DNA signals were detected. Once the purity and stability of the final membrane pellet was ascertained, the Ct-NEs were coated with the selected membranes. The NC assembly was obtained by exploiting the electrostatic interaction between the positive charged Ct and the negative charged plasma membrane phospholipids. The main advantages of this types of NC are the capability to join both the nanosized features of SNEs and biological properties coming from the cell source. Each membrane deposition was confirmed by DLS and Cryo-TEM analysis which showed the typical increment of size values given by the presence of cell membrane layers.

Initially, the attention was put on the building of CM-NEsoSome costing in a SNEs coated with a cancer cell membrane of U87, a human primary glioblastoma cell line, to exploit the homotypic adhesion properties to cancer cells active targeting. The obtained CM-NEsoSome had a nanometric distributions and demonstrated a good biocompatibility and cell internalization. These results open to the conveyance of several lipophilic compounds ranging from drugs and biomolecules to contrast agent compounds.

Then, we moved toward another biological source of cell membrane to realize a NDDS able to target an inflamed tissue as plaque. In this case, the role of macrophage and monocyte membrane coating was investigated and compared for the assembly an M and M0 NEsoSome to target the AS plaque. Both the formulations showed nanosized dimensions as proved by DLS and Cryo-TEM. The *in vitro* uptake in TNF- α activated HUVECs showed a faster internalization of macrophage coated material as compared to monocyte and uncoated NCs. It must be highlighted that M-NEsoSome showed a better accumulation when compared to uncoated NEsoSome probably due to the presence of cell adhesion molecules driving monocyte accumulation on inflamed tissue. The selectivity was also proved by analysing the accumulation of all formulations in a control system of control not TNF- α treated HUVECs. In this case, there was not a significant difference between Ct-NEs and membrane coated formulations. These data even if preliminary demonstrate good selectivity of M0-NEsoSome on inflamed ECs in respect to sane ECs. The developed NCs represent an innovative cell-derived biocompatible system able to bring together the biological nature of cell membranes with the excellent synthetic properties of Ct-NEs in terms of stability and high drug encapsulation efficacy. These results suggest that cell membrane coated SNEs could be employed for the treatment and diagnosis of several human diseases by modifying the cell membrane source.

In the recent years nanotechnologies got the attention of food industries for both the development of food supplements and for the improvement of tasting and nutritional values of food products. Consequently, there is a great interest in the development of food grade formulations with attractive production cost for the industries. As SNEs could also be employed as oral drug delivery system, we proposed a food grade formulation with improved mucus adhesion properties for the delivery of lipophilic substances as CUR. At first, FG and PG formulations have been morphologically, thermodynamically, and chemically compared. No differences between them from both size and stability perspectives were observed. Moreover, the improvement bioaccessibility of encapsulated CUR was proved by *in vitro* digestion model. In detail, the nano-formulations of CUR significantly increased the bio-accessibility of CUR compared to the free CUR digestion and could successfully stabilize it against CUR degradation.

Conclusively, the Ct and Ct-NAC mucus-adhesive properties were compared for the first time within an innovative and accessible intestine-on-chip platform, InOA-chip, proving that thiolated Ct NEs possess much better mucus adhesive properties, because of S-S bonds formation with

the mucin produced by the Caco-2 monolayers. The proposed totally FG system opens a new route in nutraceutical field, being a novel emulsion-based formulation with enhanced mucus-adhesiveness thanks to the Ct salification with NAC. Nonetheless, the chosen non-covalent thiol functionalization of chitosan opens the door to an immediate use of such formulation with no need for safety clinical tests.

In conclusion, this thesis proved the versatile application of SNEs as starting building block of both sophisticated active targeted drug delivery systems and nutraceutical oral delivery attractive for food industries.

Chapter 6: Side works

During the three years of PhD, I have the opportunity to collaborate in other activity involving O/W NEs as lipophilic molecules encapsulation strategy which led to publication of the following works. I was responsible for preparing and characterizing nanoemulsions for use as encapsulation strategies in both polymeric microparticles and cellulose layers. Additionally, I analysed the encapsulation and release capabilities of these formulations.

Tunable Release of Curcumin with an In Silico-Supported Approach from Mixtures of Highly Porous PLGA Microparticles

Concetta Di Natale^{1,2,†}, Valentina Onesto^{1,†}, Elena Lagreca^{1,3}, Raffaele Vecchione^{1,} and Paolo Antonio Netti^{1,2,3}*

¹*Center for Advanced Biomaterials for Health Care (CABHC), Istituto Italiano di Tecnologia, Largo Barsanti Matteucci 53, 80125 Napoli, Italy*

²*Interdisciplinary Research Centre on Biomaterials (CRIB), University of Naples Federico II, P.le Tecchio 80, 80125 Naples, Italy*

³*Department of Chemical Materials and Industrial Production (DICMAPI), University of Naples Federico II, P.le Tecchio 80, 80125 Naples, Italy*

**Author to whom correspondence should be addressed.*

†These authors contributed equally.

Published articles: Materials 2020, 13(8), 1807; <https://doi.org/10.3390/ma13081807>

*Received: 5 March 2020 / Revised: 3 April 2020 / Accepted: 9 April 2020 / Published: 11 April 2020
(This article belongs to the Special Issue Biodegradable and Biocompatible Polymer-Based Materials for Biomedical Engineering)*

Abstract

In recent years, drug delivery systems have become some of the main topics within the biomedical field. In this scenario, polymeric microparticles (MPs) are often used as carriers to improve drug stability and drug pharmacokinetics in agreement with this kind of treatment. To avoid a mere and time-consuming empirical approach for the optimization of the pharmacokinetics of an MP-based formulation, here, we propose a simple predictive in silico-supported approach. As an example, in this study, we report the ability to predict and tune the release of curcumin

(CUR), used as a model drug, from a designed combination of different poly(D,L-lactide-co-glycolide) (PLGA) MPs kinds. In detail, all CUR–PLGA MPs were synthesized by double emulsion technique and their chemical–physical properties were characterized by Mastersizer and scanning electron microscopy (SEM). Moreover, for all the MPs, CUR encapsulation efficiency and kinetic release were investigated through the UV–vis spectroscopy. This approach, based on the combination of *in silico* and experimental methods, could be a promising platform in several biomedical applications such as vaccinations, cancer-treatment, diabetes therapy and so on.

Keywords: PLGA MPs; drug delivery; curcumin; *in silico*; release model; first-order equation

1. Introduction

In recent decades, polymeric microparticles (MPs) have been widely used as drug delivery systems for the controlled release of small molecules, proteins, or peptides¹⁻⁴. The reason of this great diffusion is due to several attractive features such as the use of non-laborious techniques^{5,6}, low production costs⁶, simplicity in industrial scale-up⁷ and possibilities of different ways of administration (oral, ocular, parental, inhalation)^{8,9}. Particularly, biodegradable MPs composed of PLGA, a random copolymer of poly(glycolic acid) (PGA) and poly(lactic acid) (PLA), are well-established drug delivery systems for small macromolecules involved in the treatment of several important diseases including cancer¹⁰. PLGA is also a Food and Drug Administration (FDA) and European Medicine Agency (EMA) approved polymer for ophthalmologic, and other medical applications. PLGA shows relatively high miscibility with other polymers and solvents¹⁰, and, moreover, it is able to encapsulate both hydrophilic and lipophilic drugs¹¹. The use of PLGA MPs has many advantages, including biocompatibility, non-immunogenicity, non-toxicity, and the possibility of monitoring the polymer degradation in physiological environments to obtain a controlled drug delivery¹¹. Particularly, PLGA biodegradation involves a hydrolytic and an auto-catalytic degradation which includes hydration, hydrolytic degradation, auto-catalytic degradation and solubilization^{10,12,13}. Usually, the degradation time decreases by increasing the glycoside units content, but the pharmacokinetics characteristics of PLGA MPs are defined also by other factors such as initial MW^{6,13}, the monomer composition ratio of the PLGA matrix^{14,15}, stereochemistry (composition in D and L), end-group functionalization¹⁶, drug type¹⁷ and pH value of the release medium^{1,14-16,18,19}. In addition, the porosity of MPs can influence the drug release; for example, a relatively high porosity facilitates water penetration into particles leading to a direct drug release

from the porous and faster MPs degradation resulting again in a faster drug release²⁰. By contrast, a low degree of porosity can hinder water diffusion into MPs reducing the rate of polymer degradation²¹. The combination of these complex factors, without understanding their kinetics and dynamics, makes it difficult to predict and control the release of a drug.

Mathematical models represent a fundamental tool to optimally design new pharmaceutical systems, to study drug formulations and to evaluate *in vitro* and *in vivo* releases²²⁻²⁴. They rely on the model fitting of experimental data and equations and they enable a quantitative interpretation of the values obtained from a drug release assay²⁵. Release systems can be divided into those that release drug following a slow zero-or first-order kinetics and in controlled release patterns that provide an initial burst, followed by a slow zero-or first-order release of the sustained drug, to maintain as long as possible the desired pharmaceutical concentration in the target tissues or in the blood²⁶. In this regard, the shape and dimension of the system designed to achieve a specific drug release profile as well as the amount and type of the active agent, adjuvants and polymer can be predicted by mathematical models, in order to obtain a fine control on the drug release kinetics²⁵. *In silico* models can help to understand more deeply the physical and chemical mechanisms of drug release also reducing the number of experiments. They are particularly useful to analyse different conditions and strategies when the effects of diverse phenomena are joined²⁷. For example, mathematical modelling and parametric analysis were used to analyse the temperature effects of the controlled drug release process from PLGA biodegradable nanoparticles²⁸. Usually, empirical or mechanistic models are applied in the drug delivery field and in particular, the second ones, taking into account both physical and chemical phenomena that occur during the drug release, show a very high predictive ability towards specific experimental conditions^{29,30}.

In this study, we aim to develop a smart approach, based on the combination of *in silico* and experimental methods, to predict and control the release of a specific drug. We chose curcumin as a model drug and encapsulated it into PLGA MPs in three different ways: as water phase, as oil phase and as nano-emulsion. We decided to use curcumin since it is a powerful active substance by itself (ex. anti-inflammatory^{31,32}, anticancer³¹) and a hydrophobic molecule with a log P value of ~3.0, which allows it to be dissolvable in common organic solvents and partially soluble in polar solvents including water³³. These characteristics are common to many hydrophobic drugs (prostaglandin, doxorubicin) making curcumin (CUR) an ideal model drug.

Additionally, these features allowed us to perform three different kinds of encapsulation, providing different kinds of release, which then could be combined to obtain tenable kinetic release profiles in a predictive way.

The MPs were synthesized by double emulsion technique and their chemical–physical properties were characterized by Mastersizer, UV–vis and microscopy technologies. In the end, a non-linear first order *in silico* model was used to predict and tune (mixing the proper quantity of the three formulations) its release from MPs which was later confirmed by the experimental data. We think that the use of an *in silico* model, in combination with experimental data, could be very useful to design MPs with desired drug release profiles in order to control therapeutic dosages.

2. Materials and Methods

Materials

Poly (lactic-co-glycolic acid) (PLGA) RESOMER® RG 504 H, 38,000–54,000 Dalton, lactide–glycolide = 50:50, was purchased from Boehringer Ingelheim (Ingelheim am Rhein, Kreis, Germany) Curcumin (*Curcuma longa*, Turmeric, powder, M.W. = 368.38, CUR), dichloromethane (DCM), ammonium bicarbonate (ABC), dimethyl sulfoxide (DMSO), Mowiol® 40–88 (poly(vinyl)alcohol (PVA) MW 27,000–32,000 PVA) and Tween 20 were purchased from Sigma-Aldrich (Milan, Italy). Soybean oil and Lipoid E80 lecithin were purchased from Lipoid (Lipoid AG, Steinhausen/ZG, Switzerland). Bidistilled water was pre-treated with a Milli-Q R Plus System (Millipore Corporation, Bedford, OH, USA).

Methods

CUR–MPs Production

CUR in Oil Phase (CUR–Oil) and Water Phase (CUR–Water) Formulation

CUR–MPs were prepared by the water/oil/water double emulsion/solvent evaporation technique as already reported³⁴. A gas foaming porous agent, ammonium bicarbonate (ABC), at a concentration of 7.5 mg/mL was added in the first emulsion to obtain highly porous particles. Twelve milligrams of curcumin were loaded in DCM for the oil phase preparation, while the same

amount of drug was dissolved in 100 μ L of ethanol and 900 μ L of water plus 1 mL of DMSO in the water phase formulation.

CUR-O/W 20% Oil Nano-Emulsions (CUR-NEs) as Water Phase

The CUR-NEs was prepared as previously reported^{31,34,35}. Briefly, 1.2 mg of egg-lecithin (surfactant) was dissolved in 5 mL of soybean oil (oil phase). After, 20.83 mg of CUR was added to the mixture. The final emulsion was obtained by adding 19.3 mL of Milli-Q water to oil phase. After the process, 100 μ L of CUR-NE was used to produce CUR-NE-MPs as described in the previous paragraph.

CUR-MPs Characterization

Confocal Microscopy

All three CUR-MPs formulations were characterized by confocal microscopy (Leica SP5 microscope (Wetzlar, Germania)) to evaluate the signal of the molecule inside them. In detail, fluorescence images were acquired using an HCX IRAPO L 40 \times /0.95 water objective and a 488 nm laser as an excitation source as already described³⁶.

Microparticle Size and Polydispersity Index (PDI)

The mean size and the PDI of all CUR-MPs were determined by static light scattering (Mastersizer 3000, Malvern Instruments, Malvern, UK) using a concentration of 3 mg/mL in water.

Scanning Electron Microscopy (SEM)

CUR-MPs morphology was evaluated by SEM microscopy as already described ^[40]. Concisely, 20 μ L were deposited on a standard SEM pin stub and analysed by FESEM ULTRA-PLUS (Zeiss) (Milan, Italy) at 5 kV with the SE2 detector. Moreover, the internal porous structure of the MPs was investigated using a PDMS 2 mm in thickness cured at 80 $^{\circ}$ C for 30 min. After cooling, MPs were deposited on it and another PDMS layer 2mm in thickness was used to cover them up. Finally, the solid PDMS block was frozen in liquid nitrogen (-196 $^{\circ}$ C) and sectioned using the Leica CryoUltra Microtome EM-FC7-UC7 (Milan, Italy).

Entrapment Efficiency (% η) of CUR inside MPs

The % η of curcumin inside the three formulations of MPs was measured dissolving 10 mg of MPs in 1 mL of DMSO for 30 min, at room temperature. The solution was then analysed by UV–vis (UV–Visible-V-730 UV–Visible Spectrophotometer, Jasco, (Cremella, (LC), Italy) following the signal at 426 nm. The quantity of curcumin-loaded was obtained through the Beer–Lambert law using 58,547 dm³·mol⁻¹·cm⁻¹ as the molar extinction coefficient of curcumin in DMSO³⁷. All experiments were performed in triplicate.

In Vitro Release Study

In Silico Approach

Curcumin in oil phase, water phase and nano-emulsion experimental release data were fitted using MATLAB® (v.R2019a) (Turin, Italy) employing an exponential growth model. In particular, the curcumin release C_r was described by:

$$\text{Eq. 1 } C_r = a(1 - e^{-bt})$$

where a and b are the model parameters, and $y=0$ at $t=0$ the initial conditions.

A simple release kinetics prediction under the non-linear first-order assumption of **Eq. 1** was developed by **Eq. 2**:

$$\text{Eq1 } C_r = \sum_{n=1}^n C_n a_n (1 - e^{-b_n t}) / \sum_{n=1}^n C_n$$

$$\text{with } \sum_{n=1}^n C_n = C_1 + C_2 + \dots + C_n = 100$$

where a_n and b_n are the model parameters, C_n is the percentage of weighted curcumin MPs, n is the number of different MP formulations considered.

In Vitro Cumulative Release of CUR from MPs

In vitro curcumin release profile was obtained by the UV–vis technique (V-730 UV–Visible Spectrophotometer, Jasco, Cremella, (LC), Italy)). Aliquots of 5 mg of the three different microparticle formulations were suspended in 1.5 mL of phosphate buffer saline PBS at pH 7.2, vortexed under magnetic stirring at 550 rpm and incubated at 37 °C. At defined time intervals, 1

mL of PBS was removed without removing particles. The supernatants were then diluted 1:1 in ethanol and analysed by UV–vis using as molar extinction coefficient $28,648 \text{ dm}^3 \cdot \text{mol}^{-1} \cdot \text{cm}^{-1}$ ³⁸. The experiments were achieved in triplicate.

3. Results and Discussion

CUR-MPs Production and Morphological Characterization

CUR-MPs were produced through the double emulsion technique using the method of solvent evaporation³⁶. Three different configurations were obtained (CUR–NE, CUR–oil and CUR–water) to produce microspheres with curcumin molecules embedded inside or outside the porous structures. This strategy was designed to produce MPs with different drug release kinetics in physiological conditions. To compare the differences between the microparticles, their morphology was evaluated using Confocal and SEM microscopies. In particular, as shown in **Figure 1 A, B**, CUR–oil and CUR–water microparticles were visibly homogeneous with a high fluorescent signal corresponding to the embedded curcumin molecules. In detail, in the oil configuration, all curcumin was outside the porous structure as expected, while in the water conformation most of it was located inside the pores. Some aggregation phenomena were instead visible in the CUR–NE microparticles, probably due to the instability of the nano-emulsion during the production process (**Figure 1 C**).

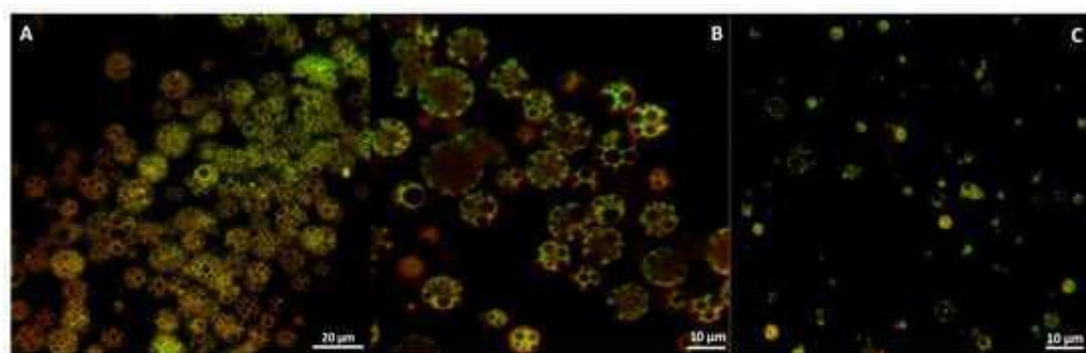


Figure 1. Confocal images of CUR-loaded microparticles: **A)** CUR–oil, **B)** CUR–water and **C)** CUR–nano-emulsions (NEs).

Similar considerations can be made analysing microparticles by SEM microscopy. In general, CUR–oil and CUR–water microparticles showed a homogeneous polymeric surface

(**Figure 2 A, B**) and by investigating their internal porous structure it was possible to confirm an open porosity for both the strategies of production (**Figure 2 D, E**). As for CUR–NE microparticles, they displayed good open porosity as the configurations just described (**Figure 2 F**) but their polymeric surface showed a slightly porous structure (**Figure 2 C**), maybe some nano-emulsion droplets aggregated on the surface generating a closed superficial porosity.

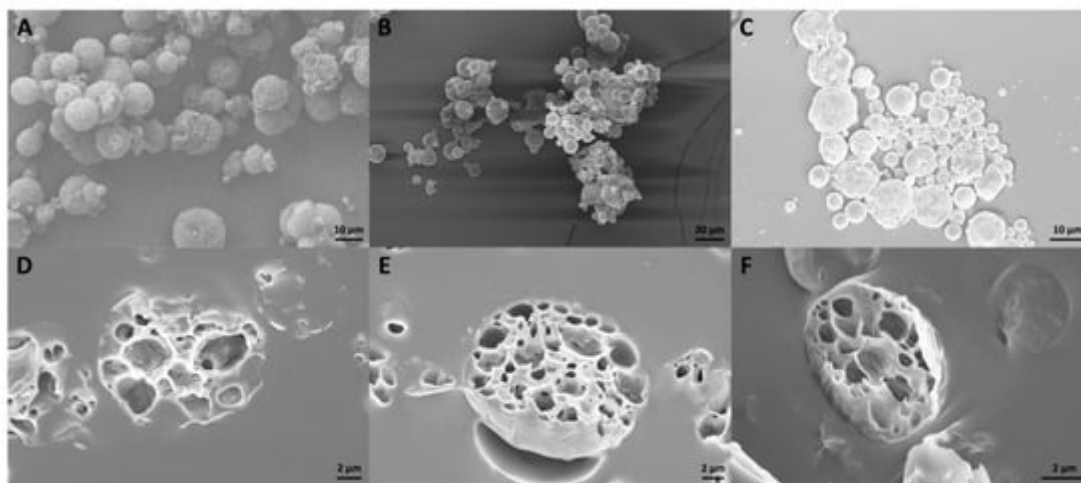


Figure 2. SEM microscopy of microparticles (MPs) microstructure. **A)** CUR–oil, **B)** CUR–water and **C)** CUR–NEs. In addition, their internal porosity was evaluated, depositing them on a PDMS layer 2 mm in thickness and cutting a PDMS block: **D–F)** CUR–oil, CUR–water and CUR–NE, respectively.

The homogeneity of MPs was also confirmed by analysing their size with a Malvern Mastersizer. The obtained results showed that CUR–oil and CUR–water microparticles have a uniform distribution with a mean diameter of 13.36 μm and 9.32 μm (**Figure 3 A, B**). Contrarily, as for the CUR–NE, despite having an average diameter of 7.9 μm , they expose a less sharp curve with a large peak at $\cong 1$ μm typical of the nano-emulsion used in this study, corroborating our hypothesis about its instability during the production phase of the microparticles (**Figure 3 C**).

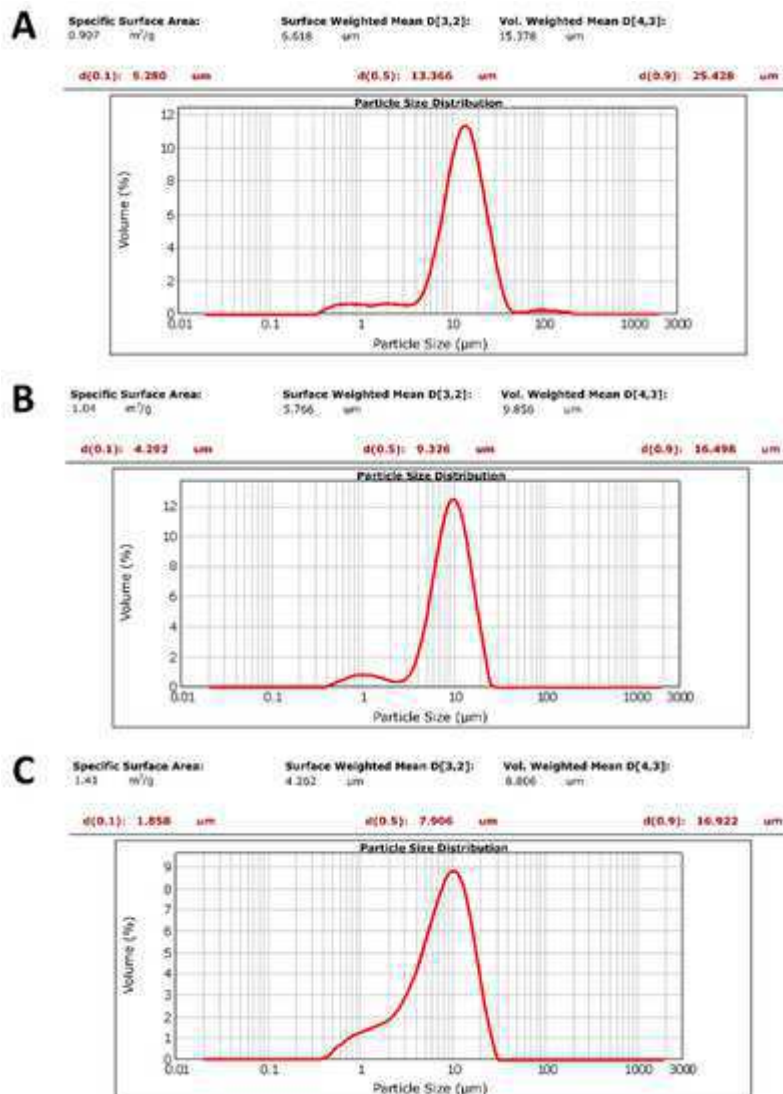


Figure 3. CUR-MPs dimensional analysis by Mastersizer at 3 mg/mL in water solution: **A)** CUR-oil, **B)** CUR-water and **C)** CUR-NE microparticles.

%η of CUR inside MPs

To evaluate the amount of curcumin encapsulated into MPs, 10 mg of each formulation was dissolved in a basic solution as reported in the **Materials and Methods** section. **Table 1** summarizes the %η for all three preparations; in particular, CUR-oil and CUR-water reached encapsulation efficiencies of 40.01 ± 0.3 and 42.30 ± 3.5 , respectively. As for the CUR-NE, the %η was 31.02 ± 0.5 and it was maybe due to the instability of the nano-emulsion during the

microparticle production steps (e.g., high speed, pH, time for solvent evaporation) as argued in the previous paragraph.

Table 4. % η of CUR-MPs

MPs	%η \pm SD
CUR-NE	31.02 \pm 0.5
CUR-oil	40.01 \pm 0.3
CUR-water	42.30 \pm 3.5

Release Study

In Silico Prediction

Release rate studies are important to control, tune and adjust the drug dose during a time-long therapy such as for diabetes³⁹, chemotherapy⁴⁰ and other chronic diseases as neurological⁴¹ or inflammation diseases^{42,43}. To this end, mathematical modelling can provide valuable information on the mechanism of the release process²⁵.

For measuring CUR release kinetics, the experimental release data of the three MP formulations were fitted using a non-linear first-order equation. Data fittings are shown in **Figure 4** together with the extracted model parameters **a** and **b**. The correlation coefficient R^2 and adjusted R^2 values of CUR-water, CUR-NE and CUR-oil were 0.99, 0.95, 0.98 and 0.98, 0.94

and 0.98, respectively. Therefore, the experimental data were not far from the calculated ones, indicating the suitability of the non-linear first-order kinetic equation model.

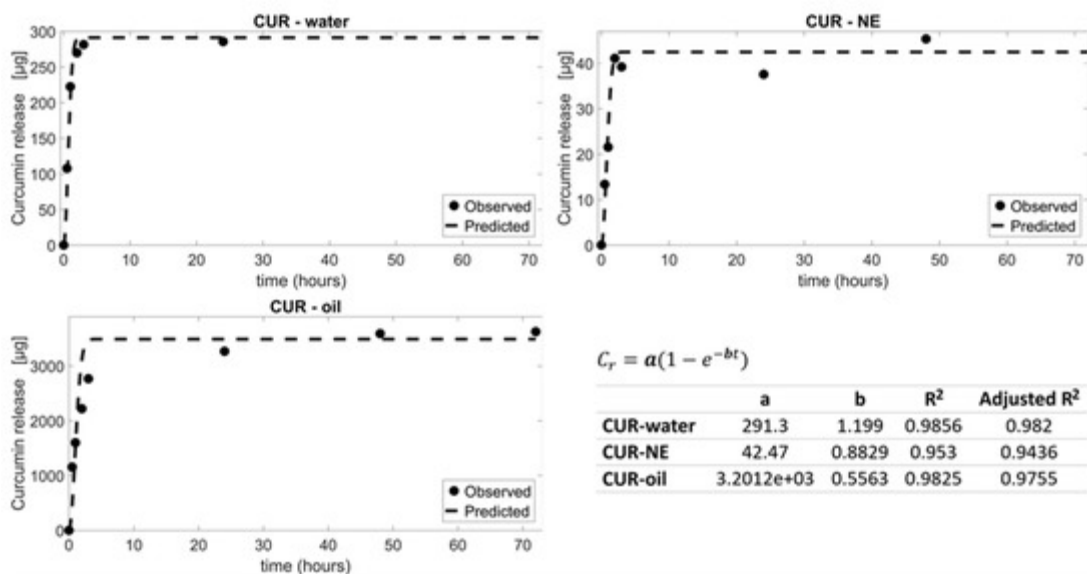


Figure 4. CUR–water, CUR–oil and CUR–NE experimental data were fitted with non-linear first-order models (dashed lines). The corresponding fitting parameters a and b are showing the table as well as the R² and adjusted R² values.

Once acquired the mathematical equations which describe the dependence of release as a function of time, a quantitative combination of non-linear first-order models (**Equation 2**) describing the three CUR–MP kinetics was used for simulating further releases of the encapsulated molecule. Some possible combinations are shown in **Figure 5**. Mathematical modelling of curcumin release kinetics has been used to design several controlled MP-based drug delivery systems to release a specific concentration of curcumin in the target tissues with the desired timing. This tool is very useful to predict releases, avoiding the necessity of realizing experiments.

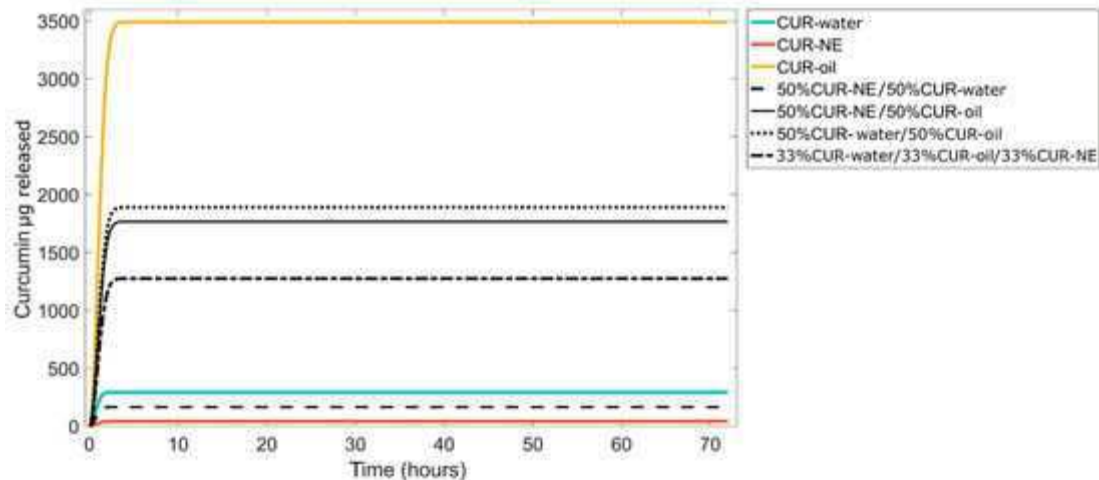


Figure 5. Predictive curcumin release kinetics can be obtained combining different CUR–water, CUR–oil and CUR–NE amounts by non-linear first-order models.

***In Vitro* CUR Release**

With the aim to understand the reliability and accuracy of the *in silico* studies, experimental *in vitro* release profiles of curcumin were performed. Particularly, four different combinations used for theoretical studies were analysed: **(i)** 50% of CUR–oil plus 50% CUR–water, **(ii)** 50% of CUR–oil plus 50% CUR–NE, **(iii)** 50% of CUR–water–50% CUR–NE and **(iv)** 33% of all three formulations. Moreover, the release of curcumin from the single formulations was also evaluated as control. Interestingly, as shown in **Figure 6 A, B**, a perfect correlation between hypothetical and experimental results was obtained, confirming that mathematical models can be a great support to reduce the number of experiments and to analyse different conditions and strategies.

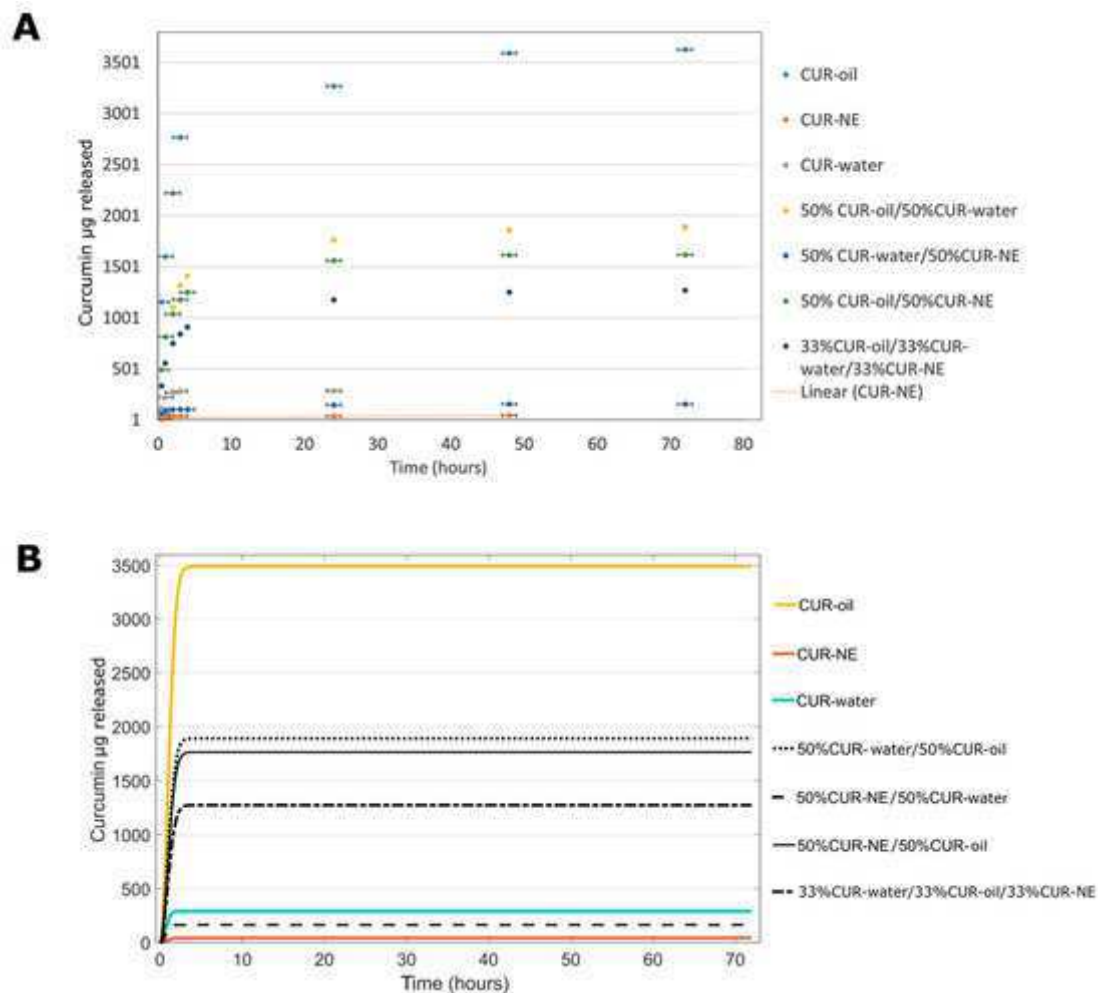


Figure 6. Correlation of curcumin released from different MP combinations: **A)** experimental *in vitro* release, in PBS at pH 7.2, 550 rpm and 37 °C and **B)** *in silico* release.

The amounts of curcumin released from each case coming from *in silico* and *in vitro* experiments after 72h, were summarized in **Table 2**. As we can see, the CUR–water and CUR–NE formulations can guarantee a fast release; after 72 h, all CUR is released, but they are able to release only 285 ± 2.95 and 45.35 ± 4.21 µg of curcumin, respectively. In addition, for these formulations, a percentage of release more than 100% is reported; numbers over 100%, but still close to this value, are potentially due to random and systematic errors coming from the evaluation methods. Intermediary situations can be achieved by mixing them with CUR–oil configuration, indeed, using the 50% of CUR–oil MPs with 50% of CUR–water or CUR–NE, 60% of the drug can be released after 72 h with an amount of >1 mg. This situation was maintained even by using

33% of the three formulations together. The same results were confirmed by the *in silico* data (**Table 2**). The obtained outcomes underline how, thanks to our approach, we are able to finely regulate the quantity of the drug to be released, generating a powerful platform for the drug delivery field.

Table 2. *In silico* and *in vitro* curcumin release experiments ($n = 3$).

MPs	µg of CUR Released <i>In Silico</i> (72 h)	% CUR Released <i>In Silico</i> (72 h)	µg of CUR Released <i>In Vitro</i> (72 h)	% CUR Released <i>In Vitro</i> (72 h)
CUR–oil	3491	77.4	3626±15	80±10
CUR–water	291.3	107.4	285±3	105±4
CUR–NE	42.47	99.2	45±4	106±3
50%CUR–oil/50%CUR–water	1891	64.7	1886±16	64±16
50%CUR–oil/50%CUR–NE	1766	63.3	1617±0.3	58±9
50%CUR–water/50%CUR–NE	166	95.6	155±2	89±12
33%CUR–oil/33%CUR water/33%CUR–NE	1275	62.4	1270±15	62±14

4. Conclusions

This project was undertaken to design curcumin-loaded PLGA MP-based formulations with tuneable kinetic release by using a combination of different PLGA MPs. We demonstrated that the rate of curcumin released PLGA MPs can be controlled by playing on the encapsulation strategy which has an effect on the MP microstructure and on the drug distribution within the MPs. Moreover, thanks to the use of a non-linear first-order mathematical model we were able to predict and obtain intermediate situations capable of guaranteeing prolonged or fast drug releases by combining the starting PLGA MPs. The perfect agreement obtained between experimental and in silico methods, confirmed that mathematical modelling could be a valuable support to reduce the number of experiments during the development of novel personalized therapies, especially for the long-term ones.

Our approach can be easily extended to other molecules besides curcumin, and it will be useful to release drugs to the target sites with a controlled timing and amount, maximizing the therapeutic efficiency and thus decreasing the side effects.

Author Contributions

Conceptualization, C.D.N., R.V., P.A.N., C.D.N. and E.L. performed microparticles production and all related experiments, V.O. performed in silico models, C.D.N. writing—original draft preparation, C.D.N., V.O. and R.V. writing—review and editing. All authors have read and agreed to the published version of the manuscript.

Acknowledgments

The authors would like to thank Dr. Valentina Mollo for her great support in SEM imaging and Dr. Fabio Formigini for his support in confocal imaging.

References

- 1 Patel, V., Akbari, B., Deshmukh, A., Goyani, M. & Patel, A. A Review on PLGA Based Solvent Induced In-situ Forming Implant. *Research Journal of Pharmaceutical Dosage Forms and Technology* **8**, 127 (2015).
- 2 Guo, W., Quan, P., Fang, L., Cun, D. & Yang, M. Sustained release donepezil loaded PLGA microspheres for injection: Preparation, in vitro and in vivo study. *Asian Journal of Pharmaceutical Sciences* **10**, 405-414, doi:<https://doi.org/10.1016/j.ajps.2015.06.001> (2015).

- 3 Chereddy, K. K., Vandermeulen, G. & Pr at, V. PLGA based drug delivery systems: Promising carriers for wound healing activity. *Wound Repair and Regeneration* **24**, 223-236, doi:<https://doi.org/10.1111/wrr.12404> (2016).
- 4 Jamaledin, R. *et al.* Progress in Microneedle-Mediated Protein Delivery. *Journal of Clinical Medicine* **9**, 542 (2020).
- 5 Han, F. Y., Thurecht, K. J., Whittaker, A. K. & Smith, M. T. Bioerodable PLGA-Based Microparticles for Producing Sustained-Release Drug Formulations and Strategies for Improving Drug Loading. *Frontiers in Pharmacology* **7**, doi:10.3389/fphar.2016.00185 (2016).
- 6 Amoyav, B. & Benny, O. Microfluidic Based Fabrication and Characterization of Highly Porous Polymeric Microspheres. *Polymers* **11**, 419 (2019).
- 7 Rezvantalab, S. & Keshavarz Moraveji, M. Microfluidic assisted synthesis of PLGA drug delivery systems. *RSC Advances* **9**, 2055-2072, doi:10.1039/C8RA08972H (2019).
- 8 Hu, Y., Li, M., Zhang, M. & Jin, Y. Inhalation treatment of idiopathic pulmonary fibrosis with curcumin large porous microparticles. *International Journal of Pharmaceutics* **551**, 212-222, doi:<https://doi.org/10.1016/j.ijpharm.2018.09.031> (2018).
- 9 Rezaul H Ansary, M. B. A. a. M. M. R. Biodegradable Poly(D,L-lactic-co-glycolic acid)-Based Micro/Nanoparticles for Sustained Release of Protein Drugs - A Review. *Tropical Journal of Pharmaceutical Research* **13**, 1179-1190, doi:10.4314/tjpr.v13i7.24 (2014).
- 10 Kapoor, D. N. *et al.* PLGA: a unique polymer for drug delivery. *Therapeutic Delivery* **6**, 41-58, doi:10.4155/tde.14.91 (2015).
- 11 Swider, E. *et al.* Customizing poly(lactic-co-glycolic acid) particles for biomedical applications. *Acta Biomaterialia* **73**, 38-51, doi:<https://doi.org/10.1016/j.actbio.2018.04.006> (2018).
- 12 Makadia, H. K. & Siegel, S. J. Poly Lactic-co-Glycolic Acid (PLGA) as Biodegradable Controlled Drug Delivery Carrier. *Polymers* **3**, 1377-1397 (2011).
- 13 Xu, Y., Kim, C.-S., Saylor, D. M. & Koo, D. Polymer degradation and drug delivery in PLGA-based drug-polymer applications: A review of experiments and theories. *Journal of Biomedical Materials Research Part B: Applied Biomaterials* **105**, 1692-1716, doi:<https://doi.org/10.1002/jbm.b.33648> (2017).
- 14 Physicochemical Properties and Applications of Poly(lactic-co-glycolic acid) for Use in Bone Regeneration. *Tissue Engineering Part B: Reviews* **19**, 380-390, doi:10.1089/ten.teb.2012.0443 (2013).
- 15 Washington, M. A. *et al.* Monomer sequence in PLGA microparticles: Effects on acidic microclimates and in vivo inflammatory response. *Acta Biomaterialia* **65**, 259-271, doi:<https://doi.org/10.1016/j.actbio.2017.10.043> (2018).
- 16 Takeuchi, I., Tomoda, K., Hamano, A. & Makino, K. Effects of physicochemical properties of poly(lactide-co-glycolide) on drug release behavior of hydrophobic drug-loaded nanoparticles. *Colloids and Surfaces A: Physicochemical and Engineering Aspects* **520**, 771-778, doi:<https://doi.org/10.1016/j.colsurfa.2017.02.054> (2017).

- 17 Wang, J. *et al.* Encapsulation and release of doxycycline from electrospray-generated PLGA microspheres: Effect of polymer end groups. *International Journal of Pharmaceutics* **564**, 1-9, doi:<https://doi.org/10.1016/j.ijpharm.2019.04.023> (2019).
- 18 Panyam, J., Williams, D., Dash, A., Leslie-Pelecky, D. & Labhasetwar, V. Solid-state Solubility Influences Encapsulation and Release of Hydrophobic Drugs from PLGA/PLA Nanoparticles. *Journal of Pharmaceutical Sciences* **93**, 1804-1814, doi:<https://doi.org/10.1002/jps.20094> (2004).
- 19 Keles, H., Naylor, A., Clegg, F. & Sammon, C. Studying the release of hGH from gamma-irradiated PLGA microparticles using ATR-FTIR imaging. *Vibrational Spectroscopy* **71**, 76-84, doi:<https://doi.org/10.1016/j.vibspec.2014.01.012> (2014).
- 20 Keles, H., Naylor, A., Clegg, F. & Sammon, C. Investigation of factors influencing the hydrolytic degradation of single PLGA microparticles. *Polymer Degradation and Stability* **119**, 228-241, doi:<https://doi.org/10.1016/j.polymdegradstab.2015.04.025> (2015).
- 21 Peppas, N. A. & Narasimhan, B. Mathematical models in drug delivery: How modeling has shaped the way we design new drug delivery systems. *Journal of Controlled Release* **190**, 75-81, doi:<https://doi.org/10.1016/j.jconrel.2014.06.041> (2014).
- 22 Wojcik-Pastuszka, D. *et al.* Evaluation of the Release Kinetics of a Pharmacologically Active Substance from Model Intra-Articular Implants Replacing the Cruciate Ligaments of the Knee. *Materials* **12**, 1202 (2019).
- 23 Mircioiu, C. *et al.* Mathematical Modeling of Release Kinetics from Supramolecular Drug Delivery Systems. *Pharmaceutics* **11**, 140 (2019).
- 24 Jakhmola, A. *et al.* Experimental and theoretical study of biodirected green synthesis of gold nanoflowers. *Materials Today Chemistry* **14**, 100203, doi:<https://doi.org/10.1016/j.mtchem.2019.100203> (2019).
- 25 Dash, S., Murthy, P. N., Nath, L. & Chowdhury, P. Kinetic modeling on drug release from controlled drug delivery systems. *Acta Pol Pharm* **67**, 217-223 (2010).
- 26 Casalini, T., Rossi, F., Lazzari, S., Perale, G. & Masi, M. Mathematical Modeling of PLGA Microparticles: From Polymer Degradation to Drug Release. *Molecular Pharmaceutics* **11**, 4036-4048, doi:10.1021/mp500078u (2014).
- 27 Lucero-Acuña, A., Gutiérrez-Valenzuela, C. A., Esquivel, R. & Guzmán-Zamudio, R. Mathematical modeling and parametrical analysis of the temperature dependency of control drug release from biodegradable nanoparticles. *RSC Adv* **9**, 8728-8739, doi:10.1039/c9ra00821g (2019).
- 28 Luta, I. & Maria, G. Semi-empirical vs. mechanistical kinetic models used to design drug delivery systems. *UPB Scientific Bulletin, Series B: Chemistry and Materials Science* **74**, 99-112 (2012).
- 29 Naghipoor, J. & Rabczuk, T. A mechanistic model for drug release from PLGA-based drug eluting stent: A computational study. *Computers in Biology and Medicine* **90**, 15-22, doi:<https://doi.org/10.1016/j.compbiomed.2017.09.001> (2017).
- 30 Battisti, M. *et al.* Non-invasive Production of Multi-Compartmental Biodegradable Polymer Microneedles for Controlled Intradermal Drug Release of Labile Molecules. *Frontiers in Bioengineering and Biotechnology* **7**, doi:10.3389/fbioe.2019.00296 (2019).

- 31 Fotticchia, T. *et al.* Enhanced Drug Delivery into Cell Cytosol via Glycoprotein H-Derived Peptide Conjugated Nanoemulsions. *ACS Nano* **11**, 9802-9813, doi:10.1021/acsnano.7b03058 (2017).
- 32 Calcagno, V. *et al.* Oil Core–PEG Shell Nanocarriers for In Vivo MRI Imaging. *Advanced Healthcare Materials* **8**, 1801313, doi:<https://doi.org/10.1002/adhm.201801313> (2019).
- 33 Quagliariello, V. *et al.* Cardioprotective Effects of Nanoemulsions Loaded with Anti-Inflammatory Nutraceuticals against Doxorubicin-Induced Cardiotoxicity. *Nutrients* **10**, 1304 (2018).
- 34 Vecchione, R. *et al.* Curcumin bioavailability from oil in water nano-emulsions: In vitro and in vivo study on the dimensional, compositional and interactional dependence. *Journal of Controlled Release* **233**, 88-100 (2016).
- 35 Vecchione, R. *et al.* Tunable stability of monodisperse secondary O/W nano-emulsions. *Nanoscale* **6**, 9300-9307 (2014).
- 36 Barik, A. *et al.* Evaluation of a new copper(II)–curcumin complex as superoxide dismutase mimic and its free radical reactions. *Free Radical Biology and Medicine* **39**, 811-822, doi:<https://doi.org/10.1016/j.freeradbiomed.2005.05.005> (2005).
- 37 Veisheh, O. Drug delivery: Week-long diabetes therapy. *Nature Biomedical Engineering* **1**, 0090, doi:10.1038/s41551-017-0090 (2017).
- 38 Kalaydina, R. V., Bajwa, K., Qorri, B., Decarlo, A. & Szewczuk, M. R. Recent advances in "smart" delivery systems for extended drug release in cancer therapy. *Int J Nanomedicine* **13**, 4727-4745, doi:10.2147/ijn.S168053 (2018).
- 39 Kang, Y. J., Cutler, E. G. & Cho, H. Therapeutic nanoplatfoms and delivery strategies for neurological disorders. *Nano Convergence* **5**, 35, doi:10.1186/s40580-018-0168-8 (2018).
- 40 Di Natale, C. *et al.* The level of 24-hydroxycholesteryl esters decreases in plasma of patients with Parkinson's disease. *Neuroscience Letters* **672**, 108-112, doi:<https://doi.org/10.1016/j.neulet.2018.02.041> (2018).
- 41 Ulbrich, W. & Lamprecht, A. Targeted drug-delivery approaches by nanoparticulate carriers in the therapy of inflammatory diseases. *Journal of The Royal Society Interface* **7**, S55-S66, doi:10.1098/rsif.2009.0285.focus (2010).
- 42 Alteriis, R. d. *et al.* A method to tune the shape of protein-encapsulated polymeric microspheres. *Scientific Reports* **5**, 12634, doi:10.1038/srep12634 (2015).
- 43 La Manna, S., Di Natale, C., Florio, D. & Marasco, D. Peptides as Therapeutic Agents for Inflammatory-Related Diseases. *International Journal of Molecular Sciences* **19**, 2714 (2018).

© 2020 by the authors. Licensee MDPI, Basel, Switzerland. This article is an open access article distributed under the terms and conditions of the Creative Commons Attribution (CC BY) license (<http://creativecommons.org/licenses/by/4.0/>).

Engineered Bacterial Cellulose Nanostructured Matrix for Incubation and Release of Drug-Loaded Oil in Water Nanoemulsion

Concetta Di Natale,^{1,2,3} Vincenza De Gregorio,^{1,2} Elena Lagreca,^{2,3} Francesca Mauro,^{2,3} Brunella Corrado,^{1,2} Raffaele Vecchione,^{2,*} and Paolo Antonio Netti^{1,2,3}

¹ Interdisciplinary Research Centre on Biomaterials, University of Naples Federico II, Naples, Italy

² Istituto Italiano di Tecnologia, Naples, Italy

³ Department of Chemical Materials, Industrial Production Engineering, University of Naples Federico II, Naples, Italy

✉Corresponding author.

*Correspondence: Raffaele Vecchione, ti.tii@enoihccev.eleaffaR

This article was submitted to *Biomaterials*, a section of the journal *Frontiers in Bioengineering and Biotechnology*. *Front Bioeng Biotechnol.* 2022 Mar 9;10:851893. doi: 10.3389/fbioe.2022.851893. PMID: 35356776; PMCID: PMC8959586.

Abstract

Bacterial cellulose (BC) is a highly pure form of cellulose produced by bacteria, which possesses numerous advantages such as good mechanical properties, high chemical flexibility, and the ability to assemble in nanostructures. Thanks to these features, it achieved a key role in the biomedical field and in drug delivery applications. BC showed its ability to modulate the release of several drugs and biomolecules to the skin, thus improving their clinical outcomes. This work displays the loading of a 3D BC nanonetwork with an innovative drug delivery nanoemulsion system. BC was optimized by static culture of SCOBY (symbiotic colony of bacteria and yeast) and characterized by morphological and ultrastructural analyses, which indicate a cellulose fiber diameter range of 30–50 nm. BC layers were then incubated at different time points with a nanocarrier based on a secondary nanoemulsion (SNE) previously loaded with a well-known antioxidant and anti-inflammatory agent, namely, coenzyme-Q10 (Co-Q10). Incubation of Co-Q10–SNE in the BC nanonetwork and its release were analyzed by fluorescence spectroscopy.

Keywords: bacterial cellulose, drug delivery, nanocellulose network, nanoemulsion, antioxidant

1. Introduction

In the last few years, the choice of appropriate drug delivery systems has achieved great attention in the pharmaceutical field. A successful drug delivery is influenced by several factors¹ including the identification of a suitable biomaterial³ to be used as a building block for the assembly of the final system⁴. For example, very recently, nanostructure plasmalogen-loaded cubosomes or exosomes were reported as innovative delivery systems for the lipophilic antioxidant compound, opening new opportunities for bioinspired nanoassemblies^{5,6}. In this context, another interesting material, which is synthesized from bacteria and presents a nanostructured matrix useful for drug encapsulation and release, is the bacterial cellulose (BC); it possesses a great versatility in terms of *in situ* modulation, post-synthesis chemical modifications, biocompatibility, or ease of sterilization^{7,8}. In addition, it also shows high purity and water absorption capacity, as well as single mechanical properties, good permeability, or resistance to degradation⁹⁻¹¹. Thanks to these properties, BC is achieving great interest in biomedical research concerning, for example, the wound dressing for skin burns or the microsurgery for the restoration of artificial blood vessels^{7,12}. From the chemical point of view, BC is organized in a tridimensional (3D) nanofibrillar network, and this singular property makes it a suitable macromolecular support for drug encapsulation and, therefore, for the development of specific controlled release systems^{13,14}. Several studies displayed the ability of BC networks to modulate the release and bioavailability of drugs in percutaneous administration, and hence, they were suggested as supports for topical or transdermal drug delivery¹⁵. For example, BC fibers loaded with silver nanoparticles, in topic formulations, demonstrated an antibacterial activity up to 99.99% against *Escherichia coli* and *Staphylococcus aureus*^{16,17}. Other studies instead showed the ability of nanofibrils as aerogels to encapsulate drugs such as anti-inflammatories, anticancer, steroids or biomolecules as peptides, and proteins or antibodies¹⁸. Apart from drug loading, the possibility of regulating their release is also remarkable, and BC nanofibers revealed the ability to modulate the release of both hydrophobic and hydrophilic compounds, thus providing versatile materials with respect to drug delivery¹⁹. Several studies, indeed, revealed as BC nanofibers can allow a sustained and controlled release of antioxidant molecules such as quercetin and vanillin or cinnamic acid for food or cosmetic applications^{14,20,21}.

The present work proposes a method to load the BC nanonetwork with stabilized lipophilic compounds and allow its release in a time frame of hours which is compliant with skin applications.

To the best of our knowledge, no Co-Q10 nanocarrier has ever been encapsulated within cellulose fibres. In detail, we used an ultra-stable oil-in-water (O/W) SNE coated by a thin layer of chitosan (Ct) ²²⁻²⁴, a positively charged polyelectrolyte, able to encapsulate lipophilic molecules such as curcumin^{22,25-27}, lycopene²⁸, and Co-Q10²⁹. In the latter stage of work, the nanocarriers were loaded with Co-Q10 acting as antioxidant and anti-inflammatory agents meant for oral delivery, proving high loading capability and molecular stability preservation. However, Co-Q10 is also very well-known as an antioxidant for skin applications³⁰. Starting from these considerations, here, we propose the development of a BC-Co-Q10-SNE nanonetwork for a double release approach where the cellulose network releases the Co-Q10-loaded SNE which, upon degradation, can finally release active Co-Q10 to the skin. Our BC was produced by the SCOBY using optimized conditions in terms of humidity (98%) and temperature (30°C), as well as the culture media volume that assured the correct moist status, avoiding the production of a thick layer with BC exfoliation ^{20,31}. Several spectroscopic techniques such as scanning electron microscopy (SEM) and infrared ray (IR) were used for BC morphological and chemical characterizations, while Co-Q10-SNE loading and release were studied by confocal microscopy and fluorescence, respectively, by following Co-Q10 autofluorescence.

This study aims to be a proof of concept for a new use of BC as a drug delivery system; future analysis will indeed focus on the production of inflamed micro-tissues which will subsequently be treated with the BC-Co-Q10-SNE described in this study.

2. Material and methods

Materials

Both soybean oil (density at 20°C of 0.922 g mL⁻¹) and the surfactant Lipoid E80 (egg lecithin powder 80–85% enriched with phosphatidyl choline (PC) and 7–9.5% content in phosphatidyl ethanolamine (PE)) were purchased from Lipoid GmbH and used without further purification. Millipore Milli-Q water was used for the preparation of all nanoemulsions and solutions. Chitosan (Ct, LMW 90–150 kDa, and DDA 84% determined *via* ¹H-NMR) was purchased from Sigma-Aldrich (Milan, Italy). Ubidecarenone, Coenzyme-Q10 (Co-Q10), was kindly offered by the Faravelli Group. Kombucha SCOBY was purchased from KEFIRA, and glucose and agar were purchased from Sigma-Aldrich.

Methods

Media preparation and SCOBY culture

For Kombucha SCOBY (KEFIRA) culture, a tea broth and an agar plate were prepared with the following protocol: 860 ml of deionized water (dH₂O) was boiled before adding 140 g/L of glucose; 10 sachets (20 g) of black tea were added and steeped for 10 min. Consequently, the tea bags were removed, and the sweetened tea was cooled at room temperature; then, apple vinegar (140 mL/L) was added. The medium was autoclaved at 121°C for 15 min. For solid medium, the agar was autoclaved separately. To improve the fermentation process of the SCOBY, one piece (1×1 cm) of the SCOBY was aseptically added into the liquid broth and cultured for 3 days. Then, an aliquot of 1 mL of the previously fermented SCOBY, which acts as a starter, was inoculated into the culture broth at a concentration of 0.05% v/v (1 mL/20 mL). For BC production, starters of the SCOBY were cultured in 50 mL tubes, and two different experimental phases were performed: uncontrolled fermentation conditions (UCC) and controlled fermentation conditions (CC). For the CC, the static fermentation process took place in a dark CO₂ incubator in a controlled humidified atmosphere (≥80%) with constant temperature at 30°C for 3 days, to guarantee an optimal environment for symbiont growth. The cap of the tube was removed and perforated parafilm, previously sterilized, and was used to cover the lid and increase the exchange of O₂ with the external surface. This process was repeated in triplicates. Tests were performed in triplicates as well. Viable count assay was performed, as reported earlier.

Live/Dead Assay

To select the SCOBY pieces to use for the experimental phase, the viability percentage was assessed by using the Live/Dead BacLight Bacterial Viability Stain Kit (Molecular Probes, Eugene, and OR). First, the best concentration of the viability kit stain mixture (SYTO9 and propidium iodide (PI)) was selected, which allowed us to distinguish live cells from dead cells (SYTO9: PI, 1:2 v/v). Briefly, freshly grown SCOBY pieces were opportunely cut, harvested, and washed three times with 0.85% sodium chloride (NaCl) solution. Then, 30 µL of a mixture of SYTO9 and PI (1:2) was diluted in a final volume of 5 ml, and each SCOBY piece was incubated with 1 ml in darkness for 15 min at room temperature, according to the manufacturer's instructions. The non-viable SCOBY were prepared by 95% ethanol treatment of bacteria for

30 min (positive control). The SCOBY pieces were washed twice with 0.85% NaCl after the treatments and examined under a confocal microscope (Confocal Leica TCS SP5 II femtosecond laser scanning system, Leica). Filters were set to 493–522 nm for SYTO9 and 618–676 nm for PI. Confocal images were obtained with 40x objective (optical zoom 1.5). Each sample was scanned at randomly selected areas as a series of vertical optical sections, each one 0.50 μm thick. Quantitative analyses of each SCOBY piece were carried out by analysing the digital images of live (green) and dead (red) bacteria by ImageJ software. Each image was divided in regions of interest (ROIs) with comparable areas, and thresholding was performed. The fluorescence intensity per unit area was measured and calculated as the percentage of viable cells. Thereafter, the culture parameter was set, maintaining the temperature at 30°C and the humidity (>98%) for controlled experimental cultures (CCs). To obtain the CC condition, the samples were placed in an incubator at 30°C by inserting a 10 cm high tank with an evaporating surface of 20 cm to obtain constant humidity >80% without water refill during the entire experimental phase. Conversely, for uncontrolled experimental cultures (UCCs), SCOBY pieces were cultured at room temperature (\sim 23°C) and environmental humidity (\sim 50%).

Ultrastructural characterization of the BC layer

For ultrastructural analysis of the fibrillar structure of BC, the BC layers obtained by UCC and CC were primarily fixed with 4% paraformaldehyde. Then, it was fixed with 2.5% of glutaraldehyde in 0.1 M of sodium cacodylate and was left for 1–4 h at the room temperature. In due course of time, it was washed thrice for 10 min in 0.1 M sodium cacodylate and sucrose and buffered at the normal temperature. It was then buffered with 1% osmium tetroxide (OsO_4) in 0.1 M sodium cacodylate for 1 h at 4°C and afterward again, washed thrice with 0.1 M sucrose buffer solution. Dehydration was performed on the sample using ethanol at 30, 50, 70, and 95% for 15–60 min at 4°C. Finally, 100% of ethanol was applied for 15–60 min at the room temperature thrice. Image analyses were performed by ImageJ software by using the DiameterJ plugin³². First of all, the scale bar of the image was measured by using the scale option after using the zoom option from the toolbar. SEM images (1024×768 pixels) were obtained, as already described^{2,33-36 37 1}, and then segmented using the algorithms provided by “DiameterJ Segment” to convert the image into binary forms. Then, segmented images were processed by DiameterJ to measure the diameter of the cellulose bundles and fibres. In addition, DiameterJ was also used to measure the BC network parameters as the mean pore area, porosity percent, and numbers of pores:

$$\text{Mean pore area} = \frac{\text{Total number of black pixel coated pores}}{\text{Total number of pores in image}} \quad \text{Eq. 1}$$

$$\% \text{porosity} = \frac{\text{Total number of black pixels}}{\text{Total number of pixels in image}} \quad \text{Eq. 2}$$

Infrared spectroscopy

The BC chemical structure was confirmed by IR. BC sheet of 1 cm. The measurements were carried out in the range of 500–4,000 cm^{-1} in absorption or transmission modes (64 scans, 4 cm^{-1} resolution) (Thermo Fisher Scientific Instruments, Nicolet 6,700, Waltham, MA, United States). The spectra were subject to ATR correction, smoothing, and baseline correction to be normalized³⁸.

Co-Q10-SNE production and characterization

At first, a primary Co-Q10 negatively charged oil-in-water (O/W) nanoemulsion (NE) at 20 wt% of oil concentration was prepared, as previously reported^{24,39,40}. Briefly, first the oil phase was obtained by adding the surfactant to the soybean oil. For the analysis, 5.8 g of Lipoid E80 was dissolved in 24 ml of soybean oil at 60°C and mixed using the immersion sonicator (Ultrasonic Processor VCX500 Sonic and Materials). An amount of 4.08 g of Co-Q10 was dissolved in the oil phase at 60°C for 1 h, then added dropwise to the aqueous phase (Milli-Q water) and mixed again using the immersion sonicator. The pre-emulsion was passed at 2000 bar through the high-pressure valve homogenizer (Microfluidics M110PS) for three individual cycles to greatly reduce the initial size; then, the reservoir was continuously refilled for 200 steps.

Co-Q10-NE was then functionalized with Ct to have a positively charged SNE. In detail, to achieve the secondary emulsion, a first layer of Ct was deposited above the primary one by following an already developed procedure^{23,24}. Briefly, a 0.1 M acetic acid solution of Ct pH 4 (0.2 wt%) was prepared, and the 20 wt% oil O/W NE was then added to the Ct solution under vigorous stirring for 15 min to allow uniform Ct deposition. Final concentrations of oil and Ct were 10 and 0.1 wt%, respectively, while the pH of the final NE (SNE) was 4. O/W NE and SNE were characterized by measuring the size, polydispersity index (PDI), and ζ -potential values through a dynamic light scattering (DLS) instrument (Zetasizer ZS, Nanoseries ZEN 3600, Malvern Instruments Ltd., Malvern, United Kingdom, $\lambda = 632.8 \text{ nm}$). All the samples were diluted up to a

droplet concentration of approximately 0.025 wt% by using Milli-Q water. A detecting angle of 173 was used. A default refractive index ratio (1.5900) and three runs for each measurement (1 run lasting 100 s) were used in the calculations of the particle size distribution. ζ -potential analysis was carried out by setting 30 runs for each measurement. The morphology of Co-Q10-SNE was observed by Cryo-TEM analysis. For the preparation of the frozen-hydrated sample, the plunge freezing method was performed. Briefly, a drop of 3 μ L of the sample was deposited on 200-mesh holey carbon grids (Ted Pella, United States); then, it was inserted in the chamber of a FEI Vitrobot Mark IV (FEI Company, the Netherland) at 4°C and 90% of humidity. The droplet of the sample was blotted with a filter paper for 1 s (blot force 1, drain time 0.5 s) and then, the grid was plunged into liquid propane. Then, the grid was stored in liquid nitrogen in a grid box until it was finally transferred to a cryo-specimen 626 holder (Gatan, Inc., United States) and loaded into the Cryo-transmission electron microscope (Cryo-TEM) for imaging. To obtain the image of the nanocarriers, we used a Tecnai G2 20, a Cryo-TEM transmission electron microscope (FEI Company, the Netherlands) equipped with a LaB6 emitter (acceleration voltage of 200 kV) and recorded with a 2 × 2 k CCD-Eagle 2HS camera. The frozen-hydrated sample is a radiation-sensitive material, so to avoid damaging it, the observation was carried out in a low-dose mode.

Co-Q10-SNE encapsulation and release: confocal microscopy and fluorescence

For the experiment, 5 mg of cellulose layers (5 mm diameter) were suspended in 1.5 mL of Co-Q10-SNE and incubated at room temperature at different time points (15 min and 30 min) with a gentle agitation. All the tests were executed in triplicates. All samples were stored at 4°C, and SNE adsorption on cellulose layers was evaluated by confocal microscopy. Samples were imaged using a Leica TCS SP5 STED-CW gated microscope (Leica-Microsystems, Mannheim, Germany) with HCX IRAPO L 25.0×0.95 water objective⁴¹⁻⁴³. A laser source of 488 nm was used to excite the Co-Q10 in the oil core. Moreover, a semi-quantitative analysis was performed on at least five images for each z-plane to obtain the mean fluorescence intensity of the loaded Co-Q10-SNE. Using ImageJ software, the mean gray value (MGV) of the green channel was measured for each image^{44,45}. Co-Q10-SNE release studies were carried out by suspending 5 mg of BC-Co-Q10-SNE in 1.5 ml of water. Samples were incubated at 37°C and shaken under gentle conditions. At fixed time points (15, 30 min, 1, 2, 3, and 24 h), 1 ml of the sample was withdrawn

after cellulose layer sedimentation using centrifugation for 5 min at 10,000 rpm (MicroCL21R, Centrifuge, ThermoScientific, United States). The pellet was resuspended in the same volume of fresh buffer. The collected supernatants were analysed by fluorescence (Microplate Readers Perkin Elmer); the excitation wavelength was 450 nm, and the maximum emission was recorded between 470 and 600 nm. The fluorescence intensity peak was determined at 551 nm. All the tests were executed in triplicates.

3. Results and discussion

Cellulose production: morphological and chemical characterization

In order to validate the SCOBY (**Figure 1A**) for BC production in static culture, preliminary viability assay was performed by using Live/Dead assay. SCOBY portions (1cmx1cm) were observed under a confocal microscope in the central and peripheral areas, obtaining a reliable measurement of the entire sample. SCOBY pieces on which symbiont viability reaches at least 50% were used for the experimental phase, as reported in representative images and 3D reconstruction (**Figure 1B**). Quantitative analysis of the SCOBY portion showed a viability of $79 \pm 3.5\%$ by measuring the intensity of green (for viable bacteria) and red (for non-viable bacteria) fluorescence measured by the area. SCOBY pieces with a strong reduction in the cell viability were not used for the experimental phase (data not showed). Once the SCOBY pieces to use for BC production are selected, two different culture conditions were set: a temperature of 30°C and the humidity >98% for the controlled experimental culture (CC) and room temperature (~23°C) and environmental humidity (~50%) for the uncontrolled experimental culture (UCC). To carry out the morphological characterization of the BC produced in UCC at different stages of maturation, BC layers were produced in static conditions without refreshing the medium. Each layer (about 1 mm thick) was separated from the layer below due to a variation of the medium/air interface and a reduction in the volume of the medium over time with a reduced humidity. The BC layers obtained with this procedure showed different ripeness degrees, starting from the bottom (in direct contact with the liquid suspension) with the lowest ripeness up to the more superficial ones (in direct contact with air), which appear to be, from a macroscopic analysis, more consistent and thicker >1 mm. These tests made it possible to observe a variation in the cellulose consistency based on the degree of maturation whose chemistry was studied by IR spectroscopy. In detail, three layers (internal, intermediate, and external) were obtained at 72 h, and they showed the

typical BC peaks⁴⁶⁻⁴⁸ with the bands at $3,353\text{ cm}^{-1}$ and $2,924\text{ cm}^{-1}$ relative to the stretching of the OH and CH groups, respectively; a peak observed at $1,738\text{ cm}^{-1}$ and $1,640\text{ cm}^{-1}$ associated with the stretching of the C = O groups, and the bending of the OH groups referred to absorbed water molecules into cellulose fibres, a peak at $1,046\text{ cm}^{-1}$ corresponding to the vibration of the pyranose ring–C–O–C, and the peak at 889 cm^{-1} related to the presence of β -glycosidic bonds (**Figure 2**). The three layers also revealed a similar degree of polymerization with the presence of the peak at $1,738\text{ cm}^{-1}$, even if, its intensity grows as the superficiality of the layer increases (**Figure 2**). To avoid the development of this crosslinked BC, which could hinder the correct SNE incubation, BC was grown under CC conditions, as explained earlier, and the correct maturation level was analysed by IR. From the morphological analysis, the samples grown under CC conditions appear to have an adequate hydration status, highlighted by the lower degree of compactness, as well as greater transparency. In contrast, the unique layer produced under UCC conditions is thicker and not transparent at all, indicating a greater degree of compactness and less hydration, which is reflected in a greater degree of crosslinking in the IR spectrum (**Figure 3 red spectrum**). Spectra of UCC and CC BC obtained at 72 h, corroborated our hypothesis; indeed, BC obtained in CC conditions showed only the maturation peak at $1,640\text{ cm}^{-1}$ (**Figure 3, violet spectrum**) in contrast with the UCC BC which revealed the crosslinked band at $1,738\text{ cm}^{-1}$ (**Figure 3 red spectrum**). IR spectra strongly confirmed that the moisture content seemed to be directly related to the degree of compactness (revealed by the crosslinking) of BC, demonstrating that the adjusted humidity environment allows reaching a loosening of the cellulose structure useful for nanocarriers' penetration upon incubation.

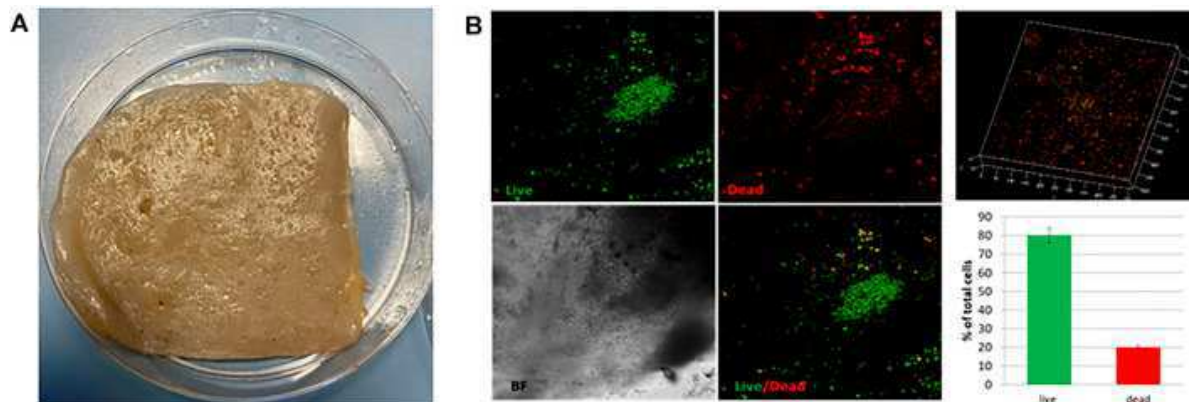


Figure 1. **A)** Representative image of the SCOBY portion for BC production. **B)** Live/Dead fluorescence images of the SCOBY. 3D reconstruction of the observed portion and the percentage of live (green) and dead (red) bacteria.

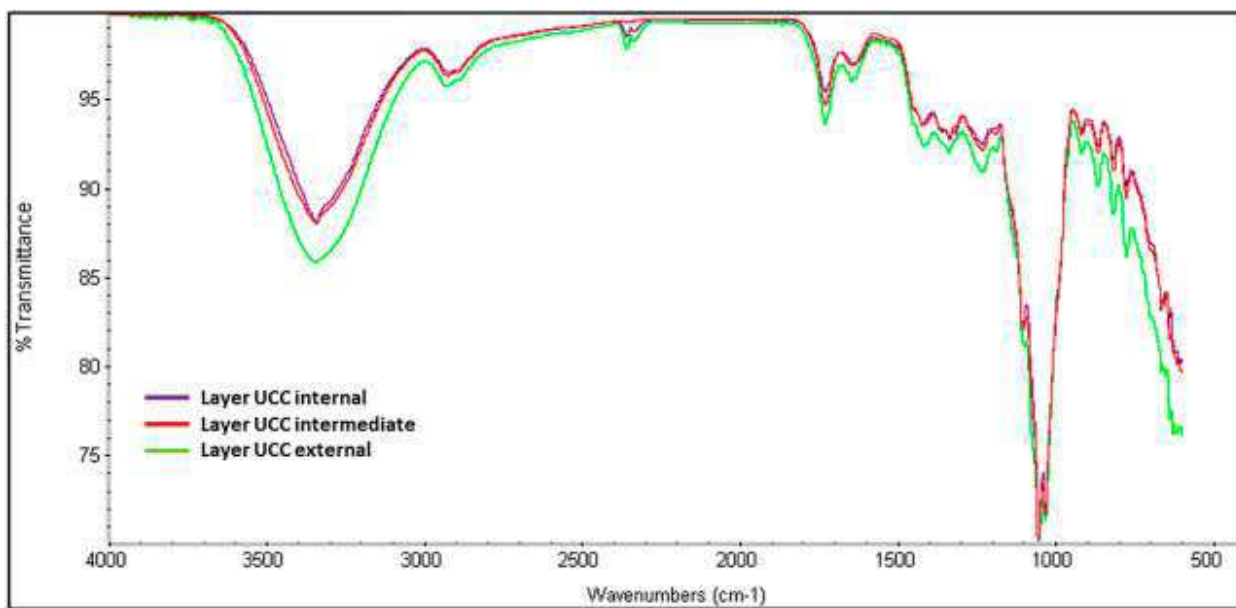


Figure 2. IR analysis of UCC internal, intermediate, and external layers obtained at 72 h.

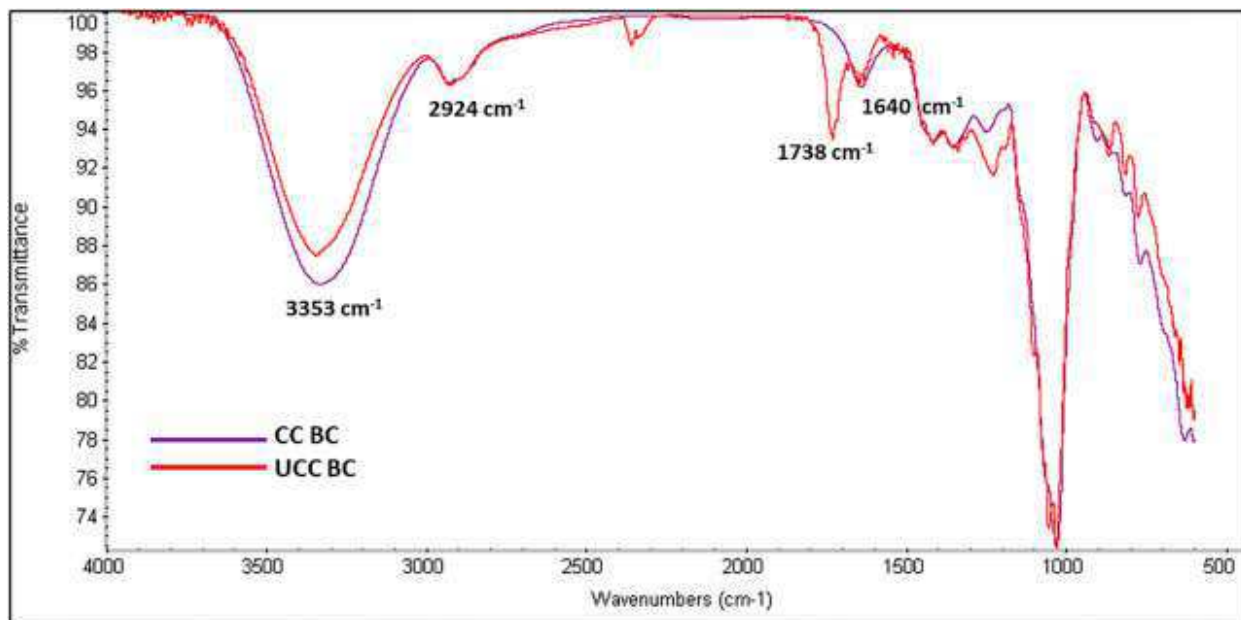


Figure 3. IR spectra of CC (violet spectrum) and UCC BC (red spectrum) at 72 h.

Ultrastructural characterization of BC

To achieve the ultrastructural characterization of the BC produced in UCC or in CC, BC layers were produced in static conditions without refreshing the medium (**Figure 4A**). Representative SEM images showed a different degree of compactness of the cellulose fiber network. In particular, the external layer in UCC highlighted a greater degree of compactness, as shown in **Figure 4B**. Quantitative data of the SEM images showed for the single layer obtained in CC a significantly greater mean pore area and porosity percentage with a smaller number of pores ($p < 0.05$) than the layers obtained in UCC, especially the superficial layer (External). In detail, the porosity values are 39.0, 41.7, and 35.9, while the mean pore area values are 0.0107, 0.0151, and 0.0129 μm^2 for the external, intermediate, and internal layers, respectively, indicating a slight difference between the superficial layer and the most internal layers obtained in UCC although not statistically significant (**Figure 4C**).

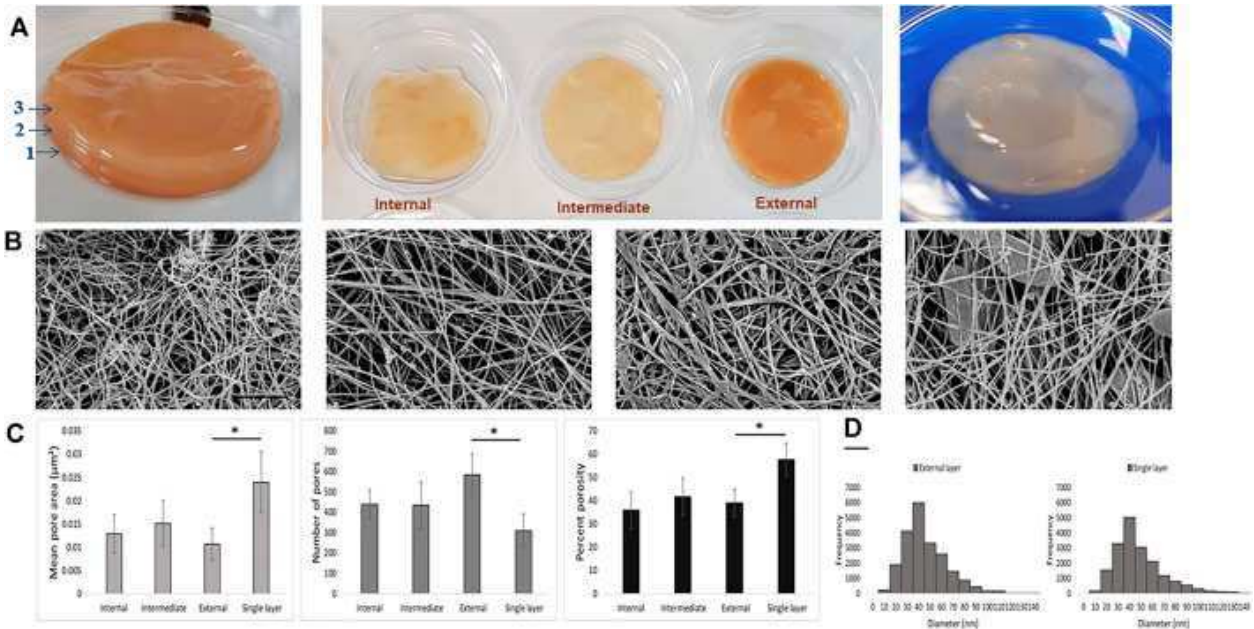


Figure 4. **A)** Qualitative images of BC layers produced under UCC (left and middle) and CC (right). **B)** Representative SEM images of the different BC layers (internal, intermediate, external, and single layer, from left); scale bar 1 μm . **C)** Mean pore area, number of pores, and porosity percentage of BC networks of the different BC layers. **D)** Fiber diameter histogram of external and single BC layers produced in UCC and CC, respectively.

At last, all samples showed the fiber diameters in a range of 30–50 nm, and a comparable fiber frequency was also reported (**Figure 4D**), indicating that the main difference among BC produced by the SCOPY is in assembly of the fiber rather than in the single fibers.

Co-Q10-SNE encapsulation and release by BC

As stated in the **Materials and Method** section, primary and secondary Co-Q10-NEs were produced by a method developed in our laboratory³⁹. Co-Q10-NE and Co-Q10-SNE size distribution and uniformity were evaluated by DLS measurements, as reported in **SI. Figures S1A, B**. In detail, Co-Q10-NE displayed an average size of 112.4 ± 0.65 nm with a Pdl of 0.12 ± 0.04 and a surface charge of -46.8 ± 0.40 mV (**SI, Figure S1C**), while Co-Q10-SNE reported an average size of 103.0 ± 1.0 nm with a Pdl of 0.090 ± 0.025 and a charge of $+39.9 \pm 0.07$ mV (**SI, Figure S1C**), in agreement with those reported in the literature^{23,28,40}. Before starting incubation experiments, we also evaluated the chemical stability of our SNEs over time, and as shown in **SI Figure S1D**, they remained stable for up to 30 days, without any variation in size or PDI. Nanocarriers' uniformity and stability were also confirmed by Cryo-TEM analysis (**SI Figure S2**), where Co-Q10-SNE showed monodispersed spherical nanostructures of ~ 100 nm.

As to incubation experiments, $1\text{cm} \times 1\text{cm}$ layers of BC were used and incubated at two different time points (15 and 30 min) with 1 mL of Co-Q10-SNE. The correct incubation was then evaluated by confocal microscopy, following the autofluorescence of Co-Q10 at 551 nm, as shown in **Figures 5A,B and SI Figure S3**. Confocal analysis revealed no difference in the fluorescence intensity of both samples (**Figure 5A, SI Figure S3A**) underlying as the ultrastructure of BC allows a complete loading of SNEs already at 15 min. This result was corroborated by Co-Q10-SNE release studies where similar quantities of the Co-Q10-SNE were released from both BC samples. These analyses were carried out by fluorescence, following the maximum of Co-Q10-SNE emission at 551 nm. In detail, 5 mg of BC-Co-Q10-SNEs were suspended in 1.5 mL of water and incubated at 37°C for different time periods from 15 to 1,440 min and after 1 mL of the supernatant was removed at each time and analysed. The quantification of release kinetics showed that for both samples (BC incubated at 15 and 30 min), the Co-Q10-SNE fluorescence signal increased during the time reaching the saturation point from 120 to 1.440 min (**Figure 5 B, SI Figure S3 B**). These results were reached optimizing the BC preparation process to obtain a single not a crosslinked layer of nanofibers. Indeed, by conducting

preliminary experiments on UCC BC layers, we noted that more external layers were not able to incubate the Co-Q10-SNE, and encapsulation is mostly superficial in all the samples analysed, both at 15 and 30 min (SI Figures S4 A–F).

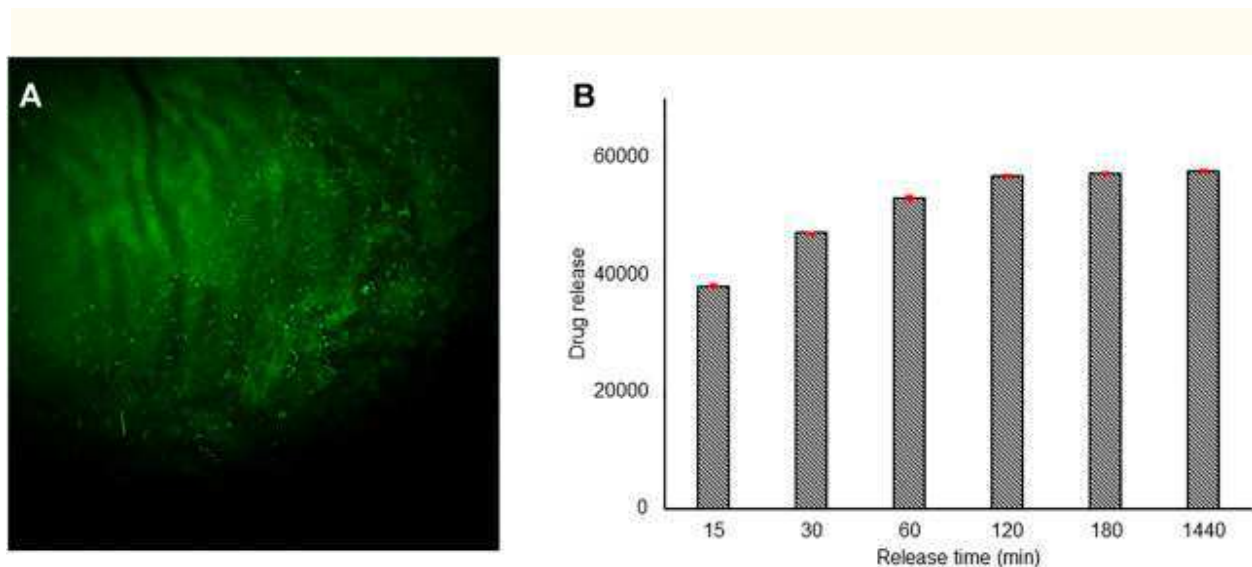


Figure 5. Confocal images of the BC-Co-Q10 SNE, **A)** 15 min incubation time λ_{exc} 450 nm, λ_{emiss} 470–600 nm. **B)** Release kinetic studies of the Co-Q10 SNE from BC incubated for 15 min.

The reported results show that the BC networks produced with our conditions can carry out a sustained release of drugs. Our double release approach based on the use of a drug-encapsulated nanocarrier within BC could help obtain a prolonged antioxidant drug release, enhancing their therapeutic effects; it is, indeed, reported that encapsulated antioxidants show a better stability, and their gradual and sustained release leads to a superior antioxidant profile⁴⁹. However, simple drug encapsulation in BC is not able to completely achieve the described effects, for example, CUR loaded in cellulose acetate electrospun nanofibers showed a great initial burst that gradually increased over time in an uncontrolled manner⁵⁰. Conversely, we proposed a delivery system which can guaranty a controlled and time-sustained release highly wished for antioxidants. In addition, by tuning the SNE size²⁴, in principle, we may easily tune the release kinetics according to the required needs.

4. Conclusion

The current research work was carried out to evaluate the potential application of BC as a drug delivery system (an explicative final system was reported in **SI Figure S5**). The BC layers were prepared starting from the SCOBY culture using UCC and CC conditions. Preliminary incubation studies showed that under UCC conditions, only the innermost layer, the least crosslinked layer, started to incubate the nanocarrier (**SI Figure S4**), and therefore, to reproduce the best loading conditions, we optimized the BC preparation process, to assure the production of a mature not crosslinked BC nanonetworks. Characterization data showed that CC-BC layers were mature, and IR data corroborate these results, demonstrating the presence of chemical bands related to BC nanofibers that are not crosslinked. The Co-Q10-SNE loading, and *in vitro* release studies revealed that BC matrices can encapsulate the drug already in 15 min; indeed, confocal images and fluorescence kinetic studies highlighted no differences with the BC incubated for 30 min. In detail, the quantification of release kinetics demonstrated that for both samples, the Co-Q10-SNE fluorescence signal increases in intensity during the time reaching the saturation point from 120 to 1.440 min. The obtained results concluded that our BC produced in CC conditions could represent a novel matrix for the delivery of drug-encapsulated nanocarriers. Indeed, thanks to the optimization of BC synthesis, it could guaranty enough hydration to demonstrate for the first time the ability to incubate O/W nanoemulsions, which are ideal nanocarriers for the encapsulation and stabilization of lipophilic and water-labile molecules, such as Co-Q10. Additionally, by playing with the SNE size and with BC synthesis conditions, we may modulate nanocarriers and therefore biomolecule release to the skin. However, further research works are required to explore this potential application. Future analysis will indeed focus on the production of inflamed micro-tissues that will be then healed with the BC-Co-Q10-SNE and appropriately analysed to evaluate the therapeutic power of the proposed system.

Acknowledgments

The author thanks Dr. Fabio Formigini for his help to acquire confocal images and Dr. Valentina Mollo for her support in the acquisition of Cryo-TEM images.

Author Contributions

CD and EL performed Co-Q10-SNE encapsulation and release (confocal microscopy and fluorescence confocal analysis) and IR BC analysis; EL prepared and characterized Co-Q10-SNE; VD, BC, and FM produced and characterized BC by SEM. CD, VD, EL, and RV wrote the original draft, and all authors revised the original manuscript. RV and PN contributed to conceptualization.

Funding

This work was supported by “PON—Mise Imprese e Competitività 2014/2020—Bando Fabbrica Intelligente, Agrifood e Scienze della Vita-Biomatrix”.

Supplementary Information

The Supplementary Material for this article can be found online at: <https://www.frontiersin.org/articles/10.3389/fbioe.2022.851893/full#supplementary-material>

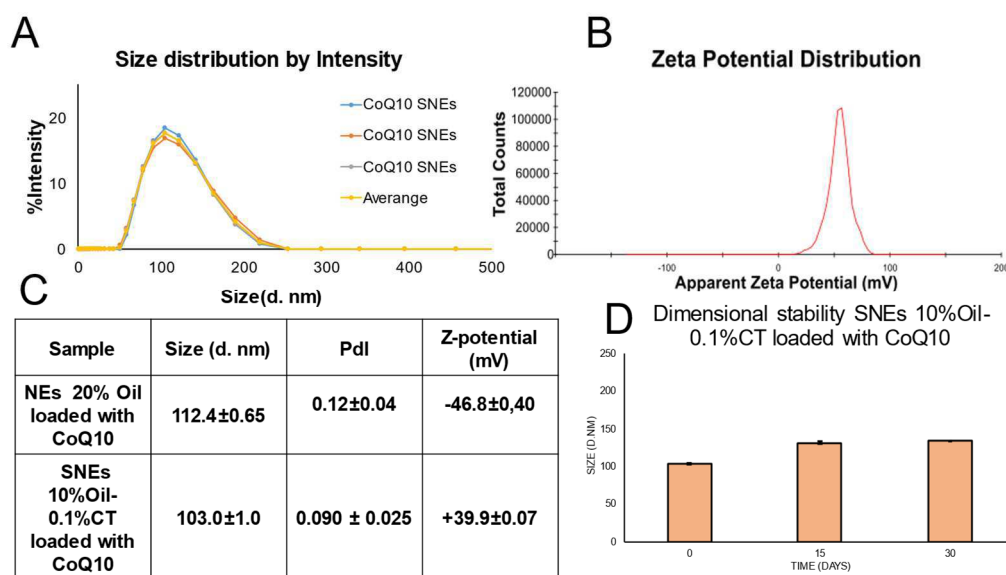


Figure S1. A-B) Example of Size distribution by Intensity of Co-Q10-SNE formulations (blue-orange –gray) obtained by DLS with the average values in yellow and PDI distribution. **C)** Average value of size, PDI and ζ - potential distribution of both Co-Q10-NE and Co-Q10-SNE. **D)** Dimensional Stability of Co-Q10-SNE.

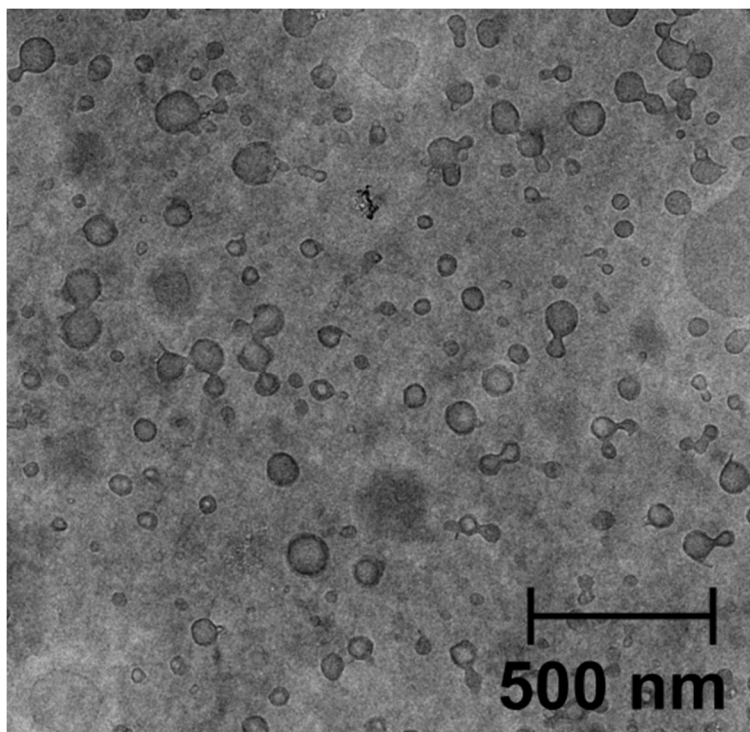


Figure S2. Cryo-TEM analysis of Co-Q10-SNE.

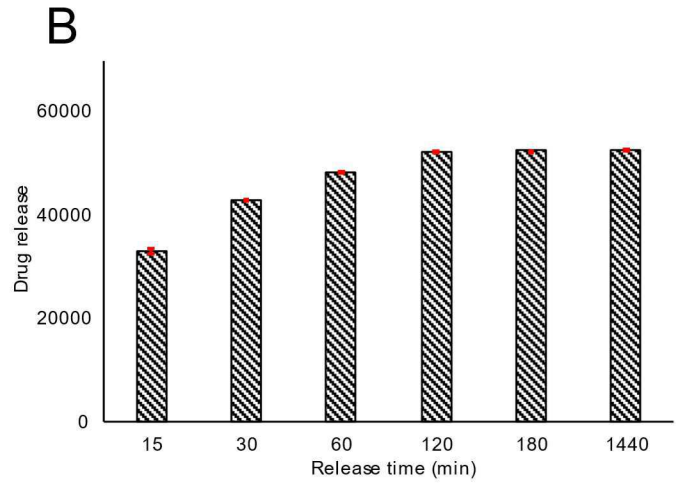
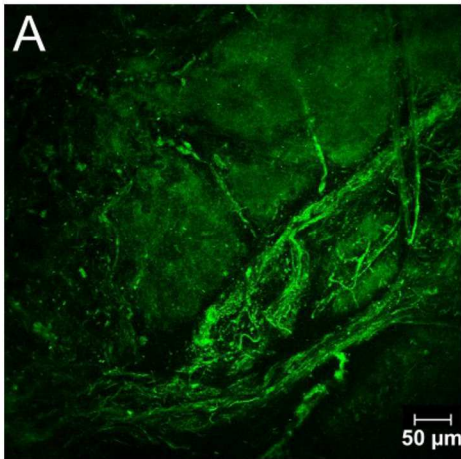


Figure S3. Confocal images of BC-Co-Q10-SNE, **A)** 30 min incubation time λ_{exc} 450 nm, λ_{emiss} 470-600nm. **B)** Release kinetic studies of Co-Q10-SNE from BC incubated for 30 min.

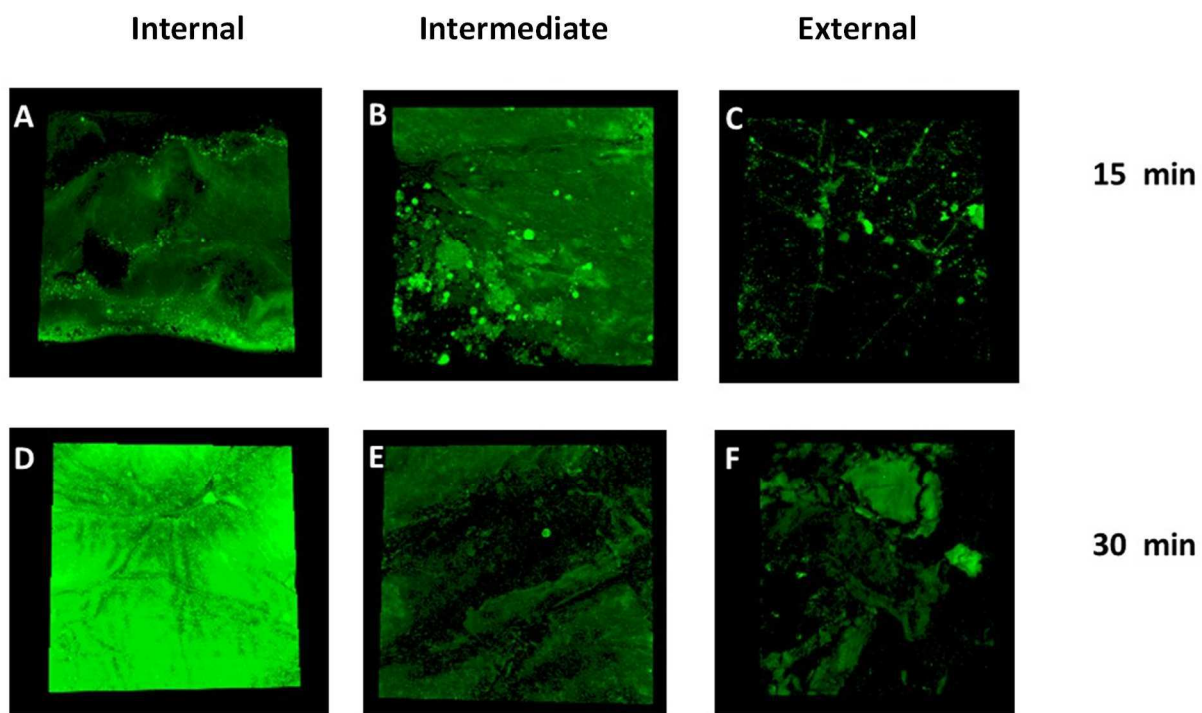


Figure S4. Confocal images of UCC internal, intermediate, and external layer, incubated with Co-Q10-SNE at **A-B-C)**15 min incubation time, **D-E-F)** 30 min; λ_{exc} 450 nm, λ_{emiss} 470-600nm.

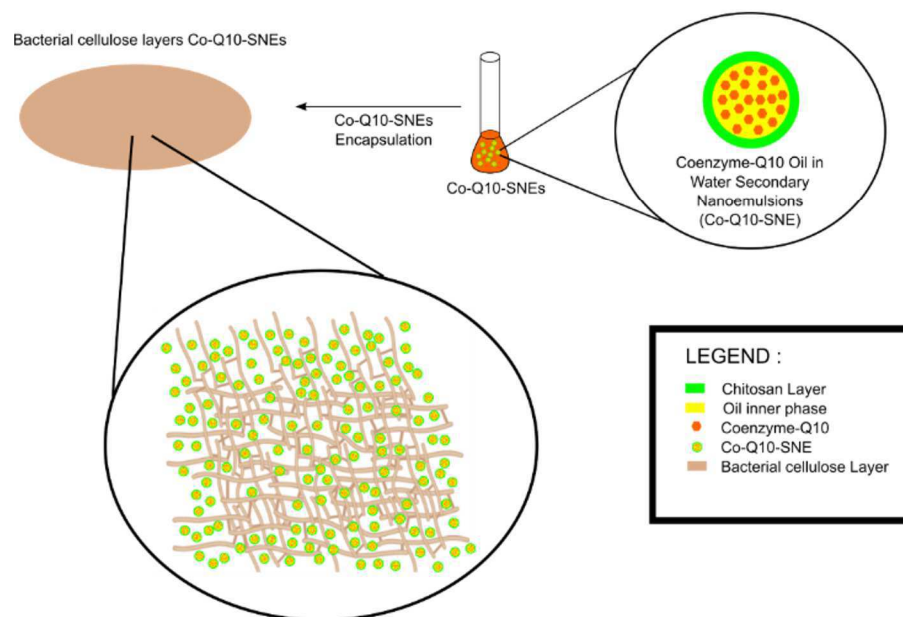


Figure S5. Schematic representation of BC-Co-Q10-SNE assembly.

References

- 1 La Manna, S., Di Natale, C., Onesto, V. & Marasco, D. Self-assembling peptides: From design to biomedical applications. *International Journal of Molecular Sciences* **22**, 12662 (2021).
- 2 Di Natale, C. *et al.* Design of biodegradable bi-compartmental microneedles for the stabilization and the controlled release of the labile molecule collagenase for skin healthcare. *Journal of Materials Chemistry B* **9**, 392-403 (2021).
- 3 Lagreca, E. *et al.* Recent advances in the formulation of PLGA microparticles for controlled drug delivery. *Progress in biomaterials* **9**, 153-174 (2020).
- 4 Martín del Valle, E. M., Galan, M. A. & Carbonell, R. G. Drug delivery technologies: the way forward in the new decade. *Industrial & engineering chemistry research* **48**, 2475-2486 (2009).
- 5 Angelova, A. *et al.* Plasmalogen-based liquid crystalline multiphase structures involving docosapentaenoyl derivatives inspired by biological cubic membranes. *Frontiers in Cell and Developmental Biology* **9**, 617984 (2021).
- 6 Mathews, P. D., Mertins, O., Angelov, B. & Angelova, A. Cubosomal lipid nanoassemblies with pH-sensitive shells created by biopolymer complexes: A synchrotron SAXS study. *Journal of Colloid and Interface Science* **607**, 440-450 (2022).
- 7 Carvalho, T., Guedes, G., Sousa, F. L., Freire, C. S. & Santos, H. A. Latest advances on bacterial cellulose-based materials for wound healing, delivery systems, and tissue engineering. *Biotechnology journal* **14**, 1900059 (2019).
- 8 de Oliveira Barud, H. G. *et al.* A multipurpose natural and renewable polymer in medical applications: Bacterial cellulose. *Carbohydrate Polymers* **153**, 406-420 (2016).
- 9 Badshah, M., Ullah, H., Wahid, F. & Khan, T. Properties and Applications of Modified Bacterial Cellulose-Based Materials. *Current Nanoscience* **17**, 351-364 (2021).
- 10 Blanco Parte, F. G. *et al.* Current progress on the production, modification, and applications of bacterial cellulose. *Critical reviews in biotechnology* **40**, 397-414 (2020).
- 11 Gregory, D. A. *et al.* Bacterial cellulose: A smart biomaterial with diverse applications. *Materials Science and Engineering: R: Reports* **145**, 100623 (2021).
- 12 Klemm, D., Schumann, D., Udhardt, U. & Marsch, S. Bacterial synthesized cellulose - Artificial blood vessels for microsurgery. *Progress in Polymer Science (Oxford)* **26**, 1561-1603, doi:10.1016/S0079-6700(01)00021-1 (2001).
- 13 Tan, T. H., Lee, H. V., Yehya Dabdawb, W. A. & Hamid, S. B. B. O. A. A. in *Materials for Biomedical Engineering: Nanomaterials-based Drug Delivery* 131-164 (2019).
- 14 Li, X. *et al.* Nanoformulations of quercetin and cellulose nanofibers as healthcare supplements with sustained antioxidant activity. *Carbohydrate Polymers* **207**, 160-168, doi:10.1016/j.carbpol.2018.11.084 (2019).
- 15 Almeida, I. *et al.* Bacterial cellulose membranes as drug delivery systems: An in vivo skin compatibility study. *European Journal of Pharmaceutics and Biopharmaceutics* **86**, 332-336 (2014).

- 16 Volova, T. G. *et al.* Antibacterial properties of films of cellulose composites with silver nanoparticles and antibiotics. *Polymer Testing* **65**, 54-68 (2018).
- 17 Fortunati, E. *et al.* Nano-biocomposite films with modified cellulose nanocrystals and synthesized silver nanoparticles. *Carbohydrate polymers* **101**, 1122-1133 (2014).
- 18 Gopi, S., Balakrishnan, P., Geethamma, V. G., Pius, A. & Thomas, S. in *Applications of Nanocomposite Materials in Drug Delivery* 75-95 (Elsevier, 2018).
- 19 Picheth, G. F. *et al.* Bacterial cellulose in biomedical applications: A review. *International journal of biological macromolecules* **104**, 97-106 (2017).
- 20 Trombino, S. *et al.* Design and synthesis of cellulose derivatives with antioxidant activity. *Macromolecular bioscience* **8**, 86-95 (2008).
- 21 Morais, E. S. *et al.* Anti-inflammatory and antioxidant nanostructured cellulose membranes loaded with phenolic-based ionic liquids for cutaneous application. *Carbohydrate Polymers* **206**, 187-197, doi:10.1016/j.carbpol.2018.10.051 (2019).
- 22 Vecchione, R. *et al.* Curcumin bioavailability from oil in water nano-emulsions: In vitro and in vivo study on the dimensional, compositional and interactional dependence. *Journal of Controlled Release* **233**, 88-100 (2016).
- 23 Vecchione, R. *et al.* Ultrastable liquid–liquid interface as viable route for controlled deposition of biodegradable polymer nanocapsules. *Small* **12**, 3005-3013 (2016).
- 24 Vecchione, R. *et al.* Tunable stability of monodisperse secondary O/W nano-emulsions. *Nanoscale* **6**, 9300-9307 (2014).
- 25 Langella, A. *et al.* In vitro study of intestinal epithelial interaction with engineered oil in water nanoemulsions conveying curcumin. *Colloids and Surfaces B: Biointerfaces* **164**, 232-239 (2018).
- 26 Fotticchia, T. *et al.* Enhanced drug delivery into cell cytosol via glycoprotein H-derived peptide conjugated nanoemulsions. *ACS nano* **11**, 9802-9813 (2017).
- 27 Vecchione, R. *et al.* Oil/water nano-emulsion loaded with cobalt ferrite oxide nanocubes for photo-acoustic and magnetic resonance dual imaging in cancer: In vitro and preclinical studies. *Nanomedicine: Nanotechnology, Biology and Medicine* **13**, 275-286 (2017).
- 28 Quagliariello, V. *et al.* Cardioprotective effects of nanoemulsions loaded with anti-inflammatory nutraceuticals against doxorubicin-induced cardiotoxicity. *Nutrients* **10**, 1304 (2018).
- 29 Quagliariello, V. *et al.* Nano-encapsulation of coenzyme Q10 in secondary and tertiary nano-emulsions for enhanced cardioprotection and hepatoprotection in human cardiomyocytes and hepatocytes during exposure to anthracyclines and trastuzumab. *International Journal of Nanomedicine* **15**, 4859 (2020).
- 30 El-Leithy, E. S., Makky, A. M., Khatib, A. M. & Hussein, D. G. Optimization of nutraceutical coenzyme Q10 nanoemulsion with improved skin permeability and anti-wrinkle efficiency. *Drug development and industrial pharmacy* **44**, 316-328 (2018).
- 31 Lahiri, D. *et al.* Bacterial cellulose: Production, characterization and application as antimicrobial agent. *International Journal of Molecular Sciences* **22**, doi:10.3390/ijms222312984 (2021).

- 32 Hotaling, N. A., Bharti, K., Kriel, H. & Simon, C. G. DiameterJ: A validated open source nanofiber diameter measurement tool. *Biomaterials* **61**, 327-338, doi:<https://doi.org/10.1016/j.biomaterials.2015.05.015> (2015).
- 33 Di Natale, C. *et al.* Structural insights into amyloid structures of the C-terminal region of nucleophosmin 1 in type A mutation of acute myeloid leukemia. *Biochimica et Biophysica Acta - Proteins and Proteomics* **1867**, 637-644, doi:10.1016/j.bbapap.2019.01.010 (2019).
- 34 Di Natale, C. *et al.* Effects of surface nanopatterning on internalization and amyloid aggregation of the fragment 264-277 of Nucleophosmin 1. *Colloids and Surfaces B: Biointerfaces* **197**, doi:10.1016/j.colsurfb.2020.111439 (2021).
- 35 Di Natale, C., Onesto, V., Lagreca, E., Vecchione, R. & Netti, P. A. Tunable Release of Curcumin with an In Silico-Supported Approach from Mixtures of Highly Porous PLGA Microparticles. *Materials* **13**, 1807 (2020).
- 36 Bagheri, N. *et al.* Electroanalytical Sensor Based on Gold-Nanoparticle-Decorated Paper for Sensitive Detection of Copper Ions in Sweat and Serum. *Analytical Chemistry* **93**, 5225-5233, doi:10.1021/acs.analchem.0c05469 (2021).
- 37 Florio, D. *et al.* Self-assembly of bio-inspired heterochiral peptides. *Bioorganic Chemistry* **114**, doi:10.1016/j.bioorg.2021.105047 (2021).
- 38 Di Natale, C. *et al.* Effects of surface nanopatterning on internalization and amyloid aggregation of the fragment 264-277 of Nucleophosmin 1. *Colloids and Surfaces B: Biointerfaces* **197**, 111439 (2021).
- 39 Quagliariello, V. *et al.* Nano-encapsulation of coenzyme Q10 in secondary and tertiary nano-emulsions for enhanced cardioprotection and hepatoprotection in human cardiomyocytes and hepatocytes during exposure to anthracyclines and trastuzumab. *International Journal of Nanomedicine*, 4859-4876 (2020).
- 40 Profeta, M. *et al.* Cell membrane-coated oil in water nano-emulsions as biomimetic nanocarriers for lipophilic compounds conveyance. *Pharmaceutics* **13**, 1069 (2021).
- 41 Jamaledin, R. *et al.* Recombinant Filamentous Bacteriophages Encapsulated in Biodegradable Polymeric Microparticles for Stimulation of Innate and Adaptive Immune Responses. *Microorganisms* **8**, 650 (2020).
- 42 Di Natale, C. *et al.* Design of biodegradable bi-compartmental microneedles for the stabilization and the controlled release of the labile molecule collagenase for skin healthcare. *J. Mater. Chem. B* (2020).
- 43 Battisti, M. *et al.* Non-invasive Production of Multi-Compartmental Biodegradable Polymer Microneedles for Controlled Intradermal Drug Release of Labile Molecules. *Frontiers in Bioengineering and Biotechnology* **7**, doi:10.3389/fbioe.2019.00296 (2019).
- 44 Celetti, G., Di Natale, C., Causa, F., Battista, E. & Netti, P. A. Functionalized poly (ethylene glycol) diacrylate microgels by microfluidics: In situ peptide encapsulation for in serum selective protein detection. *Colloids and Surfaces B: Biointerfaces* **145**, 21-29 (2016).
- 45 Di Natale, C. *et al.* The level of 24-hydroxycholesteryl esters decreases in plasma of patients with Parkinson's disease. *Neuroscience Letters* **672**, 108-112, doi:10.1016/j.neulet.2018.02.041 (2018).

- 46 Keshk, S. M. A. S., Razek, T. M. A. & Sameshima, K. Bacterial cellulose production from beet molasses. *African Journal of Biotechnology* **5**, 1519-1523 (2006).
- 47 Castro, C. *et al.* Structural characterization of bacterial cellulose produced by *Gluconacetobacter swingsii* sp. from Colombian agroindustrial wastes. *Carbohydrate Polymers* **84**, 96-102 (2011).
- 48 Tabarsa, T., Sheykhnazari, S., Ashori, A., Mashkour, M. & Khazaeian, A. Preparation and characterization of reinforced papers using nano bacterial cellulose. *International Journal of Biological Macromolecules* **101**, 334-340, doi:10.1016/j.ijbiomac.2017.03.108 (2017).
- 49 Khalil, I. *et al.* Nanoantioxidants: Recent trends in antioxidant delivery applications. *Antioxidants* **9**, doi:10.3390/antiox9010024 (2020).
- 50 Khoshnevisan, K. *et al.* Cellulose acetate electrospun nanofibers for drug delivery systems: Applications and recent advances. *Carbohydrate Polymers* **198**, 131-141, doi:10.1016/j.carbpol.2018.06.072 (2018).

Copyright © 2022 Di Natale, De Gregorio, Lagreca, Mauro, Corrado, Vecchione and Netti.

This is an open-access article distributed under the terms of the Creative Commons Attribution License (CC BY). The use, distribution or reproduction in other forums is permitted, provided the original author(s) and the copyright owner(s) are credited and that the original publication in this journal is cited, in accordance with accepted academic practice. No use, distribution or reproduction is permitted which does not comply with these terms.

List of publication

1. Alessia La Rocca, Vincenza De Gregorio, Elena Lagreca, Raffaele Vecchione, Paolo Antonio Netti, Giorgia Imparato, Colorectal cancer bioengineered microtissues as model to replicate tumor-ECM cross-talk and assess drug delivery systems *in vitro*, *UnderSubmission*
2. Elena Lagreca, Raffaele Vecchione, Chiara Di Cicco, Federica D'Aria, Alessia La Rocca, Vincenza De Gregorio, Luana Izzo, Raffaele Crispino, Valentina Mollo, Emiliano Bedini, Giorgia Imparato, Alberto Ritieni, Concetta Giancola, Paolo Antonio Netti, Physicochemical and *in vitro* biological validation of food grade secondary oil in water nanoemulsions with enhanced mucus-adhesion properties, *Colloids and Surfaces A: Physicochemical and Engineering Aspects*, Volume 654,2022,129998, ISSN 0927-7757,(<https://doi.org/10.1016/j.colsurfa.2022.129998>)(<https://www.sciencedirect.com/science/article/pii/S0927775722017538>)
3. Di Natale C, De Gregorio V, Lagreca E, Mauro F, Corrado B, Vecchione R, Netti PA. Engineered Bacterial Cellulose Nanostructured Matrix for Incubation and Release of Drug-Loaded Oil in Water Nanoemulsion. *Front Bioeng Biotechnol*. 2022 Mar 9;10:851893. Doi: 10.3389/fbioe.2022.851893. PMID: 35356776; PMCID: PMC8959586.
4. Di Natale C, Lagreca E, Panzetta V, Gallo M, Passannanti F, Vitale M, Fusco S, Vecchione R, Nigro R, Netti P.A, *Morphological and Rheological Guided Design for the Microencapsulation Process of Lactobacillus paracasei CBA L74 in Calcium Alginate Microspheres*. *Frontiers in Bioengineering and Biotechnology*, 2021. **9**.
<https://www.frontiersin.org/articles/10.3389/fbioe.2021.660691> , DOI=10.3389/fbioe.2021.660691, ISSN=2296-4185
5. Profeta, M.; Di Natale, C.; Lagreca, E.; Mollo, V.; Netti, P.A.; Vecchione, R. Cell Membrane-Coated Oil in Water Nano-Emulsions as Biomimetic Nanocarriers for Lipophilic Compounds Conveyance. *Pharmaceutics* 2021, 13, 1069. <https://doi.org/10.3390/pharmaceutics13071069>
6. Lagreca, E., Onesto, V., Di Natale, C. *et al.* Recent advances in the formulation of PLGA microparticles for controlled drug delivery. *Prog Biomater* **9**, 153–174 (2020).
<https://doi.org/10.1007/s40204-020-00139-y>
7. Di Natale, C.; Onesto, V.; Lagreca, E.; Vecchione, R.; Netti, P.A. Tunable Release of Curcumin with an *In Silico*-Supported Approach from Mixtures of Highly Porous PLGA Microparticles. *Materials* **2020**, 13, 1807. <https://doi.org/10.3390/ma13081807>
8. Di Natale, C., De Rosa, D., Profeta, M., Jamaledin, R., Attanasio, A., Lagreca, E., Scognamiglio P.L., Netti, P.A. & Vecchione, R. (2021). Design of biodegradable bi-compartmental microneedles for the stabilization and the controlled release of the labile molecule collagenase for skin healthcare. *J. Mater. Chem. B*, 2021,**9**, 392-403, DOI
<https://doi.org/10.1039/D0TB02279A>
9. Quagliariello V, Vecchione R, De Capua A, Lagreca E, Iaffaioli RV, Botti G, Netti PA, Maurea N. Nano-Encapsulation of Coenzyme Q10 in Secondary and Tertiary Nano-Emulsions for Enhanced Cardioprotection and Hepatoprotection in Human Cardiomyocytes and Hepatocytes During Exposure to Anthracyclines and Trastuzumab. *Int J Nanomedicine*. 2020 Jul 9;15:4859-4876. doi: 10.2147/IJN.S245170. PMID: 32764923; PMCID: PMC7359894.

Acknowledgements

I would like to express my gratitude to my primary supervisor, Prof. Netti, for providing me with this opportunity. I would also like to thank Ing. Raffaele Vecchione for his invaluable help and advice with this thesis. In addition, I extend my deep appreciation to Dr. Concetta Di Natale, also known as Conny, who not only guided me through the project but also became a good friend.

I believe that research is collaboration and cross-pollination of ideas, and I would like to thank all the professors and researchers from external departments who have made themselves available to collaborate towards the completion of this thesis project. Special thanks go to Dr. Elisabetta Caiazzo for her great assistance in finalizing Chapter 3. I would like to thank Prof. Maffia and Prof. Ialenti for their contribution to Chapter 3. I would like to thank Prof. Giancola, Prof. Ritieni, Prof. Bedini, Dr. Izzo, Dr. Di Cicco, Dr. D'Aria, Dr. Imparato, Dr. La Rocca, Dr. Crispino and Dr. De Gregorio for their contribution to Chapter 4. I would also like to thank Dr. Chino from the Department of Chemical Sciences of University of Naples Federico II and Prof. Marasco and Dr. La Manna from the Department of Pharmacy of University of Naples Federico II for making themselves available to use their equipment when necessary.

I am grateful to Dr. Valentina Mollo for her teachings in cell biology and electron microscopy and her constant support. The support and assistance provided by Dr. Fabio Fomiggini were greatly appreciated. Moreover, I would like to thank my lab colleagues and friends, Rezvan Jamaledin "Rose", Valentina Onesto, Roberta D'Auria, Raffaele Crispino, Imma Tufano, Rosa Sorrentino, Nicoletta Martone, Brunella Corrado, Alessandro Attanasio, Denise Pagliara, Francesco Rippa, Erika Caianiello, Roberta Passariello, Giuseppe Cesarelli, and Alessia La Rocca for their constant support during PhD years. I wish to acknowledge the help provided by the staff at the IIT - Center for Advanced Biomaterials for Healthcare, especially Dr. Raffaella Della Moglie e Dr. Pasquale Caruso, and all PhD students and researchers who gave extra hours to the confocal microscope and cell hood reservations.

Lastly, I would like to express my sincere gratitude to my sister Valeria for revising the English of this thesis. I also appreciate the support I received from the rest of my family. I thank my boyfriend Raffaele for his unwavering support and belief in me, without which this achievement would not have been possible.